Measurement and Source Apportionment of reactive Volatile Organic Compounds (VOCs) in South Asia

A thesis

submitted by

Chinmoy Sarkar

for the degree of

Doctor of Philosophy

Indian Institute of Science Education and Research Mohali

Knowledge City, Sector 81, SAS Nagar, Manauli PO 140306

Mohali, India

April 2016

Declaration

I hearby declare that I wrote the dissertation submitted without any unauthorised external assistance and used only sources acknowledged in the work. All textual passages which are appropriated verbatim or paraphrased from published and unpublished texts as well as all information obtained from oral sources are duly indicated and listed in accordance with bibliographical rules. In carrying out this research, I complied with the rules of standard scientific practice as formulated in the statutes of the Indian Institute of Science Education and Research, Mohali.

Date:

Place: Mohali

Chinmoy Sarkar

In my capacity as the supervisor of the candidate's thesis work, I certify that the above statements by the candidate are true to the best of my knowledge.

Dr. Vinayak Sinha

(Supervisor)

Acknowledgements

I would like to thank my supervisor Dr. Vinayak Sinha for his unwavering and creative guidance. Without his guidance this dissertation would not have been possible.
My sincere gratitude to the Founding Director of IISER Mohali, Professor N. Sathyamurthy for his support and to enable my participation in the SusKat-ABC campaign.
I am also thankful to my monitoring committee members Dr. Ramesh Ramachandran and Dr. Baerbel Sinha for insightful suggestions and motivation.
I thank all my group members - Vinod, Saryu, Praphulla, Gaurav, Harshita, Haseeb, Abhishek, Saurav, Savita, Ashish, Pallavi, Tess and Vaishali for their constant support.
I am grateful to IISER Mohali for providing advanced infrastructure and the Atmospheric Chemistry Research Facility.
I thank Ministry of Human Resource and Development (MHRD) for my PhD fellowship. I also thank the Department of Science and Technology (DST) India, International Centre for Integrated Mountain Development (ICIMOD) Nepal, Institute for Advanced Sustainability Studies (IASS) Potsdam, European Geosciences Union (EGU), World Meteorological Organization (WMO), International Geosphere-Biosphere Program (IGBP) for their support and funding to attend various international scientific events.
I also thank Dr. Mark G. Lawrence, Dr. Arnico Panday, Dr. Achim Edtbauer, Dr. Maheswar Rupakheti, Dr. Joost de Gouw, Dr. Rui Li and Dr. Bob Yokelson for their help.
I thank my friends, Shruti Arya, Satyam Srivastava, Sumyra Sidiq and Shilpa Setia. Special thanks to Shruti Arya for the constant support, care and useful discussions.
My deepest gratitude to my parents and family members for their love and support.

Chinmoy Sarkar

List of Publications

1. Sarkar C., Sinha V., Kumar V., Rupakheti M., Panday A., Mahata K. S., Rupakheti D., Kathayat B., and Lawrence M. G.: Overview of VOC emissions and chemistry from PTR-TOF-MS measurements during the SusKat-ABC campaign: high acetaldehyde, isoprene and isocyanic acid in wintertime air of the Kathmandu Valley, Atmos. Chem. Phys., 16, 3979-4003, doi:10.5194/acp-16-3979-2016, 2016.

2. Sarkar C., Kumar V. and Sinha V.: Massive emissions of carcinogenic benzenoids from paddy residue burning in North India, Curr. Sci., 104, 1703-1706, 2013.

3. Sarkar C., Sinha V., Sinha B., Rupakheti M., Panday A., Bhave P., and Lawrence M. G.: Source apportionment of VOCs in the Kathmandu Valley during the SusKat-ABC international field campaign using positive matrix factorization, In preparation for Atmos. Chem. Phys. Discuss., 2016.

4. Kumar V., **Sarkar C.** and Sinha V.: Influence of post-harvest crop residue fires on surface ozone mixing ratios in the N.W. IGP analyzed using two years of continuous in-situ trace gas measurements. J. Geophys. Res. Atmos., 120, doi: 10.1002/2015JD024308, 2016.

5. Sinha V., Kumar V. and **Sarkar C.**: Chemical composition of pre-monsoon air in the IndoGangetic Plain measured using a new PTR-MS and air quality facility: high surface ozone and strong influence of biomass burning: Atmos. Chem. Phys., 14, 5921-5941, 10.5194/acp-14-5921-2014, 2014.

6. Sinha, B., Sangwan, K. S., Maurya, Y., Kumar, V., **Sarkar, C.**, Chandra B., P. and Sinha, V.: Assessment of crop yield losses in Punjab and Haryana using two years of continuous in-situ ozone measurements, Atmos. Chem. Phys., 15, 9555-9576, 10.5194/acp-15-9555-2015, 2015.

7. Pawar, H., Garg, S., Kumar, V., Sachan, H., Arya, R., **Sarkar, C.**, Chandra, B., P.

and Sinha, B.: Quantifying the contribution of long-range transport to Particulate Matter (PM) mass loadings at a suburban site in the North-Western Indo-Gangetic Plain (IGP), 15, 9501-9520, doi:10.5194/acp-15-9501-2015, Atmos. Chem. Phys., 2015.

Synopsis

Volatile Organic Compounds (VOCs) are important atmospheric constituents that affect human health, air quality and climate. Chronic exposure to certain VOCs can aggravate cardiovascular diseases and cancer risks. Through their participation in chemical reactions with hydroxyl radicals and nitrogen oxides in the atmosphere, they influence the formation of secondary pollutants such as tropospheric ozone and secondary organic aerosol (SOA). Both tropospheric ozone and secondary organic aerosol are important from the standpoint of air quality and climate due to their impact on human health, crop productivity and the radiative forcing of the atmosphere. Further, through reactions with the hydroxyl radicals (the detergent of the atmosphere), photodissociation reactions and radical recycling reactions, VOCs strongly influence ambient OH reactivity and the budget of HO_x (OH+HO_2) radicals which control the removal rates of gaseous pollutants, in particular greenhouse gases such as methane from the atmosphere. These effects are manifest by volatile organic compounds at ppt-ppb concentration levels in the atmosphere. Due to analytical challenges associated with measuring VOCs at such low concentrations in ambient air, our understanding of ambient VOC speciation and the role played by them in varied ecosystems during key atmospheric processes is still evolving. In particular, their specific role over the South Asian region is poorly understood due to paucity of in-situ measurements. Despite the fact that one seventh of the world population lives in the Indo-Gangetic Plain (IGP) and the fertile region sustains agricultural food crop production for much of South Asia, the lack of VOC speciation data over this region precludes a robust scientific understanding of emission sources and atmospheric chemistry of climate and air quality relevant atmospheric constituents.

Chapter 1: Introduction

The first chapter of this thesis presents an overview of the importance of VOCs in the at-

mosphere and a complete literature review of the current state of knowledge with respect to the emissions and chemistry of VOCs over South Asia.

After summarizing these aspects, I present the motivation for my thesis work which addresses five main questions and will contribute to advancing global scientific understanding of VOC emissions and chemistry over South Asia:

1. What is the chemical composition and speciation of VOCs in ambient fire plumes influenced by post-harvest paddy straw fires in the north-west Indo Gangetic Plain (IGP)?

2. What is the time and mass resolved chemical speciation of VOCs in the Kathmandu Valley in winter as observed in the PTR-TOF-MS mass scans?

3. How do the VOCs present in ambient Kathmandu air individually and collectively affect the ozone formation chemistry and air quality?

4. What are the quantitative contributions of specific emission sources (e.g., traffic, biomass co-fired brick kilns) to ambient concentrations of individual VOCs and the ozone production potential?

5. What should be the mitigation strategy for the improvement of air quality in the Kathmandu Valley based on the in-situ observations?

Chapter 2: Quantifying ambient VOCs present at concentrations of few ppt-ppb: Analytical considerations and challenges

Ambient air represents a very challenging chemical matrix to quantify VOCs present at few ppt-ppb range. The matrix varies in chemical composition by day and night in response to emissions and meteorological changes. In particular the presence of water vapour and more abundant gases such as carbon dioxide, methane, oxygen can present complex analytical challenges. Traditionally VOC measurements in the atmosphere were pioneered by improvements in gas chromatographic (GC) techniques, wherein air samples collected in canisters/adsorbents are analyzed after sufficient preconcentration. Today variants of gas chromatographic techniques can measure a suite of VOCs at concentrations as low as 0.1 ppt (parts-per-trillion). Despite these advantages, issues that arise during collection, storage and pre-concentration steps can lead to measurement artefacts. In particular several oxygenated VOCs such as acetaldehyde, methanol and acetone and short-lived reactive VOCs cannot be reliably quantified using conventional gas chromatographic methods. Moreover, the disadvantage for ambient emission activity related studies, using these GC

based methods is the sub-optimal time resolution of measurements (typically hourly). In the past several decades, various new spectroscopic methods have also emerged for specific VOCs, but remain limited in scope for VOC measurements in ambient air. In such a context, highly mass and time resolved mass spectrometric methods are better suited and have revolutionized the ambient air VOC studies in the past decade. These permit real time quantification in a rapidly changing atmosphere so that accurate and specific emission activity information can be discerned by careful analysis of the measurements.
In this regard, high sensitivity proton transfer reaction mass spectrometry (PTR-MS) is the most advanced and sensitive technique currently available to detect volatile organic compounds at trace concentrations of few ppt in the ambient air in real time (few seconds time resolution) over an appropriate mass range for VOCs ($>$ 200 amu). Within the instrument, organic species with a proton affinity greater than water are chemically ionised by proton transfer with the reagent hydronium (H_3O^+) ions and the products are then separated (using a quadrupole or time-of-flight analyzer) before detection using secondary electron multipliers or channeltrons. The key advantage of this type of ionization is that all major constituents of ambient air (e.g., Nitrogen (78%); Oxygen (21%), Water Vapour, Argon, Carbon dioxide, Methane) do not have a proton affinity greater than that of water and hence do not undergo detection, leading to simpler mass spectra. In particular, no pre-concentration or storage of sample is necessary for achieving ppt detection limit. Moreover, the soft ionization method ensures that there is little fragmentation.
In this chapter I discuss and describe these important measurement aspects which also highlight the novelty of my thesis work from a measurement perspective.
In my thesis, I employed two different versions of the PTR-MS instrument, namely the PTR-Q-MS which uses a quadrupole as mass analyzer and a PTR-TOF-MS which uses a time-of-flight mass analyzer.
Both PTR-Q-MS and PTR-TOF-MS were deployed for the first time in South Asia during these studies, in Mohali and in Kathmandu, respectively. The major advantage of PTR-TOF-MS over PTR-Q-MS is its high mass resolution and detection limit of few tens of ppt that permits identification of several rarely measured or previously unmeasured compounds based on their monoisotopic masses and therefore identification/contribution of different isobars at a nominal mass is made possible.

Chapter 3: Massive Emissions of Carcinogenic Benzenoids from Paddy residue burning in North India

In this chapter I investigated the VOC speciation in ambient plumes influenced by post harvest paddy residue fires in the N.W. IGP and compared ambient enhancements due to this activity for a suite of chemical compounds, in particular for carcinogenic benzenoids, carbon monoxide and nitrogen oxides.

Benzenoids are organic pollutants emitted mainly by traffic and industrial sources. Here, using the combination of online in-situ measurements of several benzenoids and methyl cyanide (a biomass burning tracer) for the time in India, satellite remote sensing data of fire counts and back trajectory of air masses at a site in Mohali, we show that massive amounts of benzenoids are released from post-harvest paddy residue burning. Two periods, one that was not influenced by paddy residue burning (Period 1, 18:00-03:30 IST; 5-6 October, 2012) and another which was strongly influenced by paddy residue burning (Period 2, 18:00-03:30 IST; 3-4 November, 2012) were chosen to assess normal and perturbed levels. Peak values of 3830 ppb CO, 100 ppb NO_x, 40 ppb toluene, 16 ppb benzene, 24 ppb for sum of all C8-benzenoids and 13 ppb for sum of all C9-benzenoids were observed during Period 2 with the average enhancements in benzenoid levels more than 300%. The ozone formation potential of benzenoids matched CO with both contributing 5 ppb h^{-1} each. Such high levels of benzenoids for 1-2 months in a year aggravate smog events and can enhance cancer risks in north western India.

Chapter 4: Overview of VOC emissions and chemistry from PTR-TOF-MS measurements during the SusKat-ABC campaign

The Kathmandu Valley in Nepal suffers from severe wintertime air pollution. Volatile organic compounds (VOCs) are key constituents of air pollution, though their specific role in the Valley is poorly understood due to insufficient data. During the SusKat-ABC (Sustainable Atmosphere for the Kathmandu Valley-Atmospheric Brown Clouds) field campaign conducted in Nepal in the winter of 2012-2013, a comprehensive study was carried out to characterize the chemical composition of ambient Kathmandu air, including the determination of speciated VOCs by deploying a Proton Transfer Reaction Time of Flight Mass Spectrometer (PTR-TOF-MS) - the first such deployment in South Asia. 71 ion peaks (for which measured ambient concentrations exceeded the 2σ detection limit)

were detected in the PTR-TOF-MS mass scan data, highlighting the chemical complexity of ambient air in the Valley. Of the 71 species, 37 were found to have campaign average concentrations greater than 200 ppt and were identified based on their spectral characteristics, ambient diel profiles and correlation with specific emission tracers as a result of the high mass resolution ($m/\Delta m > 4200$) and temporal resolution (1 minute) of the PTR-TOF-MS. The highest average VOC mixing ratios during the measurement period were (in rank order): acetaldehyde (8.8 ppb), methanol (7.4 ppb), acetone (4.2 ppb), benzene (2.7 ppb), toluene (1.5 ppb), isoprene (1.1 ppb), acetonitrile (1.1 ppb), C8-aromatics (∼1 ppb), furan (∼0.5 ppb), and C9-aromatics (0.4 ppb). Distinct diel profiles were observed for the nominal isobaric compounds isoprene ($m/z = 69.070$) and furan ($m/z = 69.033$). Comparison with wintertime measurements from several locations elsewhere in the world showed mixing ratios of acetaldehyde (∼9 ppb), acetonitrile (∼1 ppb) and isoprene (∼1 ppb) to be among the highest reported till date. Two "new" ambient compounds namely, formamide ($m/z = 46.029$) and acetamide ($m/z = 60.051$), which can photochemically produce isocyanic acid in the atmosphere, are reported in this study along with nitromethane (a tracer for diesel exhaust) which has only recently been detected in ambient studies. Two distinct periods were selected during the campaign for detailed analysis: the first was associated with high wintertime emissions of biogenic isoprene, and the second with elevated levels of ambient acetonitrile, benzene and isocyanic acid from biomass burning activities. Emissions from biomass burning and biomass co-fired brick kilns were found to be the dominant sources for compounds such as propyne, propene, benzene and propanenitrile which correlated strongly with acetonitrile ($r^2 > 0.7$), a chemical tracer for biomass burning. The calculated total VOC OH reactivity was dominated by acetaldehyde (24.0%), isoprene (20.2%) and propene (18.7%), while oxygenated VOCs and isoprene collectively contributed to more than 68% of the total ozone production potential. Based on known SOA yields and measured ambient concentrations in the Kathmandu Valley, the relative SOA production potential of VOCs were: benzene > naphthalene > toluene > xylenes > monoterpenes > trimethylbenzenes > styrene > isoprene. The first ambient measurements from any site in South Asia of compounds with significant health effects such as isocyanic acid, formamide, acetamide, naphthalene and nitromethane have been reported in this study. Our results suggest that mitigation of

intense wintertime biomass burning activities, in particular point sources such biomass co-fired brick kilns, would be important to reduce the emission and formation of toxic VOCs (such as benzene and isocyanic acid) in the Kathmandu Valley and improve its air quality.

Chapter 5: Source Apportionment of VOCs in the Kathmandu Valley during the SusKat-ABC international field campaign using Positive Matrix Factorization

In this chapter, receptor modelling was performed using the US Environmental Protection Agency's (EPA) Positive Matrix Factorization (PMF) model version 5.0 to apportion the VOC dataset obtained during the SusKat-ABC field campaign in the Kathmandu Valley to specific sources.

In the PMF model, an ambient data set is viewed as a data matrix X of i by j dimensions consisting of i number of samples and j chemical species. The objective of multivariate receptor modeling is to identify the number of source profile factors "p" that can explain the observed VOC composition and temporal characteristics at a site, the species profile "f" of each source, and the amount of mass g contributed by each source profile factor to each individual sample, along with the residual "e" (a measure of data not attributed to any source factor profiles) according to the following equation:

$$X_{ij} = \sum_{k=1}^{p} g_{ik} f_{kj} + e_{ij} \quad (1)$$

Positive matrix factorization model (EPA PMF version 5.0) was applied for the source apportionment of the dataset of 37 VOCs measured using PTR-TOF-MS during the SusKat-ABC field campaign (19 December 2012-30 January 2013) in the Kathmandu Valley. Total eight source categories were resolved by the PMF model after applying the new "constrained model operation". These are - traffic, residential biofuel use and waste disposal, mixed industrial emissions, biomass co-fired brick kilns, unresolved industrial emissions, solvent evaporation, mixed daytime source and biogenic emissions. The unresolved industrial emissions and traffic factor contributed most to the total VOC mass loading (17.9% and 16.8%, respectively) followed by mixed industrial emissions (14.0%),

residential biofuel use and waste disposal (10.9%), solvent evaporation (10.8%), biomass co-fired brick kilns (10.4%), biogenic emissions (10.0%) and mixed daytime factor (9.2%). Conditional probability function (CPF) analyses were performed to identify the physical locations associated with different sources. Source contributions to individual VOCs showed biomass co-fired brick kilns significantly contribute to the elevated concentrations of several health relevant VOCs such as carcinogenic benzene. Biogenic emissions contributed most (24.2%) to the total daytime ozone production potential even in winter followed by solvent evaporation (20.2%), traffic (15.0%) and unresolved industrial emissions factor (14.3%). Secondary organic aerosol (SOA) production was dominated by biomass co-fired brick kilns (28.9%) and traffic (28.2%). Comparison of the PMF derived results with REAS, EDGAR and existing Nepalese inventory showed that all the inventories overestimate the contribution of residential biofuel use and underestimate the contribution of traffic in the Kathmandu Valley.

Contents

List of Publications **vii**

Synopsis **xvi**

1 Introduction **1**

1.1 The Atmosphere 1

1.2 Volatile Organic Compounds (VOCs): sources and sinks in the troposphere 5

1.3 Importance of VOCs for tropospheric chemistry 7

1.4 Status of VOC research in South Asia 13

1.5 Research motivation and thesis outline 14

2 Quantifying ambient VOCs present at concentrations of few ppt-ppb: Analytical considerations and challenges **17**

2.1 Gas Chromatography 18

2.1.1 Sample acquisition 20

2.1.2 Sample preparation 21

2.1.3 Sample separation 21

2.1.4 Detection 23

2.2 Proton Transfer Reaction Mass Spectrometry (PTR-MS) 24

2.2.1 Ion source 26

2.2.2 Drift tube 27

2.2.3 Mass analyzers 29

2.2.4 Detector 37

3 Massive Emissions of Carcinogenic Benzenoids from Paddy residue burning in North India **39**

3.1 Abstract . . . 39

3.2 Introduction . . . 40

3.3 Materials and methods . . . 42

3.3.1 Site Description . . . 42

3.3.2 Benzenoids and Methyl Cyanide measurements using Proton Transfer Reaction Mass Spectrometry (PTR-MS) . . . 42

3.3.3 Sampling of ambient air . . . 44

3.3.4 Carbon monoxide (CO), nitrogen oxides (NO_x) and PM measurements . . . 44

3.3.5 Trajectory Analysis and MODIS Data . . . 45

3.4 Results and discussion . . . 45

3.5 Conclusions . . . 52

4 Overview of VOC emissions and chemistry from PTR-TOF-MS measurements during the SusKat-ABC campaign **53**

4.1 Abstract . . . 53

4.2 Introduction . . . 55

4.3 Materials and methods . . . 58

4.3.1 Site Description and prevalent meteorology . . . 58

4.3.2 VOC measurements using PTR-TOF-MS . . . 61

4.4 Results and discussion . . . 67

4.4.1 Identification of VOCs present in ambient air using PTR-TOF-MS mass scans . . . 67

4.4.2 General trends in VOC concentrations during the SusKat-ABC campaign . . . 73

4.4.3 Comparison with wintertime VOC mixing ratios elsewhere . . . 78

4.4.4 Diel profiles as a tool to constrain emission sources: VOCs emitted from biomass burning activities in the Kathmandu Valley . . . 80

4.4.5 Diel profiles of rarely measured VOCs and correlation with emission tracer VOC compounds for constraining their sources 85
4.4.6 High isoprene in the Kathmandu Valley: a daytime biogenic source and contributions from combustion sources 88
4.4.7 OH reactivity and Ozone Production Potential of VOCs 90
4.4.8 SOA formation potential of VOCs in the Kathmandu Valley 93
4.4.9 VOCs with direct health implications for exposed population . . . 95
4.5 Conclusions 96

5 Source Apportionment of VOCs in the Kathmandu Valley during the SusKat-ABC international field campaign using Positive Matrix Factorization 101
5.1 Abstract 101
5.2 Introduction 102
5.3 Materials and methods 105
5.3.1 Positive Matrix Factorization (PMF) 105
5.3.2 Implementation of PMF 107
5.3.3 Conditional probability function (CPF) analyses 116
5.4 Results and Discussion 116
5.4.1 Identification of PMF factors 116
5.4.2 Factor 1 - Traffic 116
5.4.3 Factor 2 - Residential biofuel use and waste disposal 118
5.4.4 Factor 3 - Mixed industrial emissions 121
5.4.5 Factor 4 - Biomass co-fired brick kilns 122
5.4.6 Factor 5 - Unresolved industrial emissions 123
5.4.7 Factor 6 - Solvent evaporation 125
5.4.8 Factor 7 - Mixed daytime 126
5.4.9 Factor 8 - Biogenic emissions 127
5.4.10 Conditional probability functions (CPF) to determine source directionality 130

5.4.11 Source contribution to total VOC mass loading and comparison with emission inventory . . . 132
5.4.12 Source contribution to individual VOCs . . . 136
5.4.13 Source contribution to daytime ozone production potential and SOA formation . . . 142
5.5 Conclusions . . . 144

6 Conclusions: Major findings and outlook **145**

List of Figures and Tables **151**

Bibliography **161**

Chapter 1

Introduction

1.1 The Atmosphere

The Earth's atmosphere consists of different layers and these different layers of the atmosphere are characterized by distinct temperature and pressure regimes which vary with altitude. The troposphere is the lowermost part of the atmosphere that extends from the Earth's surface up to 10-18 km depending on the latitude and the season. This layer is characterized by rapid vertical mixing and decrease in temperature with altitude due to adiabatic cooling associated with convection. The temperature in the troposphere ranges from 288 K (at the surface) to 217 K at the tropopause (∼18 km) and the pressure ranges from 1013 hPa (at the surface) to 75.65 hPa (at ∼18 km). The stratosphere extends from ∼20 km up to ∼50 km where temperature increases with altitude due to absorption of solar ultraviolet energy by ozone and exothermic photodissociation reactions. Vertical mixing is slow in this layer. The temperature in the stratosphere ranges from 217 K to 271 K and the pressure ranges from 55.29 hPa to 0.798 hPa. The mesosphere extends from ∼50 km up to ∼90 km wherein temperature decreases with altitude and rapid vertical mixing occurs. The temperature in the mesosphere ranges from 271 K to ∼210 K and the pressure ranges from 0.798 hPa to ∼0.0003 hPa. Thermosphere extends from ∼90 km up to ∼500 km and is characterized by high temperatures due to absorption of short-wavelength radiation by N_2 and O_2 and photoionization that leads to the formation of ions.

Figure 1.1 shows a pictorial representation of the discrete layers in the atmosphere and the variation of temperature with altitude. Among all the layers, troposphere (the lowermost part near the surface) contains more than 90% of all air molecules and most of the chemical reactions occur in this layer. Many of these reactions can contribute to the formation of secondary pollutants such as ozone and secondary organic aerosol (Atkinson., 2000; Carlton et al., 2009). Stratospheric ozone protects us from the harmful ultraviolet (UV) rays (wavelength between 240-290 nm) by absorbing it and therefore ozone in the stratosphere is known as the 'good ozone'. In the troposphere ozone acts as a criteria pollutant above certain threshold concentrations of few tens of ppb affecting air quality, crop productivity and human health (IPCC, 2013; Haggen-Smit., 1952; Giles., 2005; Ashworth et al., 2015; Sinha et al., 2015; Jerrett et al., 2009). Therefore, tropospheric ozone when present in excess is known as 'bad ozone'.

Volatile Organic Compounds (VOCs) fuel the formation of ozone in the troposphere along with other secondary pollutants such as secondary organic aerosol (SOA). Both tropospheric ozone and secondary organic aerosol are important from the standpoint of air quality and climate due to their impact on human health, crop productivity and the radiative forcing of the atmosphere. Recently, the Fifth Assessment Report (AR5) of the Intergovernmental Panel on Climate Change (IPCC, 2013) estimated the contribution of non-methane volatile organic compounds (NMVOCs) to climate (+0.05 to +0.15 W m^{-2}) and rated the current level of scientific understanding of NMVOCs on climate as only "medium", which is much below that of aerosols for which the level of scientific understanding is rated to be "high". The effects of NMVOCS on climate occur primarily through chemical feedbacks and hence studies related to VOC emissions and chemistry are urgently required, in particular over under-studied regions like South Asia.

The troposphere can be regarded as a large reactor where emitted reactant molecules are photochemically oxidized by atmospheric oxidants such as the hydroxyl radical and removed by chemical degradation and deposition (Karl et al., 2010; Park et al., 2013). The atmospheric lifetime or residence time of a species determines how long the species tends to reside in the global atmosphere before it is removed and hence is a very important quantity in atmospheric studies.

Figure 1.2 shows the temporal and spatial scale of several reactive atmospheric con-

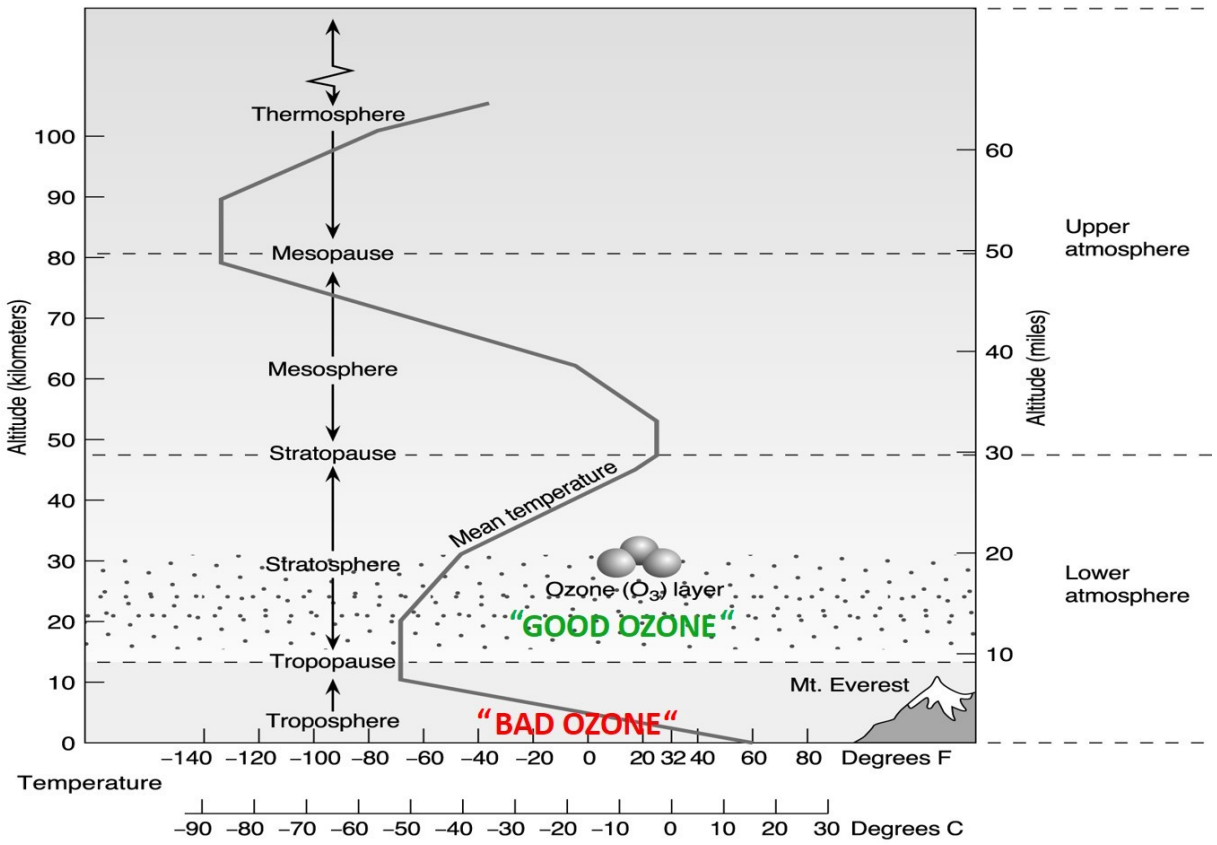

Figure 1.1: Variation of temperature at different layers of the atmosphere (Source: James E. Girard, Principles of Environmental Chemistry, 2010, 'Reproduced with kind permission from Jones & Bartlett Learning, Burlington, Massachusetts, United States')

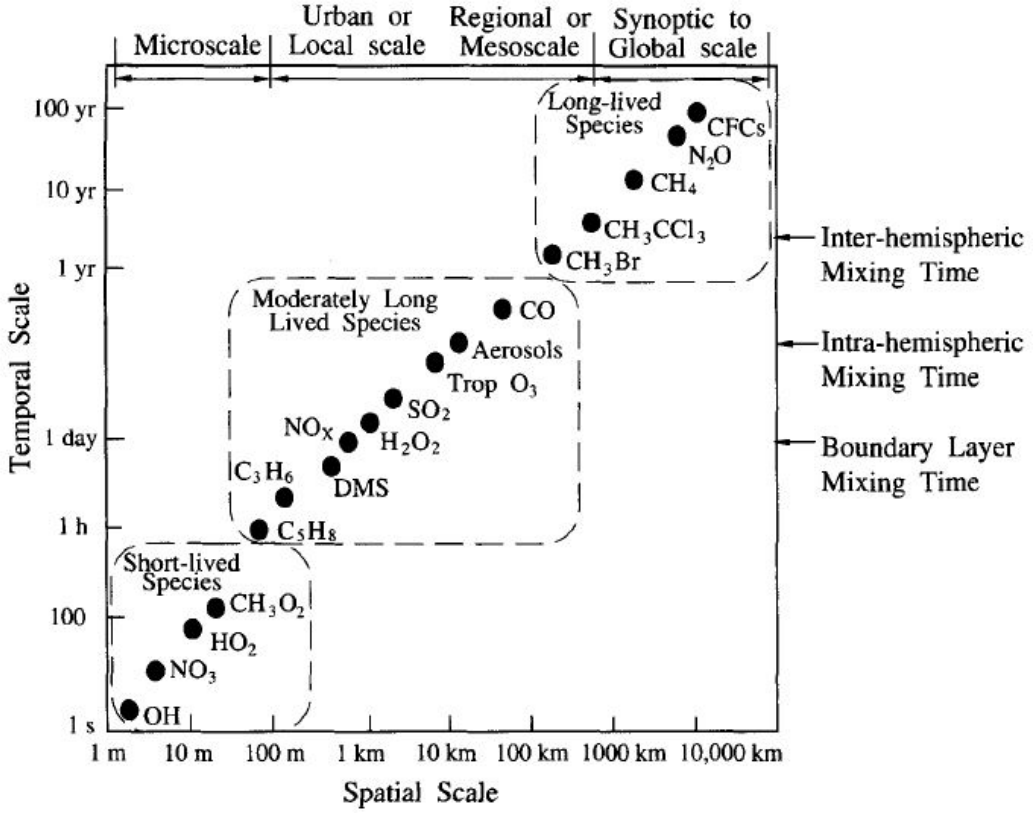

Figure 1.2: Spatial and temporal scales of variability for reactive constituents of the atmosphere (Source: Seinfeld and Pandis, Atmospheric Chemistry and Physics: From Air Pollution to Climate Change, Second Edition, 2006, 'Reproduced with kind permission from John Wiley & Sons Ltd., UK')

stituents. The y-axis shows the time scale of a constituent in the atmosphere i.e., the lifetime or residence time of that constituent whereas x-axis shows the spatial scale which gives an indication of how far these constituents may be transported. The atmospheric lifetime or residence time can be defined as,

$$\tau = \frac{Q}{R} \tag{1.1}$$

Where, Q is the amount/concentration of the species in the atmosphere, and R is the rate of removal of the species (generally represented by a first order loss process) from the atmosphere. For example, reaction of methane with hydroxyl (OH) radicals represent the main removal process of methane in the troposphere ($CH_4 + OH \rightarrow CH_3 + H_2O$). Assuming average [OH] concentration = 1×10^6 molecules cm^{-3} (Levy., 1971; Monks.,

2005) and the typical rate coefficient for this reaction at the surface = 3.5×10^{-15} cm^3 $molecule^{-1}$ s^{-1} (Atkinson et al., 2006), the atmospheric lifetime of methane is calculated as follows:

$$\tau = \frac{[CH_4]}{k_{(CH_4+OH)}[OH][CH_4]} = \frac{1}{k_{(CH_4+OH)}[OH]} = \frac{1}{(3.5 \times 10^{-15} \ \ cm^3 molec^{-1} s^{-1})(1 \times 10^6 \ \ molec cm^3)} = \sim 9.2 \ \ yrs \tag{1.2}$$

Short-lived species such as the OH radical can have an atmospheric lifetime of few milliseconds in polluted air whereas long-lived species such as methane (a Green House Gas (GHG)) can have lifetimes on the timescales of several years. Most VOCs have tropospheric lifetimes in the intermediate range between those of short-lived radicals and the long-lived GHGs and are present at very low concentrations, usually in parts-per-trillion (ppt) to parts-per-billion (ppb) range. Quantification of VOCs in a complex matrix (i.e., the troposphere) which is composed of both short-lived and long-lived species and variable amounts of water vapour therefore presents a major analytical challenge.

1.2 Volatile Organic Compounds (VOCs): sources and sinks in the troposphere

According to the definition provided by the International Union of Pure and Applied Chemistry (IUPAC), Volatile Organic Compounds (VOCs) are carbon containing compounds which possess high vapour pressure (> 10 Pa at 25°C) and low boiling point (below 260°C) at standard atmospheric pressure (101.3 kPa). All gaseous organics including aliphatic, aromatic and halogenated hydrocarbons, aldehydes, esters, acids, alcohols and ketones are considered to be VOCs but carbon monoxide (CO) and carbon dioxide (CO_2) have traditionally been excluded from the definition of VOCs due to their larger abundances (CO: tens of ppb to few ppm; CO_2 = 380-400 ppm).

VOCs can have both biogenic and anthropogenic sources (Hewitt., 1999). Globally, biogenic sources exceed the emission of VOCs (815-1530 Tg y^{-1}) from anthropogenic sources (71-175 Tg y^{-1}) (Guenther et al., 1995; Warneck and Williams., 2012). Among biogenic

VOCs, isoprene is the single largest contributor with a global budget of 530 Tg y^{-1} (Guenther et al., 2006). Biomass burning is a significant source of numerous VOCs including many oxygenated compounds, nitriles and aromatics (Andreae and Merlet., 2001) with global emission estimates of 25-80 Tg y^{-1}. Oxygenated VOCs can also be produced in the atmosphere due to the photooxidation of hydrocarbons (Singh., 2004; Sommariva et al., 2011). Fossil fuel emissions are an anthropogenic source of VOCs such as alkanes, alkenes and aromatics and play a profound role in urban environments, despite smaller contributions on the global scale. In the South Asian region (specifically in India and Nepal), the major anthropogenic sources of VOCs are thought to be traffic, biomass burning, residential biofuel use and waste disposal, industrial and brick kiln emissions. According to the EDGAR (Emission Database for Global Atmospheric Research) v4.2 emission inventory (2008), the total NMVOC emission from India and Nepal were reported to be 11.3 Tg y^{-1} and 0.316 Tg y^{-1}. The removal of VOCs in the troposphere occurs by photochemical oxidation and deposition. These removal processes can occur on time scales of minutes to months for most VOCs (Atkinson and Arey., 2003). During the daytime, reactions with the hydroxyl radical (OH) constitute the major sink for a large number of VOCs. The primary production of hydroxyl radicals in turn depends on photolysis of O_3 and subsequent reaction with water vapour of some of the excited oxygen atoms. This can be expressed by the following set of reactions (Leighton., 1961),

$$O_3 + h\nu \longrightarrow O_2 + O(^1D) \quad (\lambda < 335nm) \qquad \text{[R1]}$$

$$O(^1D) + M \longrightarrow O(^3P) + M \quad (M = N_2O_2) \qquad \text{[R2]}$$

$$O(^3P) + O_2 + M \longrightarrow O_3 + M \quad (M = air) \qquad \text{[R3]}$$

$$O(^1D) + H_2O \longrightarrow 2OH \qquad \text{[R4]}$$

[R1],[R2] and [R3] constitute a null cycle, in which no net production of ozone occurs. The photolysis rate coefficient of O_3 (k_1) at solar zenith angle of 0° is 6×10^{-5} s^{-1} while

the rate coefficient of [R3] (k_3) is 2.6-4.0 $\times$ 10^{-11} cm^3 $molec^{-1}$ s^{-1} (Seinfeld and Pandis., 2006). The formation of OH from $O(^1D)$ is much faster with a rate coefficient of 2.2 $\times$ 10^{-10} cm^3 $molec^{-1}$ s^{-1} (Seinfeld and Pandis., 2006). The $O(^1D)$ formed as a result of the photolysis of O_3 can either collisionally quench back to stable $O(^3P)$ or can form 2 molecules of OH radicals. At normal temperature and pressure (298 K and 1 atm) and 80% relative humidity, $\sim$40% of the total $O(^1D)$ formed in the troposphere may form OH radicals (Seinfeld and Pandis., 2006). Photolysis of nitrous acid (HONO), dark reactions of O_3 with alkenes and photolysis of formaldehyde and other carbonyl compounds in presence of NO can also act as sources of the OH radical in the troposphere (Atkinson., 2000). Typically the average daytime OH radical concentrations are of the order of 1 $\times$ 10^6 molecules cm^{-3} (Levy., 1971; Monks., 2005). Photolysis, reactions with ozone and nighttime reactions with nitrate (NO_3) radical also act as sinks of VOCs (Warneke et al., 2004).

A list of the dominant sources and sinks along with global budgets and atmospheric lifetimes for some major atmospheric VOCs relevant to this thesis work are summarized in Table 1.1 (Source References: Warneck and Williams. (2012); Millet et al. (2008); Singh. (2004); Marandino et al. (2005); Jardine et al. (2015); Martinez et al. (2004); Sekimoto et al. (2013); Barnes et al. (2010); Borduas et al. (2014); Roberts et al. (2014)).

1.3 Importance of VOCs for tropospheric chemistry

VOCs in the troposphere can react chemically to form secondary pollutants such as tropospheric ozone and secondary organic aerosol and some VOCs also have direct health impacts.

Tropospheric ozone is a short-lived secondary pollutant and is important due to its impact on air quality, human health and crop productivity (IPCC, 2013; Haggen-Smit., 1952; Giles., 2005; Ashworth et al., 2015; Sinha et al., 2015; Jerrett et al., 2009). In the troposphere, ozone is produced due to photolysis of NO_2 ($\lambda < 420$ nm).

$$NO_2 + h\nu \longrightarrow NO + O(^3P) \qquad [R5]$$

Table 1.1: Overview of some important VOCs in the troposphere: approximate atmospheric lifetimes, major sources, sinks and global budgets

VOCs	Chemical formula	Atmospheric lifetime	Major sources (Tg y^{-1})	Major sinks (Tg y^{-1})
Acetonitrile*[1]	CH_3CN	∼7 months	Biomass burning (1.2)	Reaction with OH (0.3), uptake by oceans (1.2)
Benzene[2]	C_6H_6	∼10 days	Industrial and fossil fuel (1.5), biofuel (2), biomass burning (2.7)	Reaction with OH
Toluene[3]	C_7H_8	∼2 days	Industrial and fossil fuel (4.7), biofuel (1.1), biomass burning (1.8)	Reaction with OH
Isoprene[4]	C_5H_8	∼1.5 hours	Emissions from deciduous trees (570)	Reaction with OH
Monoterpenes[5]	$C_{10}H_{16}$	∼1-5 hours	Emissions from coniferous and deciduous trees (140)	Reaction with OH and O_3
Formaldehyde[6]	HCHO	∼10 hours	Oxidation of hydrocarbons	Photolysis and reaction with OH
Methanol[7]	CH_3OH	∼4.9 days	Terrestrial plant growth (80), plant decay (23), biomass burning (12), atmospheric production (35), urban sources (5), oceans and biogenic (85)	Gas phase oxidation by OH (88), dry deposition in land (40), wet deposition (13), uptake by oceans (101)
Acetaldehyde[8]	CH_3CHO	∼19.2 hours	Hydrocarbon oxidation (128), vegetation (23), ocean emissions (57), biomass burning (3), anthropogenic emissions (2)	Reaction with OH (188), photolysis (22), dry and wet deposition (3)
Acetone[9]	CH_3COCH_3	∼15 days	Hydrocarbon oxidation (20-36), vegetation (25-75), ocean emissions (0-15), biomass burning (7-11), anthropogenic emissions (2)	Photolysis (14-30), reaction with OH (11-25), wet and dry deposition (46-96)
Dimethylsulfide (DMS)[10]	CH_3SCH_3	∼2 days	Ocean emissions (50), soils and vegetation (1)	Reaction with OH and NO_3
Naphthalene[11]	$C_{10}H_8$	∼1 day	Vehicle exhaust and residential heating	Reaction with OH
Nitromethane[12]	CH_3NO_2	∼2 years	Diesel vehicle exhaust	Photodissociation
Formamide, Acetamide[13]	$HCONH_2$, CH_3CONH_2	∼1-4 days	Photooxidation of alkyl amines, industrial sources	Photolysis, chemical reactions with OH, NO_3, O_3
Isocyanic acid[14]	HNCO	-	Biomass combustion, photooxidation of amines and amides, diesel engines	Wet and dry deposition, photolysis, reaction with OH

∗Global budget of acetonitrile is not balanced and its sink is always estimated to be larger than the source (Sanhueza et al., 2004); 1-4,6. (Warneck and Williams., 2012); 5. (Atkinson and Arey., 2003) 7 and 8. (Millet et al., 2008); 9. (Singh., 2004) and (Marandino et al., 2005); 10. (Jardine et al., 2015); 11. (Martinez et al., 2004); 12. (Sekimoto et al., 2013); 13. (Barnes et al., 2010), (Borduas et al., 2014); 14. (Roberts et al., 2014).

$$O(^3P) + O_2 + M \longrightarrow O_3 + M \quad [R6]$$

O_3 reacts with nitric oxide (NO) to produce NO_2 and O_2 ($k_7 = 1.8 \times 10^{-14}$ cm^3 s^{-1}; Atkinson et al. (2004)).

$$O_3 + NO \longrightarrow NO_2 + O_2 \quad [R7]$$

The reactions [R5]-[R7] constitute a 'null cycle' in which no net production of O_3 occurs and a photo-stationary state between O_3-NO-NO_2 is formed on timescale of few 100 seconds during the daytime (Mannschreck et al., 2004).

VOCs (represented here as the generic hydrocarbon, RH) react with OH radicals in presence of O_2 to produce alkyl peroxy (RO_2) radicals (Sinha et al., 2012) which can further undergo reaction with NO, and produce alkoxy radicals and one molecule of NO_2 ($k_9 \geq 10^{-12}$ cm^3 molecule^{-1} s^{-1} and $k_{10} = 7.5\text{-}9 \times 10^{-12}$ cm^3 molecule^{-1} s^{-1}; Seinfeld and Pandis. (2006); Finlayson-Pitts and Pitts. (2000)).

$$RH + OH \longrightarrow R + H_2O \quad [R8]$$

$$R + O_2 + M \longrightarrow RO_2 + M \quad [R9]$$

$$RO_2 + NO \longrightarrow RO + NO_2 \quad [R10]$$

These alkoxy radicals can undergo further reactions to produce hydro peroxy (HO_2) radicals and lower carbonyl compounds ($k_{11} = 8\text{-}9.5 \times 10^{-15}$ cm^3 molecule^{-1} s^{-1}; Seinfeld and Pandis. (2006)).

$$RO + O_2 \longrightarrow \text{carbonylcompound} + HO_2 \quad [R11]$$

HO_2 can react with NO to produce OH and another molecule of NO_2 ($k_{12} = 8.1 \times 10^{-12}$ cm^3 molecule^{-1} s^{-1}; Seinfeld and Pandis. (2006)).

$$HO_2 + NO \longrightarrow OH + NO_2 \quad [R12]$$

Therefore from one molecule of VOC, in principle at least 2 molecules of NO_2 can be produced which can undergo photolysis to produce 2 molecules of O_3 in the troposphere outside the O_3-NO-NO_2 photo-stationary state. In reality, depending on the structure of a VOC, multiple conversions of NO to NO_2 can occur during its complete oxidation and for each such conversion a molecule of O_3 can be formed. Thus, VOCs tend to fuel the formation of surface ozone.

[R8] is the slowest step among [R8]-[R12] and its rate coefficient depends on the nature of the R group. Therefore [R8] acts as the rate determining step for the ozone production from VOCs. This underscores the importance of VOC OH reactivity/NO_x OH reactivity for ozone production in the troposphere. In the troposphere, both VOCs and NO_x compete for the available OH radicals. At a high VOC/NO_x ratio, OH will react primarily with VOCs whereas at a low VOC/NO_x ratio, reaction with NO_x dominates. Therefore, at high VOC/NO_x ratios when VOC OH reactivity dominates, radical-radical reactions of the following type can act as the major chain termination reaction ($k_{13} = 2.9 \times 10^{-12}$ cm^3 $molecule^{-1}$ s^{-1}; Seinfeld and Pandis. (2006)),

$$HO_2 + HO_2 \longrightarrow H_2O_2 + O_2 \qquad \text{[R13]}$$

At low VOC/NO_x ratios when NO_x OH reactivity dominates, formation of nitric acid occurs and this reaction acts as the major chain termination reaction ($k_{14} = 1.1 \times 10^{-11}$ cm^3 $molecule^{-1}$ s^{-1} at 1 atm; Seinfeld and Pandis. (2006)).

$$OH + NO_2 + M \longrightarrow HNO_3 + M \qquad \text{[R14]}$$

The non-linearity of ozone production on initial concentrations of hydrocarbons and NO_x can be visualized using ozone isopleth plots (Figure 1.3). In a NO_x limited regime (where VOC OH reactivity dominates), [R13] acts as the chain termination reaction and maximum ozone production becomes directly dependent on NO_x and can be expressed by the following equation (Jacob., 1999),

$$P_{O_3} = 2k_{(HO_2+NO)}\left(\frac{P_{HO_x}}{k_{(HO_2+HO_2)}}\right)^{1/2}[NO] \qquad (1.3)$$

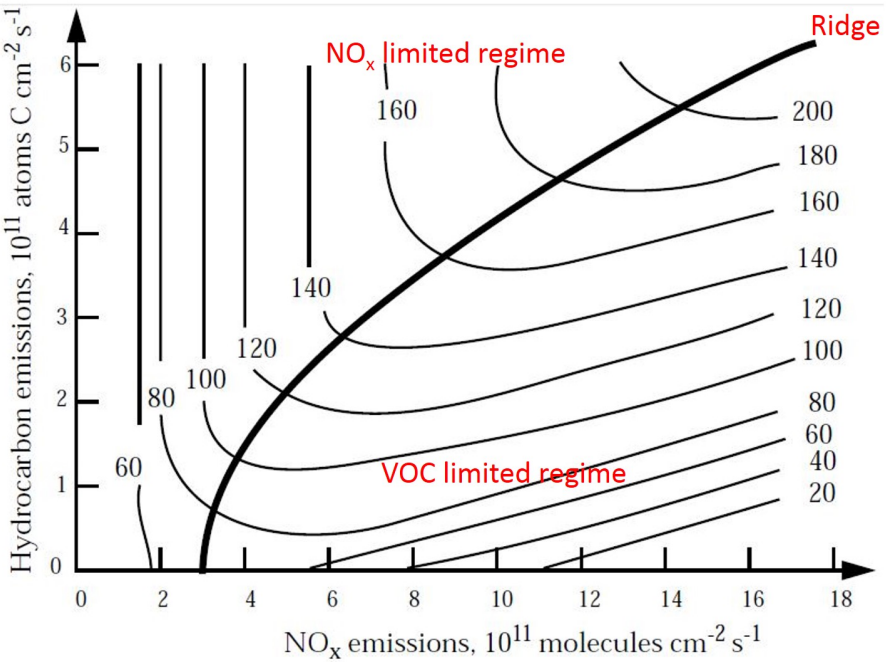

Figure 1.3: Ozone isopleth diagram showing dependence of ozone production on emissions of VOCs and NO_x (Source: Daniel J. Jacob, Introduction to Atmospheric Chemistry, 1999, 'Reproduced with kind permission from Princeton University Press, New Jersey, United States')

Where, P_{O_3} is the maximum ozone production, P_{HO_x} is the production rate of HO_x (OH + HO_2) radicals, [NO] is the concentration of NO. In a VOC limited regime (where NO_x OH reactivity exceeds the VOC OH Reactivity), [R14] acts as the chain termination reaction and the maximum ozone production is given by (Jacob., 1999),

$$P_{O_3} = 2k_{(RH+OH)} \frac{P_{HO_x}}{k_{(OH+NO_2+M)}} \frac{[RH]}{[NO_2][M]} \tag{1.4}$$

Where, [RH], [NO_2] and [M] are the concentrations of VOCs, NO_2 and the reaction partner (N_2 or O_2). It is clear from Equation (1.4) that in a VOC limited regime, maximum ozone production has a linear dependence on VOC concentrations (i.e., [RH]) and inverse dependence on NO_x. Therefore in a VOC limited regime, reduction of NO_x can lead to increased O_3 production.

The ability of VOCs to form secondary organic aerosol (SOA) in the troposphere which has direct climatic impacts as a radiative forcing agent of the atmosphere (IPCC, 2013), is also very important.

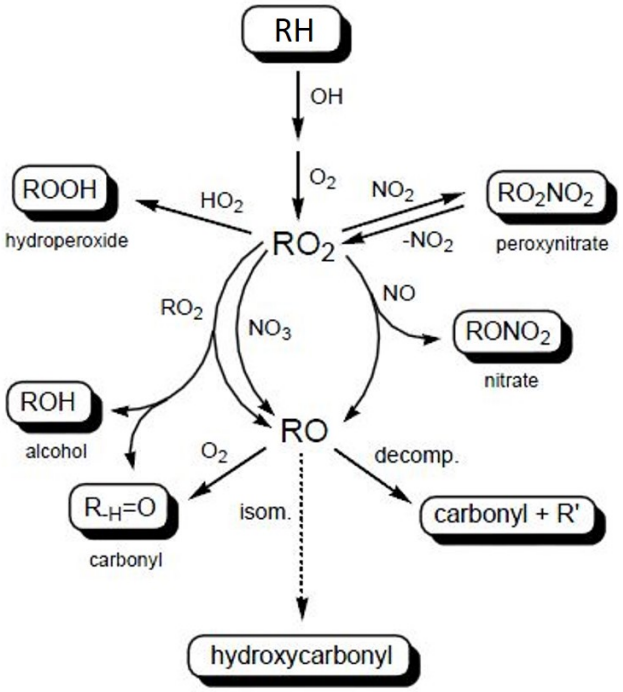

Figure 1.4: Schematic of first generation product formation from VOCs (Source: Hallquist et al. (2009))

Globally, anthropogenic SOA contributes 27 TgC y^{-1} that includes 17 TgC y^{-1} SOA from biomass burning whereas biogenic SOA contributes 88 TgC y^{-1} (Hallquist et al., 2009). Initial oxidation of VOCs with OH radical leads to the formation of a set of first generation products containing at least one oxygenated functional group such as aldehyde (-C(=O)H), ketone (-C(=O)-), alcohol (-OH), carboxylic acid (-C(=O)OH), hydroperoxide (-OOH), nitrate ($-ONO_2$), peroxyacyl nitrate ($-C(=O)OONO_2$) and percarboxylic acid (-C(=O)OOH) groups. All these first generation products are less volatile and more water soluble. Figure 1.4 shows a general schematic for the formation of these first generation products from VOCs in the troposphere. Oxidation of these first generation products further can form second generation products with even lower volatility and higher solubility. These second generation products contribute to secondary organic aerosol (SOA). Ozonolysis of terpenes (α-pinene, β-pinene) can also form SOA in the troposphere (Presto et al., 2005; Iinuma et al., 2013). The SOA yield always depends on the available NO_x concentrations. Recently, several studies on terpene ozonolysis, isoprene oxidation and photooxidation of benzene, toluene and m-xylene have reported that SOA yields for all

these compounds are highest at lower NO_x concentrations (Presto et al., 2005; Kroll et al., 2006; Ng et al., 2007). However, for some of the higher molecular weight sesquiterpenes such as longifolene and aromadendrene a reverse dependence was observed i.e., maximum SOA yield at higher NO_x concentrations (Ng et al., 2007a).

1.4 Status of VOC research in South Asia

The specific role of ambient Volatile Organic Compounds (VOCs) in South Asia is poorly understood due to lack of in-situ ambient data, large emission uncertainties, and inadequate understanding of their chemical transformations. Several studies have been carried out to understand emissions and chemistry of air pollutant trace gases (CO, SO_2, O_3, NO_x) and particulate matter (PM_{10}, $PM_{2.5}$) in this region (Kulshrestha et al., 1997; Lal et al., 2000; Gadi et al., 2003; Ahammed et al., 2006; Ghude et al., 2008; Lal et al., 2008; Gaur et al., 2014; Pudasainee et al., 2006; Panday et al., 2009; Sharma et al., 2012; Gurung and Bell., 2012). However, only few studies on VOC measurements have been reported in the literature from India and Nepal.

A study by Srivastava. (2005) reported variability of benzene-toluene-ethylbenzene-xylene (BTEX) and chlorobenzene concentrations in Delhi during 2001. Another study (Srivastava et al., 2005) reported a comparison of BTEX and chlorobenzene concentrations in residential areas, commercial areas, industrial areas, traffic intersections and petrol pumps in Delhi during 2001. A similar study was carried out in Mumbai during 2001-2002 by Srivastava et al. (2006). A comparison of the emissions from refueling stations in Delhi and Mumbai reported very high BTEX concentrations (50-800 μg m^{-3}) (Srivastava et al., 2005). An indoor air quality study in Mumbai showed that benzene concentrations were always above the National Ambient Air Quality Standards guidelines (NAAQS; annual average < 5 μg m^{-3}) at nine different indoor locations (Srivastava and Devotta., 2007). Source apportionment studies based on these offline measurements using chemical mass balance (CMB) model were also carried out for Delhi and Mumbai (Srivastava., 2004; Srivastava et al., 2005) which reported vehicular exhaust and evaporative emissions to be the major contributors to BTEX. A previous study also reported emissions of BTEX, alkanes (ethane, propane, i-butane, n-butane, i-pentane, n-pentane, n-hexane, n-heptane

and n-decane), alkenes (ethylene, acetylene and propylene) and other hydrocarbons from an industrial area in Mumbai (Mohan Rao et al., 1997). Mixing ratios of fifteen carbonyl compounds and BTEX compounds were reported from Kolkata during the summer of 2006 and associated health risks for these compounds were discussed (Dutta et al., 2009). Another recent study from Kolkata estimated the consequences of BTEX emissions on human health in terms of non-cancer and cancer risk due to inhalation exposure (Majumdar et al., 2011). A study on non-methane hydrocarbons (C_2-C_5 NMHCs) was carried out in Ahmedabad during 2002 by Sahu and Lal. (2006). Recently, Lal et al. (2012) reported light NMHCs (C_2-C_5) measurements from Kanpur and Hissar in the Indo-Gangetic Plain (IGP) during December, 2004.

With regard to quantification of volatile organic compounds in the Kathmandu Valley in Nepal, only two previous studies were reported. Sharma et al. (2000) reported measurements of light NMHCs (C_2-C_6) in downtown Kathmandu and a rural site in Nagarkot in November 1998 using thirty-eight whole air samples analyzed offline with a Gas Chromatography-Flame Ionization Detector (GC-FID). Measurements of seven monocyclic aromatic hydrocarbons were reported by Yu et al. (2008) at a suburban site in Kathmandu during January-February, 2003 using long path differential optical absorption spectroscopy (DOAS). Recent studies from our group have reported VOCs using PTRMS technique (Sinha et al., 2014; Sarkar et al., 2013, 2016; Kumar et al., 2016; Chandra and Sinha, 2016). Large scale studies need to include VOC speciation as an integral component of the experimental design and have rarely been done so till date.

1.5 Research motivation and thesis outline

From the preceding discussion, it is clear that very little data and information is currently available to understand the emissions and chemistry of VOCs in South Asia. Until 2011, there had been no deployment of high time and mass resolution techniques such as proton transfer reaction mass spectrometry in South Asia. Figure 1.5 shows sites in the world where VOC speciation studies using the PTR-MS technique (as red circles) had been carried out until 2011. It can be noted that no study was performed in the South Asian region (the red square) before 2011. The closest study using the PTR-MS technique was

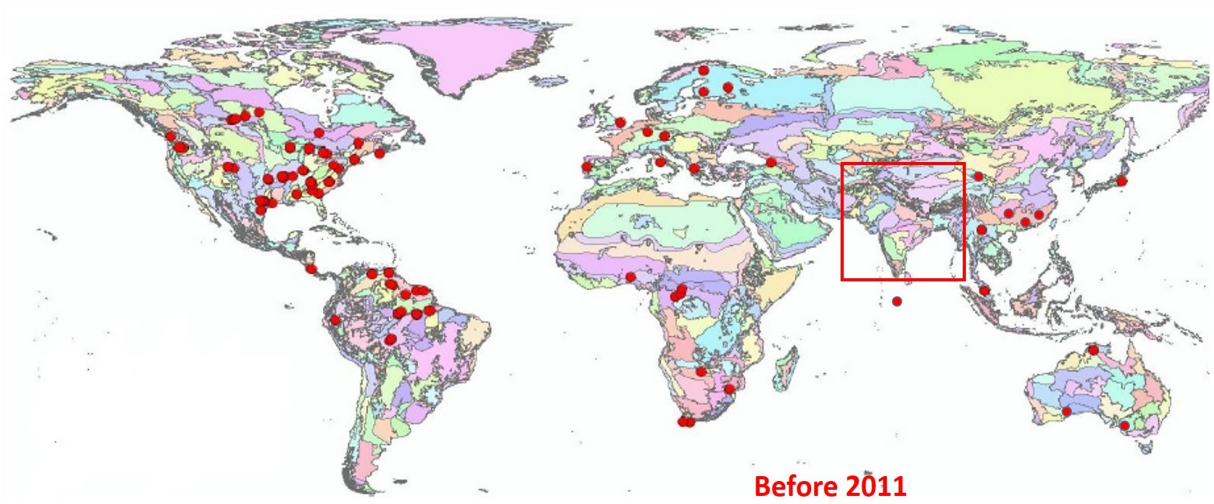

Figure 1.5: World map showing previous VOC speciation studies including PTR-MS technique (Figure adapted from: Guenther et al. (2006)). Red square shows no study performed in South Asia before 2011

performed during the INDOEX campaign over the Indian Ocean (Lelieveld et al., 2001; Sprung et al., 2001).

The main motivation of this thesis work was to deploy Proton Transfer Reaction Mass Spectrometry (PTR-MS) for elucidating the speciation, emissions and chemistry of VOCs at two South Asian sites - Mohali (India) and Kathmandu (Nepal). Analytical details and advantages of the PTR-MS technique over other offline methods of VOC measurements are discussed in Chapter 2 of this thesis. This thesis then focuses on the following five scientific questions:

1. What is the chemical composition and speciation of VOCs in ambient fire plumes influenced by post-harvest paddy straw fires in the north-west Indo Gangetic Plain (IGP)?

2. What is the time and mass resolved chemical speciation of VOCs in the Kathmandu Valley in winter as observed in the PTR-TOF-MS mass scans?

3. How do the VOCs present in ambient Kathmandu air individually and collectively affect the ozone formation chemistry and air quality?

4. What are the quantitative contributions of specific emission sources (e.g., traffic, biomass co-fired brick kilns) to ambient concentrations of individual VOCs and the ozone production potential?

5. What should be the mitigation strategy for the improvement of air quality in the Kathmandu Valley based on the in-situ observations?

The first question is addressed in Chapter 3 of this thesis wherein implications of the paddy straw fire emissions for formation of tropospheric ozone, secondary organic aerosol and human health are also discussed. The second and third questions are addressed in Chapter 4 which analyzes VOC speciation in ambient air of the Kathmandu Valley in winter. Several new findings, in particular the first experimental evidence in ambient air for the formation of isocyanic acid from precursor compounds such as acetamide and formamide, which were observed for the first time in ambient air worldwide, are reported. The relative contributions of major VOCs involved in ozone formation are also discussed. The final chapter (Chapter 5) of this thesis describes the application of a Positive Matrix Factorization (PMF) model on the observed ambient dataset for source apportionment of VOCs in the Kathmandu Valley during winter. The model is able to explain much of the observed VOC variability providing source apportionment of the major VOC emission sources. Overall, the thesis work has provided significant advancement of global scientific understanding regarding VOC emissions and chemistry in Kathmandu and Mohali, and revealed the unique chemical complexity of air over the South Asian region.

Chapter 2

Quantifying ambient VOCs present at concentrations of few ppt-ppb: Analytical considerations and challenges

Ambient air represents a challenging chemical matrix for quantifying VOCs. The matrix varies in chemical composition by day and night in response to emissions and meteorological changes and the low concentration range of VOCs (typically ppt-ppb range) implies even small interferences from more abundant atmospheric constituents can compromise the detection of VOCs. In particular the presence of water vapour and gases such as ozone, carbon dioxide, methane and oxygen can lead to complex analytical challenges.
Gas chromatography (GC) based techniques are the most widely employed analytical technique used for VOC measurements in the atmosphere. Due to the low concentrations (few ppt-ppb) involved, air samples collected in canisters/adsorbents require preconcentration. At present, variants of gas chromatographic techniques can measure a suite of VOCs at concentrations as low as 0.1 ppt (parts-per-trillion) (Xu et al., 2003; Christian et al., 2004; Jones et al., 2014). Also other major advantages of using GC-based methods are its lower cost and ease in handling. Despite these advantages, issues that arise during collection, storage and pre-concentration steps can lead to several measurement artefacts.

In particular, several oxygenated VOCs such as acetaldehyde, methanol and acetone and short-lived reactive VOCs cannot be reliably quantified using most conventional offline gas chromatographic methods as not all VOCs are quantitatively retained in canisters in which samples are collected. Moreover, the disadvantage for ambient emission activity related studies, using these GC based methods is the sub-optimal temporal resolution of the measurements (typically hourly). In the past several decades, various new spectroscopic methods have also emerged for quantifying specific VOCs (Paton-Walsh et al., 2014; Platt and Stutz., 2008), but remain limited in scope for VOC measurements in ambient air. In such a context, highly mass and time resolved mass spectrometric methods (such as proton transfer reaction mass spectrometry) are better suited and have provided new insights in ambient air VOC studies in the past decade (de Gouw and Warneke., 2007; Blake et al., 2009). These permit real time quantification in a rapidly changing atmosphere so that accurate and specific emission activity information can be discerned by careful analysis of the measurements.

In this chapter, the mass spectrometry technique (specifically proton transfer reaction mass spectrometry) used for quantification of ambient VOCs during my thesis work has been discussed in detail. For completeness and comparison, I have also described the principle behind offline gas chromatographic (GC) methods of VOC quantification, so that an overview of advantages and disadvantages intrinsic to both techniques can be discerned.

2.1 Gas Chromatography

Gas chromatography (GC) is a well-established method to separate and identify compounds from a mixture. The basic principle of GC involves solvation of a mixture in a highly diffused gas (the mobile phase), which carries the analytes through the separation system. Interactions between the mobile phase and an immiscible bed of material (the stationary phase) then determine how fast the analyte will move through the bed. Interaction (or adsorption) of analytes with the stationary phase results in separation of the analyte molecules. For appreciable gas phase and stationary phase interactions, the mobile phase must have a high diffusion coefficient. Nitrogen (N_2), hydrogen (H_2) and helium (He) are commonly used as the carrier gas (mobile phase) in gas chromatogra-

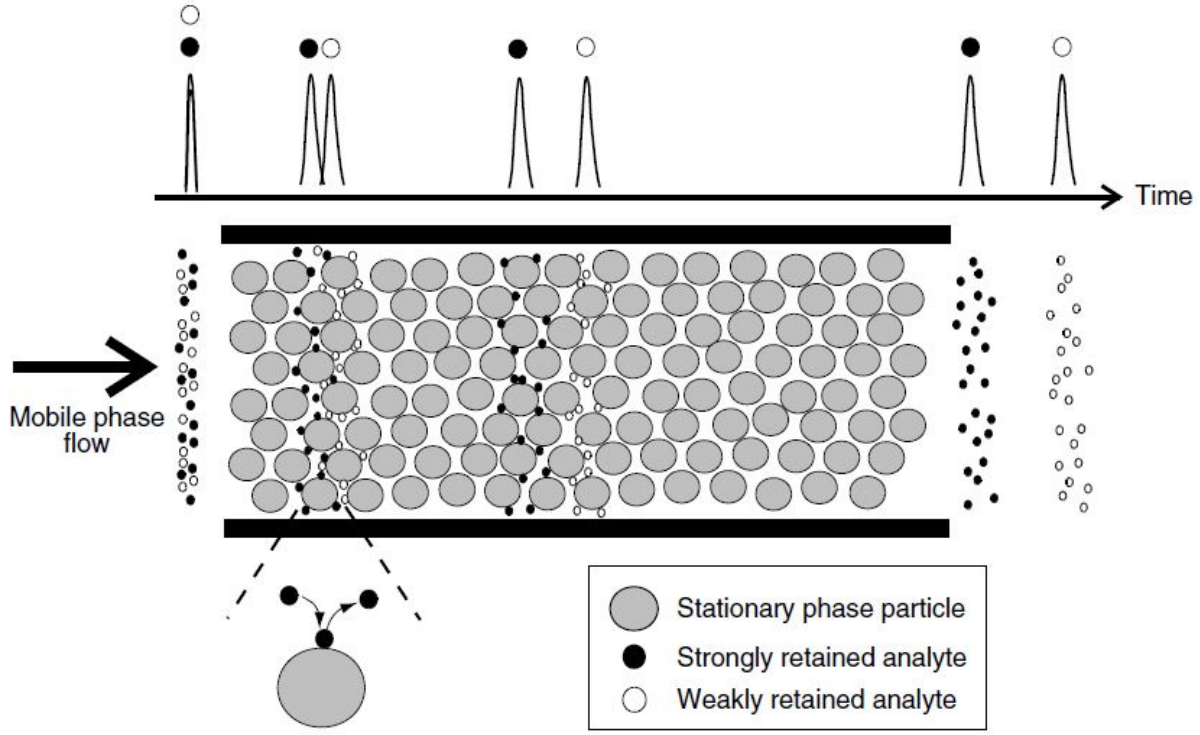

Figure 2.1: Schematic of chromatographic separation (Source: Dwayne E. Heard, Analytical Techniques for Atmospheric Measurement, 2006, 'Reproduced with kind permission from John Wiley & Sons Ltd., UK')

phy but helium is generally preferred over hydrogen as the use of hydrogen can lead to the formation of some in-column unstable species due to hydrogenation in some types of columns. Figure 2.1 illustrates how this separation occurs.

The time taken by a compound to be eluted from the column is termed as the retention time, and is used for the identification of analytes. Depending on the application, a variety of detectors (e.g., flame ionization detector (FID); electron capture detector (ECD); mass selective detector (MSD)) can be coupled to the gas chromatography column. Once the analyte band reaches the detector upon proper separation, it produces a Gaussian-shaped peak. The area under the peak is used to determine the concentration. In practice, ideal Gaussian peaks are not always obtained, causing larger measurement uncertainties. In practice, calibration with gaseous mixtures that contain known concentrations of compounds permit the sensitivities of gas chromatographic systems to be established which are then employed for quantification of the compounds present in the ambient air samples. A GC consists of mainly four parts - a) a highly pure and regulated carrier gas source with

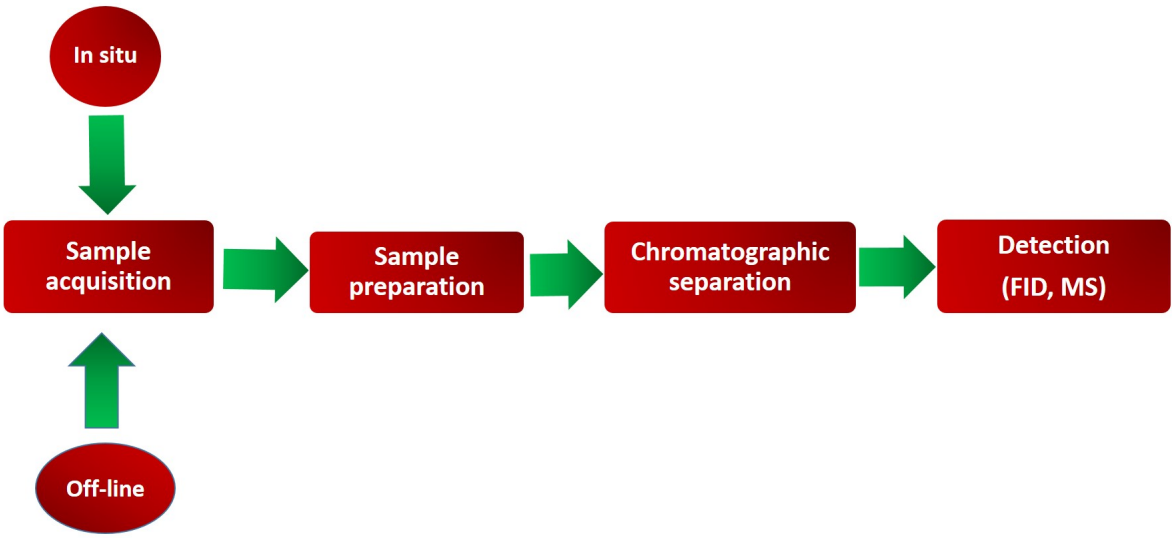

Figure 2.2: Flow diagram of a generic gas chromatography based system

traps for water, hydrocarbons and oxygen, b) an inlet which introduces vaporized sample to the carrier gas, c) a column where separation occurs and d) a detector. Generally, injection ports and sampling valves are used as an inlet. Separation in the column of GC is highly temperature dependent and therefore it is placed in a well-regulated oven. The detector generates a stable electrical signal for pure carrier gas which is considered as the baseline. Hence the purity of gases is essential for accurate quantification as contamination can preclude good peak separation due to "meandering" baselines. Figure 2.2 shows the flow diagram of a typical chromatographic system.

2.1.1 Sample acquisition

The sample acquisition process is the first step in any GC analysis. Stainless steel canisters of 1-10 L volume are generally used for the collection of whole air samples. Glass flasks made of borosilicate glass can also be used after proper conditioning for sample collection and storage (Pollmann et al., 2008). Samples are filled in the canisters by vacuum release or by pressurizing the sample using Teflon diaphragm pumps. To minimize the interaction with canister walls and to retain sample integrity, coating methods such as electropolishing, silica or Teflon coating are used in the canisters. Stable molecules such

as methane, carbon monoxide can be stored easily in the canisters while less volatile compounds create problems due to analyte condensation in the canister walls. To avoid this condensation problem, solid phase adsorbents are used as an alternative sample acquisition method. Adsorbents possess strong retention characteristics (surface area > 1000 m^3 g^{-1}) when carbon-based (e.g., charcoal) or with low surface area (< 50 m^3 g^{-1}) when based on Tenax TA (2, 6-diphenylene oxide) polymers. Samples can be introduced either dynamically (typically in minutes) or via diffusional sampling (typically over several days) in the adsorbent tubes. Carbon-based adsorbents are generally appropriate for volatile hydrocarbons, chlorofluorocarbons (CFCs) and organic nitrates whereas polymeric adsorbents are used for less volatile species such as aromatics and monoterpenes. However, the analysis of atmospheric oxygenated compounds is challenging using these methods due to irreversible retention on the adsorbents which causes loss to canister walls and strong influence of even trace amounts of moisture.

2.1.2 Sample preparation

Presence of water in atmospheric samples can cause large changes in the stationary phase affinity of columns. Water is typically removed from the sample using condensation traps or stripping coils. Inorganic adsorbents such as potassium carbonate (K_2CO_3) and magnesium perchlorate ($Mg(ClO_4)_2$) can also be used to remove water. Permeation membranes such as Nafion (tetrafluoroethylene-perfluoro-3, 6-dioxa-4-methyl-7-octenesulfonic acid copolymer) are also used for continuous drying of samples. However, this type of drier is not suitable for the quantification of polar compounds. Table 2.1 lists different types of adsorbents and their volatility range.

2.1.3 Sample separation

Separation of atmospheric samples by GC can be done using either packed columns or capillary columns. In packed columns, finely divided inert materials are used as coating in the stationary phase to minimize its thickness and maximize the area. The coated material is packed in a metal, glass or plastic tube with an outside diameter of 1/8 to

Table 2.1: Common adsorbents used in GC and their respective volatility range

Adsorbent	Volatility range
Molecular sieve (13X and 5$\mathring{A}$)	1,3 butadiene (13X), nitrous oxide (5$\mathring{A}$)
Carbosieve SIII	C_2 - C_5
Carboxen 1003	C_2 - C_5
SulfiCarb	C_3 - C_8
Carbograph 5TD	$C_{3/4}$ - $C_{6/7}$
Carbograph 1TD	$C_{5/6}$ - C_{14}
Carbograph 2TD	C_8 - C_{20}
Tenax TA	C_7 - C_{30}
Quartz wool/Silica beads	C_{30} - C_{40}

1/4 inch. Generally this type of column is used in the analysis of methane, CO_2 and N_2O. Capillary columns are suitable for separation of less volatile compounds. In capillary columns, the stationary phase is coated in the inner surface of an open tube with inner diameter of 0.1-0.5 mm and typical column length of 30 m. The major advantage of capillary columns is that they produce very narrow peaks. Capillary columns can be of two types - porous layer open tubular (PLOT) columns and wall-coated open tubular (WCOT) columns. PLOT columns are used for highly volatile non-methane hydrocarbons in the carbon atom range of C_1-C_7. PLOT consists of a thin porous layer of finely divided solid (Al_2O_3 doped with KCl or Na_2SO_4) coated on the walls of the tube. Rapid separations in the column occur via adsorption instead of phase transition. More than 100000 sites are typically available for adsorption in the column. PLOT type columns are unfavorable for the separation of polar oxygenated compounds as strong retention can occur for these species. This type of column can also lead to peak broadening for the species with high boiling points for the same reason. So, for the analysis of higher molecular weight species namely mono-aromatics, VOCs, CFCs, HCFCs and monoterpenes, WCOT columns are used. In WCOT, a viscous liquid namely methylpolysiloxane (non-polar) or phenyl-methylpolysiloxane (slightly polar) is used as the stationary phase. Columns are generally 50 m long with film thickness of 1-5 μm. To reduce the peak broadening, a temperature gradient is also used in WCOT. It is a well-established method for the analysis of semi-volatile and C_5-C_{12} species.

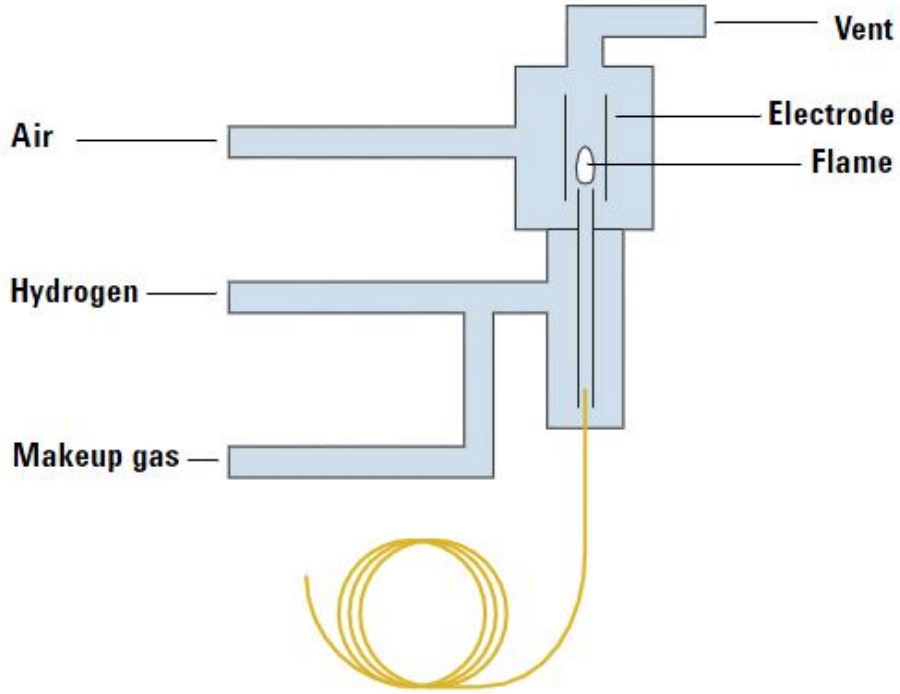

Figure 2.3: Schematic of a flame ionization detector (FID) (Source: Agilent Technologies, Santa Clara, California, USA)

2.1.4 Detection

Flame ionization detector (FID) is generally used in GC due to its high sensitivity, wide linearity and long-term reliability. For a sample volume of 1 L, the detection limit of FID can be in ppt (10-12) range. In the FID, very few ionized particles are produced from an air/hydrogen flame. Production of ions increase in presence of carbon-based materials. In the FID, mixing of carrier gas with hydrogen occurs first and then it is burnt in the air. Two electrodes are used in FID, one of which is placed near the flame. Also a polarizing voltage is used to collect ions from the flame. FID responds to anything that appears in the flame and creates ions. The current collected in the FID increases whenever a component appears in the flame and a chromatogram is created after amplification of the collected current.

In my thesis I wanted to undertake VOC speciation in ambient air and from point sources in real time in order to relate it to in-situ emission and meteorological changes. For such studies the slower temporal resolution of the GC based techniques would have been

less desirable. Although the GC based methods have an advantage in the speciation of isomers such as monoterpenes, in order to overcome the major limitations (e.g., detection of oxygenated VOCs) intrinsic to most GC based methods, I opted for the highly mass and time resolved analytical technique of proton transfer reaction mass spectrometry (PTR-MS) using which VOC speciation for a large number of emission tracer molecules (e.g., acetonitrile), reactive compounds (e.g., acetaldehyde) and toxic compounds (e.g., benzene) can be performed at detection limits of few ppt within few seconds.

2.2 Proton Transfer Reaction Mass Spectrometry (PTR-MS)

Proton transfer reaction mass spectrometry (PTR-MS) overcomes some of the disadvantages of gas chromatography (GC) based analytical technique. This technique was pioneered and popularized by Professor Werner Lindinger and co-workers at the University of Innsbruck in Austria and was introduced in mid 1990s for atmospheric VOC measurements (Hansel et al., 1995; Lindinger et al., 1998). The development of this technique was made possible by improving the existing selected ion flow tube mass spectrometry (SIFT-MS) method through introduction of a hollow cathode discharge source to generate highly pure ($> 95\%$) reagent hydronium ion (H_3O^+) and a short length drift tube. Introduction of a drift tube in place of the flow tube reduced the formation of hydrated hydronium ions [$H_3O^+(H_2O)$] and other cluster ions due to substantial ion-molecule collisions. Proton transfer reaction mass spectrometry is a soft chemical ionization (CI) mass spectrometric technique wherein analyte VOC molecules with a proton affinity (P.A.) greater than that of water vapour (165.2 kcal mol^{-1}) undergo chemical ionization with the reagent hydronium ions (H_3O^+) and form protonated molecular ions (with m/z = molecular ion + 1), permitting detection of VOCs. The reaction of VOCs (represented as R) with H_3O^+ can be expressed as,

$$R^{\cdot} + H_3O^+ \longrightarrow RH^+ + H_2O \qquad \text{[R15]}$$

Table 2.2: Proton affinities of different species present in the atmosphere (from proton affinity list provided by Ionicon Analytik GmbH, Innsbruck, Austria)

Classification	Molecule	Proton Affinity (kcal mol^{-1})
Inorganic gases	O_2	100.6
	N_2	118.0
	CO_2	129.2
	H_2O	165.2
Alkanes	Methane	129.9
	Ethane	142.5
	Propane	150.5
Alkenes	Ethylene	162.6
	Propene	179.6
Alkynes	Acetylene	153.3
	Propyne	178.8
Aromatics	Benzene	179.3
	Toluene	187.4
	p-Xylene	190.0
	Phenol	195.0
Oxygenated compounds	Formaldehyde	170.4
	Methanol	180.3
	Ethanol	185.6
	Acetaldehyde	183.8
	Acetone	194.1
Acids and Nitriles	Formic acid	177.3
	Acetic acid	186.9
	Acetonitrile	186.2
	Propanenitrile	189.8
Amides	Formamide	196.5
	Acetamide	206.5

As major atmospheric gases such as nitrogen, oxygen, carbon dioxide and methane have proton affinities lower than water vapour, they do not cause interferences in the detection of the trace level VOCs. Table 2.2 lists a number of atmospheric trace gases along with their respective proton affinities.

The PTR-MS instrument consists of four main units - 1) an ion source where production of highly pure ($> 95\%$) reagent hydronium ions (H_3O^+) occurs, 2) a drift tube reactor where non-dissociative (typically) H^+ transfer from H_3O^+ to analyte VOCs occurs, 3) a mass analyzer that separates ions based on their m/z ratio, which can be a quadrupole or time of flight analyzer and 4) a detector.

Detailed descriptions of each component are provided below:

2.2.1 Ion source

The ion source consists of two parts - in the first part vapour of ultrapure water undergoes plasma discharge in a hollow cathode chamber leading to the following reactions,

$$e^- + H_2O \longrightarrow H_2O^{\cdot +} + 2\,e^- \quad \text{[R16]}$$

$$e^- + H_2O \longrightarrow H_2^+ + 2\,e^- + O^{\cdot} \quad \text{[R17]}$$

$$e^- + H_2O \longrightarrow H_2 + O^+ + 2\,e^- \quad \text{[R18]}$$

$$e^- + H_2O \longrightarrow H^+ + OH^{\cdot} + 2\,e^- \quad \text{[R19]}$$

The ions produced by these reactions together with the water vapour then enter into a second chamber where ion molecule reactions occur,

$$O^+ + H_2O \longrightarrow H_2O^{\cdot +} + O^{\cdot} \quad \text{[R20]}$$

$$H_2^+ + H_2O \longrightarrow H_2O^{\cdot +} + H_2 \quad \text{[R21]}$$

$$H^+ + H_2O \longrightarrow H_2O^{\cdot +} + H^{\cdot} \quad \text{[R22]}$$

Finally, this $H_2O^{\cdot +}$ reacts with water vapour to produce hydronium ions (H_3O^+) that act as reagent ions in the PTR-MS,

$$H_2O^{\cdot +} + H_2O \longrightarrow H_3O^+ + OH^{\cdot} \quad \text{[R23]}$$

Optimization of the ion source is needed to keep its efficiency high as coating effects can decrease the efficiency. For the PTR-MS systems used in this thesis work, voltages were set to 80-120 V for the first chamber and 60-100 V for the second chamber of the ion

source. Also a water flow of 3-5 sccm was used.

2.2.2 Drift tube

The ionization process of VOCs occur in the drift tube according to reaction R1. From the ion source H_3O^+ ions enter the drift tube via a Venturi-type inlet and due to an applied electric drift field these H_3O^+ ions move towards the detection part of the drift tube undergoing collisions with the analyte VOCs along the way. Proton transfer reactions take place due collision with VOCs that possess a proton affinity greater than that of water vapour. The ionization process in proton transfer reaction is associated with energy transfers of 0-2 eV. For a single VOC (R) reacting with the hydronium ions, it can be shown that the protonated VOC ions ($[RH^+]$) can be expressed as follows (de Gouw and Warneke., 2007),

$$[RH^+] = [H_3O^+]_0(1 - e^{-k[R]t}) \tag{2.1}$$

Where, k is the rate coefficient for the proton transfer reaction (typical value $\geq 10^{-9}$ cm^3 s^{-1}), t is the reaction time and, $[H_3O^+]_0$ is the concentration of reagent ions injected from the ion source and [R] is the concentration of the VOC. It is assumed that the only loss of reagent ions occurs through proton transfer reactions with VOCs. As only a small fraction of H_3O^+ ions react in the drift tube under typical instrumental conditions, equation 2.1 can be reasonably approximated as,

$$[RH^+] = [H_3O^+]_0[R]kt \tag{2.2}$$

This above expression is valid unless $[RH^+]$ becomes very high (> 10 ppm). Signals proportional to $[RH^+]$ and $[H_3O^+]$ are measured by the detection system and re-arrangement of equation 2.2 provides the number density of VOC injected inside the drift tube according to,

$$[R] = \frac{[RH^+]}{kt[H_3O^+]} \tag{2.3}$$

The number density of [R] is then converted to a mixing ratio using drift tube pressure and temperature and this mixing ratio is typically expressed in parts-per-billion by volume (ppbv). The conversion of number density to mixing ratio can be illustrated with an

example. If the number density of methanol is 2.69 $\times$ 10^{17} molecules m^{-3} then the mixing ratio of methanol ($C_{methanol}$) can be expressed as,

$$C_{methanol} = \frac{n_{methanol}}{n_{air}} \tag{2.4}$$

Where $n_{methanol}$ and n_{air} are the number densities of methanol and air, respectively. Now the number density of air (n_{air}) can be obtained from,

$$n_{air} = \frac{A_v P}{RT} \tag{2.5}$$

Where, A_v is the Avogadro's number (6.023 $\times$ 10^{23} molecules mol^{-1}), R is the universal gas constant, P and T are the air pressure and temperature. At standard temperature and pressure (STP; 273.15 K and 1013 hPa) the n_{air} will be 2.69 $\times$ 10^{25} molecules m^{-3}. Therefore at STP, the mixing ratio of methanol will be,

$$C_{methanol} = \frac{2.69 \times 10^{17} \ \text{mol}}{2.69 \times 10^{25} \ \text{mol}} = 10^{-8} \ \text{mol/mol} = 10 \ \text{nmol/mol} = 10 \ \text{ppb} \tag{2.6}$$

Analyte VOC molecules can form cluster ions in the drift tube apart from the desired product ion (RH^+), which can complicate the interpretation of mass spectra.

$$RH^+ + nH_2O \longleftrightarrow RH^+(H_2O)_n \qquad \text{[R24]}$$

This can be reduced by applying a strong electric field on drift tube which enhances the kinetic energy of the reagent ions. If an electric field E is applied over the length of the drift tube, the average drift velocity of the ions will be,

$$v_d = \mu \times E \tag{2.7}$$

Where μ is the ion mobility. This ion mobility is generally expressed in terms of the reduced mobility (μ_0),

$$\mu_0 = \frac{p}{p_0} \times \frac{T_0}{T} \times \mu = \frac{N}{N_0} \times \mu \tag{2.8}$$

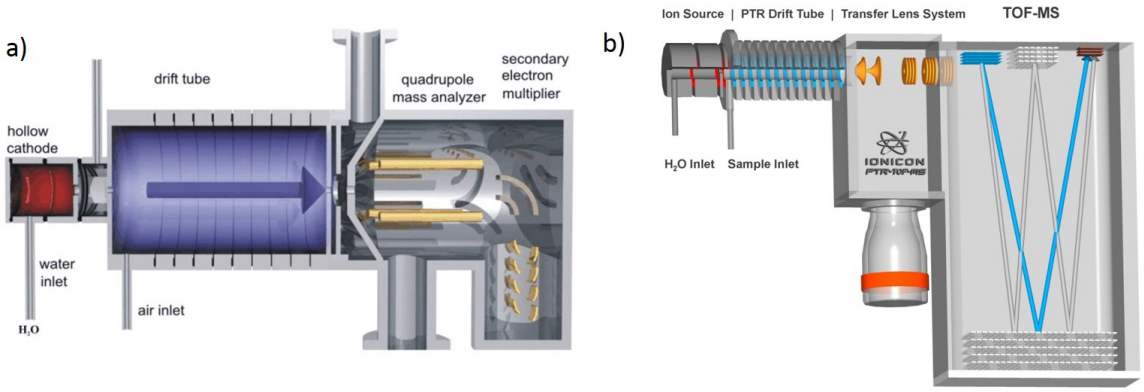

Figure 2.4: Schematic of a) PTR-Q-MS (Figure adapted from M. Schwarzmann, 2001) and b) PTR-TOF-MS (Source: Ionicon analytik GmbH, Innsbruck, Austria)

Where, T, p and N are the temperature, pressure and number density in the drift tube, respectively. N_0 is the number density at standard temperature (T_0 = 273.15 K) and pressure (p_0 = 1 atm). Substituting μ in equation 2.8 gives,

$$v_d = (\mu_0 N_0) \times (\frac{E}{N}) \tag{2.9}$$

Thus drift velocity is a function of E/N ratio which is expressed in Townsend unit (1 Td = 10^{-17} V cm^2). High E/N ratios reduce ion clustering within the drift tube but may cause fragmentation. In addition to the drift velocity the transmission efficiency of individual VOCs through the mass analyzer also needs to be taken into account, as do minor losses within the drift tube. Hence for achieving better accuracy, calibration experiment derived sensitivity factors (expressed in normalized ion counts per ppb of VOC; Sinha et al. (2014)) are preferred for VOC quantification.

2.2.3 Mass analyzers

In the PTR-MS technique, two types of mass analyzers have been employed till date - 1) a quadrupole (Q) mass analyzer and 2) a time-of-flight (TOF) mass analyzer. Figure 2.4 represents the schematic of both PTR-Q-MS and PTR-TOF-MS.

A quadrupole mass analyzer consists of four parallel cylindrical metal rods typically of 10-20 mm radius and 20 cm length. Among these four rods, two opposite rods are positively charged and other two are negatively charged. Ions entering the quadrupole region

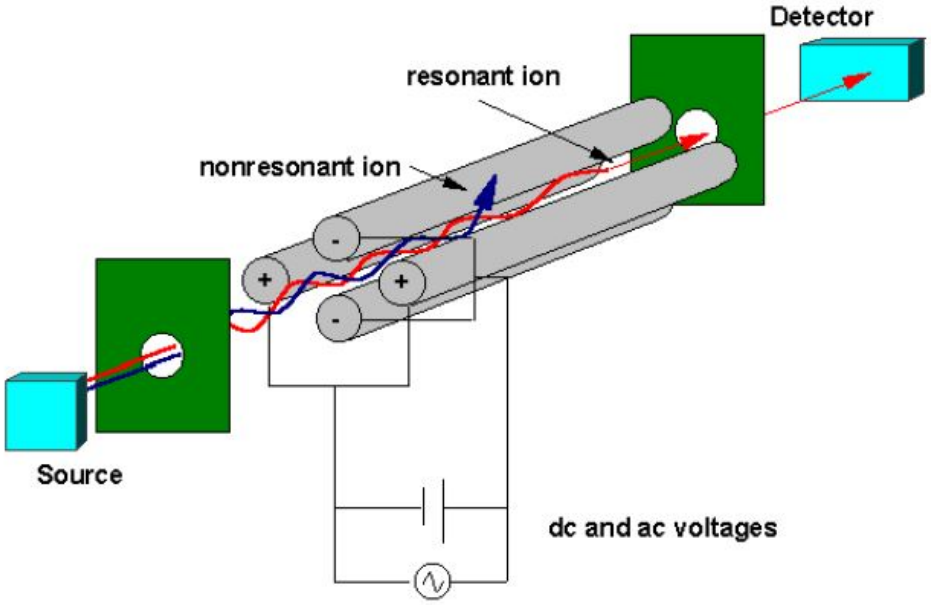

Figure 2.5: Schematic of a quadrupole mass analyzer (Source: Ionicon analytik GmbH, Innsbruck, Austria)

are subjected to a DC voltage and a high frequency AC voltage applied to the four rods and only one ion is transmitted at a time as the other ions do not have a stable trajectory. Figure 2.5 presents a schematic of the quadrupole.

Depending on the applied voltages and frequency, ions with a specific m/z ratio are transmitted through the quadrupole. This is shown using the equation of motion (Matthieu equation). Ions travelling along the z-axis are influenced by the total electric field originating from the applied potentials on the rods:

$$\phi_0 = +(U - cos\omega t) \quad \text{and} \quad -\phi_0 = -(U - cos\omega t) \tag{2.10}$$

Where, ϕ_0 is the potential applied to the rods, ω is the angular frequency ($= 2\pi\nu$, ν is the RF field frequency), U is direct potential (varies between 500 to 2000 V) and V is zero-to-peak amplitude of RF voltage (varies between 0 to 3000 V). Figure 2.6 shows different components of applied potentials in the quadrupole.

When ions are accelerated along the z axis between the quadrupole rods, they also have

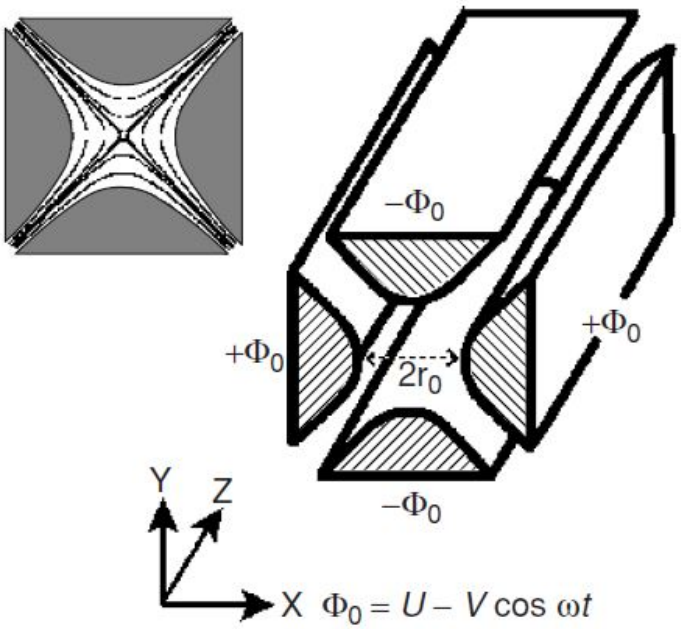

Figure 2.6: Contribution of components of applied potential for different directions (x, y and z- axis) in a quadrupole (Source: Hoffmann and Stroobant, Mass Spectrometry Principles and Applications, 2007, 'Reproduced with kind permission from John Wiley & Sons Ltd., UK')

acceleration components along x and y axis due to the forces induced by the electric fields:

$$F_x = m\frac{d^2x}{dt^2} = -ze\frac{\delta\phi}{\delta x} \quad \text{and} \quad F_y = m\frac{d^2y}{dt^2} = -ze\frac{\delta\phi}{\delta y} \tag{2.11}$$

Where, ϕ is a function of ϕ_0 and can be expressed as,

$$\phi_{x,y} = \frac{\phi_0(x^2 - y^2)}{r_0^2} = \frac{(U - Vcos\omega t)(x^2 - y^2)}{r_0^2} \tag{2.12}$$

Differentiation and rearrangement will give equations of motion (Paul equation):

$$\frac{d^2x}{dt^2} + \frac{2ze}{mr_0^2}(U - Vcos\omega t)x = 0 \quad \text{and} \quad \frac{d^2y}{dt^2} - \frac{2ze}{mr_0^2}(U - Vcos\omega t)y = 0 \tag{2.13}$$

An ion will have stable trajectory if it never hits the rods i.e., if x and y never becomes equal to r_0. To obtain the values of x and y, Matthieu differential equations are used

which can be represented as:

$$\frac{d^2u}{d\zeta^2} + (a_u - 2q_u cos2\zeta) = 0 \tag{2.14}$$

Where, $\zeta = \omega t/2$. Incorporating value of ζ in the above equation and solving it gives,

$$a_u = a_x = -a_y = \frac{8zeU}{m\omega^2 r_0^2} \quad \text{and} \quad q_u = q_x = -q_y = \frac{4zeV}{m\omega^2 r_0^2} \tag{2.15}$$

This equation shows that a relationship between the coordinates of ions and time can be established. For a quadrupole both r_0 and ω remains constant and U and V are varied. Therefore, x and y can be determined as a function U and V for a specific time span. Based on the stability areas of the ions along x and y axis, U and V can be expressed as,

$$U = a_u \frac{m}{z} \frac{\omega^2 r_0^2}{8e} \quad \text{and} \quad V = q_u \frac{m}{z} \frac{\omega^2 r_0^2}{4e} \tag{2.16}$$

The quadrupole mass analyzer has mass resolution of ∼1 amu over the whole mass range which is sufficient to separate two ions with different nominal masses. The response time of the quadrupole mass analyzer can be as low as 100 ms. The PTR-Q-MS can be operated in two different modes - a) multiple ion detection (MID) mode and b) scan mode. A dwell time of 200 ms is usually set for the primary ion while for the other masses dwell time > 200 ms is used depending on the expected concentration levels. In the scan mode, masses over specific mass range of the PTR-Q-MS can be chosen. As scan mode operates over the whole mass range, the time taken to finish a cycle of measurement is longer in duration relative to the MID mode. Operating the PTR-Q-MS in a mass scan mode permits possibilities for identifying new compounds.

Validation studies to assess the reliability of attributing VOCs to specific m/z ratios using the PTR-Q-MS have been carried out by inter comparing with other analytical techniques (e.g., GC-FID) and have been extensively reviewed in the literature (de Gouw and Warneke., 2007; Blake et al., 2009). The results of these studies showed that for PTR-Q-MS, VOCs such as methanol, acetonitrile, acetaldehyde, acetone, isoprene, benzene, toluene, sum of C8-aromatics and sum of C9-aromatics are the major contributors at m/z ratios 33, 42, 45, 59, 69, 79, 93, 107 and 121, respectively (de Gouw and Warneke.,

2007). Both acetone and propanal contribute to m/z = 59 but several studies have shown propanal contributes maximum up to 10%. Therefore, acetone is considered as the major contributor at m/z = 59. Detection of isoprene at m/z ratio 69 can have interference in the biomass burning plumes and urban areas due to presence of furan at the same nominal mass (Christian et al., 2004). Measurement of both benzene and toluene can have slight humidity dependence (Warneke et al., 2001). Two propylbenzene isomers and three trimethylbenzene isomers can contribute to m/z ratio of 121 which can also have very small interferences due to $C^{35}C^{37}Cl_2^+$ ions from CCl_4 (Śpanél and Smith., 1999). However this interference should be a constant offset as the variability of CCl_4 is extremely low in the atmosphere.

In the time of flight (TOF) mass analyzer, ions are first accelerated by applying an electric field and then the time taken by each ion to reach the detector is measured which can be attributed to specific m/z ratios of ions. TOF can be of two types - linear TOF (TOF) and reflectron TOF (RTOF or VTOF). Figure 2.7 shows a basic schematic of a linear time of flight analyzer (LTOF). In LTOF, ions are accelerated first towards a flight tube due to a potential difference between the extraction grid and an electrode. Then ions enter in a field-free region after leaving the acceleration region where separation of ions occur according to their velocities. After the separation, ions reach at the other edge of the flight tube near the detector. The time taken by ions to pass through the field free region between source and the detector is used to determine the mass-to-charge ratio.

If a potential V_s is applied to accelerate an ion with mass m and total charge q, then it's electric potential energy (E_{el}) can be expressed as,

$$E_{el} = qV_s = zeV_s \tag{2.17}$$

Now if this electric potential energy is converted to the kinetic energy (E_k) then,

$$E_k = \frac{1}{2}mv^2 = zeV_s = E_{el} \tag{2.18}$$

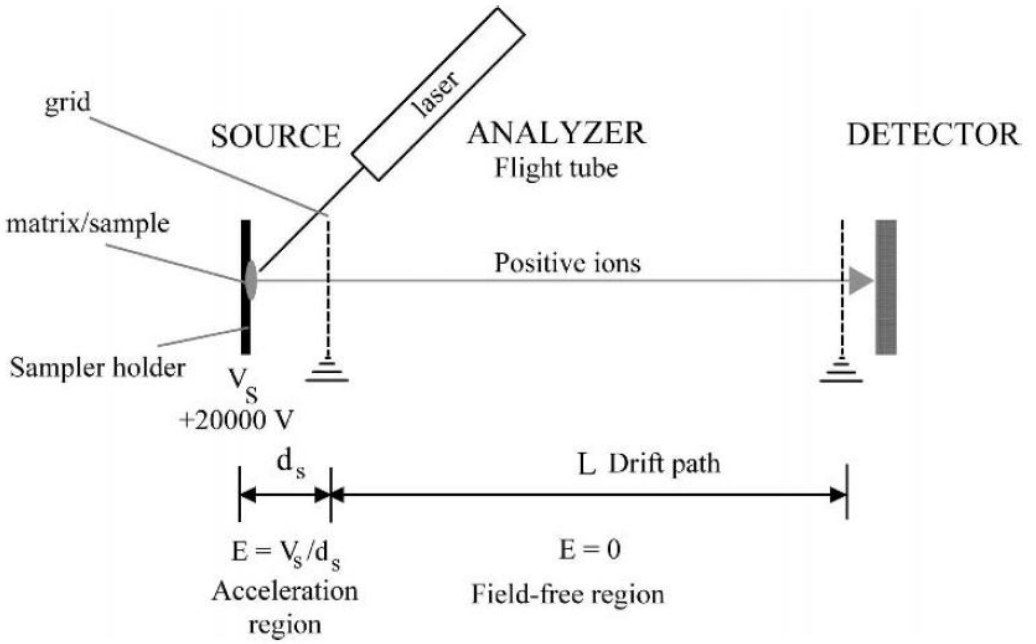

Figure 2.7: Schematic of a linear time-of-flight (LTOF) mass analyzer (Source: Hoffmann and Stroobant, Mass Spectrometry Principles and Applications, 2007, 'Reproduced with kind permission from John Wiley & Sons Ltd., UK')

Therefore the velocity of ion leaving the source can be expressed as,

$$v = (\frac{2zeV_s}{m})^{1/2} \tag{2.19}$$

Now if the ion has to travel a distance L then the time taken by the ion will be,

$$t = \frac{L}{v} \tag{2.20}$$

Putting value of v we get,

$$t^2 = \frac{m}{z}(\frac{L^2}{2eV_s}) \tag{2.21}$$

Therefore m/z can be calculated from measurement of t^2. Also it shows that ions with lower mass will reach the detector first.

In the reflectron TOF, an electrostatic reflector (also called as reflectron) is used to improve the mass resolution. This reflectron acts as an ion mirror by creating a retarding field and deflects the ions. After the deflection, ions are send back to the flight tube. The reflectron is placed opposite to the ion source behind the field free region. After reflection

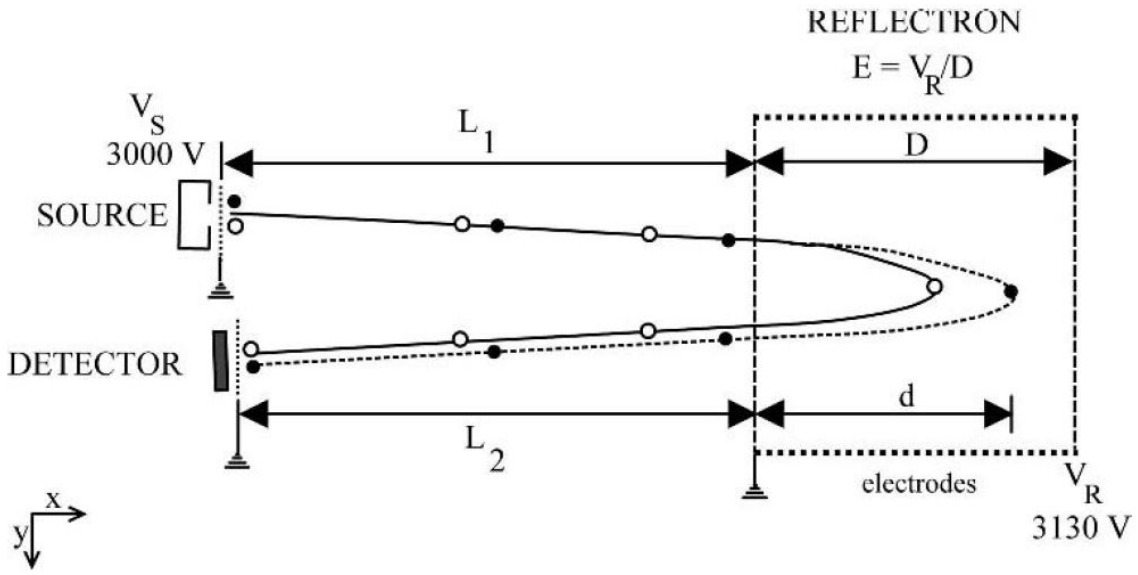

Figure 2.8: Schematic of a reflectron time-of-flight (RTOF) mass analyzer (Source: Hoffmann and Stroobant, Mass Spectrometry Principles and Applications, 2007, 'Reproduced with kind permission from John Wiley & Sons Ltd., UK')

of the ions at the reflectron they are captured by a detector positioned either off-axis or co-axially on the source side. The advantage of the reflectron is it corrects the kinetic energy dispersion for the ions with same m/z ratio. As a result, ions having more kinetic energy penetrates the reflectron more deeply as compared to the ions with less kinetic energy and therefore ions with more velocity (hence more velocity) will take more time to get out of the reflectron. Figure 2.8 shows a schematic of a reflectron TOF.
If V_R is the potential and D is the length of the reflectron, then the electric field in the reflectron will be,

$$E = \frac{V_R}{D} \tag{2.22}$$

Now if an ion with charge q and kinetic energy E_k having a velocity v_{ix} penetrates the reflectron to a depth d then,

$$d = \frac{E_k}{qE} = \frac{qV_s}{(qV_R/D)} = \frac{DV_s}{V_R} \tag{2.23}$$

The mean velocity in the reflectron will be $v_{ix}/2$ as the x component of the velocity (v_x) becomes equal to zero. Therefore the penetration time (t_0) at the distance d will be,

$$t_0 = \frac{d}{(v_{ix}/2)} \tag{2.24}$$

Now inside the reflectron, the total flight length is 2d and therefore total reflectron time (t_r) will be,

$$t_r = 2t_0 = \frac{2d}{v_{ix}/2} = \frac{4d}{v_{ix}} \tag{2.25}$$

If L_1 and L_2 are distances covered by the ions before and after the reflectron then, L_1+L_2 will be the flight length outside the reflectron and time taken to cover this distance will be,

$$t = \frac{L_1 + L_2}{v_{ix}} \tag{2.26}$$

So the total flight time taken by the ions will be,

$$t_{TOT} = t + t_r = \frac{L_1 + L_2 + 4d}{v_{ix}} \tag{2.27}$$

Substituting v_{ix} by $(2zeV_s/m)^{1/2}$ gives,

$$t_{TOT}^2 = \frac{m}{z}\frac{(L_1 + L_2 + 4d)^2}{2eV_s} \tag{2.28}$$

It can be seen from the above equation that m/z is related to total flight time.
The mass resolution (FWHM method) of a commercial PTR-TOF-MS sold by Ionicon Analytik is greater than 4000 amu. Such high mass resolution and hence high specificity of PTR-TOF-MS enables us to identify VOCs based on their monoisotopic masses so that exact elemental formulae can be obtained. Therefore nominal isobars such as isoprene (a biogenic tracer) and furan (a combustion tracer) which appear at m/z ratio 69 in PTR-Q-MS can be separated by PTR-TOF-MS as they appear at m/z 69.070 and 69.033, respectively. The dynamic range is much better than that of a quadrupole mass analyzer.

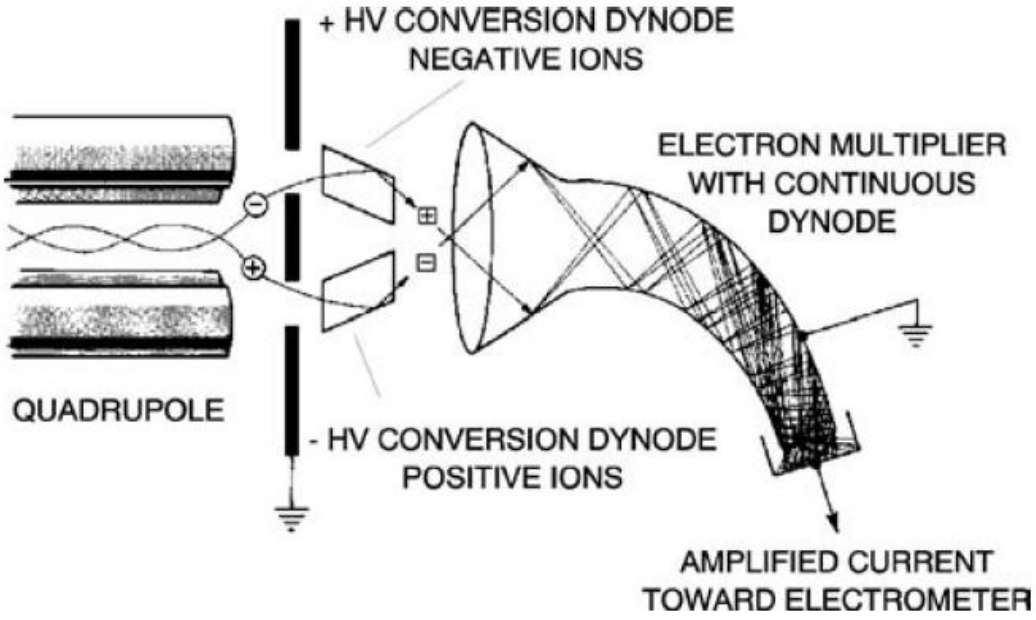

Figure 2.9: Schematic of continuous dynodes or channeltrons (Source: Hoffmann and Stroobant, Mass Spectrometry Principles and Applications, 2007, 'Reproduced with kind permission from John Wiley & Sons Ltd., UK')

2.2.4 Detector

In the PTR-Q-MS, a secondary electron multiplier (SEM) is typically used as a detector which comprises of a conversion dynode, a series of further dynodes and a collector. In an SEM, to increase detection efficiency, ions are first accelerated to high velocity using a conversion dynode at high potential (±3 to ±30 kV). Any ion (positive or negative) hitting the conversion dynode causes the emission of several secondary particles which can be positively charged, negatively charged or neutral. The first dynode converts these secondary particles/ions to electrons and then amplifies them by a "cascade" effect to produce an amplified current. The PTR-Q-MS used in this thesis for the VOC quantification contains a Balzers SEM as the detector. Generally this SEM operates between 1400-2100 V when it is new and between 2500-3500 V when it becomes old.

The PTR-TOF-MS used for the VOC quantification in this thesis employed a channeltron detector. Figure 2.9 represents the schematic of a channeltron or continuous dynode electron multiplier. Channeltron has good secondary emission properties and comprises of a curve-shaped lead-doped glass. Due to the uniform electric resistance of the walls, a

continuous accelerating field is created along the length of the tube by applying a voltage. The secondary electrons produced due to the collision of secondary particles from the conversion dynode with the curved inner wall, are then accelerated leading to the formation of more secondary electrons in the electron multiplier. Therefore a cascade of electrons is produced resulting in an amplified current that can be measured.

Chapter 3

Massive Emissions of Carcinogenic Benzenoids from Paddy residue burning in North India

3.1 Abstract

Benzenoids are organic pollutants emitted mainly by traffic and industrial sources. Here, using the combination of online in-situ measurements of several benzenoids and methyl cyanide (a biomass burning tracer) for the time in India, satellite remote sensing data of fire counts and back trajectory of air masses at a site in Mohali, we show that massive amounts of benzenoids are released from post-harvest paddy residue burning. Two periods, one that was not influenced by paddy residue burning (Period 1, 18:00-03:30 IST; 5-6 October, 2012) and another which was strongly influenced by paddy residue burning (Period 2, 18:00-03:30 IST; 3-4 November, 2012) were chosen to assess normal and perturbed levels. Peak values of 3830 ppb CO, 100 ppb NO_x, 40 ppb toluene, 16 ppb benzene, 24 ppb for sum of all C8-benzenoids and 13 ppb for sum of all C9-benzenoids were observed during Period 2 with the average enhancements in benzenoid levels more than 300%. The ozone formation potential of benzenoids matched CO with both contributing 5 ppb h^{-1} each. Such high levels of benzenoids for 1-2 months in a year aggravate smog events and can enhance cancer risks in north western India.

3.2 Introduction

Biomass burning affects the environment across varied spatial and temporal scales in several regions of the world (Crutzen and Andreae., 1990). It contributes significantly to the global atmospheric budgets of gases and aerosol, perturbs regional atmospheric composition and amplifies reaction rates responsible for the formation of secondary air pollutants such as ozone and secondary organic aerosol, impairing regional air quality (Andreae and Merlet., 2001). In north-western India, large scale burning of crop residue takes place twice a year during the post harvest months of October-November (mainly rice) and April-May (mainly wheat) (Venkataraman et al., 2006; Streets et al., 2003). 12,685 km^2 of paddy crop area in Punjab alone was reported to have been burnt in October 2005 (Badarinath et al., 2006).

While previous crop residue burning studies in India (Gupta et al., 2004; Venkataraman et al., 2006; Sahai et al., 2007) have focused on nutrient loss of soils and long lived climate relevant gases like methane, nitrous oxide, carbon dioxide and carbon monoxide, till date no study within India has investigated the impact of paddy residue burning on regional levels of reactive and carcinogenic benzenoid compounds such as benzene, toluene, xylenes, ethylbenzene and trimethylbenzenes. Benzenoid compounds and methyl cyanide are known to be emitted during biomass burning (Andreae and Merlet., 2001). In fact the predominant emission source of atmospheric methyl cyanide (global budget 0.4-1.0 Tg y^{-1} (Holzinger et al., 1999) is biomass burning, a reason why it is considered an excellent chemical tracer of biomass burning emissions (Holzinger et al., 1999).While methyl cyanide has a long atmospheric lifetime of about 9 months and health risks posed by it are unknown, benzenoid compounds collectively termed BTEX (benzene, toluene, ethylbenzene and xylene) are considered carcinogenic and mutagenic even at ambient levels of few tens of ppb (WHO, 2010). Unlike methyl cyanide for which biomass burning is the major source, traffic and solvent industry emissions are regarded as the main sources of atmospheric benzenoids (Rasmussen and Khalil., 1983). Total global emissions of benzene, toluene and xylenes are estimated to be 15 Tg y^{-1} (Olivier et al., 1996). In India the few studies of ambient BTEX levels reported in the literature ((Hoque et al., 2008; Kumar and Tyagi., 2006) and references therein) are from urban sites in cities like Delhi, Mumbai

and Kolkata. The analytical techniques used were offline methods based on passive or active sampling on adsorbents (with large potential for artifacts due to transfer losses) and quite slow typically providing only highly averaged (daily or weekly level) temporal information.

Considering the large quanta of crop residue (116-289 Tg y^{-1})(Venkataraman et al., 2006) burnt every year in India, benzenoid emissions and environmental impacts therefrom could be quite significant owing to both direct health impacts (e.g., carcinogenic and mutagenic) and indirect effects (e.g., through its atmospheric reaction products participating in secondary pollutant formation). The high hydroxyl radical reactivity of benzenoids fuels photochemical production of ozone and secondary organic aerosol, resulting in intensification of smog episodes. Phenolics and cresols are the major first generation products during atmospheric oxidation of most benzenoids. Moreover, a significant fraction of the benzenoid mass can partition to form aerosol. While benzenoids themselves are hydrophobic, their conversion to phenolics and cresols in the atmosphere results in formation of more polar (hence hydrophilic) aerosol that can increase the water vapour uptake by atmospheric aerosol and enhance fog formation. Recently air pollution episodes gripped large parts of North India between 26 October and 8 November 2012, even affecting the capital, Delhi (Singh., 2012). A major factor deemed responsible for the acute smog was the transport of pollutant laden air masses from the paddy residue burning regions in Punjab and Haryana.

Here, we employ the combination of online ambient air chemical measurements (1 measurement every minute) obtained by deploying a high sensitivity proton transfer reaction mass spectrometer (PTR-MS) for the first time in India in tandem with IISER Mohali's air quality station, air mass back trajectories and satellite remote sensing data of fire events. Methyl cyanide and benzenoid compounds were measured concomitantly with carbon monoxide, nitrogen oxides and aerosol mass concentrations ($PM_{2.5}$ and PM_{10}) at the receptor site in Punjab (Mohali; 30.667°N, 76.729°E and 310 m asl). Data measured on 3 November, 2012 (a day that was impacted by air masses which had passed over the burning fields less than 72 hours ago) and on 5 October, 2012 (a day in the same season but before crop residue burning activity had commenced), were used to quantify enhancements in ambient levels of methyl cyanide and benzenoids due to the paddy

residue fires.

3.3 Materials and methods

3.3.1 Site Description

All the measurements were performed at IISER Mohali's Atmospheric Chemistry Facility (iisermohali.ac.in/facilities/AtmosChemfacility/index.html) installed on the roof top of the Central Analytical Facility Building within the IISER Mohali campus (∼20 m above ground level), which is a suburban site in the north-western Indo-Gangetic Plain (IGP) (30.667°N, 76.729°E ; 310 m above mean sea level). The wind sector spanning south to north-west (180-315°) is mainly rural and agricultural land and was the main fetch region observed in the periods covered by this study. The IISER atmospheric chemistry facility is unique in South Asia, and consists of a high sensitivity proton transfer reaction mass spectrometer (PTR-MS) (India's first PTR-MS), an online ambient air quality station and a meteorological station. Below we detail the analytical details of the measurements.

3.3.2 Benzenoids and Methyl Cyanide measurements using Proton Transfer Reaction Mass Spectrometry (PTR-MS)

Proton transfer reaction mass spectrometry (PTR-MS) is a technique in which analyte VOC molecules with a proton affinity (P.A.) greater than that of water vapour (P.A. of water 165 kcal mol^{-1}) undergo soft chemical ionization with reagent hydronium ions (H_3O^+) to form protonated molecular ions (with m/z = molecular ion + 1). Nitrogen, oxygen, carbon dioxide and methane have a lower P.A. than water vapour and do not cause interferences in the detection of the trace VOCs. The instrument at IISER Mohali is a high sensitivity model (HS Model 11-07HS-088) manufactured by Ionicon Analytik Gesellschaft, Austria. It has four main parts, namely 1) the ion source which produces a pure stream of H_3O^+ ions (> 95%) by plasma discharge of water vapour 2) a reaction chamber in which ionization of VOCs takes place, 3) a quadrupole mass analyzer to separate the product ions and 4) a secondary electron multiplier for detection and amplification of the ion signal. The use of the PTR-MS technique in diverse fields has been

reviewed in detail elsewhere (Blake et al., 2009; de Gouw and Warneke., 2007).

To ensure proper data quality assurance, careful maintenance checks and performance characterization in terms of detection limits and sensitivities for respective VOCs are carried out through regular calibrations. The instrument was calibrated for the measured compounds (range 0.3-20 ppb) using a custom ordered VOC gas standard containing methyl cyanide, benzene, toluene, p-xylene and 1,2,4-trimethylbenzene (Apel-Riemer Environmental, Inc., Colorado, USA), as per the protocols detailed in the works of Sinha et al. (Sinha et al., 2009, 2012). The instrumental background was also determined by sampling zero air. Methyl cyanide, benzene, toluene, sum of C8-aromatics (xylenes and ethylbenzene) and sum of C9-aromatics (trimethylbenzenes) were measured at the mass to charge ratios of m/z 42, m/z 79, m/z 93, m/z 107 and m/z 121, respectively in the selected ion monitoring mode. These VOC-m/z identifications are in keeping with extensive validation studies from diverse ecosystems around the world (de Gouw and Warneke., 2007). The extensive reviews of (de Gouw and Warneke., 2007) and (Blake et al., 2009) and works of Warneke et al. (2001, 2003) and (de Gouw., 2003) have demonstrated that the detection of toluene (m/z = 93), C8- and C9-aromatics (m/z = 107 and 121, respectively) using PTRMS technique does not suffer from any known isobaric interferences. With a more highly mass resolved PTR-MS in an even more complex chemical environment in the Kathmandu Valley, I was also not able to observe any competing isobaric species (Sarkar et al., 2016). The total uncertainties were determined to be 6.1%, 6.3%, 7.3%, 8.1% and 6.8% for methyl cyanide, benzene, toluene, p-xylene and 1,2,4-trimethylbenzene, respectively, calculated using the root mean square propagation of individual uncertainties like the 5% accuracy error inherent in the VOC gas standard concentration, the 2σ instrumental precision error while measuring the compounds at 3 ppb, and the flow uncertainty of 2% for each mass flow controller used during the calibration. Detection limits defined as the 2σ noise while measuring at levels of $\sim$0.3 ppb, are 0.1 ppb, 0.06 ppb, 0.08 ppb, 0.09 ppb and 0.09 ppb for methyl cyanide, benzene, toluene, p-xylene and 1,2,4-trimethylbenzene, respectively.

3.3.3 Sampling of ambient air

Teflon (inner diameter 3.12 mm) was used as inlet tubing for the gas analyzers which were collocated at circa 20 m above ground. The inlets were protected from dust particles using Teflon and Nucleopore membrane particle filters (filter diameter 47 mm). Ambient air was drawn into the instruments continuously. The total sampling plus inlet residence time for all the instruments was < 70 s.

3.3.4 Carbon monoxide (CO), nitrogen oxides (NO_x) and PM measurements

Carbon monoxide (CO) was measured using non-dispersive infra red (NDIR) filter correlation spectroscopy (Thermo Fisher Scientific, Model No 48i). The one minute data has an uncertainty and detection limit of 7% and 40 ppb, respectively. This technique has been validated extensively (de Gouw et al., 2009). For quality assurance of the dataset, zero drift calibration is done frequently (at least once every day) and span calibrations (100-1500 ppb) are carried out at least once every month.

NO_x (sum of NO and NO_2) was measured using the chemiluminescence technique (Thermo Fisher Scientific, Model No 42i). The one minute data has an uncertainty and detection limit of 7% and 0.05 ppb, respectively. Zero drift and span calibration (5 point calibration in the range 10-50 ppb) are carried out at least once every week and once every four weeks, respectively.

$PM_{2.5}$ and PM_{10} mass concentrations were measured by the standard β-attenuation technique (Thermo Fisher Scientific, Model No 5014i Beta) that has a detection limit of < 1 μg m^{-3}. The instrument is calibrated at least once every 8 weeks.

The meteorological parameters such as wind speed, wind direction, solar radiation, ambient temperature and relative humidity were also measured using separate sensors manufactured by Met One Instruments Inc., Rowlett.

3.3.5 Trajectory Analysis and MODIS Data

Back trajectory ensemble calculations for air masses arriving at Mohali (30.667°N, 76.729°E) and New Delhi (28.519°N, 77.213°E) (20 m agl) on 5 October 2012 (18:30 IST) and on 3 November 2012 (18:30 IST) respectively, were performed using the NOAA HYSPLIT model using GDAS (Global Data Acquisition System) meteorology (Draxler and Rolph., 2012; Rolph., 2012). The trajectories were plotted on a map using Pan Map GIS software (Figure 3.1). Only those trajectories that were consistent with the terrain height of the measurement site (< 400 m above mean sea level at Mohali and > 400 m above mean sea level at Shimla) were considered for further analysis.

Moderate Resolution Imaging Spectroradiometer (MODIS) (NASA/University of Maryland, 2002, MODIS Hotspot / Active Fire Detections Data set, http://maps.geog.umd.edu) remote sensing fire count data was used to detect paddy residue burning activity in North India (including Bihar, Jharkhand, Rajasthan, Madhya Pradesh) for two 96 hour periods from 2 October 2012 to 5 October 2012 and from 31 October 2012 to 3 November 2012.

3.4 Results and discussion

Figure 3.1 shows the MODIS fire counts data (red crosses) from 2-5 October 2012 and from 31 October-3 November 2012. Two periods were considered: The first period (5 October 2012 18:00 IST-6 October 2012 03:30 IST; hereafter termed Period 1) had no discernible influence of paddy residue burning while the second period (3 November 2012 18:00 IST-4 November 2012 03:30 IST; hereafter termed Period 2) was intensely influenced by paddy residue burning as can be seen in the 72 hour back trajectories for both Mohali and Delhi and the 96 hour fire counts data.

Period 1 measurements are representative of a period not influenced by paddy residue burning but still characterized by similar meteorology and dynamics as Period 2. The back trajectories for Delhi are plotted to highlight that during Period 2, the paddy residue burning emissions were also affecting Delhi and chemical perturbation of atmospheric composition in Delhi would be similar to that experienced at Mohali.

Figure 3.2 shows the enhancements in methyl cyanide (CH_3CN), carbon monoxide (CO), sum of nitrogen dioxide and nitrogen monoxide (NO_x), toluene and benzene during Pe-

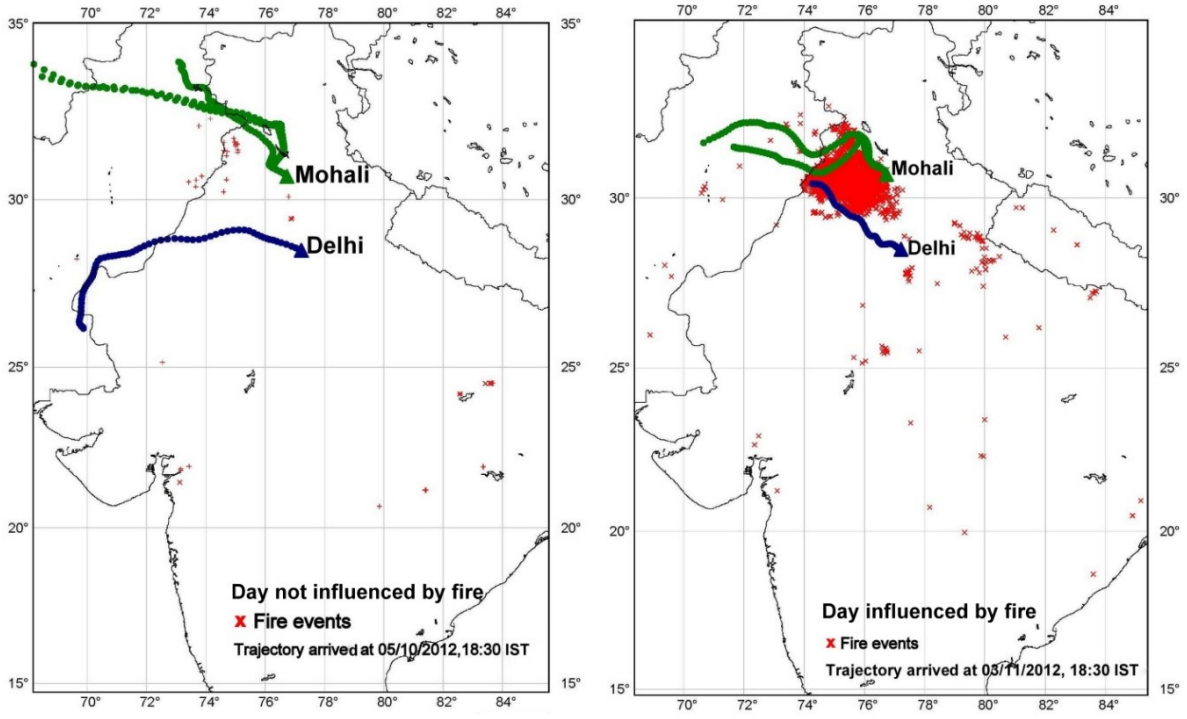

Figure 3.1: 72-hour back trajectories of air masses that arrived at 18:30 IST in Mohali and Delhi on 5 October 2012 and 3 November 2012 (also shown are the 96 hour MODIS fire count data as red markers)

riod 1 (black cross) relative to Period 2 (red triangle) between 18:00-03:30 IST at Mohali. During Period 1, it can also be seen that the profile of the measured species is rather flat. However the levels of all the measured species increases rapidly during Period 2, from 18:30 IST till 21:30 IST and remains high until 01:00 IST. Thereafter, mixing ratios decrease and by 03:30 IST they reduce to levels typical of Period 1. The increase coincides with the arrival of air masses (shaded bar) that had spent considerable time over regions where paddy residue burning was active and enhancements in the biomass burning tracer methyl cyanide provide added confirmation. Further, the decrease in the profiles from circa 03:30 IST during Period 2 also coincided with a change in the direction of the back trajectory to a more northerly sector (not shown) in which paddy residue burning was absent.

Peak values of 100 ppb NO_x , 40 ppb toluene and 16 ppb benzene were observed for more than 30 minutes during Period 2. Such high levels for benzene and toluene have only been previously reported ((Hoque et al., 2008; Kumar and Tyagi., 2006) and references therein) from congested traffic roads in Delhi, Mumbai and Kolkata and demonstrate that paddy residue burning emissions can rival even the high emissions from urban traffic regionally. The paddy straws are made of cellulose and hemicellulose, lignin, extractives and trace minerals which are composed mainly of C, H, N and O (Koppmann et al., 2005). In chamber studies where crop residue alone was burnt, direct benzenoid emissions from the paddy residue have been reported in numerous previous studies (e.g., Stockwell et al. (2015); Christian et al. (2004); Yokelson et al. (2013)). The mechanistic reasons for emissions of benzenoids when plant residue is combusted have been discussed by Koppmann et al. (2005).

The average nocturnal boundary layer (NBL) height obtained for Period 1 and Period 2 using the NOAA HYSPLIT model was 1.5 times higher in Period 1 compared to Period 2 (Period 1 NBL = 89 m ; Period 2 NBL = 61 m). While calculating the degree of enhancements, the difference in NBL dilution was taken into account. Table 3.1 summarizes the results. All gas and aerosol parameters show significant enhancement (> 1.5) for Period 2 but in particular the benzenoid compounds show the highest enhancements (3.3 to 4.7). By quantifying the "baseline" and "perturbed" ambient concentrations of benzenoids and co-emitted gases and aerosol including the chemical tracer for the emission

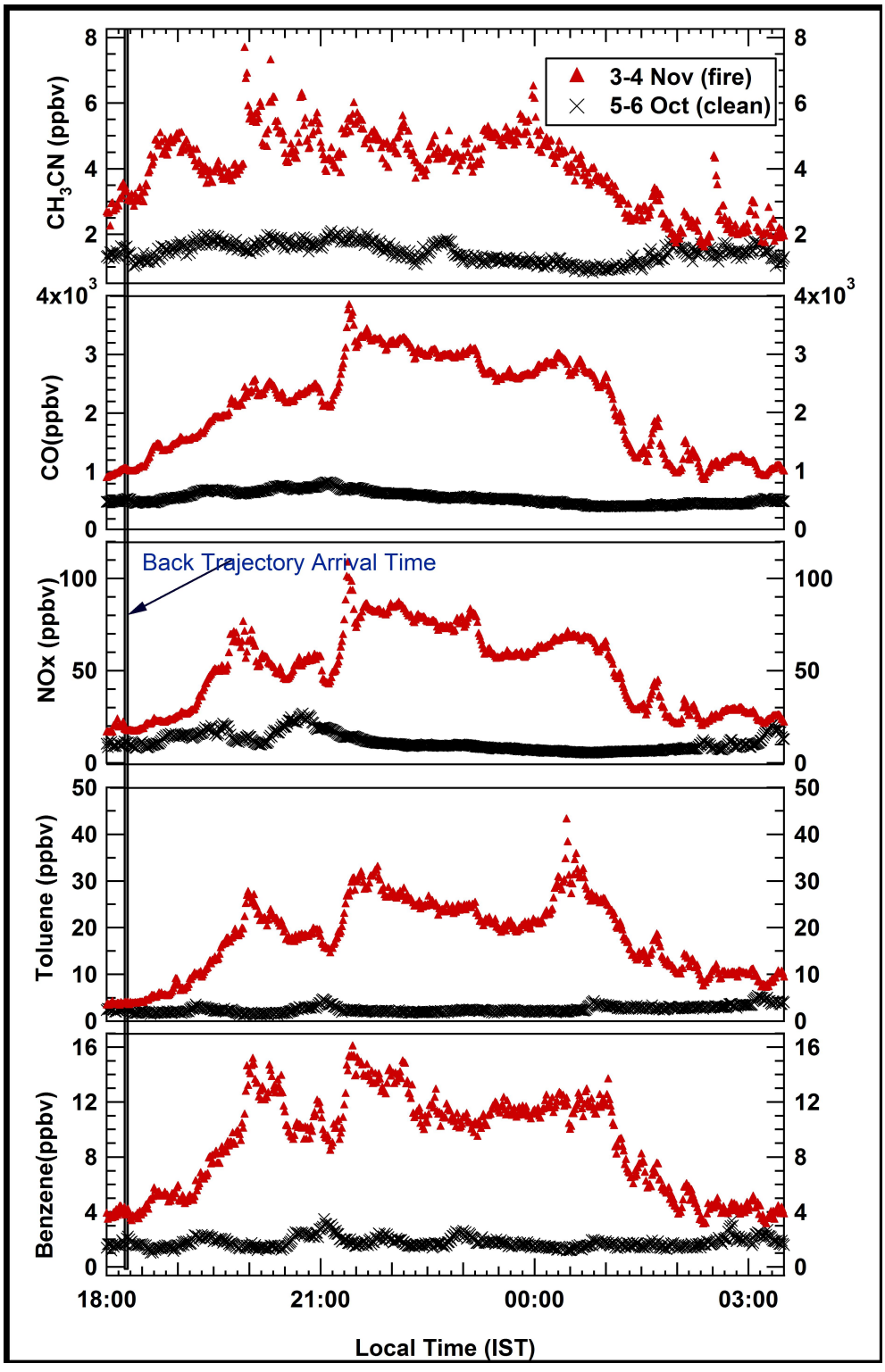

Figure 3.2: Ambient mixing. ratios (n = 570) in ppb of methyl cyanide, carbon monoxide, nitrogen oxides, toluene and benzene from 18:00-03:30 IST duirng Period 1 (black cross; non-fire influenced) and Period 2 (red triangles) fire influenced

Table 3.1: Enhancement ratios during the period not influenced by crop residue burning (clean period; 18:00-03:30) and period influenced by crop residue burning (18:00-03:30), typical chemical lifetimes, ozone and secondary organic aerosol formation potentials of the measured species

Measured species	Clean period Avg±Sdev	Crop residue burning Avg±Sdev	Crop residue burning (max)	Degree of enhancement	Lifetime	Ozone prod. pot.	SOA yield (%)
Methyl cyanide*	1.1±0.4	4.0±1.2	7.7	1.8	268.5 d	0.001	-
Benzene*	2.7±0.6	8.9±3.5	16.0	3.3	4.7 d	0.1	27.2-29
Toluene*	3.8±1.1	17.8±8.0	43.1	4.7	1.6 d	0.7	7.3-13.2
C8-aromatics*	3.3±0.9	13.0±5.0	24.3	3.9	0.5 d	1.8	2.8-8.7
C9-aromatics*	1.9±0.7	6.5±2.4	12.9	3.4	0.2 d	2.3	-
CO*	838±161	2117±784	3830	2.5	60 d	4.9	-
NO_x(NO+NO_2)	16.7±7.0	50.2±21.7	108.3	3.0	2 d	-	-
$PM_{10}^{\#}$	250±64	402±123	587	1.6	-	-	-
$PM_{2.5}^{\#}$	137±23	240±63	320	1.8	-	-	-

$*$measured in ppb; $^{\#}$measured in μg m^{-3}; ^{a}rate coefficient data were taken from (Atkinson et al., 2004) and [OH] = 3×10^6 molecules cm^{-3} was considered; lifetime is defined as time taken for level to reduce to 1/e of initial value; ^{b} SOA yield reported in (Ng et al., 2007) was taken.

activity during the case study, my observations and analysis clearly show ambient concentration enhancements of more than 300% (refer Table 3.1) occurred for all benzenoids. I note that ambient concentrations (C) are a function of the emissions (E), loss rate (L) and dilution effect (D) of boundary layer dynamics (meteorological conditions) and can be expressed as:

$$C = f(E, L, D) = E - L - D \tag{3.1}$$

I accounted for the boundary layer dilution effect while loss rate/sinks (controlled by the hydroxyl radical) are unlikely to change in the ambient environment as hydroxyl radicals are buffered. Hence, in this case the ambient concentration enhancements are a direct consequence of the emissions from the paddy residue burning activity (the additional emission source). As the ambient concentration enhancements are massive ($> 300\%$ for all benzenoids), it is reasonable to conclude that the emissions of benzenoids are also massive in this case. Recent works from our group using 3-year and 2-year long measurements (Chandra and Sinha, 2016; Kumar et al., 2016) further demonstrate the representativeness of such events in the north-western IGP. The average benzenoid concentrations were 3-4 times higher than the background concentrations (with peak concentrations as high as

10-15 times) even several km downwind after atmospheric dilution and dispersion. This suggests that the actual benzenoid emissions and concentrations at the fields where the paddy residue fires were active would be much higher i.e., at least an order of magnitude higher which is massive for ambient conditions. These higher concentrations of benzenoids are what the nearest villages are likely to experience as exposure. Note, the atmospheric lifetimes of benzene and toluene are ∼8-9 days and ∼2-3 days, respectively. Therefore, the benzene concentrations that reach the nearby villages could be at least one order of magnitude higher than the concentrations observed at IISER Mohali.

The crop residue burning activity occurs twice a year (paddy residue burning in Oct-Nov and wheat residue burning in April-May) and lasts for at least one month for each type of crop residue burning (Kumar et al., 2016). This means that in a year, at least two months (60 days) are intensely influenced by crop residue burning in the north-western IGP. Now taking the National Ambient Air Quality Standard (NAAQS) for benzene (< 1.6 ppb; annual average), the exposure should not exceed 584 ppb (365 × 1.6 ppb) in a year. But if we consider the average benzene concentration of ∼10 ppb (which was observed in this case study at IISER Mohali), the exposure of benzene during the two months of crop residue burning becomes higher (60 × 10 ppb = 600 ppb) than the NAAQS limit for a year at a site several km downwind. Also note that the average concentrations of benzene and other aromatics could be at least one order of magnitude higher in the nearby areas where the crop residue fires were active. This indicates that the exposure to the benzenoids would be much higher and can contribute to the cancer prevalence in this region. A recent study from our group (Chandra and Sinha, 2016) on the health risk assessment of benzene has conclusively shown that due to the influence of post-harvest paddy residue burning, at least 468 out of 46.8 million adults and 155 out of 6.2 million children experience enhanced cancer risk in Punjab and Haryana.

The enhancement in nitrogen oxides by a factor of 3 has strong implications for the regional levels of ozone. An excess of nitrogen monoxide relative to ozone at night would result in chemical titration of the ozone mainly through the following reaction bringing down nighttime ozone levels within minutes.

$$NO + O_3 \longrightarrow NO_2 + O_2 \qquad [R25]$$

However when transported to downwind sites, with the first rays of sunlight, intense ozone production would result due to the photolysis of the nitrogen dioxide (at $\lambda < 460$ nm) which would further be fueled by reactive volatile organic compounds present in the air masses. Table 3.1(Column 7) shows the high ozone production potential in ppb O_3 h^{-1} due the benzenoids and CO calculated using Equation (1) (Sinha et al., 2012).

$$Ozone\ production\ potential = (\sum k_{VOC_i+OH}[VOC_i]) \times [OH] \times n \tag{3.2}$$

where k_{VOC_i+OH} is the pseudo first order rate coefficient for the reaction of species VOC_i with OH; $[VOC_i]$ is the concentration of the measured VOC and n= 2. $[VOC_i]$ was replaced by the measured [CO] and n = 1 in Equation 1 for calculating the O_3 production potential due to CO.

The total ozone production potential due to just benzenoids and CO is quite high ($\sim$10 ppb h^{-1}). Note also that the ozone production potential due to the measured benzenoids rivals the ozone production potential due to CO during Period 2. Even if 50% of the high production potential (since higher O_3 production potential is typically accompanied by higher O_3 loss potential) were to translate into net ozone production, the peak ozone value due to the benzenoids and CO chemistry would be 5 ppb h^{-1} higher. Due to increased daytime O_3 and NO_x, more hydroxyl radicals would be formed (since O^1D from ozone photolysis reacts with H_2O and produces OH radicals) and oxidant chemistry would be amplified (as VOC + OH produces HO_2 and NO keeps recycling OH by converting HO_2 to OH), aggravating photochemical smog. Besides the primary health impact due to carcinogenic benzenoids and high ozone, significant fine mode aerosol in the form of secondary organic aerosol would be expected to be formed as shown in Table 3.1. In particular almost 30% of the reacting benzene mass concentration could form secondary organic aerosol (Column 8; Table 3.1). During the chemical transformations which occur in multiple steps, the more polar and hence hydrophilic water absorbing secondary organic aerosols could coat onto the existing atmospheric particles causing them to swell up with water affecting visibility, air quality and cloud properties (Rosenfeld et al., 2008).

3.5 Conclusions

On a regional scale in the agricultural regions and villages of north-western India, paddy residue burning may dominate benzenoid emissions from traffic and industrial sources and the impact of crop residue burning from India on the global budget of benzenoids will require further such studies in different seasons and regions of India.

Every year during Oct-Nov, $\sim 90\%$ of the days are influenced by paddy residue burning in the north-western Indo Gangetic Plain (IGP). These events are similar to the event chosen here for the case study in terms of emissions and spatio-temporal character. Recent works from our group using 3-year and 2-year long measurements (Chandra and Sinha, 2016; Kumar et al., 2016) further demonstrate the representativeness of such events in the north-western IGP. It is disconcerting to note that several paddy growing regions of India are also regions with very high prevalence of cancer (e.g., Malwa belt in Punjab). The exposure of the population to sustained high levels of carcinogenic benzenoids in the air they breathe for several months in a year could certainly be a contributory factor to cancer prevalence and warrants detailed multidisciplinary epidemiological and environmental studies. It is worth mentioning that though the Ministry of Environment and Forests, Government of India stipulated new ambient air quality standards (NAAQS) in 2009 regarding permissible exposure to benzene in air (NAAQS for benzene: annual average < 1.6 ppb), no standards are available for the other benzenoids. Currently, the national monitoring network for benzenoid VOCs is very sparse and does not even exist for methyl cyanide, for which this study reports the first measurements. Future efforts should focus on national monitoring of ambient benzenoids using online analytical techniques to establish their spatial and temporal variability and constrain contribution of its different sources for mitigation.

Chapter 4

Overview of VOC emissions and chemistry from PTR-TOF-MS measurements during the SusKat-ABC campaign

4.1 Abstract

The Kathmandu Valley in Nepal suffers from severe wintertime air pollution. Volatile organic compounds (VOCs) are key constituents of air pollution, though their specific role in the Valley is poorly understood due to insufficient data. During the SusKat-ABC (Sustainable Atmosphere for the Kathmandu Valley-Atmospheric Brown Clouds) field campaign conducted in Nepal in the winter of 2012–2013, a comprehensive study was carried out to characterize the chemical composition of ambient Kathmandu air, including the determination of speciated VOCs by deploying a Proton Transfer Reaction Time of Flight Mass Spectrometer (PTR-TOF-MS)–the first such deployment in South Asia. 71 ion peaks (for which measured ambient concentrations exceeded the 2σ detection limit) were detected in the PTR TOF-MS mass scan data, highlighting the chemical complexity of ambient air in the Valley. Of the 71 species, 37 were found to have campaign average concentrations greater than 200 ppt and were identified based on their spectral character-

istics, ambient diel profiles and correlation with specific emission tracers as a result of the high mass resolution ($m/\Delta m > 4200$) and temporal resolution (1 min) of the PTR-TOF-MS. The concentration ranking in the average VOC mixing ratios during our wintertime deployment was acetaldehyde (8.8 ppb) > methanol (7.4 ppb) > acetone + propanal (4.2 ppb) > benzene (2.7 ppb) > toluene (1.5 ppb) > isoprene (1.1 ppb) > acetonitrile (1.1 ppb) > C8-aromatics ($\sim$ 1 ppb) > furan ($\sim$ 0.5 ppb) > C9-aromatics (0.4 ppb). Distinct diel profiles were observed for the nominal isobaric compounds isoprene (m/z = 69.070) and furan (m/z = 69.033). Comparison with wintertime measurements from several locations elsewhere in the world showed mixing ratios of acetaldehyde ($\sim$ 9 ppb), acetonitrile ($\sim$ 1 ppb) and isoprene ($\sim$ 1 ppb) to be among the highest reported till date. Two "new" ambient compounds namely, formamide (m/z = 46.029) and acetamide (m/z = 60.051), which can photochemically produce isocyanic acid in the atmosphere, are reported in this study along with nitromethane (a tracer for diesel exhaust) which has only recently been detected in ambient studies. Two distinct periods were selected during the campaign for detailed analysis: the first was associated with high wintertime emissions of biogenic isoprene, and the second with elevated levels of ambient acetonitrile, benzene and isocyanic acid from biomass burning activities. Emissions from biomass burning and biomass co-fired brick kilns were found to be the dominant sources for compounds such as propyne, propene, benzene and propanenitrile which correlated strongly with acetonitrile ($r^2 > 0.7$), a chemical tracer for biomass burning. The calculated total VOC OH reactivity was dominated by acetaldehyde (24.0%), isoprene (20.2%) and propene (18.7%), while oxygenated VOCs and isoprene collectively contributed to more than 68% of the total ozone production potential. Based on known SOA yields and measured ambient concentrations in the Kathmandu Valley, the relative SOA production potential of VOCs were: benzene > naphthalene > toluene > xylenes > monoterpenes > trimethylbenzenes > styrene > isoprene. The first ambient measurements from any site in South Asia of compounds with significant health effects such as isocyanic acid, formamide, acetamide, naphthalene and nitromethane have been reported in this study. Our results suggest that mitigation of intense wintertime biomass burning activities, in particular point sources such biomass co-fired brick kilns, would be important to reduce the emission and formation of toxic VOCs (such as benzene and isocyanic acid) in the Kathmandu Valley.

4.2 Introduction

The Kathmandu Valley is a bowl-shaped basin at an altitude of $\sim$ 1300 m that is surrounded by the Shivapuri, Phulchowki, Nagarjun and Chandragiri mountains which have an altitude range of 2000–2800 m above mean sea level and is prone to poor air quality and air pollution episodes (Panday et al., 2009). In particular during the winter mornings, due to the combination of suppressed mixing, katabatic wind flows and the topography of the basin, pollutants remain trapped under an inversion layer close to the surface of the Valley (Kitada et al., 2003; Regmi et al., 2003). Previous studies in similar Valley sites such as Santiago de Chile and Mexico City have investigated the coupling of topography, meteorology, atmospheric dynamics, emissions and chemical processes in exacerbating air pollution episodes and suggested ways to mitigate the air pollution and improve air quality (Molina et al., 2007; de Foy et al., 2006; Schmitz., 2005; Rappenglück et al., 2005). In contrast, only few such studies have been carried out within the Kathmandu Valley. Previous studies in the Kathmandu Valley have examined pollution in relation to carbon monoxide (CO), nitrogen oxides (NO_x), sulfur dioxide (SO_2), ozone (O_3) (Panday and Prinn., 2009; Larssen et al., 1997; Yu et al., 2009; Ramana et al., 2004; Pudasainee et al., 2006) and particulate matter (Gurung and Bell., 2012; Sharma et al., 2012). An early study by Davidson et al. (1986) reported ambient average concentrations of 2 ppm CO during the winter season of 1982–1983. Offline measurements of nitrogen dioxide (NO_2) and sulphur dioxide (SO_2) performed by Larssen et al. (1997) examined the average pollution exposure in different regions of the Valley and found that the brick kiln region south-east of the Valley and cities were most severely affected. With regard to quantification of volatile organic compounds in downtown Kathmandu and a rural site in Nagarkot, data pertaining to light C2–C6 compounds was obtained in a study in November 1998 using thirty-eight whole air samples analyzed offline with a GC-FID (Sharma et al., 2000). Subsequently Yu et al. (2008) measured mixing ratios of seven monocyclic aromatic hydrocarbons, using long path differential optical absorption spectroscopy (DOAS) at a suburban site in Kathmandu during January–February 2003. All these initial studies highlighted that traffic sources were major contributors to air pollution in the Kathmandu Valley (Yu et al., 2008). In the time since these studies, due to rapid urbanization and population growth

over the last decade, the wintertime air quality has deteriorated severely. Yet very little information is currently available with regard to the emissions and chemistry of volatile organic compounds in the Kathmandu Valley. Except for a handful of species, most of which were measured only periodically using offline sampling methods, virtually no in-situ data is available from the region with regard to the concentration and speciation of several important volatile organic compounds.

Volatile organic compounds (VOCs), in particular the reactive ones, have atmospheric lifetimes ranging from minutes to days (Atkinson., 2000) and exert a profound influence on regional air quality through their participation in chemical reactions leading to the formation of secondary pollutants such as tropospheric ozone and secondary organic aerosol (SOA). Both tropospheric ozone and secondary organic aerosol are important from the standpoint of air quality and climate due to their impact on health and the radiative forcing of the atmosphere (IPCC, 2013). Further, through reactions with the hydroxyl radicals (the detergent of the atmosphere Lelieveld et al., 2004), photodissociation reactions and radical recycling reactions, VOCs strongly influence ambient OH reactivity and the budget of HO_x (OH, HO_2) radicals which control the removal rates of gaseous pollutants, including most greenhouse gases from the atmosphere. Inhalation of certain VOCs present in air also produces direct adverse health effects. For example benzene and nitromethane are reported to be human carcinogens by the World Health Organization (WHO, 2010).

In order to address gaps in our scientific understanding of the air pollution in the Kathmandu Valley, a large scale scientific experiment called the Sustainable Atmosphere for the Kathmandu Valley-Atmospheric Brown Clouds (SusKat-ABC) campaign was carried out in the winter of 2012–2013 by an international team of scientists. An overview of the campaign objectives, measurement suite and sites will be presented in the overview paper (Rupakheti et al., 2016) while an overview of the meteorology and pollution transport processes will be presented in a second overview paper (Panday et al., 2016). We present here results derived from the in-situ measurements of speciated VOCs using a proton transfer reaction time of flight mass spectrometer (PTR-TOF-MS), the first such deployment in South Asia. Another version of this type of instrument, which has lower mass resolution, namely a proton transfer reaction quadrupole mass spectrometer (PTR-Q-MS) has

been previously deployed in the North-West Indo-Gangetic Plain in Mohali, India ((Sinha et al., 2014), Chapter 3).

With a mass resolving power ($m/\Delta m$) of more than 4200, PTR-TOF-MS measurements enable identification of several compounds based on their exact monoisotopic mass (molecular formula) and have fast time response ($\sim$ 1 min). These attributes were leveraged to quantify a suite of ambient VOCs at a suburban site (Bode; 27.689^0N, 85.395^0E, 1345 m a.m.s.l.) in the Kathmandu Valley during December 2012–January 2013. Oxygenated VOCs such as methanol, acetaldehyde, sum of acetone and propanal, aromatic VOCs such as benzene, toluene, sum of C8-aromatics and sum of C9-aromatics, isoprene, furan and acetonitrile were quantified every minute and their diel emission profiles analyzed to constrain major sources. Careful analysis of the ambient mass spectra from 21–210 Th was undertaken to identify several "new" or rarely quantified VOCs based on their monoisotopic masses (and therefore molecular formula), spectral characteristics observed at a particular m/z in a 0.005 amu bin relative to the ion peak, ambient diel profiles and correlation with specific emission tracer molecules such as acetonitrile (a tracer for biomass burning). By contrasting periods in the chemical dataset based on the dominance of biogenic emission sources and emissions from brick kilns co-fired with biomass, respectively, VOCs emitted from brick kilns were constrained. The measured VOC concentrations in the Kathmandu Valley were compared with previous wintertime measurements from other urban/suburban sites and megacities. The diel profiles of rarely detected and measured VOCs such as nitromethane and isocyanic acid were correlated with tracer VOCs. The major VOC contributors to the total measured reactive carbon, the VOC OH reactivity, ozone production potential and secondary organic aerosol formation potential were elucidated through detailed analyses. Finally, information pertaining to direct health impacts of some of the quantified VOCs detected in this complex chemical environment are discussed with conclusions and outlook for future VOC studies in the region.

Figure 4.1: Location of the measurement site (Bode; red circle) along with surrounding cities (Kathmandu, brown circle; Patan, blue circle and Bhaktapur, pink circle), brick kilns (white markers), major industries (yellow triangles), forest areas (green tree symbols), airport (blue marker) and major river path (sky blue path) in the Google Earth image of the Kathmandu Valley (obtained on 22 May 2015 at 14:55 LT)

4.3 Materials and methods

4.3.1 Site Description and prevalent meteorology

The Kathmandu Valley is a bowl-shaped basin in the Himalayan foothills. The average altitude of the Valley is 1300 m above mean sea level (a.m.s.l.). It is encircled by a ring of mountains that range from 2000–2800 m a.m.s.l., with about five mountain passes approximately 1500–1550 m a.m.s.l. (Panday et al., 2009). VOC measurements during this study were performed in the winter season from 19 December 2012 till 30 January 2013 at Bode (27.689^0N, 85.395^0E; 1345 m a.m.s.l.), which is a suburban site located in the westerly outflow of Kathmandu city.

Figure 4.1 shows a zoomed view of the land use in the vicinity of the measurement site (Bode; red circle; image derived using Google Earth on 22 May 2015 at 14:55 LT) in relation to the surrounding cities – Kathmandu ($\sim$ 10 km to the west; brown circle),

Patan ($\sim$ 12 km south-west of the site; blue circle) and Bhaktapur ($\sim$ 5 km south-east of the site; pink circle), major point sources and forested areas. Most of the agricultural fields near the site have unpaved tracks and were sold as small plots, and are largely uncultivated. At some distance, there are agricultural fields on which rice is sown in the summer and either potatoes/vegetables or wheat is sown in winter. The major road (Bhaktapur road) is about 1 km south of the site. In 2011, the total population of Kathmandu, Patan and Bhaktapur cities were: 1,003,285 (population density: 20,289 km^{-2}), 226,728 (population density: 14,966 km^{-2}) and 83,658 (population density: 12,753 km^{-2}), respectively according to Central Bureau of Statistics (2011). The region east of the site was usually downwind but it is important to note that several brick kilns (white marker in Figure 4.1; around 10 brick kilns) were located south-east of the site at about 1 km distance. Major industries (yellow triangles in Figure 4.1) were concentrated primarily in the cities of Kathmandu (Balaju industrial area) and Patan (Patan industrial area), while Bhaktapur industrial area was located in the south-east direction within 2 km of the measurement site. About 20 small industries, mainly pharmaceuticals, plastic, tin, electronics and fabrics were located in this industrial area. Also a few plastic, electronics, wood, aluminium and iron industries were located within 3 km from the Bode site in the south-east direction. The Tribhuvan international airport was located west of the site ($\sim$ 4 km from Bode).

The region north of the site has a small forested area (Nilbarahi Jungle in Figure 4.1; $\sim$ 0.5 km^2 area) and a reserve forest (Gokarna Reserve Forest in Figure 4.1; $\sim$ 1.8 km^2 area) at approximately 1.5 and 7 km from the measurement site, respectively. Other nearby forest areas were located adjacent to the international airport (Mrigasthali and Bhandarkhal Jungle; 8–10 km from the site). The forests in the Kathmandu Valley consist of broad-leaved evergreen mixed forest of *Schima castanopsis* at the base (up to 1800 m a.m.s.l.), oak-laurel forest in the middle (1800 to 2400 m a.m.s.l.), and oak forest at the top, while the conifer tree species *Pinus roxiburghii* (Khote Salla) and *Pinus wallichianna* (Gobre Salla) are also found (Department of Plant Resources, Nepal., 2015). Other major tree species are *Melia azedarach* (Bakaino), *Schima wallichii* (Chilaune), *Castanopsis indica* (Dhale Katus), *Piptanthus nepalensis* (Suga Phul), *Persia bombycina* (Kaulo), *Madhuca longifolia* (Mauwa), *Celtis australis* (Khari), *Quercus semecarpifolia* (Khasru),

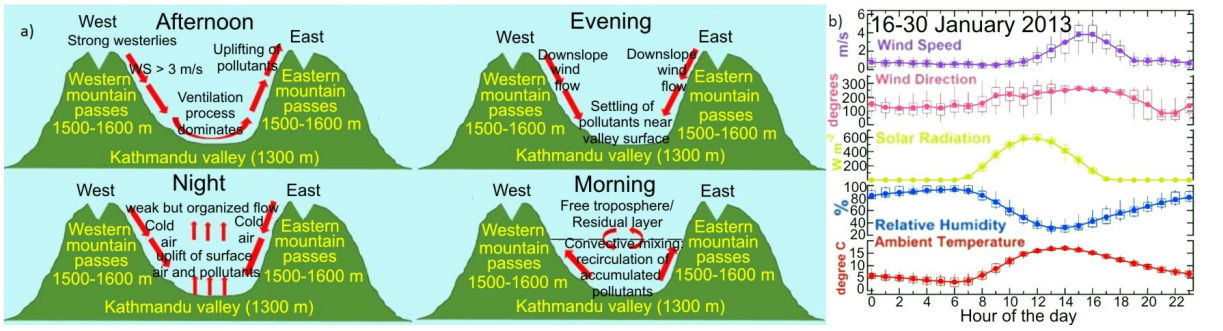

Figure 4.2: a) Schematic of wind flow during different times of the day in the Kathmandu Valley. b) Box and whisker plots of the measured meteorological parameters (wind speed, wind direction, solar radiation, relative humidity and ambient temperature) at the Bode site (16-30 January 2013)

and *Cryptomeria japonica* (Dhupi salla) (Department of Plant Resources, Nepal., 2015). The general meteorological conditions within the Kathmandu Valley remain fairly similar throughout the winter season (Regmi et al., 2003; Panday et al., 2009) and it is worth mentioning that the winter of 2012–2013 was not anomalous. Conditions were calm during the mornings with shallow boundary layer and therefore what we see in the morning hours are emissions from the previous night and emissions from morning activities around the measurement site within a radius of few km, rather than regional emissions. Cold pooling of air at night resulting in dilution of pollution was observed in the diel profiles of VOCs for period 1 when the 24/7 brick kilns were largely un-operational (for e.g. between midnight and 05:00 LT). Shortly after sunrise, the surface air mixes in with air that was aloft. Finally during the afternoon (10:00–15:00 LT), westerly winds sweep the valley from west to east at wind speeds of 3–4 ms^{-1} advecting the emissions, some of which may get transported across the mountain passes (Kitada et al., 2003; Regmi et al., 2003; Panday et al., 2009).

Figure 4.2b shows the box and whisker plots for the meteorological parameters measured at Bode from 16–30 January 2013 derived from the one minute temporal resolution data acquired using meteorological sensors (Campbell Scientific Loghborough, UK) installed on the rooftop ($\sim$ 25 m above ground and $\sim$ 5 m away from the instrument inlet). Daytime (08:00–17:00 LT) average ambient temperature for the measurement period was observed to be 12.2 ± 4.5 degreeC. It is worth mentioning that most mornings were associated with dense fog (average ambient RH$>$ 90% with visibility $<$ 100m) whereas the afternoons

were associated with high speed westerly winds ($> 4\text{ms}^{-1}$). Wind speeds from other wind sectors were generally lower (average wind speeds $\sim 1\text{ms}^{-1}$). The early morning wind flow was normally from the south-east wind sector which comprised of several brick kilns and Bhaktapur city. Evening hours were also associated with dense fog and the relative humidity (RH) was generally greater than 90% throughout the night. Minimum RH levels ($\sim$ 35%) were observed during midday. The sunrise typically occurred between 07:00–08:00 and sunset timings were around 17:00 Nepal Standard Time (NST), respectively. The range of atmospheric pressure during the campaign was 856–866 hPa.

4.3.2 VOC measurements using PTR-TOF-MS

Volatile organic compounds (VOCs) over the mass range (21–210 amu) were measured using a commercial high sensitivity proton transfer reaction time of flight mass spectrometer (Model PTR-TOF-MS 8000; Ionicon Analytic GmbH, Innsbruck, Austria). This instrument has been described in detail by Jordan et al. (2009) and is a more recent development of the PTR technique (Lindinger et al., 1998) that enables higher mass resolution at ppt level detection limit (Ruuskanen et al., 2011; Müller et al., 2010; Park et al., 2013; Stockwell et al., 2015). Briefly, the instrument consists of a hollow cathode ion source which produces a pure flow of the H_3O^+ reagent ions, a drift tube where analyte VOCs undergo ionization and an orthogonal acceleration reflectron time of flight mass analyzer and multi-channel plate detector. The instrument was operated at a drift tube pressure of 2.2 mbar, drift tube temperature of 600 degreeC and drift tube voltage of 600 V, resulting in an operating E/N ratio of $\sim$ 135 Td (1 Td = 10^{-17}V cm^{-2}; de Gouw and Warneke., 2007). Table 4.1 summarizes the relevant instrumental details. The high mass resolution of the instrument ($m/\Delta m > 4200$ at m/z 21.022 and > 4800 at m/z 205.195) and detection limit of few tens of ppt permitted identification of several rarely measured or previously unmeasured compounds based on their monoisotopic masses.

The PTR-TOF-MS 8000 used in this work was installed in a room on the second floor of a building at the suburban measurement site at Bode, Kathmandu. Ambient air was sampled continuously from the rooftop ($\sim$ 20 m above ground) through a Teflon inlet line that was protected with a Teflon membrane particle filter to ensure that dust and

debris did not enter the sampling inlet. Teflon membrane particle filters similar to the ones used in the Kathmandu study have been used without issues in several previous PTR-MS VOC studies by some of the authors (e.g. Sinha et al. (2010)), including at another South Asian site in Mohali, India (Sinha et al., 2014). The filters were changed on seven occasions during the 40 day long deployment from 19 December 2012 to 30 January 2013. The inlet lines used in Kathmandu were prepared prior to deployment by continuous purging at different flow rates in the laboratory at Mohali for more than three days and zero air was sampled through these lines. After purging, the background signals were always comparable to background signals observed during direct injection of zero air without a long inlet line for the m/z ion peaks reported in this work. Bearing in mind that the ambient air (range of ambient temperature: 5–15^{0}C) was drawn in under 25 seconds (residence + sampling time; determined by spiking the inlet with sesquiterpenes emitted from an orange peel) into the PTR-TOF-MS, the probability of inlet effects for sticky compounds is not high. In any case, the part of the inlet line that was indoors was well insulated and heated to 40^{0}C all the time to ensure there were no condensation effects. Instrumental background checks using zero air were performed at intervals of 3–4 days during the campaign.

Data acquisition of mass spectra was accomplished using the TofDaq software (version 1.89; Tofwerk AG, Switzerland). This software controls the timing of the pulser (used to pulse the ions produced in the drift tube and channel them into the time-of-flight region) and stores the raw data as a series of mass spectra in HDF5 format along with relevant instrumental metadata. The raw mass spectral data was then analyzed using the PTRMS-viewer software (version 3.1; Ionicon Analytic GmbH, Innsbruck, Austria) enabling peak search, peak fits and mass assignments. Mass axis calibration was accomplished using the following intrinsic ions: $H_3^{18}O^+$ (monoisotopic mass 21.022) and $H_3^{18}O^+.H_2O$ (monoisotopic mass 39.033). In addition the transmission values of benzene (m/z = 79.054), toluene (m/z = 93.070), xylenes (m/z = 107.086), trimethylbenzenes (m/z = 121.101), dichlorobenzene (m/z = 146.976) and trichlorobenzene (m/z = 180.937) were employed. Further analysis of the dataset was carried out using the IGOR Pro software (version 6.0; WaveMetrics, Inc.).

The instrument was calibrated twice (10 January 2013 and 15 January 2013) during the

field deployment by dynamic dilution of VOCs using a 17-component VOC gas standard (Ionimed Analytik GmbH, Austria at $\sim$ 1ppm; stated accuracy better than 8%). Calibration for these seventeen VOCs namely formaldehyde, methanol, acetonitrile, acetaldehyde, ethanol, acrolein, acetone, isoprene, methacrolein, 2-butanone, benzene, toluene, o-xylene, chlorobenzene, α-pinene, 1, 2-dichlorobenzene and 1, 2, 4-trichlorobenzene were carried out in the range of 2–10 ppb at various relative humidities (RH = 60, 75 and 90%). RH was controlled as per the details provided in Kumar and Sinha. (2014). In order to determine the instrumental background at all relevant m/z channels, VOC free zero air was produced by passing ambient air through an activated charcoal scrubber (Supelpure HC, Supelco, Bellemonte, USA) and a VOC scrubber catalyst maintained at 350^0C (GCU-s 0703, Ionimed Analytik GmbH, Innsbruck, Austria). Following the procedure of Stockwell et al. (2015), the measured ion signals were normalized to H_3O^+ (m/z = 19) primary ions according to the following equation:

$$\text{ncps} = \frac{I(\text{RH}^+) \times 10^6}{I(\text{H}_3\text{O}^+)} \times \frac{2}{P_{\text{drift}}} \times \frac{T_{\text{drift}}}{298.15} \tag{4.1}$$

The two calibration experiments made during the course of the campaign did not change the VOC sensitivities (values were within the precision error) as instrumental operational conditions were not changed. Usually, the sensitivity response of VOCs in a PTR-MS remain remarkably stable if instrumental operational conditions are not changed. This is borne by several previous studies (de Gouw and Warneke., 2007) including our own group's recent studies in the South Asian environment which involved a three year study (Chandra and Sinha, 2016) and a month long study (Sinha et al., 2014). Large changes in ambient humidity are known to affect the sensitivity of some VOCs (e.g. benzene, methanol). This occurs due to a change in the abundance and ratio of the primary reagent ions (H_3O^+; m/z = 19) and the hydrated hydronium ions ($H_3O^+.H_2O$; m/z = 37) within the drift tube (de Gouw et al., 2003). It assumes importance when ambient RH has large variability (e.g. very dry $<$ 20% RH to very humid $>$ 80% RH) during the measurements (e.g. during airborne measurements) and when the ratio of m37/m19 in the drift tube is typically more than 10%. For the measurements reported in this study, the ratio of the hydrated hydronium ions ($H_3O^+.H_2O$; nominal m/z = 37) to the primary ions (H_3O^+;

Table 4.1: Principal operational settings for PTR-TOF-MS parameters

Parameter	Value
Overall drift voltage (U_{drift})	600 V
Temperature at drift tube (T_{drift})	60 °C
Pressure at drift tube (P_{drift})	2.2 mbar
Length of the drift tube (L_{drift})	9.3 cm
Reaction Time (t)	92 µs
Field strength of the drift tube (E/N)*	135 Td

*E is the electric field strength (V cm^{-1}) and N is the gas number density (molecule cm^{-3}), 1 Td = 10^{-17} V cm^2 $molecule^{-1}$

nominal m/z = 19) was lower than 10%, for more than 92% of the dataset and the ratio never exceeded 16%. For the conditions during the campaign, our calibration experiments did not reveal significant humidity dependence for the VOC sensitivities (ncps ppb^{-1}). Moreover, as reported in de Gouw and Warneke. (2007) and Sinha et al. (2009), it is the absolute humidity content of the sampled air rather than the RH, which is responsible for changes in detection sensitivity of certain VOCs within the PTR-MS. The sensitivity dependence has been reported in numerous studies as function of RH because RH is more frequently used in meteorology and for no changes/small changes in temperature, RH is a good proxy of the absolute humidity. We note that during the Kathmandu deployment, while the RH variability was large (35% - 100%) most of the RH change was on account of changes in the ambient temperature rather than changes in absolute humidity of sampled air. The variability in the absolute humidity was only in the range of 20% between 19 December 2012 and 30 January 2013. Figure 4.3 shows the sensitivities (ncps ppb^{-1}) for acetonitrile (a biomass burning tracer), acetaldehyde (an oxygenated compound), isoprene (a biogenic tracer) and benzene (an aromatic compound) at different RH regimes (60, 75 and 90%) during the calibration experiments. In all cases an excellent linearity (r^2 = 0.99) was observed. Hence the sensitivity (ncps ppb^{-1}) derived at 90% RH was applied for converting the measured normalized counts per second to ppb and no further humidity corrections were deemed necessary. In order to derive the sensitivity for the sum of monoterpenes, which have a molecular ion peak at m/z = 137.132 and for which fragmentation results in ion signals at m/z 81.070 and m/z 137.132, the signal measured at m/z 137.132 was scaled by 2.63, as calibrations at the instrumental settings employed in the study clearly showed that 38% of the total molecular ion signal for monoterpene was

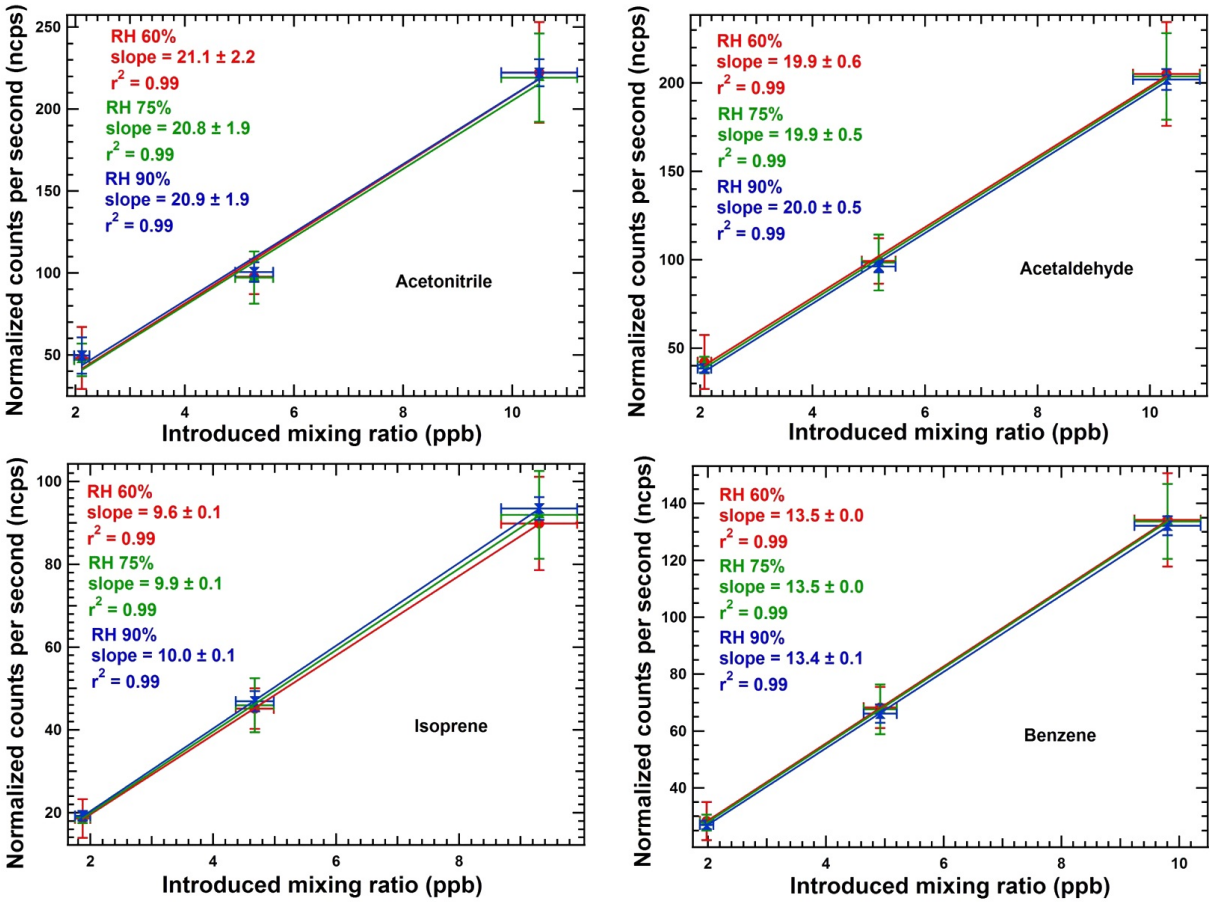

Figure 4.3: Compound specific normalized sensitivities at different relative humidities (RH 60%, 75% and 90%) for acetonitrile, acetaldehyde, isoprene and benzene during the calibration experiment performed on 10 January 2013. Horizontal bars reflect the error due to the MFC flows and the accuracy of the VOC gas standard whereas vertical bars reflect the precision error (2σ) of the measurements

detected at m/z = 137.132, consistent with fragmentation patterns reported previously by Tani et al. (2004) for similar reaction conditions in the drift tube.

Variable background concentrations were observed for both formaldehyde and methanol while sampling zero air during the calibration experiments. Hence for these two compounds and all the other compounds not present in the 17 component VOC gas standard but reported in this work, sensitivity factors were determined following the example of Stockwell et al. (2015), wherein calculated mass-dependent calibration factors based on linearly approximated transmission curve fits for oxygenated VOCs and hydrocarbons were employed. Figure 4.4a shows the linearly fitted mass-dependent transmission curve (black markers and dotted line) overlaid with the sensitivity factors of the calibrated

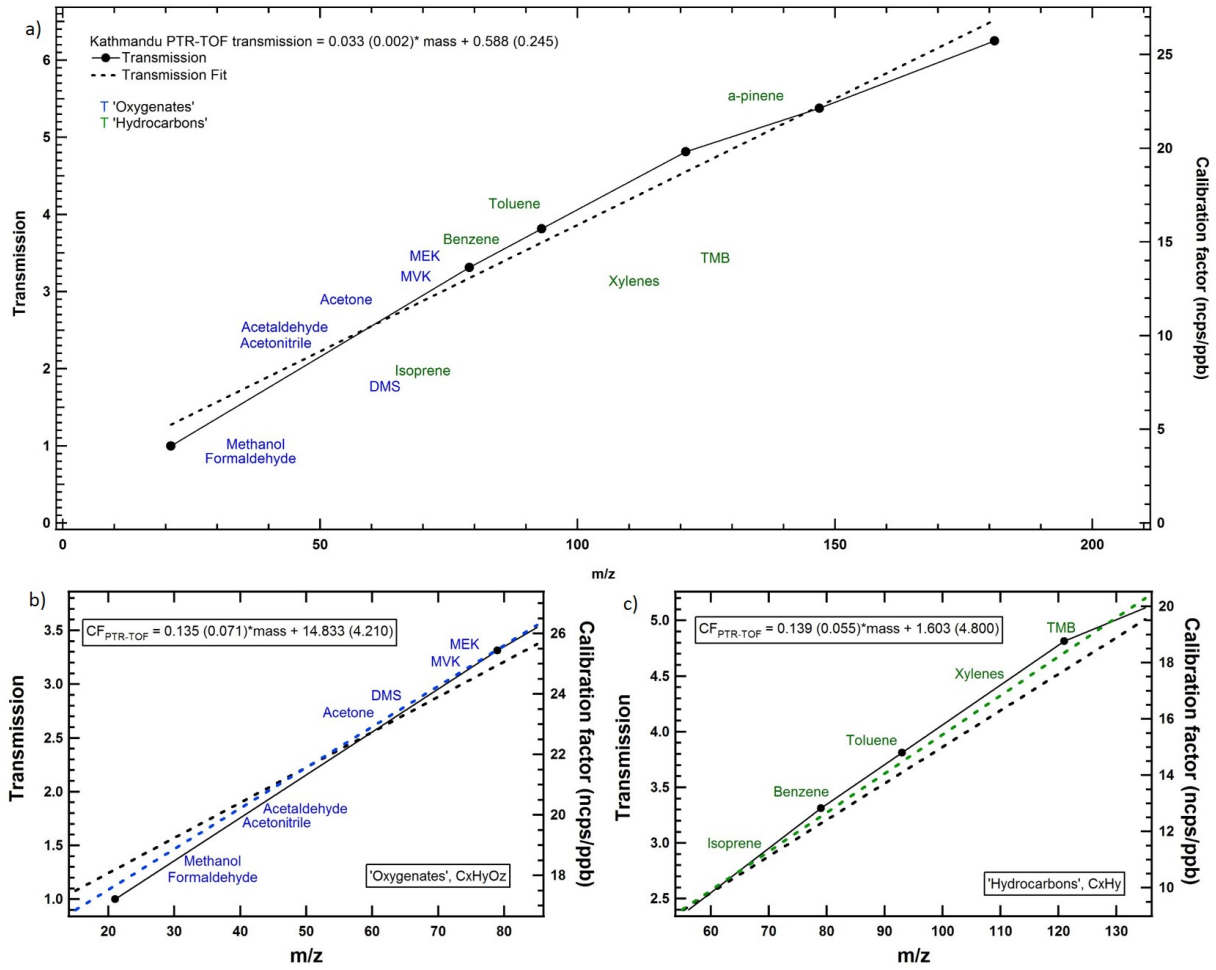

Figure 4.4: a) Normalized response of calibration factors ("CF", ncps ppb^{-1}) vs mass (calibrated species labeled by name) overlaid with linearly fitted mass-dependent transmission curve (black markers and dotted line). Approximate calibration factors for all observed masses where explicit calibrations were not available were determined using separate linear approximations namely b) oxygenated (blue) and c) hydrocarbon (green) species

compounds. Using linear approximations, mass-dependent calibration factors were determined separately for oxygenates (Figure 4.4b) and hydrocarbons (Figure 4.4c) in keeping with their different mass dependent behavior. For masses with heteroatoms other than oxygen, mass-dependent sensitivity factors were determined based on approximations used for the oxygenated compounds. For acetic acid, the sum of the signals at m/z = 61.207 (parent ion peak) and m/z = 43.018 (fragment of the parent ion), were used to derive an upper limit for its ambient concentration.

The limit of detection was defined to be 2σ of the measured normalized signal (ncps) while

measuring VOC free zero air divided by the sensitivity expressed in ncps ppb^{-1} (Sinha et al., 2014). The total uncertainty for calibrated compounds was calculated using the root mean square propagation of the accuracy error of the VOC standard, the mass flow controller's flow fluctuations during the calibration and the instrumental precision error (2σ while measuring 2 ppb of the compound). Using this approach, all calibrated VOCs had a total uncertainty of $< 20\%$ (e.g., acetaldehyde 9.9%, acetone 9.6%, isoprene 15.4%, benzene 9.4% and toluene 8.9%) whereas for the other compounds reported in this work that could not be calibrated, we estimate an overall uncertainty of $\sim$50% as also proposed by Stockwell et al. (2015) using a similar approach for quantification.

4.4 Results and discussion

4.4.1 Identification of VOCs present in ambient air using PTR-TOF-MS mass scans

The PTR-TOF-MS deployed in this study was operated over the range of 21–210 Th, with a mass resolution ($m/\Delta m > 4200$ at m/z = 21.022 and > 4800 at m/z = 205.195) sufficient to identify several compounds based on their monoisotopic masses. A maximum of 71 ion peaks (m/z) were observed in the mass spectra during the measurement period for which the measured ambient concentrations exceeded the detection limit. Among these 71 species, 37 compounds/species had an average concentration greater than or equal to 200 ppt during the study period. The molecular formula of compounds/species corresponding to these 37 ion peaks are listed in Table 4.2. Additionally Table 4.2 also provides: (1) identity of plausible organic/fragment ions (e.g. NO_2^+ due to C1–C5 alkyl nitrates), (2) sensitivity, (3) limit of detection, and (4) average $\pm 1\sigma$ variability of ambient mixing ratios observed during the study period.

In order to minimize ambiguity arising due to multiple species or fragment ions contributing to ion peaks at a given m/z ratio, the following quality control measures were employed for attribution of mass identifications to the observed ion peaks: (1) Ion peaks for which the observed mass spectra had competing/major shoulder peaks in a mass bin width of 0.005 amu centred at the relevant monoisotopic ion peak were excluded from

exclusive mass assignments (2) Next, the ambient time series of the observed ion peak assigned after step 1, was carefully examined and cases where the concentration profile was completely flat/showed no ambient variability were also excluded from mass assignments (3) Thirdly, the concentration profiles of the ion peaks ascribed to rarely reported or new compounds after step 1 and step 2, were compared to the ambient time series and diel profiles of more frequently/regularly quantified VOCs, such as acetonitrile, isoprene, benzene, toluene, acetone and acetaldehyde as their diel profiles would likely indicate the driving processes and emission sources of the compounds. During the PTR-TOF-MS field deployment, instrumental background checks revealed backgrounds as high as 170 ppt at certain m/z channels (e.g. m/z 125.958, m/z 90.947, m/z 108.957). Therefore, the 200 ppt cut off was chosen as an additional quality control measure so as to ensure attribution of ion peaks in the mass spectra only to the compounds present in the ambient air and not due to instrumental reasons. The 37 compounds that were identified accounted for 86.7% of the total mass due to all 71 ion peaks detected in the mass spectra.

Table 4.2: Most likely identity of VOCs (having average mixing ratios > 0.2 ppb) detected at specific protonated m/z ratios, molecular formula, likely mass assignment, reference of previous mass assignment, sensitivity, limit of detection (LOD), average ambient mixing ratios (± 1σ)

Protonated m/z or ion	Formula	Most Likely Identity	References of some previously reported studies	Sensitivity (ncps ppb^{-1})	LOD (ppb)	Average (Sdev) mixing ratio (ppb)
28.007	HCN	Hydrogen Cyanide	Stockwell et al. (2015); Karl et al. (2003)	18.48	0.241	1.56 (0.24)
31.018	HCHO	Formaldehyde	Inomata et al. (2010); Stockwell et al. (2015)	18.88	0.103	1.78 (0.50)
33.034	CH_3OH	Methanol	Seco et al. (2011); de Gouw et al. (2003)	19.16	0.090	7.42 (1.28)
41.039	C_3H_4	Propyne	Akagi et al. (2011); Stockwell et al. (2015)	7.17	0.080	7.67 (1.80)
42.034	CH_3CN	Acetonitrile*	Seco et al. (2011); de Gouw et al. (2003)	20.91	0.043	1.08 (0.38)
43.055	C_3H_6	Propene	Stockwell et al. (2015); Park et al. (2013)	7.45	0.048	3.98 (1.21)
44.014	NHCO	Isocyanic acid	Warneke et al. (2011)	20.64	0.067	0.90 (0.08)
45.033	C_2H_4O	Acetaldehyde*	de Gouw et al. (2003); Seco et al. (2011)	20.04	0.262	8.81 (4.58)
45.990	NO_2^+	Nitronium ion from fragmentation of C1-C5 alkyl nitrates	Aoki et al. (2007)	20.91	0.094	1.08 (0.24)
46.029	CH_3NO	Formamide		20.91	0.093	0.76 (0.16)
47.013	CH_2O_2	Formic acid	Jordan et al. (2009); Williams et al. (2001)	21.04	0.041	4.96 (1.02)
47.049	C_2H_6O	Ethanol	Park et al. (2013); Seco et al. (2011)	21.05	0.361	1.59 (0.85)
51.044	C_4H_2	1,3-Butadiyne#	Yokelson et al. (2013)	8.56	0.013	0.67 (0.14)
56.060	C_3H_5N	Propanenitrile#	Yokelson et al. (2013)	22.27	0.022	0.21 (0.05)
57.034	C_3H_4O	Acrolein*+ Methylketene	Stockwell et al. (2015); Jordan et al. (2009)	22.26	0.034	0.80 (0.26)
59.049	C_3H_6O	Acetone*+ Propanal	de Gouw et al. (2003); Seco et al. (2011)	23.47	0.074	4.21 (0.65)
60.051	C_2H_5NO	Acetamide		22.80	0.069	0.39 (0.05)

61.027	$C_2H_4O_2$	Acetic acid (sum of parent ion contributions at m/z 61.027 and fragment ion contributions at m/z 43.018)	de Gouw and Warneke. (2007); Stockwell et al. (2015); Seco et al. (2011)	22.94	0.440	7.46 (2.93)
62.026	CH_3NO_2	Nitromethane[@]	Inomata et al. (2014); Akagi et al. (2013)	23.07	0.020	0.24 (0.08)
63.026	C_2H_6S	Dimethyl Sulfide	Akagi et al. (2011); Park et al. (2013)	23.21	0.049	0.26 (0.03)
67.054	C_5H_6	1,3-Cyclopentadiene	Stockwell et al. (2015)	10.78	0.008	0.23 (0.06)
69.033	C4H_4O	Furan	Stockwell et al. (2015); Jordan et al. (2009)	24.02	0.009	0.46 (0.17)
69.070	C_5H_8	Isoprene*	Stockwell et al. (2015); de Gouw et al. (2003); Seco et al. (2011)	10.02	0.013	1.11 (0.24)
71.049	C_4H_6O	Methylvinylketone; Methacrolein; Crotonaldehyde*	Seco et al. (2011); Stockwell et al. (2015); de Gouw and Warneke. (2007)	27.17	0.017	0.35 (0.10)
73.027	$C_3H_4O_2$	Methylglyoxal	Stockwell et al. (2015); Müller et al. (2012)	24.56	0.021	0.31 (0.10)
73.063	C_4H_8O	Methylethylketone*	de Gouw et al. (2003); Stockwell et al. (2015); Park et al. (2013)	21.91	0.036	0.69 (0.12)
75.042	$C_3H_6O_2$	Hydroxyacetone	Christian et al. (2003); Heigenmoser et al. (2013); Stockwell et al. (2015)	24.83	0.066	0.63 (0.18)
79.054	C_6H_6	Benzene*	Jordan et al. (2009); de Gouw et al. (2003)	13.43	0.013	2.71 (1.17)
83.085	C_6H_{10}	Assorted Hydrocarbons	Stockwell et al. (2015)	13.01	0.008	0.45 (0.09)
87.042	$C_4H_6O_2$	2,3-Butanedione	Stockwell et al. (2015); Karl et al. (2007)	26.45	0.028	0.35 (0.08)
93.070	C_7H_8	Toluene*	Seco et al. (2011); Jordan et al. (2009)	15.78	0.006	1.53 (0.38)
97.031	$C_5H_4O_2$	2-Furaldehyde (furfural)	Ruuskanen et al. (2011); Liu et al. (2012); Li et al. (2013)	27.80	0.010	0.26 (0.07)

97.102	C_7H_{12}	Assorted Hydrocarbons	Stockwell et al. (2015)	14.96	0.006	0.23 (0.05)
105.070	C_8H_8	Styrene	Jordan et al. (2009); Stockwell et al. (2015)	16.07	0.004	0.21 (0.08)
107.086	C_8H_{10}	Xylenes*	Jordan et al. (2009); Stockwell et al. (2015)	15.36	0.004	0.97 (0.27)
121.101	C_9H_{12}	Trimethylbenzenes	Müller et al. (2012); Jordan et al. (2009)	18.30	0.004	0.38 (0.10)
129.070	$C_{10}H_8$	Naphthalene	Jordan et al. (2009); Stockwell et al. (2015)	19.40	0.009	0.33 (0.09)

* VOC sensitivities determined using VOC gas standards in calibration experiments; # Observed mass accuracy for 1,3-Butadiyne and Propanenitrile were 21 mDa and 10 mDa, respectively; @ Corrected for the ^{13}C isotopologues of acetic acid.

In cases, where the contributions of isotopologues were significant (e.g., acetic acid m/z = 61.027 and nitromethane m/z = 62.026), the signal at the concerned m/z was duly corrected (Inomata et al., 2014). Potential interferences due to isotopic contributions (e.g. ^{13}C) were also corrected whenever applicable. Out of these 37 ions which were identified with reasonable confidence, 8 contained nitrogen, 15 were oxygenated compounds, 13 were hydrocarbons and one contained sulfur. Two ion peaks (m/z = 51.044 and m/z = 56.060) could not be identified based on the exact protonated monoisotopic m/z and for these, the closest contenders namely 1,3-butadiyne (m/z = 51.023) and propanenitrile (m/z = 56.050), were tentatively assigned. Two "new" compounds, which to the best of our knowledge have not been reported in any previous study, namely - formamide (CH_3NO; protonated m/z = 46.029) and acetamide (C_2H_5NO; protonated m/z = 60.051) were also detected. We discuss their diel variability and potential sources in Section 4.4.5 along with some of the other rarely reported compounds in ambient air. Figure4.5 shows illustrative mass spectra for isocyanic acid which demonstrates that it is the major contributor in the relevant mass bin. Considering that some loss of isocyanic acid can occur due to hydrolysis in the drift tube, our measurements maybe a lower limit of the ambient concentrations of isocyanic acid.

The total reactive carbon calculated as the sum of the average mixing ratios of all the 37 compounds reported in this study was 175.8 ppbC, of which fifteen compounds alone contributed 145.4 ppbC (83% of the total) and are listed in Table 4.3. Propyne, acetaldehyde, benzene, acetic acid, acetone, propene and toluene collectively composed more than 60% of the measured reactive carbon. In Sections 4.4.2 and 4.4.4, we examine the general

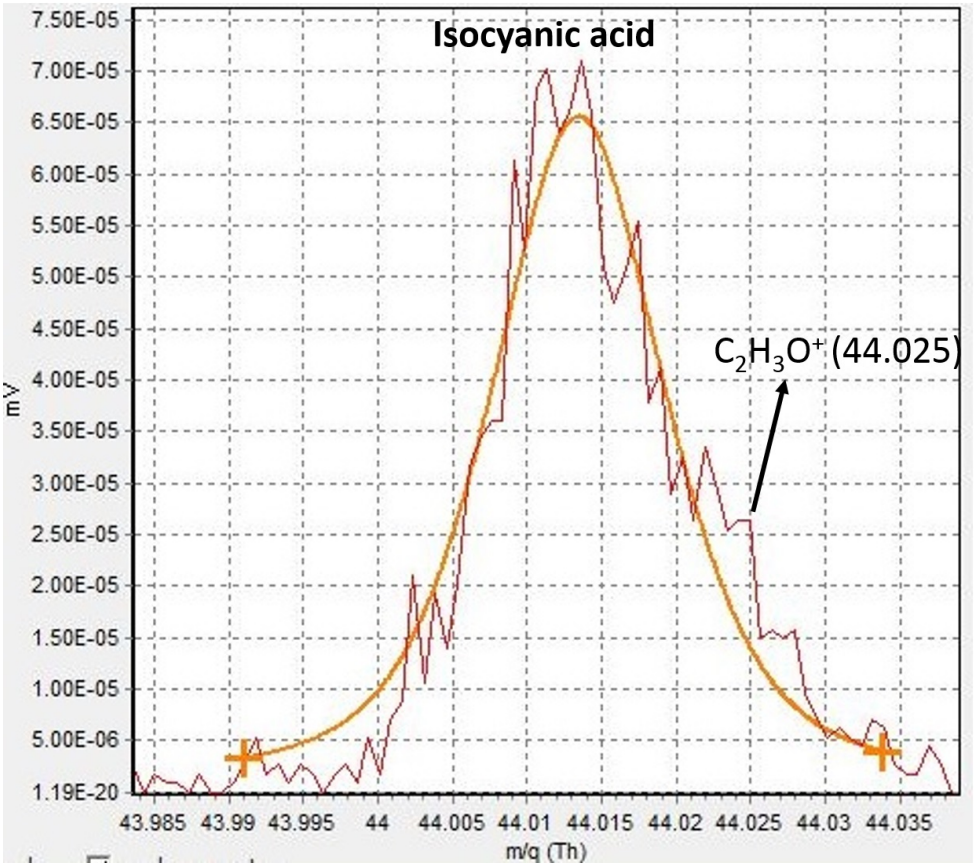

Figure 4.5: Illustrative mass spectra (30 second average) of isocyanic acid obtained at 09:24 LT on 13 January 2013

Table 4.3: Top fifteen contributing VOCs to the total reactive carbon during SusKat-ABC campaign

VOCs	Campaign average reactive carbon (ppbC)	Percentage contribution to total reactive carbon
Propyne	23.01	13.1%
Acetaldehyde	17.62	10.0%
Benzene	16.26	9.2%
Acetic acid	14.92	8.5%
Acetone	12.63	7.2%
Propene	11.94	6.8%
Toluene	10.71	6.1%
Xylenes	7.76	4.4%
Methanol	7.42	4.2%
Isoprene	5.55	3.2%
Formic acid	4.96	2.8%
Trimethylbenzenes	3.42	1.9%
Naphthalene	3.30	1.9%
Ethanol	3.18	1.8%
MEK	2.76	1.6%

trends and diel concentration profiles of the most abundant VOCs to gain more detailed insights into the emission sources and chemistry of VOCs in wintertime air of the Kathmandu Valley.

4.4.2 General trends in VOC concentrations during the SusKat-ABC campaign

Figure 4.6 shows the general trends in VOC mixing ratios (as 1 min temporal resolution data) during the period of study from 19 December 2012–30 January 2013. While the top panel represents the time series in mixing ratios of oxygenated VOCs namely methanol, acetaldehyde and the sum of acetone and propanal, the second and third panels show mixing ratios of isoprene, acetonitrile and furan, respectively. The bottom panel shows the mixing ratios of benzene, toluene, sum of C8-aromatics (xylenes and ethylbenzene), and sum of C9-aromatics (trimethylbenzenes and propylbenzenes). All these compounds collectively accounted for about 50% (total 85.4ppbC) of the total reactive carbon and are amongst the most abundant VOCs known to be present in the air influenced by urban emissions.

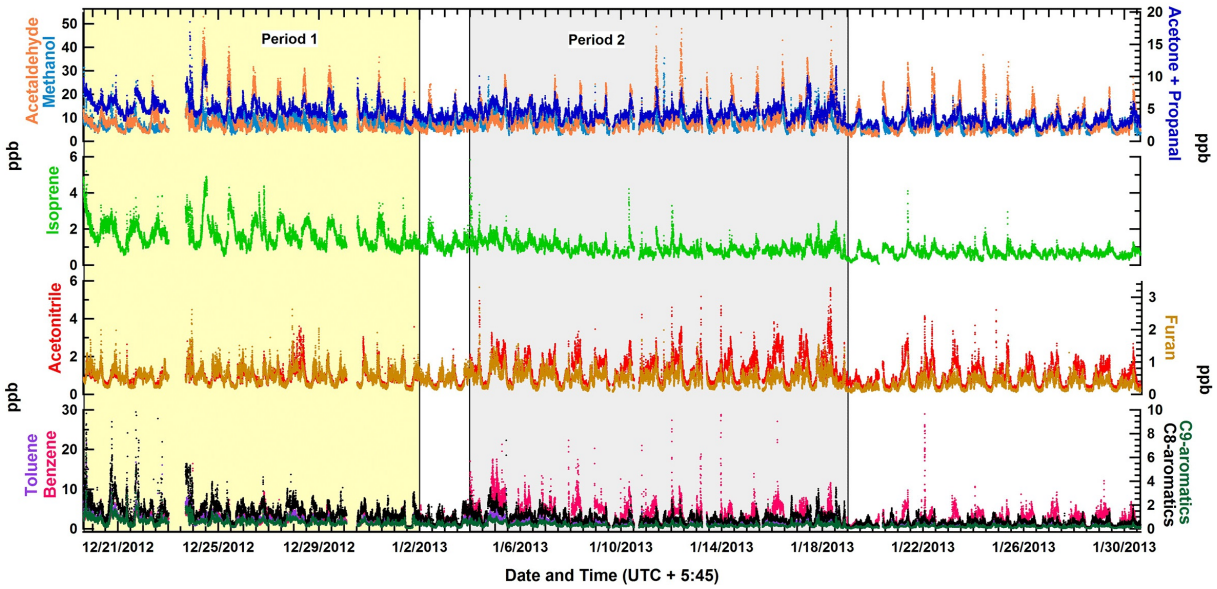

Figure 4.6: Time series of one minute time resolution data for the mixing ratios of methanol, acetaldehyde, and the sum of acetone and propanal (top panel); isoprene (second panel from top); acetonitrile and furan (second panel from bottom); benzene, toluene, the sum of C8-aromatics (xylene isomers and ethyl benzene) and the sum of C9-aromatics (isomers of trimethylbenzenes and propylbenzenes) (bottom panel) during SusKat-ABC campaign

It can be seen that the time series was characterized by two contrasting periods in terms of chemical emission signatures: period 1 (shaded in pale yellow in Figure 4.6; 19 December 2012–2 January 2013) and period 2 (shaded in grey in Figure 4.6; 4–18 January 2013). period 1 was characterized by high mixing ratios of isoprene ($>$ 3ppb) during daytime and low acetonitrile mixing ratios relative to the remainder of the measurement period (generally $<$ 2 ppb except for a plume on 28 December 2015 which was suspected to be due to garbage burning in the local vicinity), while period 2 was marked by a decrease in the amplitude of daytime isoprene and a significant increase in mixing ratios of acetonitrile (typically $>$ 3 ppb) and benzene (typically $>$ 10 ppb). The global budget of isoprene is dominated by emission from vegetation (500 Tg a^{-1}; Guenther et al., 2006), in most cases as a function of photosynthetic active radiation (PAR) and temperature. Clearly, in the early part of this winter campaign, conditions were favourable for significant isoprene emissions from vegetation. It is worth mentioning that oak and *Melia azedarach* were present in the forested regions upwind of the site and are high isoprene emitters (Geron et al., 2001). As the ambient temperature and radiation decreased and

early morning fog became frequent during the first half of January, biogenic emissions reduced in intensity (< 2 ppb). Leaf fall in deciduous trees by the end of December and more frequent leaf litter burning were likely important contributors to reduced isoprene and increased acetonitrile emission in the second half of the campaign. While the highest isoprene concentrations were driven by biogenic sources, biomass burning sources also emitted isoprene, a finding consistent with reports from another South Asian site at Mohali, India (Sinha et al., 2014).

All the brick kilns in the Kathmandu Valley are Fixed Chimney Bull Trench Brick Kilns (FCBTK), except for one Vertical Shaft Brick Kiln (VSBK) and two Hoffmann design brick kilns. FCBTKs are operated around the clock, from the first week of January to mid-April, according to our survey. Thus, our deployment fortuitously was able to contrast the periods marked by the presence and almost complete absence of operational brick kilns in the fetch region of our measurement site. Most open burning and cooking activities remain similar in December and January. Due to reduced leaf fall in January (leaf fall of deciduous trees picks up in November and peaks in December) the open burning of leaf litter with other waste is generally less in January. With regard to increased open biomass burning from other sources in January, the first week of January was the coldest period of the deployment, so one could hypothesize that the higher emissions in this period were due to more open fires being lit to keep warm. However as can be seen in Figure 4.6, the biomass burning emissions were much higher for most of January (including a rain event during 18 January 21:00 LT – 19 January 01:00 LT). Thus, the brick kiln activity is the singular feature that is prominently different between both the periods.

To the best of our knowledge and survey, the fuel burnt in the brick kilns does not differ much between the brick kilns though the type of bio-fuel employed during different times in a year can vary depending on the availability and abundance of certain types of bio-fuel. One common biofuel used in the brick kilns is the seed of the lapsi fruit (*Choerospondias axillaris*). This emission activity appears to have been captured quite well in the time series profile of acetonitrile, for which the major emission source is biomass burning ((Holzinger et al., 1999; Sinha et al., 2014), Chapter 3). It was also interesting to note the similarities in the time series of furan ($\sim$ 1 ppb), another combustion tracer, with acetonitrile. Biomass burning and biofuel use contribute to half of the global budget of

benzene ((Henze et al., 2008; Andreae and Merlet., 2001), Chapter 3) and it appears that brick kilns in Kathmandu being co-fired with biomass as fuel were a major source of benzene. A recent study by Al-Naiema et al. (2015) reported reduction in emissions (∼40% reduction of fossil CO_2, particulate matter and heavy metal emissions) when co-firing of oat hull biomass with coal was carried out for generation of electricity in the United States. We note that the case study did not investigate co-emission of toxic VOCs such as isocyanic acid, formamide, acetamide, nitromethane and naphthalene which were associated with emissions from biomass co-fired brick kilns in the Kathmandu Valley. A study conducted by Clean Energy Nepal (Raut., 2003) showed that 8 h averaged concentrations of air pollutants such as Total Suspended Particulate (TSP), PM_{10}, SO_2 and NO_x were three times higher during the brick kiln operating period relative to the period they were not operational at the same location. Significant differences exist between the electricity generation unit studied by Al-Naiema et al. (2015) and the typical biomass co-fired brick kilns that dot the Kathmandu Valley in terms of design, combustion efficiency, biomass fuel being co-fired and the end application. Thus though the same word "co-firing" is used colloquially, these are really different from an operational and environmental standpoint, with one being an efficient closed unit set up that employs good scrubbers whereas the other has numerous vents and combustion characteristics that are hardly comparable.

It is also worth mentioning that the hotspot and regional haze imagery obtained using MODIS Terra satellite (at a spatial resolution of 500 m and time resolution of 5 minutes at 05:00–06:00 LT) between 19 December 2012–30 January 2013 (data accessed at NASA worldview; http://worldview.earthdata.nasa.gov/) were similar except for a 6 day period (12–17 January 2013), wherein the regional haze was stronger. We note that calmer meteorological conditions could be a potential contributory factor for stronger haze in this period. The MODIS satellite image did not detect any active fire counts (at greater than 85% confidence limit) over the Kathmandu Valley (latitude 27.7^0N) during the whole campaign period (19 December 2012–30 January 2013). Thus, the higher chemical concentrations observed from 4–18 January and even later, appear to be linked to the re-start of the biomass co-fired brick kilns and cannot be explained by linkages with regional haze or increased open burning of biomass, considering the available evidence. We analyze the diel profiles for the two contrasting periods and some of these aspects in detail in Section

4.4.4.

In the time series it can also be seen that 19 January 2013 was characterized by the lowest VOC concentrations because of an intense rain event during the previous night. When considering the entire study period, high concentrations of OVOCs were typically observed in the early morning hours between 08:00–10:00 LT and surprisingly acetaldehyde, which is the most reactive VOC among the OVOCs, frequently reached concentrations as high as 40 ppb. In contrast methanol and the sum of acetone and propanal were generally below 20 and 10 ppb, respectively. Peak acetaldehyde concentrations of about 30–40 ppb were observed in the time series. These often correlated with peaks in the concentrations of acetonitrile and furan (chemical tracers for combustion) between 4 January 2013 and 30 January 2013 and occasionally with peaks in daytime isoprene concentrations before 2 January 2013. Biomass burning sources and photooxidation of precursor compounds co-emitted from the biomass burning appear to contribute significantly to the high concentrations of oxygenated VOCs. This points to the fact that the major sources of oxygenated VOCs during wintertime in Kathmandu are different from what are generally considered to be the most important sources based on studies conducted in several other regions of the world, where photooxidation and industrial sources dominate and has large implications for wintertime oxidation chemistry in the Valley, as these species play a key role in radical chemistry (Singh et al., 1995). For example, the observed ranking in oxygenated VOCs is different from the ranking observed during wintertime in megacities like Paris and London (methanol > acetaldehyde > acetone) (Dolgorouky et al., 2012; Langford et al., 2010). Furthermore the ranking observed for aromatic VOCs during this study (benzen > toluene > C8-aromatics > C9-aromatics) was in contrast to the ranking (toluene > benzene > C8-aromatics > C9-aromatics) observed in several urban sites such as Paris, London and Tokyo (Dolgorouky et al., 2012; Langford et al., 2010; Yoshino et al., 2012). This exemplifies that the nature and strength of emission sources for oxygenated and aromatic VOCs in the Kathmandu Valley differ from several urban areas in other parts of the world. Biomass burning sources and the manner in which regulation of benzene occurs, are likely the major causes for the observed differences.

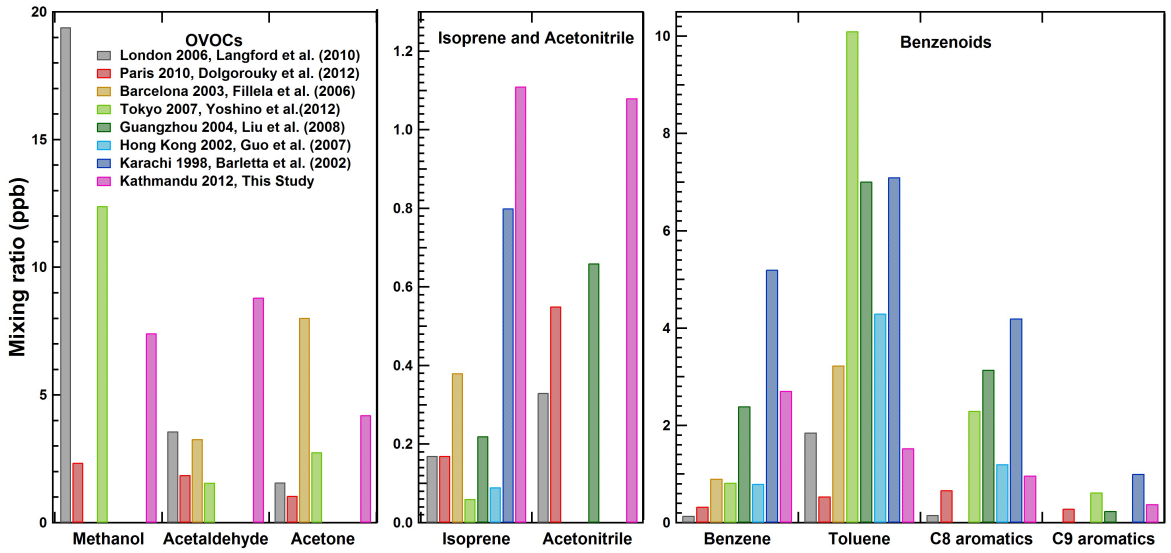

Figure 4.7: Comparison of wintertime VOC mixing ratios measured in the Kathmandu Valley with wintertime VOC mixing ratios at selected urban sites elsewhere in the world

4.4.3 Comparison with wintertime VOC mixing ratios elsewhere

Figure 4.7 provides a comparison of average VOC mixing ratios measured in the Kathmandu Valley with VOC mixing ratios reported at other urban or urban influenced environments including megacities, during winter season. The concentration ranking in the average VOC mixing ratios during our wintertime deployment was acetaldehyde (8.8 ppb)> methanol (7.4 ppb)> acetone + propanal (4.2 ppb)> benzene (2.7 ppb) > toluene (1.5 ppb)> isoprene (1.1 ppb)> acetonitrile (1.1 ppb)> C8-aromatics ($\sim$ 1 ppb) > furan ($\sim$ 0.5ppb)> C9-aromatics (0.4 ppb). As can be seen from Figure 4.7, when compared to average wintertime mixing ratios reported from several sites elsewhere in the world, the mixing ratios of acetaldehyde ($\sim$ 9 ppb), acetonitrile ($\sim$ 1 ppb) and isoprene ($\sim$ 1 ppb) in the Kathmandu Valley are among the highest measured anywhere in the world. In contrast, Kathmandu had lower methanol mixing ratios than measured in London and Tokyo (Langford et al., 2010; Yoshino et al., 2012) during winter 2006 and 2007 (19.4 and 12.4 ppb, respectively) as well as lower acetone mixing ratios than what was measured in Barcelona (8 ppb) (Filella and Peñuelas., 2006). Apart from the contribution of biogenic sources during daytime, which was major, isoprene was also emitted by biomass combustion sources in the Kathmandu Valley. Borbon et al. (2001) have previously reported that

due to traffic emissions alone, isoprene mixing ratios can reach as high as 1.8 ppb in urban areas. The Bode site was located in the outflow of Kathmandu metropolitan city and Lalitpur sub-metropolitan city and therefore the evening time increase in isoprene can also be partially due to traffic emissions during the evening rush hour. The average benzene concentrations in Kathmandu ($\sim$ 3 ppb) were notably higher than those reported in other cities except for the city of Karachi (Barletta et al., 2002). The average toluene and sum of C8-aromatics mixing ratios, however were lower than in other urban areas like Tokyo (Yoshino et al., 2012), Barcelona (Filella and Peñuelas., 2006), Karachi (Barletta et al., 2002), Hong Kong (Guo et al., 2007) and Guangzhou (Liu et al., 2008), where industrial and traffic sources are much larger than in Kathmandu. Whereas benzene is emitted in almost equal proportion from fossil fuel and biomass combustion sources (Henze et al., 2008), fossil fuel combustion and industrial processes contribute a much larger fraction to the global budgets of toluene and sum of C8 and C9-aromatics. The observed trend in concentrations of some of the aromatic compounds measured using PTR-TOF-MS in this study differs from the trend reported in a previous study by Yu et al. (2008) who employed the long path differential optical absorption spectroscopy (DOAS) technique to make measurements of monoaromatic VOCs in Kathmandu during winter 2003. In that study, xylene (a C8-aromatic compound) concentrations were reported to be the highest followed by toluene and benzene respectively. We think two reasons are responsible for differences from that study. The first reason is that the measurements by Yu et al. (2008) were carried out near a fairly busy road (Chabahil-Bouddha-Jorpati road) and a traffic intersection (Chabahil-Ringroad intersection) and consequently the aromatic VOC concentrations were primarily influenced by traffic sources. Secondly, VOC measurements using the long path DOAS technique are reported to have potentially large interferences due to ambient ozone and suspended particles (Yu et al., 2008).

Despite much larger population and more industries compared to Kathmandu, wintertime measurements in the megacities of London (Langford et al., 2010) and Paris (Dolgorouky et al., 2012) suggest that the air is much cleaner for many of the VOCs shown in Figure 4.7. The combination of the topography of Kathmandu (which results in suppressed ventilation) and the anthropogenic and biogenic emissions within the Valley appear to cause high ambient wintertime concentrations for several VOCs (e.g. acetonitrile, ac-

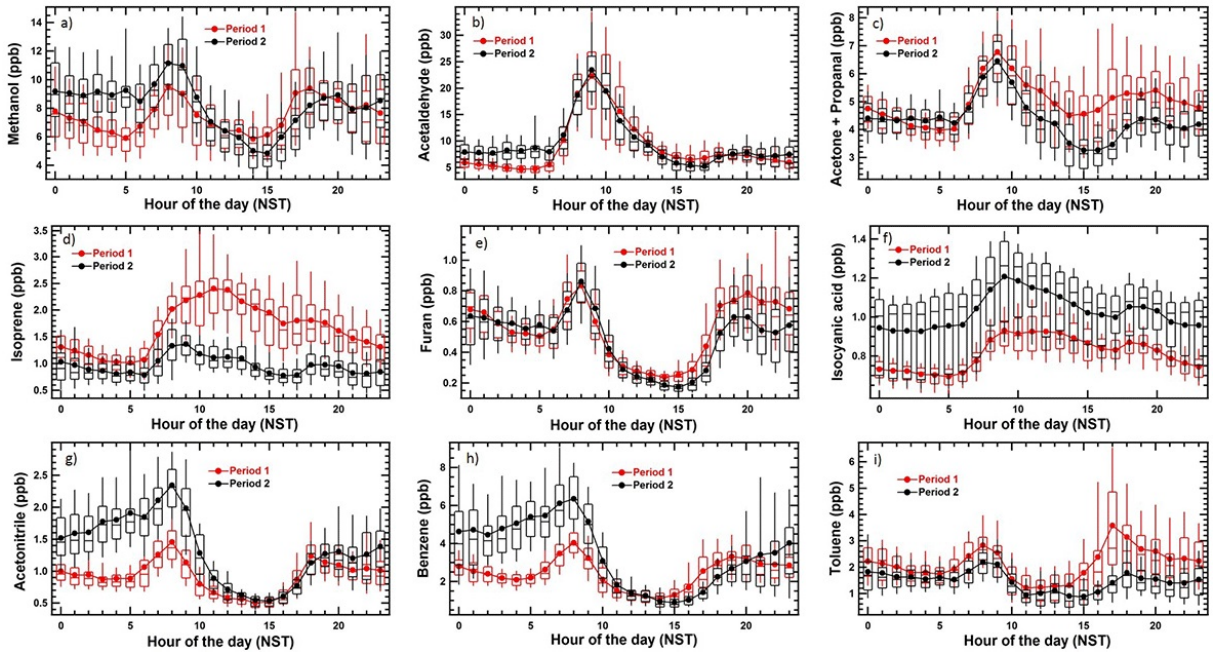

Figure 4.8: Box and whisker plots showing average, median and variability (10^{th}, 25^{th}, 75^{th} and 90^{th} percentile) for some major VOCs in the Kathmandu Valley during Period 1 and Period 2

etaldehyde, benzene and isoprene).

4.4.4 Diel profiles as a tool to constrain emission sources: VOCs emitted from biomass burning activities in the Kathmandu Valley

In order to contrast the role of diverse emission sources during period 1 and period 2, we analyzed the diel profiles of a number of VOCs. These are shown in Figure 4.8 as box and whisker plots for period 1 (derived from total number of measurements $>$ 20,500) and period 2 (derived from total number of measurements $>$ 21,500) for methanol, acetaldehyde, sum of acetone and propanal, isoprene, furan, isocyanic acid, acetonitrile, benzene and toluene. The time stamp is the start time of respective hourly data bin (e.g. 9 for data averaged between 9 and 10).

We note that the concentrations of acetonitrile (a chemical tracer for biomass combustion), methanol, benzene and isocyanic acid are significantly higher in period 2 relative to period 1, indicating that for all of them, the biomass co-fired brick kilns that became

operational in the first week of January and other forms of biomass burning (e.g. leaves and branches, garden waste and garbage) were major contributory sources. In contrast, isoprene and toluene concentrations were markedly higher during period 1 as compared to period 2. Acetaldehyde and furan did not differ much between period 1 and period 2. The high acetaldehyde concentrations suggest the possibility of high levels of peroxy acetyl nitrate (PAN). The campaign average concentration of 1.08 ppb observed at m/z 45.990 and attributed to NO_2^+ (Table 4.2), which is a fragment ion of C1–C5 alkyl nitrates (Aoki et al., 2007), appears to be consistent with the presence of a large pool of gaseous organic nitrate species too. Except for isoprene, isocyanic acid and acetaldehyde, which did not show a marked bimodal profile (morning and evening maxima), all the other VOCs shown in Figure 4.8 exhibited bimodal diel profiles to some degree, indicating the common influence of urban emission activities and biomass combustion sources for these compounds. Bimodal profiles for VOCs have previously been reported from several sites influenced by urban emissions (Staehelin et al., 1998; Stemmler et al., 2005), including our recent work in Mohali, India (Sinha et al., 2014), another site in South Asia that is somewhat closer to Kathmandu in terms of emission sources. Such bimodal profiles typically arise because morning and evening emissions get mixed into a shallow boundary layer, while the afternoon emissions are diluted under a rapidly growing boundary layer due to the surface heat flux, giving rise to a daytime minima in the diel profile. This holds for VOCs which are not formed photochemically or emitted anomalously during the daytime in large measure. Thus, bimodal diel profiles were not observed for isoprene which is emitted by terrestrial vegetation during daytime and acetaldehyde and isocyanic acid which are known to be emitted from biomass fires and produced photochemically from precursor compounds (Millet et al., 2010; Roberts et al., 2014). In general, for both period 1 and period 2, the features of diel profiles in terms of rise and fall of concentrations are similar for all the VOCs shown in Figure 4.8. The diel profiles of all VOCs also reveal at about 06:00 local time (LT), emission activities pertaining to cooking (use of biofuel and fossil fuel such as LPG)and traffic pick up, which in combination with the brick kilns emissions appears to drive the diel peaks for almost all VOCs occur at around 08:00–09:00 LT.

In addition to the typical boundary layer dynamics and emissions driving concentration profiles, the mountain meteorology appears to play a key role in the concentration peaks

observed after sunrise around 08:00–09:00 LT. If one examines the diel pattern for wind speed, wind direction, temperature and solar radiation data (available for part of the study and shown in Figure 4.2 b), it is clear that the diel meteorological conditions (e.g. surface wind flow, direction, temperature, RH) were very consistent even on different days as there is a very narrow spread in the values for each hour and the average and median always converged. The wind speeds were typically lower than 1 ms^{-1} for almost all hours of the day except between 10:00–16:00 LT, when westerly winds from the mountain passes lying west of the site swept across the Valley attaining wind speeds of 3–4 ms^{-1}, causing rapid venting and dilution. The wind direction was very consistent on daily timescales. During the evening and at night, the horizontal wind flow was mainly from the south-east direction, which changed to a westerly flow during the day. Down-slope mountain winds during nighttime result in pooling of cleaner cold air. Then shortly after sunrise, convective mixing of surface air with residual air commences the growth of the well mixed daytime boundary layer (Panday and Prinn., 2009).

The highest mixing ratios for acetaldehyde (average value of $\sim$ 25 ppb for both period 1 and period 2) and acetone (average value of $\sim$ 7 ppb for both period 1 and period 2) and indeed for most of the other VOCs were observed during morning hours about one hour after sunrise (09:00–10:00 LT). The breaking of the nocturnal boundary layer and entrainment of air masses rich in accumulated oxygenated VOCs, which were displaced by cold air from the mountain slopes after midnight contribute towards the peaks observed in all VOCs between 09:00–10:00 LT. In mountain basins such as the Kathmandu Valley, at nighttime, katabatic winds are generated due to radiative cooling of mountains that lead to pooling of cold air to the Valley bottom (Figure 4.2a). Due to this katabatic flow, less cold and less dense air parcels in the Valley bottom containing the entire Valley's surface emissions rise upward during nighttime, while relatively clean cold air parcels flow underneath. After sunrise, downward mixing of the uplifted accumulated VOCs occurs with new surface emissions, as a growing mixed layer entrains the elevated layers of the polluted air. Therefore during morning hours, mixing of oxygenated VOCs and their precursors that had accumulated during nighttime and a kick start to their photochemical production after sunrise, contributes to sharp peaks (e.g. for acetaldehyde and acetone). It should also be noted that the majority of the population in Kathmandu Valley cook

their major meals in the morning and evening hours using fuel such as liquefied petroleum gas (LPG), kerosene and firewood (Panday et al., 2009).

Contributions from biogenic sources and oxidation of alkenes to acetaldehyde are also important. Reaction of oxygenated VOCs like ethanol and methyl ethyl ketone (MEK) with hydroxyl (OH) radicals and the reaction of tropospheric ozone (O_3) with alkenes can significantly contribute to photochemical formation of acetaldehyde (Sommariva et al., 2011; Grosjean et al., 1994). After the morning peak (09:00–10:00 LT), a sharp decrease was observed in the average acetaldehyde mixing ratios (from $\sim$ 25 to $\sim$ 8 ppb during 10:00–13:00 LT) relative to methanol and acetone, which is not surprising considering its much higher OH reactivity.

The highest isoprene concentrations were observed during daytime for both period 1 and period 2 but the average concentrations were much higher during period 1 when ambient temperature and solar radiation were comparatively higher and deciduous trees had not shed much of their leaves. This clearly points to daytime biogenic emission sources of isoprene in the Kathmandu Valley. In Section 4.4.6 we investigate the spatial and temporal location of the biogenic sources. We note that while the isoprene emission profile was dominated by biogenic sources, biomass burning (Christian et al., 2003; Andreae and Merlet., 2001; Warneke et al., 2011) and traffic (Borbon et al., 2001) also contributed to the ambient isoprene as can be seen from the nighttime peaks and discussed in previous sections. Thus, the contribution of both biogenic and anthropogenic sources resulted in high isoprene even in winter in the Kathmandu Valley which is different from what has been observed at high latitude sites in winter (Seco et al., 2011).

Apart from the biomass burning practices typical of developing regions of the world, the brick kilns in the Kathmandu Valley do not only burn coal, but also burn large quantities of wood and crop residues, ca. 90 t per month per brick factory (Stone et al., 2010; Rupakheti et al., 2016), which can emit acetonitrile and benzene (refer Chapter 3). Both acetonitrile and benzene levels were much higher during nighttime and morning hours in period 2 as compared to period 1 due to more intense biomass burning in period 2. During 08:00–09:00 LT (when highest ambient acetonitrile and benzene were observed) average mixing ratios were approximately 1 and 2 ppb higher for acetonitrile and benzene, respectively during period 2 relative to period 1.

Unlike acetonitrile and benzene, toluene concentrations were higher during period 1 in comparison to period 2. Despite the dilution effect of cold air descending from the mountain slopes, benzene concentrations increased during the night in period 2, whereas toluene concentrations did not show any increase during the night in both period 1 and period 2, suggesting that biofuel and biomass burning sources (including the brick kilns co-fired with biomass) and not traffic were the driving factors responsible for nighttime increase in benzene during period 2 probably due to varied forms of biomass combustion, including the biomass co-fired brick kilns. The emission ratios of benzene/toluene from previous studies show that, for a wide variety of commonly occurring fuels, the emission of benzene can be more than twice as high as the emission of toluene (Tsai et al., 2003; Lemieux et al., 2004; Stockwell et al., 2015). The use of large number of diesel generators as an alternative power source in the Kathmandu Valley which suffers from scheduled daily power outages in some quarters of the city, could also have significant contributions to the observed high mixing ratios for aromatic VOCs.

To our knowledge, this thesis reports the first measurements of isocyanic acid from any site in South Asia. Isocyanic acid has only recently been measured in ambient air using novel mass spectrometric methods (Roberts et al., 2011), and much remains to be understood regarding its sources and sinks in different environments. The high isocyanic acid concentrations observed during the daytime suggest a strong photochemical source from hydroxyl radical initiated oxidation of alkyl amines and amides with hydroxyl radicals (Roberts et al., 2011, 2014; Zhao et al., 2014). Isocyanic acid has also been detected in diesel exhaust (Wentzell et al., 2013), tobacco smoke and wild fires and in emissions from low temperature combustion of coal (Nelson et al., 1996). From the diel profile, it is clear that around evening time there are primary emissions too but overall the secondary source dominates the ambient concentrations of isocyanic acid in this environment. Currently, global models of isocyanic acid (Young et al., 2012) do not incorporate a photochemical source. The recent model-based estimates of isocyanic acid (HNCO) by Young et al. (2012) showed annual mean concentrations of HNCO over the Indo Gangetic Plain and Nepal to be in the range of 0.2–0.5 ppb (values read from Figure 4 of Young et al. (2012). The average concentrations measured during winter in Kathmandu and in the post monsoon season in Mohali were $\sim$1 ppb (Chandra and Sinha, 2016) with clear

daytime maxima. This suggests that inclusion of isocyanic acid's photochemical sources are necessary for deriving better estimates of the global isocyanic acid budget, as these are likely significant over South Asia where biomass burning and agricultural activities can also emit precursor compounds of isocyanic acid such as alkyl amines, formamide and acetamide (Roberts et al., 2011). Our in-situ field data from the Kathmandu Valley suggests that inclusion of isocyanic acid's photochemical sources is necessary for deriving better estimates of the global isocyanic acid budget, as these are likely to be significant over South Asia where biomass burning and agricultural activities can emit alkyl amines. Serious health impairments can occur upon exposure to isocyanic acid at concentrations greater than 1 ppb, which occurred during our study for several hours during period 2. These health impacts have been previously mentioned in Roberts et al. (2011) and are also discussed in Section 4.4.9.

4.4.5 Diel profiles of rarely measured VOCs and correlation with emission tracer VOC compounds for constraining their sources

Figure 4.9a–c shows the diel profiles of propyne (m/z = 41.039), propene (m/z = 43.055) and propanenitrile (m/z = 56.060) alongside acetonitrile (an excellent tracer for biomass combustion), respectively. These diel profiles correspond to data for the entire measurement period. Strong correlation ($r^2 \geq 0.7$ for the hourly averages) with acetonitrile clearly indicates that during our wintertime study in the Kathmandu Valley, all these compounds were primarily emitted from biomass burning, despite having multiple sources (Hao et al., 1996; Akagi et al., 2011; Andreae and Merlet., 2001; Karl et al., 2003). Both propene and propyne participate in important chemical reactions in the troposphere. While propene is a source of OH radicals when it undergoes ozonolysis, propyne has been reported to produce methylglyoxal, formic acid and acetic acid in multistep reactions (Lockhart et al., 2013; Warneck and Williams., 2012). Propanenitrile has been previously detected in biomass smoke during laboratory studies (Akagi et al., 2011, 2013; Yokelson et al., 2013; Karl et al., 2003, 2007). Average propanenitrile mixing ratios observed during the measurement period were $\sim$ 0.21 ppb. Propanenitrile reacts very slowly with hydroxyl radicals

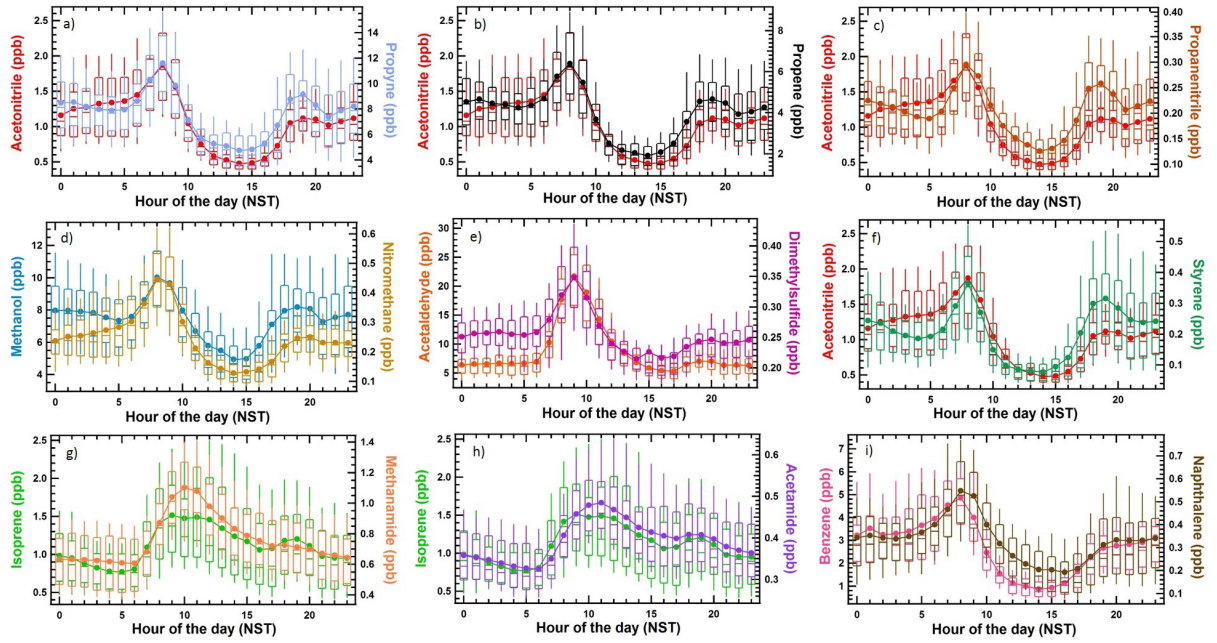

Figure 4.9: Comparison of diel box and whisker profiles of several rarely measured or previously unreported ambient VOCs with more frequently measured VOCs/emission tracers

in the atmosphere (k_{OH} is of the order of 10^{-13}cm^{3}molecule^{-1}s^{-1}) but the oxidation of propanenitrile with OH radicals can produce nitrogen compounds in the troposphere and hence could contribute to the total nitrogen budget.

Figure 4.9d–f shows the diel profiles for nitromethane, dimethyl sulfide (DMS) and styrene alongside methanol, acetaldehyde and acetonitrile. Nitromethane (measured at m/z ratio 62.026) concentrations correlated strongly with the hourly average concentrations of methanol ($r^2 = 0.81$). Nitromethane is known to be present in diesel exhaust (Inomata et al., 2013, 2014; Sekimoto et al., 2013) and biomass burning plumes (Akagi et al., 2013). The maximum nitromethane mixing ratios observed in the Kathmandu Valley were ~ 1.2 ppb which falls within the range of ambient nitromethane mixing ratios (1–9 ppb) reported previously in urban environments (Grosjean et al., 1998; Yassaa et al., 2001; Inomata et al., 2014). In the Kathmandu Valley, a large number of diesel power generators are used to supplement the main power supply. Ambient nitromethane observed in the Kathmandu Valley is therefore also likely from a combination of biomass burning sources and diesel exhaust emissions. The major sink of nitromethane in the atmosphere is its photodissociation (photodissociation lifetime of $\sim$ 10h), which produces methyl radicals

and NO_2 (Taylor et al., 1980). Therefore nitromethane can act as a NO_x source in the atmosphere and could contribute to surface ozone production.

Dimethyl sulfide measured (at m/z ratio 63.026) in the Kathmandu Valley showed good correlation with the diel profile of acetaldehyde (correlation of hourly averages: $r^2 = 0.8$). Average concentrations in the morning (09:00–10:00 LT) reached 0.4 ppb. The oxidation of DMS with nitrate radicals at night would account atleast in part for its lower nighttime concentrations of circa 0.2 ppb. Although marine phytoplankton emissions are known to be the major source of DMS in the atmosphere (Andreae and Raemdonck., 1983; Sinha et al., 2007), ambient mixing ratios up to 160 ppt have been recently reported in the Amazon rainforest, which were attributed to biogenic soil emissions (Jardine et al., 2015). Certain lichens, mosses, grasses and plant leaves can emit acetaldehyde (Kesselmeier et al., 1997; Kesselmeier and Staudt., 1999). Therefore the possibility of such vegetation on the mountain slopes and the soil acting as sources of DMS and acetaldehyde, respectively, is plausible. Inefficient combustion of sulfur rich biofuel/biomass are also potential sources of DMS (Jardine et al., 2015).

Figure 4.9g and h shows the diel profiles of formamide and acetamide alongside isoprene while Figure 4.9i shows the diel profile of naphthalene and benzene. During the measurement period, daytime maximum average values of ~ 1 and ~ 0.5 ppb were observed for formamide and acetamide, respectively. Although formamide and acetamide correlate strongly with isoprene (hourly average $r^2 \geq 0.8$), to our knowledge, biogenic sources of formamide and acetamide have not been reported previously. On the other hand short chain amides such as formamide and acetamide can be produced as a result of photochemical oxidation of alkyl amines with hydroxyl radicals and nitrogen oxides (NO_x) (Roberts et al., 2014). The presence of formamide in ambient air at concentrations as high as 1 ppb is consistent with the photochemical source of isocyanic acid discussed in the previous section. Also it is reported that both formamide and acetamide could be emitted from tobacco smoke and hence likely from pyrolysis of biomass (Ge et al., 2011). The good correlation of formamide and acetamide with isoprene's diel concentration profile suggests that the photochemical source arising from oxidation of amines dominates over any primary emission sources of amides.

The ion peak detected at m/z ratio of 129.070 in the PTR-TOF-MS spectra was at-

tributed to naphthalene. Naphthalene is the most volatile and abundant polycyclic aromatic hydrocarbon (PAH) present in the atmosphere. Previously Martinez et al. (2004) have reported vehicle exhaust and residential heating in the urban environments as major sources of naphthalene. The similarity in diel profiles of naphthalene and benzene and their strong correlation with each other (hourly average $r^2 = 0.79$), suggests that biomass burning and traffic sources dominated emissions of naphthalene in the Kathmandu Valley.

4.4.6 High isoprene in the Kathmandu Valley: a daytime biogenic source and contributions from combustion sources

Figure 4.10a shows a polar annulus plot of the hourly mean isoprene mixing ratio during the period 16–30 January 2013 (unfortunately, meteorological data for other periods of the study are unavailable). The polar annulus plot is a method of visualizing the temporal aspects of a specie's concentration with respect to wind direction. In the polar annulus plots, measured concentrations are averaged in separate time and wind direction bins and then further interpolation using Kriging technique are applied for conversion to polar coordinates (Ropkins and Carslaw., 2012). Such plots reveal important spatio-temporal information regarding emission sources. In Figure 4.10 it can be seen that isoprene had highest ambient mixing ratios ($\sim$ 1 ppb isoprene) during the daytime (07:00–14:00 LT) which is an indication of biogenic sources. Significant isoprene concentrations ($\sim$ 0.5 ppb) could also be observed during evening and nighttime which are likely from biomass combustion and traffic emission sources. Furan contributed a maximum of only $\sim$ 40 % (during nighttime) to the sum of ambient isoprene and furan. This is a very important finding as previous studies using proton transfer reaction mass spectrometers equipped with quadrupole mass analyzers, which cannot distinguish between furan and isoprene peaks due to their lower mass resolution and detect the two compounds collectively at a nominal m/z = 69, tend to attribute the evening and nighttime concentrations to furan and not isoprene. Using a novel VOC-OHM chemical kinetics reactor (Kumar and Sinha., 2014), which constrained the rate coefficient of the isobaric contributor at nominal m/z = 69, it has been demonstrated at another South Asian site in the north-west Indo Gangetic Plain (Mohali), that isoprene is the major contributor to m/z = 69. Thus it appears that

isoprene has significant contributions from both vegetation and biomass/biofuel burning sources in South Asia, which has large implications for the atmospheric oxidation in this part of the world, as discussed also in Sinha et al. (2014). While several previous studies have reported significant contributions from anthropogenic sources to isoprene in urban areas elsewhere, especially in winter (Borbon et al., 2001; Barletta et al., 2005; Hellèn et al., 2012), the in-situ measurements from Mohali and Kathmandu suggest that the magnitude of the isoprene source from anthropogenic sources may be quite important regionally in South Asia. Recently, Gilman et al. (2015) showed that in direct fire/smoke plumes from prescribed burns of selected biomass fuels common for the southeastern, southwestern or northern US, the contributions of pentadienes and cyclopentene to isoprene concentrations measured using a PTR-QMS can be quite significant. Therefore, contributions from compounds such as pentadienes and cyclopentene to the isoprene concentrations measured in the Kathmandu Valley during evening, nighttime or early morning may be significant. The non–biogenic sources of isoprene acquire greater significance in the evening, nighttime or early morning when combustion emissions are more widespread and can accumulate under shallow inversions.

What is remarkable is that in contrast to wintertime measurements of isoprene from sites elsewhere in the world due to the strong contribution from biogenic sources in the Kathmandu Valley, average wintertime concentrations of isoprene in Kathmandu were observed to be above 1 ppb (see Figure 4.6). To emphasize that the daytime isoprene concentrations were primarily controlled by biogenic emissions, we show real time data from a day (18 January 2013) where clear co-variation of the daytime isoprene concentrations occurred with changes in the solar radiation (Figure 4.10b).

High values of isoprene were generally observed from the west and northern sector (N.N.E where Nilbarahi Jungle and Gokarna Reserve Forest are located) and at appreciable wind speeds (> 3 ms^{-1}). The advection of air across the Valley in the afternoon as they flow through the mountain passes from west to east due to the high speed westerly winds has been previously described by Panday and Prinn. (2009). The forest areas on the mountain slopes appear to contribute to the high ambient isoprene concentrations measured during the afternoon hours. The average daytime (08:00–17:00 LT) isoprene concentrations observed during SusKat-ABC campaign (1.35 ppb) are comparable to the concentrations

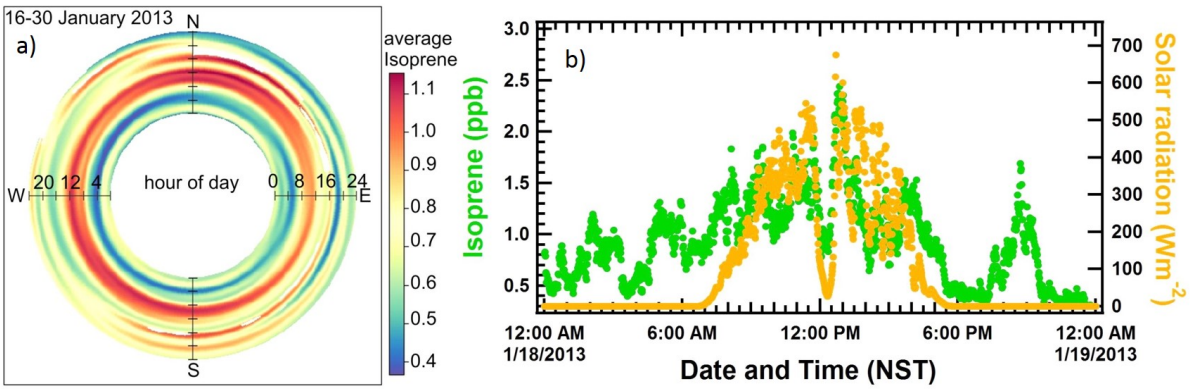

Figure 4.10: **(a)** Polar annulus plot of isoprene for the period 16–30 January 2013 highlighting the spatio-temporal variation of isoprene and its biogenic sources; **(b)** co-variation of daytime isoprene concentrations with solar radiation on 18 January, 2013.

measured in south-east Asian tropical rainforest sites (Bryan et al., 2012; Jones et al., 2011). As mentioned in the site description section, the forested areas contained tree species like oak and *Melia azedarach* which have significant isoprene emission potentials (350 μg g^{-1} dry leaf h^{-1} and 4.7μg g^{-1} dry leaf h^{-1} respectively (Simon et al., 2005; Padhy and Varshney., 2005). In the Section 4.4.7 we examine the importance of VOCs measured during this study in terms of their OH reactivity contributions and ozone formation potential.

4.4.7 OH reactivity and Ozone Production Potential of VOCs

The oxidation of VOCs (and consequently their removal rate) depends on the reactivity of VOCs with both ozone and hydroxyl radicals during daytime and the nitrate radical during nighttime. For most of the VOCs reported in this work and the typical maximum ozone concentrations observed during winter in the Kathmandu Valley (∼60–70 ppb; Putero et al. (2015)), the daytime oxidation with hydroxyl radicals is much faster relative to daytime oxidation with ozone and nighttime oxidation with nitrate radicals as $k_{VOC+OH} > k_{VOC+NO_3} > 10^3$–$10^{10}$ times k_{VOC+O_3} (Atkinson et al. (2006); kinetics.nist.gov/kinetics). For dimethyl sulfide, nighttime oxidation with nitrate radical (NO_3) can be as important as daytime oxidation with OH as $k_{DMS+NO_3} \approx k_{DMS+OH}$ (k_{DMS+NO_3} and k_{DMS+OH} are 1.1×10^{-12} cm^3 molec^{-1} s^{-1} and 5.1×10^{-12} cm^3 molec^{-1} s^{-1}, respectively; at T = 281.8 K). The hydroxyl radical reactivity of an air mass reflects the total reactive pollutant

loading of the air mass and can be used to infer its ozone formation potential (Sinha et al., 2012). While direct total OH reactivity measurements were not performed during the SusKat-ABC campaign, it is still instructive to examine the diel profile of the OH reactivity due to the suite of measured VOCs and assess the relative contributions of individual VOCs. For this analysis, we considered thirty three out of the thirty seven species that were observed at average ambient concentrations greater than 200 ppt, for which the rate coefficients with the hydroxyl radical are known. Thus, out of the thirty seven species, four namely, the nitronium ion (m/z = 45.990), isocyanic acid, and assorted hydrocarbons detected at m/z ratios of 83.085 and 97.102, respectively, were excluded from this analysis. The total VOC OH Reactivity was calculated as follows (Sinha et al., 2012):

$$Total\ VOC\ OH\ reactivity = \sum k_{VOC_i+OH}[VOC_i] \tag{4.2}$$

where k_{VOC_i+OH} is the first order rate coefficient for the reaction of VOC_i with OH radicals and [VOC_i] is the measured concentration of VOC_i. The rate coefficients were taken from the NIST chemical kinetics database (*http://kinetics.nist.gov/kinetics*), Atkinson et al. (2006) and Barnes et al. (2010).

Figure 4.11 shows the diel profile of the average sum of VOC OH reactivity due to 33 ambient VOCs, along with the diel profiles of the hourly averaged OH reactivity due to the top three contributors. The grey shaded region in Figure 4.11 represents the 10^{th} and 90^{th} percentiles of the sum of VOC OH reactivities due to the 33 ambient VOCs. The average diel profile is bimodal in nature with peaks of ca. 21 s^{-1} at 09:00 LT and ca. 13 s^{-1} at 18:00 LT. Interestingly, the nighttime value (22:00-06:00 LT) remains rather constant at ca. 12 s^{-1}. The top four contributing compounds to the total calculated VOC OH reactivity due to all 33 compounds were: acetaldehyde (24.0%) > isoprene (20.2%) > propene (18.7%). These three VOCs collectively accounted for ca. 63% of the campaign averaged total VOC OH reactivity of 12.3 s^{-1}. Table 4.4 lists the top ten VOC contributors to the total VOC OH reactivity, many of which are emitted strongly from biomass combustion sources. The influence of south easterly winds advecting primary emissions from biomass co-fired brick kilns in the morning hours is clearly discernible on the ambient OH reactivity profile.

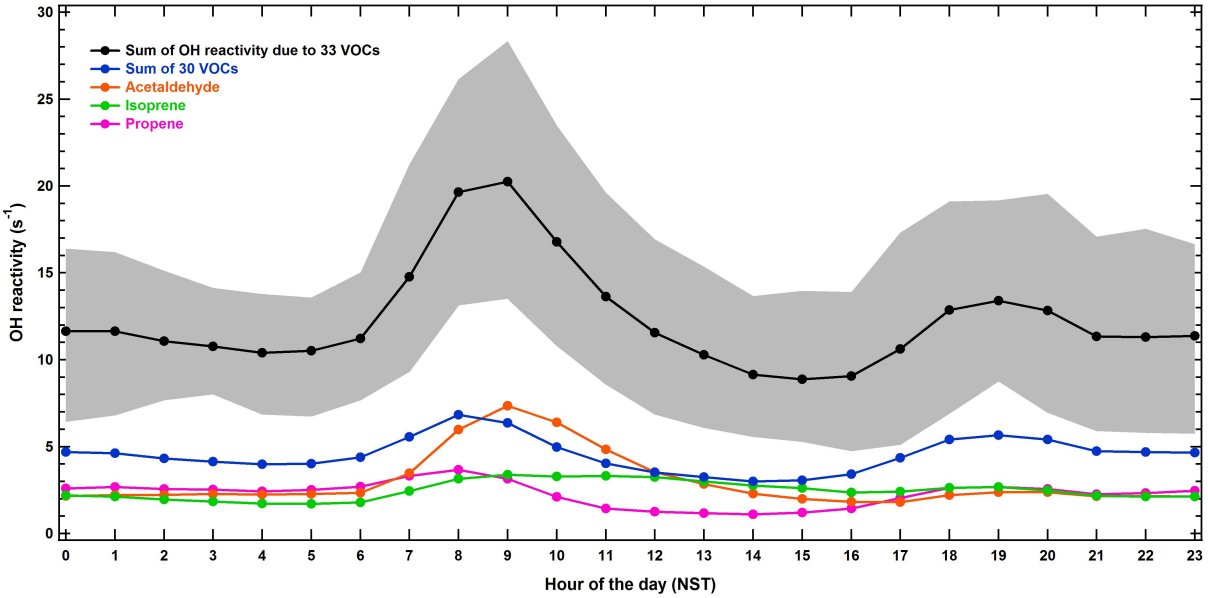

Figure 4.11: Diel profiles of the calculated total VOC OH reactivity (with 10^{th} and 90^{th} percentile contributions represented by the grey shaded region) and the major VOC contributors

For quantifying the importance of VOC and NO_x controls on the ozone production efficiency in the Kathmandu Valley, simultaneous measurements of both VOCs and NO_x are necessary. The relative ozone formation potential of VOCs can be derived as described by the following equation (Sinha et al., 2012):

$$\text{Ozone production potential} = \left(\sum k_{(\text{VOC}_i+OH)}[\text{VOC}_i]\right) \times [OH] \times n \qquad (4.3)$$

For the ozone production potential calculation, the average hydroxyl radical concentration was assumed to be [OH]= 1 × 10^6 molecules cm^{-3} with n = 2 and only data pertaining to the mid-daytime period was considered (11:00–14:00 LT). The temporal context of the analyses performed using VOC data acquired during the afternoon (11:00–14:00 LT; period using which ozone production potentials were calculated) is quite relevant considering the recently published work of Putero et al. (2015), which highlighted that hourly average concentrations of > 60 ppb are often observed during winter afternoons in the Kathmandu Valley (refer Figure 9 of Putero et al. (2015)). This shows that regional photochemistry is strong even during winter and formation of secondary pollutants contributes to hourly ozone concentrations in excess of 60 ppb. Figure 4.12a and b summarizes the results

Table 4.4: Top ten contributing VOCs to the total OH reactivity during SusKat-ABC campaign

VOCs	Campaign average speciated OH reactivity (s^{-1})	Percentage contribution to total average OH reactivity
Acetaldehyde	2.95	24.0%
Isoprene	2.47	20.2%
Propene	2.29	18.7%
Propyne	0.49	4.0%
1,3-Cyclopentadiene	0.43	3.5%
Furan	0.40	3.2%
Acrolein	0.34	2.8%
Formaldehyde	0.33	2.7%
Xylenes	0.29	2.4%
Trimethylbenzenes	0.25	2.0%

in the form of pie charts for period 1 (when most brick kilns were inactive but daytime biogenic emissions of isoprene dominated) and period 2 (when brick kilns became operational, isoprene emissions were lower and biomass burning was stronger in intensity). To ascertain the contribution of different chemical classes of compounds (e.g. OVOCs, benzenoids, isoprene) to total ozone formation potential, the 33 compounds were further divided into 5 chemical subgroups as shown. It was found that for both period 1 and period 2, oxygenated VOCs and isoprene collectively accounted for more than 68% (72% for period 1 and 68% for period 2) of the total ozone production potential. This is not surprising given that acetaldehyde and isoprene were among the highest contributors to the VOC OH reactivity. This analysis puts in perspective the relative ranking of individual VOCs and classes of VOCs to the ozone production potential in the Kathmandu Valley for potential mitigation efforts.

4.4.8 SOA formation potential of VOCs in the Kathmandu Valley

Apart from ground level ozone formation, secondary organic aerosols (SOA) can also be formed as a result of atmospheric oxidation of VOCs. The 71 detected ions collectively summed up to a total mass concentration of $\sim$160.4μgm^{-3}, out of which the 37 identified ions and VOCs reported in this work, accounted for $\sim$139.1μgm^{-3} (or 86.7%). Pudasainee

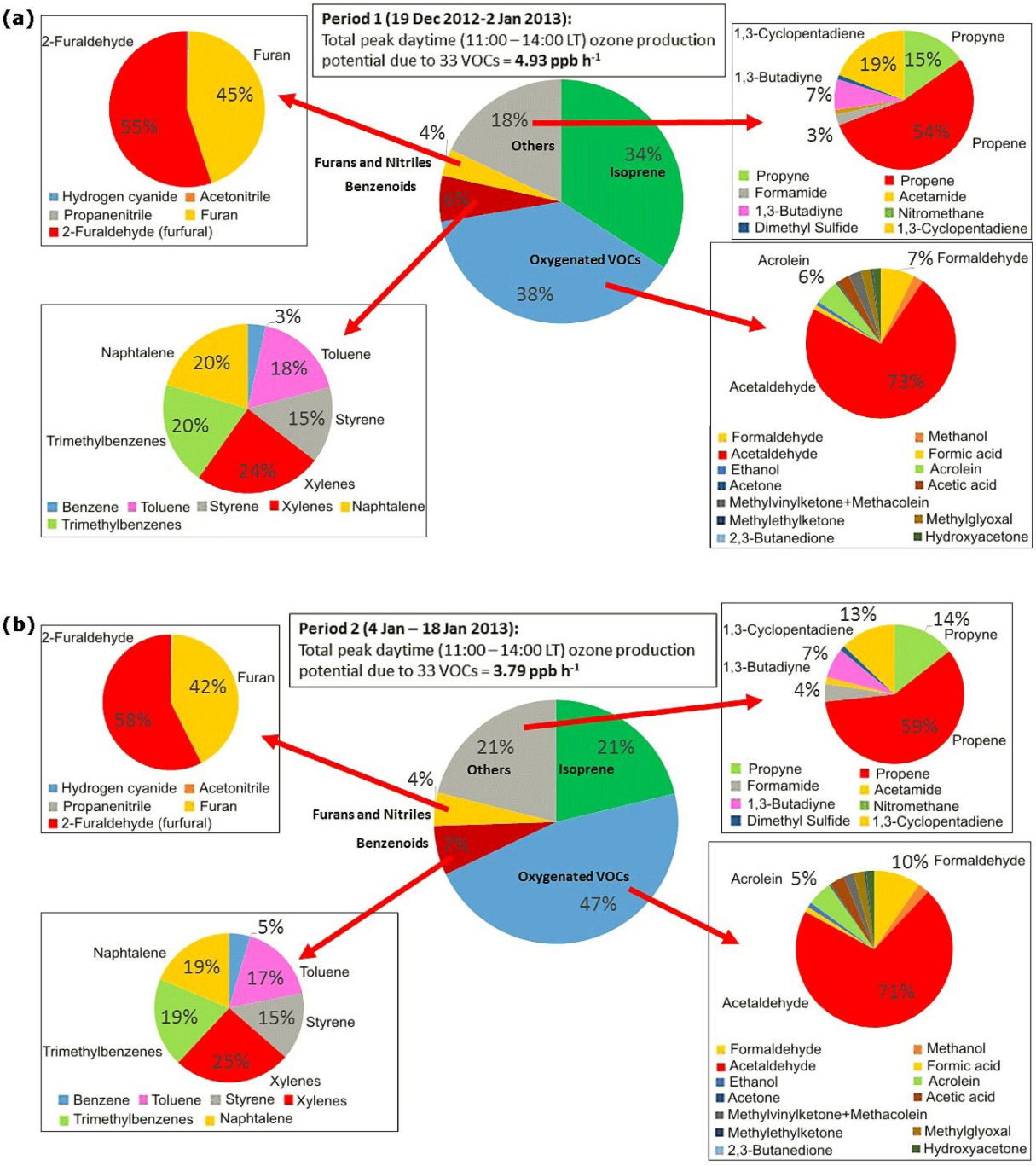

Figure 4.12: Pie charts showing contribution of different class of compounds to total ozone formation potential **(a)** for Period 1 (19 December 2012-2 January 2013) and **(b)** for Period 2 (4 January 2013-18 January 2013)

et al. (2006) previously reported NO_x rich conditions in the Kathmandu Valley and based on the SOA yields reported in the literature (e.g., 5–10% for toluene and xylenes and $\sim$ 28% for benzene; Ng et al., 2007) and the ambient concentrations of these VOCs measured during the period of study, we estimate the order of SOA production potential for these VOCs to be benzene > naphthalene > toluene > xylenes > monoterpenes > trimethylbenzenes > styrene > isoprene. Although the average ambient concentrations of the sum of monoterpenes (0.17$\pm$0.16 ppb) were below 200 ppt, it contributed significantly to the total SOA formation due to its higher SOA yield under high NO_x conditions (Lee et al., 2006).

4.4.9 VOCs with direct health implications for exposed population

Several VOCs detected in the Kathmandu Valley have consequences for human health, often at concentrations of documented concern. Benzene and formaldehyde are considered human carcinogens (Group A and B1, respectively) by WHO (2010). Among other rarely quantified ambient VOCs, short–chain amides, such as formamide and acetamide can have several health effects (Ge et al., 2011). While acetamide is considered a Group 2B human carcinogen by the International Agency for Research on Cancer http://www.iarc.fr/). nitromethane is also a Group 2B carcinogen and has been reported as a possible carcinogen to humans (Inomata et al., 2014). Some gases can result in formation of toxic secondary VOCs. For example, naphthalene is not considered to be a human carcinogen, but it can form mutagenic nitronaphthalenes by OH and NO_3 initiated reactions (Sasaki et al., 1997; Zhang et al., 2012). Atmospheric oxidation of amide compounds such as formamide and acetamide with hydroxyl radicals also contributes to the formation of isocyanic acid (Barnes et al., 2010). Ambient isocyanic acid was present at exposure levels of documented concern that can enhance human health risks for cataracts, cardiovascular diseases and rheumatoid arthritis via protein carbamylation (Wang et al., 2007; Roberts et al., 2011). Thus long term monitoring of these gases (isocyanic acid, formamide, acetamide, benzene, formaldehyde, nitromethane, naphthalene), which can cause adverse effects upon sustained exposure even at concentrations of few ppb is warranted for establishing expo-

sure and assessing health risks due to these VOCs in the Kathmandu Valley.

4.5 Conclusions

This study has comprehensively characterized the chemical composition of air in the Kathmandu Valley in terms of speciated volatile organic compounds during the SusKat-ABC wintertime campaign. The measurements performed at high time resolution (every minute) and high mass resolution ($m/\Delta m > 4200$) enabled us to identify a multitude of compounds based on their monoisotopic masses and hence exact molecular formula. Novel insights could be acquired regarding chemical processes related to ozone and secondary organic aerosol formation in a complex chemical environment affected by mountain meteorology and both anthropogenic and biogenic sources (even in winter).

A total of 71 ion peaks were observed in the mass spectra of PTR-TOF-MS that were above the detection limit of the instrument. Out of these, 37 species that had average ambient concentrations greater than 200 ppt during the campaign could be identified with reasonable confidence based on (1) spectral characteristics observed at a particular m/z in a 0.005 amu bin relative to the ion peak, (2) ambient diel profiles and (3) correlation with specific emission tracer molecules such as acetonitrile (a biomass burning tracer). 200 ppt cut off was also chosen as an additional quality control measure so as to ensure attribution of ion peaks in the mass spectra only to the compounds present in the ambient air and not due to instrumental reasons. Among these 37 species, 8 contained nitrogen, 15 contained oxygen, 13 were hydrocarbons and one contained sulfur. Based on chemical signatures of tracer compounds such as acetonitrile and isoprene, two periods with contrasting emission influences were identified during the campaign and investigated in detail. period 1 (19 December 2012–2 January 2013) was characterized by high daytime biogenic emissions of isoprene (average isoprene concentrations in period 1 and period 2 were 1.66 and 0.97 ppb, respectively) and the absence of operational brick kilns (and hence their emissions); while period 2 (4 January 2013–18 January 2013) was marked by high acetonitrile (average concentration during this Period was 1.34 ppb), benzene (3.46 ppb) and isocyanic acid (1.03 ppb) due to emissions from the biomass co-fired brick kilns and other biofuel/biomass burning activities. A clear distinction of isoprene from furan, which

had distinct emission profiles, highlighted the importance of deploying a PTR-TOF-MS for VOC measurements in the Kathmandu Valley.

Two "new" compounds which have not been reported in any previous ambient study namely, formamide (CH_3NO); protonated m/z = 46.029; campaign average 0.76 ppb) and acetamide (C_2H_5NO; protonated m/z = 60.051; campaign average 0.39 ppb) and are involved in photochemical formation of isocyanic acid were also detected. The average total reactive carbon (sum of the average mixing ratios of all the 37 species reported in this study) was 175.8 ppbC to which propyne, acetaldehyde, benzene, acetic acid, acetone, propene and toluene collectively contributed more than 60%. Isoprene concentrations as high as 3 ppb were observed frequently during the daytime, in the early part of the campaign (December 2012) and could be traced to biogenic emissions from vegetation in fetch regions upwind of the site.

The concentration ranking in the average VOC mixing ratios during our wintertime deployment was acetaldehyde (8.8 ppb) > methanol (7.4 ppb) > acetone + propanal (4.2 ppb) > benzene (2.7 ppb) > toluene (1.5 ppb) > isoprene (1.1 ppb) > acetonitrile (1.1 ppb) > C8-aromatics ($\sim$ 1 ppb) > furan ($\sim$ 0.5 ppb) > C9-aromatics (0.4 ppb). The results suggest that the emission sources of oxygenated and aromatic VOCs in the Kathmandu Valley are different compared to several cities such as Paris and London, likely due to the emissions from biomass co-fired brick kilns, open burning of biomass (e.g. garden waste, agro-residue burning and garbage burning) and extensive use of diesel generators. In comparison to wintertime mixing ratios reported from several sites elsewhere in the world, the mixing ratios of acetaldehyde ($\sim$ 9 ppb), acetonitrile ($\sim$ 1 ppb) and isoprene ($\sim$ 1 ppb) in the Kathmandu Valley are among the highest measured anywhere in the world. The major sources of propyne, propene, benzene, and propanenitrile in the Valley appeared to be biomass burning as concentrations of all these compounds correlated well with the biomass burning tracer acetonitrile ($r^2 > 0.7$) and had diel emission profiles similar to that of acetonitrile.

The top three contributing compounds to the total calculated VOC OH reactivity due to 33 compounds were: acetaldehyde (24.0%), isoprene (20.2%), and propene (18.7%), which collectively accounted for ca. 63% of the campaign averaged total VOC OH reactivity of 12.3 s^{-1}. Oxygenated VOCs and isoprene collectively accounted for more than

68% (72% for period 1 and 68% for period 2) of the total ozone production potential. Based on known SOA yields of compounds and the ambient concentrations measured in the Kathmandu Valley, it was estimated that the relative SOA production potential of VOCs was in the following order: benzene > naphthalene > toluene > xylenes > monoterpenes > trimethylbenzenes > styrene > isoprene. Several VOCs known to enhance health risks for cancer, cataract and pulmonary diseases were detected in the ambient air. The synergistic effect of these VOCs on air toxicity is difficult to quantify but likely significant. The prominent ones were: isocyanic acid, formamide, acetamide, naphthalene and nitromethane for which this study presents the first measurements in ambient air from South Asia along with benzene, a human carcinogen.

Although like all urban environment, contribution of traffic sources to ambient VOCs is significant in the Kathmandu Valley, another anthropogenic source which occupies central importance in the Kathmandu Valley (due to inefficient combustion) are the biomass co-fired brick kilns. While we did not measure particulate matter emissions from the biomass co-fired brick kilns in the Kathmandu Valley during our deployment, previous studies by Pariyar et al. (2013) and Raut. (2003) have reported and documented massive increases in PM_{10} and TSP for periods marked by the operation of the brick kilns relative to periods when they were not operational . The study conducted by Clean Energy Nepal (Raut., 2003) showed that 8 h averaged concentrations of air pollutants such as Total Suspended Particulate (TSP) , PM_{10}, SO_2 and NO_x were three times higher during the brick kiln operating period relative to the period they were not operational at the same location. The mass concentration of PM_{10} increased from $218\mu gm^{-3}$ to $603\mu gm^{-3}$ while TSP increased from $265\mu gm^{-3}$ to $634\mu gm^{-3}$. Note that these were primarily Fixed Chimney Bull Trench Brick Kilns, similar to the ones that impacted our measurements. The Bull Trench kilns are an old and inefficient technology, which have been banned even in their place of origin, India, but continue to dominate the Kathmandu Valley landscape. Thus a major conclusion of this study is that replacing the existing brick kiln technology with cleaner and more efficient brick kiln technology would aid air pollution mitigation efforts significantly. While much has been learnt about wintertime VOC speciation in Kathmandu from this study, and the first comprehensive dataset has been acquired, long term measurements and further field intensives are required.

Future studies need to focus on what happens in the Valley on seasonal and inter-annual timescales. Of particular interest would be assessing the concentrations of isoprene and acetaldehyde in summer and their atmospheric chemistry. Assessment of source specific emission ratios (inter VOC) for the major sources (brick kilns, diesel generator exhaust, leaf litter fires etc.) and improvement of existing emission inventories using the in-situ data should be undertaken. The comparison and estimation of the fraction of isoprene from vegetation and combustion will also be presented in Chapter 5 of this thesis in which source apportionment of VOCs will be performed using positive matrix factorization (PMF) model. Comprehensive air quality and policy recommendations based on all the data acquired during the SusKat-ABC study and from other sites in the Kathmandu Valley will be reported soon by Rupakheti et al. (2016) and Panday et al. (2016).

Chapter 5

Source Apportionment of VOCs in the Kathmandu Valley during the SusKat-ABC international field campaign using Positive Matrix Factorization

5.1 Abstract

Positive matrix factorization model (EPA PMF version 5.0) was applied for the source apportionment of the dataset of 37 VOCs measured using PTR-TOF-MS during the SusKat-ABC field campaign (19 December 2012-30 January 2013) in the Kathmandu Valley. Total eight source categories were resolved by the PMF model after applying the new "constrained model operation". These are - traffic, residential biofuel use and waste disposal, mixed industrial emissions, biomass co-fired brick kilns, unresolved industrial emissions, solvent evaporation, mixed daytime source and biogenic emissions. The unresolved industrial emissions and traffic factor contributed most to the total VOC mass loading (17.9% and 16.8%, respectively) followed by mixed industrial emissions (14.0%), residential biofuel use and waste disposal (10.9%), solvent evaporation (10.8%), biomass

co-fired brick kilns (10.4%), biogenic emissions (10.0%) and mixed daytime factor (9.2%). Conditional probability function (CPF) analyses were performed to identify the physical locations associated with different sources. Source contributions to individual VOCs showed biomass co-fired brick kilns significantly contribute to the elevated concentrations of several health relevant VOCs such as carcinogenic benzene. Biogenic emissions contributed most (24.2%) to the total daytime ozone production potential even in winter followed by solvent evaporation (20.2%), traffic (15.0%) and unresolved industrial emissions factor (14.3%). Secondary organic aerosol (SOA) production was dominated by biomass co-fired brick kilns (28.9%) and traffic (28.2%). Comparison of the PMF derived results with REAS, EDGAR and existing Nepalese inventory showed that all the inventories overestimate the contribution of residential biofuel use and underestimate the contribution of traffic in the Kathmandu Valley.

5.2 Introduction

Volatile Organic Compounds (VOCs) are important atmospheric constituents and are emitted from both natural and anthropogenic sources (Hewitt., 1999). They are important as precursors of surface ozone and secondary organic aerosols (SOA) and affect atmospheric oxidation capacity, climate and human health (IPCC, 2013). Thus, identification of the sources of VOCs is necessary for devising mitigation strategies to improve air quality and reduce undesired impacts of tropospheric ozone and secondary organic aerosol.

Source apportionment of VOCs can be achieved by applying source-receptor models to measured ambient datasets. Ambient VOC mixing ratios depend on the emission profiles of the sources contributing to the ambient mixture, their relative source strengths, transport and removal processes. Source receptor models perform a statistical analysis of the data to identify and quantify the contribution of different sources to the measured VOC concentrations (Watson et al., 2001). Positive matrix factorization (PMF) is currently among the most widely applied receptor model for the source apportionment of VOCs, in particular for high temporal resolution datasets (Anderson et al., 2002; Miller et al., 2002; Kim et al., 2005; Buzcu et al., 2006; Brown et al., 2007; Yuan et al., 2012). In compar-

ison to other receptor models based on principal component analysis/absolute principal component scores (PCA/APCS) (Guo et al., 2004, 2006), chemical mass balance (CMB) (Na and Pyo Kim., 2007; Morino et al., 2011) and UNMIX (Jorquera et al., 2004; Olson et al., 2007), PMF provides more robust results as it does not permit negative source contributions. Moreover, a priori knowledge about the number and signature of VOC source profiles are not needed, which is particularly useful and apt for VOC source apportionment studies in a new atmospheric chemical environment. The recently developed PMF version 5.0 also allows further refining the solution and reducing rotational ambiguity of the solutions using pre-existing knowledge of emission ratios from known point sources. Source apportionment of non-methane hydrocarbons (NMHCs) and oxygenated VOCs (OVOCs) by applying the PMF source-receptor model has been carried out in several previous studies (Shim et al., 2007; Leuchner and Rappenglück., 2010; Gaimoz et al., 2011; Bon et al., 2011; Chen et al., 2014). VOC emission inventories are frequently associated with large uncertainties (Zhang et al., 2009). This is particularly true for metropolitan cities in the developing world. Emission inventories can be evaluated bottom-up using the results obtained from source receptor models such as the PMF model. This evaluation is important to improve the accuracy of the existing emission inventories and therefore to develop effective air pollution control strategies. In this chapter I report the first application of the PMF model for VOCs source apportionment in South Asia, using the VOC dataset I measured in the Kathmandu Valley, which has been presented and analyzed in detail in Chapter 4 of this thesis.

Kathmandu is considered to be amongst the most polluted cities in Asia (Panday et al., 2009). According to the existing Nepalese emission inventory and two other emission inventories, namely REAS v2.1 (Kurokawa et al., 2013) and EDGAR v4.2 (Olivier et al., 1994), residential biofuel use is considered to be the most important anthropogenic source of VOCs in the Kathmandu Valley. It is considered to contribute ∼51% (REAS) to ∼83% (EDGAR), towards the total VOC mass loadings. In contrast, a more recent study on particulate matter (PM_{10} and $PM_{2.5}$) source apportionment conducted by International Centre for Integrated Mountain Development (ICIMOD) suggested that traffic to be the dominant source of air pollution (69%) in the Kathmandu Valley (Pradhan et al., 2012). The objective of the current study is to identify and quantify the contributions of differ-

ent emission sources to the ambient wintertime VOC concentrations in the Kathmandu Valley using positive matrix factorization (EPA PMF 5.0; Brown et al. (2015)) receptor model. VOC measurements were carried out at a suburban site in the Kathmandu Valley during SusKat-ABC field campaign (19 December 2012-30 January 2013). The measurement details and qualitative analysis of the new findings have been presented and discussed in Chapter 4 of this thesis. The VOC measurements indicated the contribution of varied emission sources such as traffic (associated with high toluene, xylenes and trimethylbenzenes), biomass co-fired brick kilns (associated with high acetonitrile and benzene) and wintertime biogenic sources (as characterized by high daytime isoprene). Based on the VOCs emission profiles, two distinct periods were identified in the dataset: the first period (19 December 2012-3 January 2013) was associated with high daytime isoprene concentrations whereas the second period (4-18 January 2013) was associated with sudden increase in acetonitrile and benzene concentrations which was suspected to be due to the kick start of the biomass co-fired brick kilns in the Kathmandu Valley. For quantitative source apportionment, hourly mean measured concentrations of all 37 VOCs measured during the instrumental deployment (19 December 2012-30 January 2013), were used for the PMF analysis. Sensitivity tests were conducted for the PMF 5.0 model version to evaluate how the new rotational tool called "constrained model operation feature" improves the representation of source profiles in the PMF model output. A total of eight source categories were determined to contribute towards VOC mixing ratios at the receptor site. These could be attributed to-solvent evaporation, mixed daytime source, biomass co-fired brick kiln emissions, residential biofuel use and waste disposal, traffic, biogenic emissions, mixed industrial emissions and an unresolved industrial emission factor. To identify the physical locations for these sources, an important prerequisite for targeted mitigation, conditional probability function (CPF) analyses were performed. Results obtained from the PMF analysis were compared with three emission inventories-the existing Nepalese inventory, REAS v2.1 (Regional Emission inventory in ASia) and EDGAR v4.2 (Emissions Database for Global Atmospheric Research) emission inventory. This comparison shows significant contribution of various industrial sources and traffic to the total VOC mass loadings, while the contribution of residential biofuel use to outdoor air pollution is overestimated in the emission inventories. Finally, the contribution of these eight

source categories to individual VOC mass concentrations, ozone formation potential and formation of secondary organic aerosol (SOA) are also analyzed and discussed.

5.3 Materials and methods

5.3.1 Positive Matrix Factorization (PMF)

The United States Environmental Protection Agency's (US EPA) Positive Matrix Factorization (PMF) 5.0 receptor model was used for source apportionment of VOCs in the Kathmandu Valley. The model is based on the multilinear engine (ME-2) approach and has been described in detail by Paatero. (1997, 1999). From a data matrix of certain number of VOCs in a given number of samples, the PMF model helps determine the total number of possible VOC source factors, the chemical fingerprint (source profile) for each factor, the contribution of each factor to each sample, and the residuals of the dataset using the following equation (Paatero and Tapper., 1994),

$$X_{ij} = \sum_{k=1}^{p} g_{ik} f_{kj} + e_{ij} \tag{5.1}$$

Where, X_{ij} is the VOC data matrix with i number of samples and j number of measured VOCs which is resolved by the PMF to provide p number of possible source factors with the source profile f of each source and mass g contributed by each factor to each individual sample, leaving the residuals e for each sample. To obtain the solution of equation (5.1), sum of the squared residuals (e^2) and variation of data points (σ^2) is inversely weighted in PMF as expressed by the following equation (Paatero and Tapper., 1994),

$$Q = \sum_{i=1}^{n}\sum_{j=1}^{m}(\frac{e_{ij}}{\sigma_{ij}})^2 = \sum_{i=1}^{n}\sum_{j=1}^{m}(\frac{X_{ij} - \sum_{k=1}^{p} g_{ik} f_{kj}}{\sigma_{ij}})^2 \tag{5.2}$$

Where, Q is the object function and a critical parameter for PMF, n is the number of samples, and m is the number of considered species. The original data should always be reproduced by the PMF model within the uncertainty considering the non-negativity constraint for both the predicted source profile and the predicted source contributions.

The explained variability (EV) as given below demonstrates the relative contribution of each factor to the individual compound and can be expressed as (Gaimoz et al., 2011),

$$EV_{kj} = \frac{\sum_{i=1}^{n} |g_{ik} f_{kj}| / \sigma_{ij}}{\sum_{i=1}^{n} (\sum_{k=1}^{p} |g_{ik} f_{kj}| + |e_{ij}|) / \sigma_{ij}} \tag{5.3}$$

The explained variability is most useful to policy makers. If the observed mass loading of a compound that is known to be harmful to human health is high, the explained variability will indicate which sources are responsible for most of its emissions and what fraction of the total observed mass is contributed by each source. Therefore, this allows planning mitigation strategies.

To ascertain the magnitude of random errors that can be caused due to the use of random seeds followed by the selection of the run with the lowest Q due to the existence of infinite solutions with different g_{ik}, f_{kj} and e_{ij} matrices but identical $Q = \sum_{i=1}^{n} \sum_{j=1}^{m} (e_{ij}/\sigma_{ij})^2$, bootstrap runs were performed. In the bootstrap runs, the timeseries is partitioned into smaller segments of a user specified length and the PMF is run on each of these smaller segments, for the same number of factors as the original model run. The model output of each bootstrap run is mapped onto the original solution using a cross correlation matrix of the factor contributions g_{ik} of a given bootstrap run with the factor contributions g_{ik} of the same time segment of the original solution using a threshold of $R > 0.6$. The bootstrap factor is assigned to the factor with which it is most strongly positively correlated, as long as the value of Pearson's R is greater than 0.6. If it cannot be attributed to any factor of the original solution it will be termed unmapped. The presence of a high fraction unmapped factor ($> 20\%$) is a clear indication of large random errors and should be investigated carefully. In our analysis no unmapped factors were present.

For each factor, the factor profile of all bootstrap runs combined is compared with the profile of the original model output. The model will provide a box and whisker plot for the mass loading (μg m^{-3}) and percentage of each compound attributed to the factor profile of each of the factors during the bootstrap runs. It will also ascertain for each compound whether or not the original solution for that factor falls into the interquartile range of the bootstrap results and provide this information in a table format.

When all sources are equally strong throughout the entire period, this bootstrap model

provides a robust estimate of the total random error. However, if one of the sources is completely absent for a significant fraction of the total hours (like the brick kilns emission source throughout the first 13 days of the SusKat-ABC campaign), the bootstrap model may overestimate the random error substantially. For such a source, mass loading of all the compounds that contribute strongly to the factor profile of the source will typically be outside the interquartile range. For the same set of compounds similar behavior could also be seen for the factor profile of several other factors. In such a situation the error estimate of the bootstrap runs should only be considered as the upper limit of the potential random error.

In addition to the random error, the PMF model has rotational ambiguity. There can be an infinite number of solutions with a different factor profile for all factors for which the model will find a different local minimum of the residual matrix while determining the factor contribution matrix. This fact that different solution for ($g_{ik}f_{kj}$) with the same sum of the scaled residuals $Q = \sum_{i=1}^{n}\sum_{j=1}^{m}(e_{ij}/\sigma_{ij})^2$ exist is called the rotational ambiguity of the model. The PMF 5.0 has a new feature named as "the constrained model operation" in which the rotational ambiguity of the model can be constrained using external knowledge of the source composition (f_{kj}) or contribution (g_{ik}) matrix. For instance, if a source was inactive for a particular period, then the contribution due to that factor during that time period could be pulled to zero in the model to provide more robust output. Alternatively, the emission ratios obtained from a particular source through samples collected at the source can also be used to constrain the model. Constraining the PMF model using such external knowledge gives rise to a penalty in Q (the object function) and a maximum penalty of 5% is recommended as a reasonable threshold (Paatero and Hopke., 2009). A detailed discussion of the use of constraints to a receptor model has been provided in previous studies (Paatero et al., 2002; Rizzo and Scheff., 2007; Paatero and Hopke., 2009; Norris et al., 2009).

5.3.2 Implementation of PMF

PMF was applied to the hourly averaged dataset of 37 ions measured using the PTR-TOF-MS from 19 December 2012-30 January 2013 during the SusKat-ABC field campaign in

the Kathmandu Valley (refer Chapter 4). All the available data during this aforementioned period were used for PMF analysis and the missing values were replaced by a missing value indicator (-999). To ensure differential uncertainties do not drive the object function Q and give undue weightage to calibrated organic ions while constructing source profiles, we followed the procedure used by Leuchner and Rappenglück. (2010) for source apportionment of VOCs in the Houston Ship Channel area and assigned a constant uncertainty of 20% for all the ions. The attribution of ions to parent compounds and corresponding detection limits were as described in chapter 4 of this thesis. Due to its erratic timeseries profile, HCN (m/z = 28.007) was classified as a weak species in the PMF input while all other ions were classified as strong species. All the input data was converted from mixing ratios (ppb) to mass concentrations (μg m^{-3}) using the relevant temperature, pressure and molecular weight. The total VOC concentration was calculated by adding the mass concentrations of all VOCs and was classified as a weak species in the PMF input. All the measured ions had a signal to noise (S/N) ratio greater than 2. Table 5.1 shows the signal to noise (S/N) ratios for all input VOC species used in the PMF along with other statistical parameters of the dataset.

PMF model runs ranging from 5 to 12 factor numbers were carried out to ascertain the best solution for this study consistent with the chemical environment of the Kathmandu Valley. Based on the $Q/Q_{theoretical}$ ratio, the physical plausibility of the factors and the rotational ambiguity of the solution, an 8-factor solution was deemed to be the best for this dataset. When less than 7 factors were employed, several source profiles appeared to be mixed, indicating inadequate resolution of sources. The solution incorporating 7-factors caused strong overlap of mixed industrial emissions with the unresolved industrial emissions factor. One of the side effects of that solution was that the factor containing daytime biogenic emissions retained the combustion source of isoprene. Even when the model was nudged towards separating the biogenic emissions and the anthropogenic combustion sources of isoprene, this separation could only be accomplished with a large penalty on Q in the 7-factor solution. The 9-factor solution had too much rotational ambiguity and assigned brick kiln emissions to two largely co-linear factors, both of which had an incomplete source profile with respect to aromatic compounds and were essentially created to better account for minor variations in the emission ratios associated with brick

Table 5.1: Statistical parameters for the measured species used as PMF input

VOCs	Category	S/N	Min	25^{th}	Median	75^{th}	Max	N[1]	Nbdl[2]
Hydrogen Cyanide	Weak	3.10	0.29	0.62	0.90	1.79	12.43	969	0
Formaldehyde	Strong	3.93	0.60	1.43	1.80	2.34	5.39	969	0
Methanol	Strong	4.00	3.31	6.69	8.51	10.32	21.79	969	0
Propyne	Strong	4.00	3.37	8.27	10.95	13.73	37.58	969	0
Acetonitrile	Strong	3.95	0.50	1.00	1.47	2.04	5.60	969	0
Propene	Strong	4.00	1.37	3.99	6.03	7.78	18.34	969	0
Isocyanic acid	Strong	3.91	0.94	1.22	1.36	1.61	2.39	969	0
Acetaldehyde	Strong	3.97	3.46	8.83	11.52	15.46	61.96	969	0
Nitronium ion	Strong	3.86	0.81	1.37	1.65	1.97	5.42	969	0
Formamide	Strong	3.71	0.55	0.93	1.20	1.51	2.67	969	0
Formic acid	Strong	4.00	2.42	6.85	7.92	9.61	17.74	969	0
Ethanol	Strong	2.78	bdl	1.16	2.21	3.49	18.63	969	51
1,3-Butadiyne	Strong	3.99	0.13	0.89	1.20	1.51	3.43	969	0
Propanenitrile	Strong	3.77	0.09	0.32	0.40	0.50	0.98	969	0
Acrolein+ Methylketene	Strong	3.95	0.40	1.14	1.51	2.06	4.09	969	0
Acetone+Propanal	Strong	3.99	3.55	6.99	8.71	10.38	23.48	969	0
Acetamide	Strong	3.53	0.51	0.69	0.82	0.97	1.53	969	0
Acetic acid	Strong	3.88	4.69	9.31	11.99	15.56	35.04	969	0
Nitromethane	Strong	3.83	0.16	0.37	0.50	0.69	1.85	969	0
Dimethyl Sulfide	Strong	3.46	0.19	0.50	0.56	0.63	2.35	969	0
1,3-Cyclopentadiene	Strong	3.97	0.14	0.36	0.50	0.70	4.42	969	0
Furan	Strong	3.98	0.19	0.66	1.14	1.52	3.38	969	0
Isoprene	Strong	4.00	0.28	1.76	2.39	3.43	11.25	969	0
Methylvinylketone; Methacrolein	Strong	3.94	0.18	0.61	0.81	1.11	3.08	969	0
Methylglyoxal	Strong	3.89	0.18	0.56	0.76	1.01	2.27	969	0
Methylethylketone	Strong	3.93	0.37	1.30	1.73	2.18	4.93	969	0
Hydroxyacetone	Strong	3.74	0.27	1.17	1.54	2.15	4.47	969	0
Benzene	Strong	4.00	0.95	3.98	6.79	10.11	37.35	969	0
Assorted Hydrocarbons	Strong	3.99	0.10	0.78	1.10	1.66	6.88	969	0
2,3-Butanedione	Strong	3.86	0.16	0.80	1.04	1.36	3.35	969	0
Toluene	Strong	4.00	0.51	3.09	4.51	6.54	30.71	969	0
2-Furaldehyde (furfural)	Strong	3.96	0.18	0.61	0.83	1.15	2.23	969	0
Assorted Hydrocarbons	Strong	3.97	0.08	0.48	0.70	1.03	3.03	969	0
Styrene	Strong	3.98	0.09	0.41	0.67	1.06	3.32	969	0
Xylenes	Strong	4.00	0.31	2.12	3.19	4.79	24.73	969	0
Trimethylbenzenes	Strong	3.99	0.17	0.94	1.39	2.14	10.44	969	0
Naphthalene	Strong	3.97	0.28	0.92	1.44	2.00	6.94	969	0

1. Number of valid hourly VOC samples; 2. Number of samples below detection limit

Table 5.2: Diagnostic for the results of the positive matrix factorization (PMF) model run

n (samples)	1006
m (species)	37
k (factors)	8
Q (theoretical)	4480.37
Q (model)	4562.89
Mean ratio VOC(estimated)/VOC(observed)	0.999

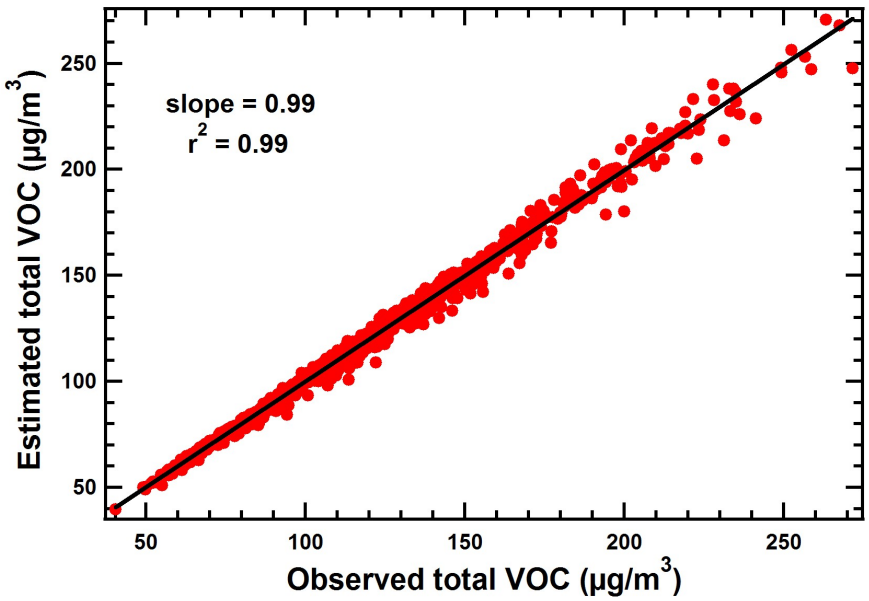

Figure 5.1: Correlation between estimated and observed VOC concentrations

kiln emissions during the firing up period and continuous operation.

The diagnostics for the 8-factor solution are summarized in Table 5.2. To identify the uncertainty associated with the PMF solution, bootstrap runs were performed for 100 times taking 96 hours as each segment length. There were no unmapped factors in the bootstrap runs.

Figure 5.1 shows the correlation between the estimated total VOC concentrations calculated using the contributions from all factors with measured total VOC concentrations. An excellent correlation ($r^2 = 0.99$) indicates that PMF model can explain almost all variance in the total VOC concentrations.

The constrained model mode was used to improve the 8-factor solution further. The original model output showed positive correlations between factors such as the biomass co-fired

brick kilns and mixed industrial emissions ($r^2 = 0.27$) as well as residential biofuel use and waste disposal factors with the traffic factor ($r^2 = 0.42$). Since this is a new feature and has only been used recently by (Brown et al., 2015) for ambient air data, a detailed description of the implementation procedure and an analysis of how the constraints affected the model output is provided here. Several constraints were used to obtain a more robust PMF solution.

Firstly, the upper limit for the emission ratio of the individual aromatic compounds to isoprene as reported by (Misztal et al., 2015) were used to constrain the factor profile of primary biogenic emissions. As a small fraction of the biogenic isoprene gets attributed to other daytime factor (mixed daytime) by the PMF model, the same constraint were used on mixed daytime factor and the solvent evaporation factor as well.

Secondly, it was assumed that aromatic compounds and acetonitrile are not photochemically produced. Acetic acid is associated with both mixed daytime and solvent evaporation, the ratios of aromatic compounds and acetonitrile to acetic acid were nudged towards 0.0001 for these factors.

Thirdly, to improve the representation of brick kiln emissions and the residential biofuel use and waste disposal in the model, the respective factors, which were clearly identified in the original model solution were nudged using the emission ratios of aromatic compounds to benzene from grab samples collected directly at the source. This was required, because in the original model output, the residential biofuel use and waste disposal factor correlate with the traffic factor ($r^2 = 0.42$) while the brick kilns emission factor correlated with the mixed industrial emissions factor ($r^2 = 0.27$). This indicates that there was substantial rotational ambiguity for these two factor pairs.

Nudging was performed by exerting a soft pull allowing for a maximum 0.2% change in Q for each constraint. A soft pull allows the change in the Q value up to a certain limit by pulling the values to a target value for an expression of elements (the emission ratio). If no minima can be found for which the change in $Q = \sum_{i=1}^{n}\sum_{j=1}^{m}(e_{ij}/\sigma_{ij})^2$ is less than 0.2% in the $g_{ik}f_{kj}$ matrix after f_{kj} has been constrained, no change was made and the original solution was retained. If the condition can be met without changing Q by more than the threshold, the revised factor profiles will be used as the base upon which the next constraint in the list of constraints will be executed.

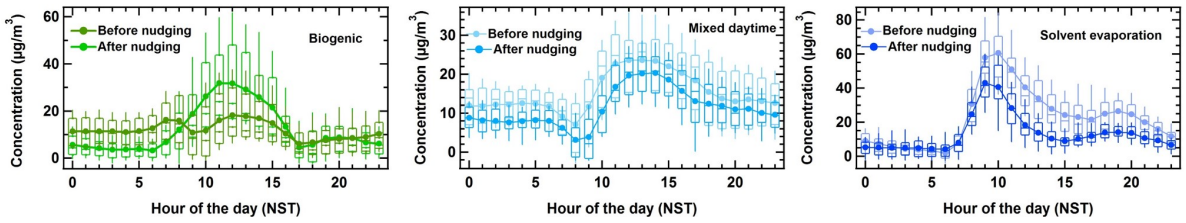

Figure 5.2: Comparison of the diel profiles of biogenic emissions, mixed daytime and solvent evaporation factors before and after nudging

Implementing the constraints mentioned above significantly improved the representation of biogenic emissions, mixed daytime and solvent evaporation factors. Figure 5.2 shows a comparison of the box and whisker plots of the biogenic emissions, mixed daytime and solvent evaporation factors before and after nudging and demonstrates the significant improvement after applying constraints.

After nudging, the contribution of the biogenic factor correlated better with solar radiation ($r^2 = 0.48$) while the mixed daytime factor correlated better with ambient temperature ($r^2 = 0.42$). The factor profile of the solvent evaporation correlates better with the rise in solar radiation and temperature after sunrise (07:00-09:00 LT; $r^2 = 0.53$). Table 5.3 represents the emission ratios used to nudge the biogenic, mixed daytime and solvent evaporation factors and provides the corresponding emission ratios before and after nudging.

It can be seen that most constraints on the aromatic to isoprene ratio could be executed without exceeding the penalty on Q. In the biogenic factor, only the naphthalene/isoprene ratio could not be constrained. The solvent evaporation and mixed daytime factors contain only a small fraction of the total daytime isoprene (8% and 7% respectively). Given the very small overall isoprene mass in these two factor profiles, few additional ratios did not meet the constraining criteria in these factor profiles (namely acetonitrile/isoprene and trimethylbenzenes/isoprene ratio in the mixed daytime factor and the xylenes/isoprene and naphthalene/isoprene ratio in the solvent evaporation factor). Some of these compounds (such as naphthalene) could not be constrained in the same factors while constraining the ERs with respect to acetic acid.

The fact that the constrained run was incapable of removing naphthalene from the source profiles of the biogenic and solvent evaporation source and the fact that the diel pro-

Table 5.3: Inter VOC emission ratios used for biogenic, solvent evaporation and mixed daytime factors to nudge the PMF model and the corresponding emission ratios before and after nudging

ERs/Isoprene	ERs used to nudge	Biogenic		Solvent	evaporation	Mixed	daytime
		before nudging	after nudging	before nudging	after nudging	before nudging	after nudging
Acetonitrile	0.002	0.06	0.00	0.00	0.004	2.78	1.75
Benzene	0.002	0.29	0.00	0.52	0.00	0.15	0.00
Toluene	0.012	0.10	0.01	0.39	0.00	4.82	0.00
Styrene	0.002	0.02	0.00	0.06	0.00	0.00	0.002
Xylenes	0.002	0.00	0.0002	0.35	0.41	4.65	0.00
Trimetylbenzenes	0.002	0.06	0.01	0.09	0.00	1.85	0.20
Naphthalene	0.002	0.31	0.30	0.36	0.60	0.00	0.002
ERs/Acetic acid	ERs used to nudge	Biogenic		Solvent	evaporation	Mixed	daytime
		before nudging	after nudging	before nudging	after nudging	before nudging	after nudging
Acetonitrile	0.0001	0.57	0.00	0.00	0.0001	0.07	0.09
Benzene	0.002	1.48	0.00	0.04	0.00	0.01	0.00
Toluene	0.0001	1.01	0.004	0.05	0.00	0.12	0.00
Styrene	0.0001	0.15	0.00	0.01	0.00	0.00	0.0001
Xylenes	0.0001	0.00	0.0001	0.04	0.01	0.12	0.00
Trimetylbenzenes	0.0001	0.59	0.004	0.01	0.00	0.05	0.01
Naphthalene	0.0001	3.08	0.15	0.04	0.01	0.00	0.0001

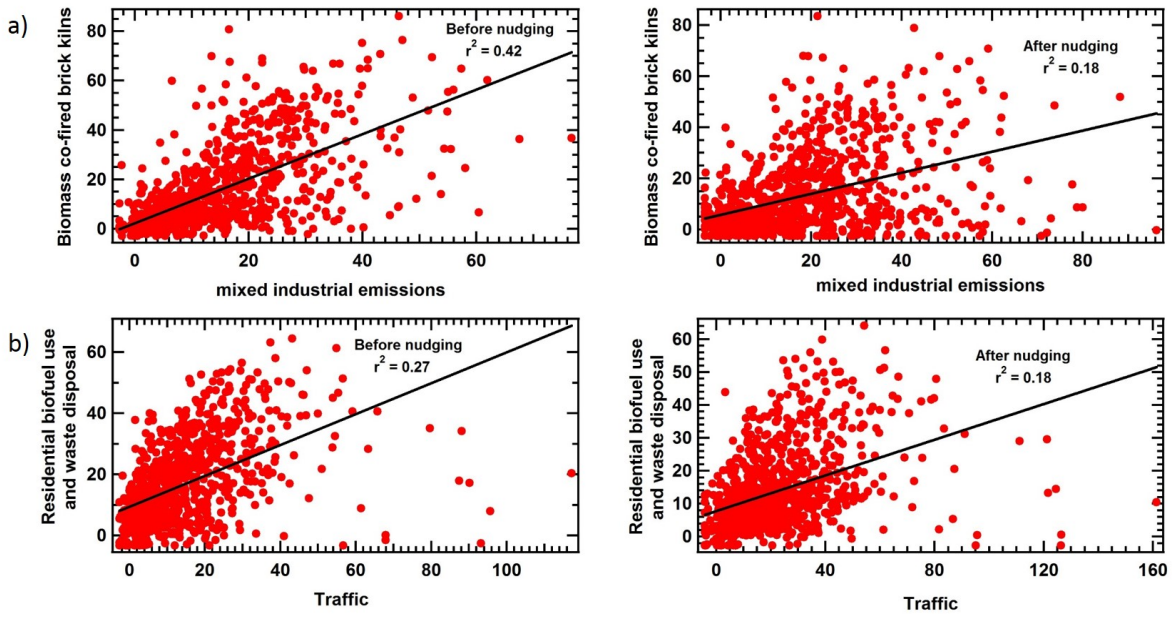

Figure 5.3: Comparison of the G-space plots between a) biomass co-fired brick kilns and mixed industrial emissions and b) residential biofuel use and waste disposal and traffic before and after nudging

files of both these factors show a weak secondary peak between 17:00-22:00 LT, seems to indicate that an additional weak combustion source with a high naphthalene emission ratio is possibly poorly represented by the current 8-factor solution. Cooking on 3 stone fires is known to emit large amounts of benzene and naphthalene (Stockwell et al., 2015) and the temporal profile of such a cooking source could overlap with that of the garbage fires. This would make it challenging for the model to separate these two sources. We, therefore, will henceforth refer to the garbage burning factor as the residential biofuel use and waste disposal factor.

Figure 5.3a shows the G-space plots for two factors, namely biomass co-fired brick kilns and mixed industrial emissions. A stronger correlation ($r^2 = 0.42$) existed in the original solution prior to nudging with ERs of grab samples, which reduced to $r^2 = 0.18$. Similarly, the correlations between residential biofuel use and waste disposal was reduced from 0.27 to 0.18, as shown in Figure 5.3b. Thus, the new solution fills the solution space better.

Table 5.4 summarizes the aromatics/benzene emission ratios derived from the PMF (before and after nudging) and its comparison with the emission ratios obtained from grab samples for biomass co-fired brick kilns and residential biofuel use and waste disposal sources.

Table 5.4: Comparison of aromatics/benzene ERs (emission ratios) obtained from PMF (before and after nudging), respective grab samples and the 3 stone firewood source reported in Stockwell et al. (2015)

ERs/Benzene	Biomass kilns	co-fired brick		3 stone firewood	Residential and waste biofuel disposal use		
	Grab samples	PMF (before nudging)	PMF (after nudging)	Stockwell et al. (2015)	Grab samples	PMF (before nudging)	PMF (after nudging)
Toluene	0.80	0.28	0.35	0.10	0.34	0.33	0.34
Styrene	0.08	0.05	0.06	0.07	0.16	0.22	0.18
Xylenes	0.58	0.16	0.22	0.08	0.25	0.28	0.25
Trimethylbenzenes	0.31	0.06	0.02	0.03	0.08	0.16	0.12
Naphthalene	0.09	0.14	0.15	0.25	0.09	0.16	0.11

For the residential biofuel use and waste disposal source, the original model run already had emission ratios very similar to the grab samples. The constrained run improved the agreement further for styrene, trimethylbenzenes and naphthalene. Constraining this factor with the ER of 3 stone firewood stoves from Stockwell et al. (2015) instead of our garbage burning grab samples resulted in a larger penalty on Q and did not improve the representation of the biogenic, mixed daytime and solvent evaporation factors.

For brick kilns, the emission ratios of the constrained model output runs diverged from the emission ratios of the grab samples. However, the temporal profile of the activity, especially the closure of the brick kilns during the first part of the campaign is better captured by the constrained run and the correlation with mixed industrial emission sources reduced significantly. The grab samples were collected on 6 December 2014, two years after the SusKat study so differences from the emission profiles observed during the SusKat-ABC campaign is a possibility. Alternatively, the differences could also stem from the inherently variable nature of this source. In particular naphthalene and benzene, were higher in the source profiles of the SusKat-ABC campaign compared to their relative abundances in the grab samples. At the time the grab samples were collected (on 6 December 2014), brick kilns were co-fired using coal, wood dust and sugarcane extracts. It is possible that in January, during peak winter season, a different type of biomass, one associated with higher benzene and naphthalene emissions (e.g., wood) was used in these biomass co-fired brick kilns, resulting in the slight disagreement between the PMF source profile and grab

sample signature for this factor.

5.3.3 Conditional probability function (CPF) analyses

For identifying the physical locations associated with different local sources, conditional probability function (CPF) analyses were performed. CPF is a well-established method to identify source locations of local sources based on the measured wind (Fleming et al., 2012). In CPF, the probability of a particular source contribution from a specific wind direction bin exceeding a certain threshold is employed which is calculated as follows:

$$CPF = \frac{m_{\Delta\theta}}{n_{\Delta\theta}} \tag{5.4}$$

Where $m_{\Delta\theta}$ represents the number of data points in the wind direction bin $\Delta\theta$ which exceeded the threshold criterion and $n_{\Delta\theta}$ is total number of data points from same wind direction bin. For this study, $\Delta\theta$ was chosen as 30° and data for wind speed > 0.5 m s^{-1} were used.

5.4 Results and Discussion

5.4.1 Identification of PMF factors

Figure 5.4 represents the factor profiles of all the 8 factors resolved by the PMF model in which grey bars indicate the mass concentrations and red lines with markers show the percentage of a species in the respective factor.
Identification and attribution of these factors is discussed in detail in the following sections.

5.4.2 Factor 1 - Traffic

More than 60% of total toluene, sum of C8-aromatics, sum of C9-aromatics and ∼37% of total assorted hydrocarbons (m/z = 97.102 and 83.085) were explained by Factor 1. Toluene and C8-aromatics contributed most (∼16% and ∼13%, respectively) to the total VOC mass of Factor 1. In addition four other compounds also contributed ≥ 5% to the

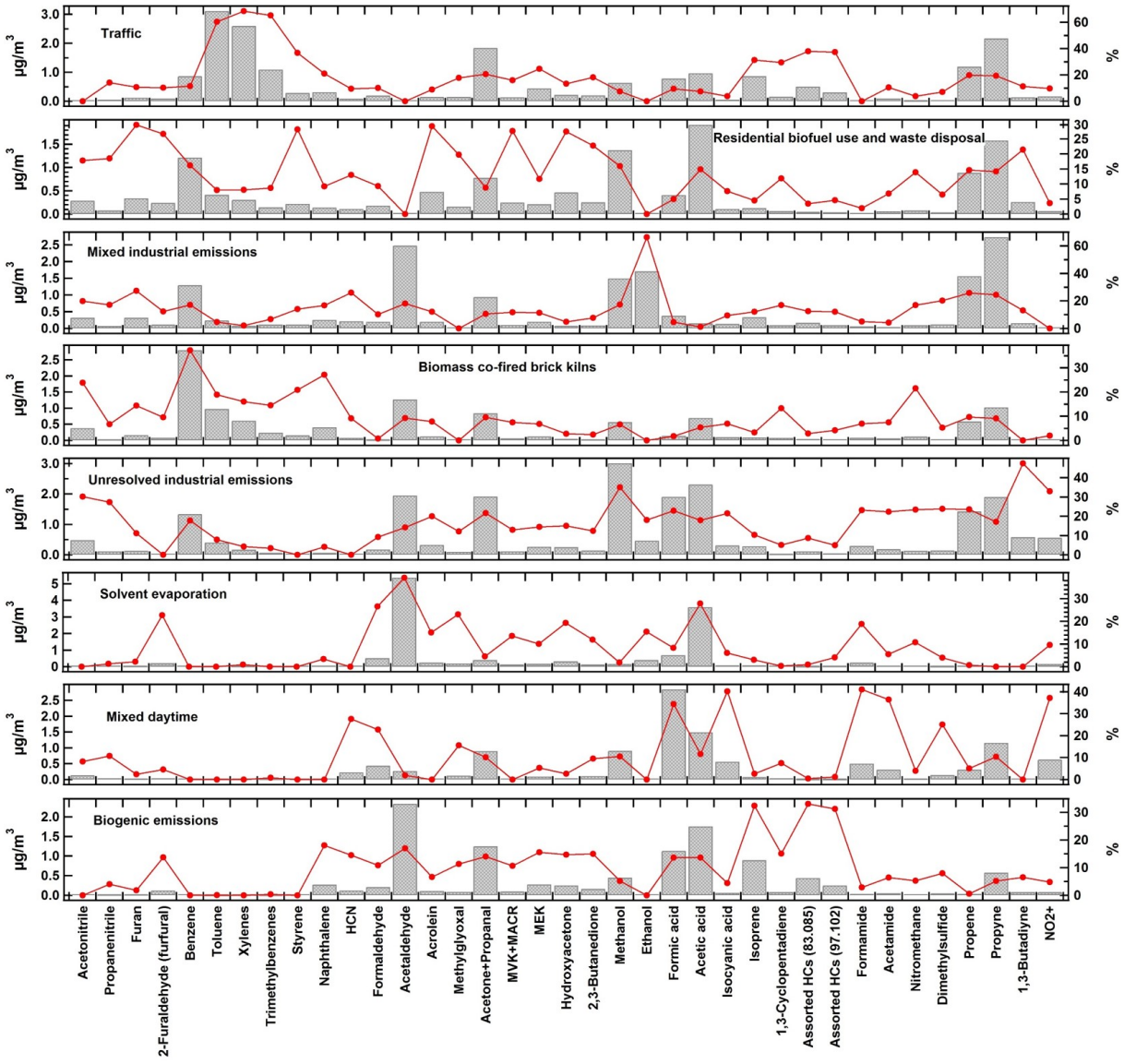

Figure 5.4: Factor profiles of the eight sources obtained by PMF analysis

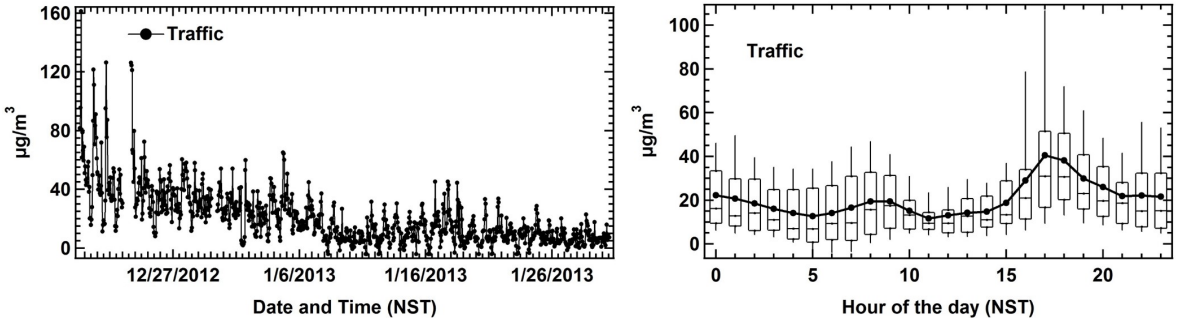

Figure 5.5: Timeseries and diel box and whisker plot for Factor 1 (Traffic)

total mass of this factor (propyne (∼11%), acetone (∼9%), propene (∼6%) and sum of C9-aromatics (∼5%)). The other 31 VOCs contributed ∼40% of the total VOC mass to this factor but their individual contributions were ≤ 5% each. The diel profile of Factor 1 (Figure 5.5) showed characteristic evening peak at 17:00 LT with an average concentration of ∼40 μg m^{-3}. This evening peak showed large variability and plume-like characteristics as the average and median diverged frequently. Occasionally, the mass contribution of this factor amounted to ∼100 μg m^{-3}. The high variability during the evening peak hour indicates that the source strength is not equal for all wind directions, but varies with fetch region.

Table 5.5 shows that the aromatics/benzene emission ratios for this factor are in good agreement with the emission ratios reported by previous studies for vehicular emissions in tunnel studies and in metropolitan sites/megacities. In view of the diel profile and observed chemical signatures, Factor 1 was attributed to traffic. It is interesting to note that ∼37% of the total styrene was present in this factor and ∼31% of the total isoprene was also explained by this factor. Few previous studies have reported traffic related sources of isoprene in urban areas (Borbon et al., 2001; Hellèn et al., 2012) and also estimated isoprene as one of the top 10 contributors to OH reactivity from traffic (Nakashima et al., 2010). Our results indicate that traffic can be a significant source of nighttime isoprene in the Kathmandu Valley.

5.4.3 Factor 2 - Residential biofuel use and waste disposal

Factor 2, too, showed regular evening hour peaks and a bimodal profile (Figure 5.6). However, the evening peak of average concentrations as high as ∼40 μg m^{-3} occurred

Table 5.5: Emission ratios of VOCs/benzene for aromatic hydrocarbons derived from the PMF model for factor attributed to traffic and comparison of ERs with previous studies for traffic source profiles

	Kathmandu PMF	Tunnel study, Stockholm[1]	Tunnel Study, Hong Kong[2]	Tunnel Study, Taipei[3]	Mexico City[4]	Los Angeles[5]
Toluene	3.41	3.89	2.27	2.80	3.47	2.45
C8-aromatics	2.89	2.81	0.87	2.53	3.55	1.38
C9-aromatics	1.20	-	0.77	2.09	2.31	0.48
Styrene	0.30	-	-	0.53	0.17	-
Naphthalene	0.19	-	0.10	-	-	-

1. Kristensson et al. (2004); 2. Ho et al. (2009); 3.Hwa et al. (2002) ; 4.Bon et al. (2011) ; 5. Borbon et al. (2013)

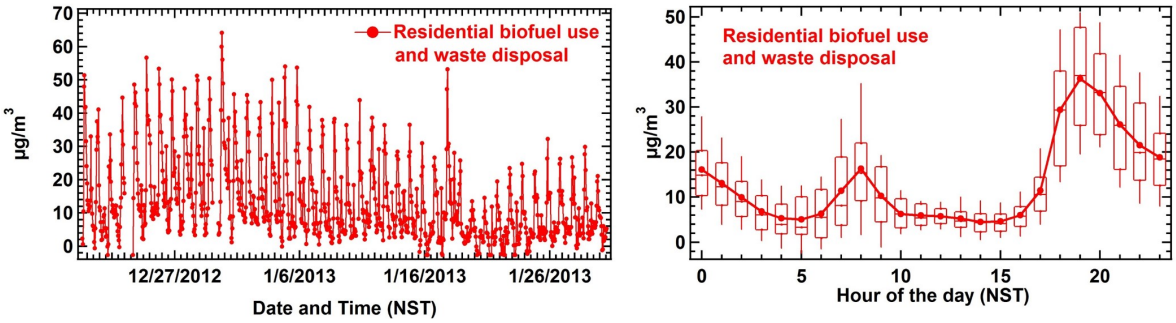

Figure 5.6: Timeseries and diel box and whisker plot for Factor 2 (Residential biofuel use and waste disposal)

after the traffic peak (at 19:00 LT) and had less variability, indicating that this source is an area source that is more equally distributed throughout the Katmandu Valley. The diel box and whisker plot also has a relatively weak morning peak (at 08:00 LT) with average concentrations of ∼18 μg m^{-3}. Figure 5.4 shows, that this factor explains 30% of total styrene, furan, 2-furaldehyde and acrolein.

Most of the VOC mass in this factor was contributed by acetic acid, propyne, methanol, benzene, propene and acetone+propanal (∼14%, ∼12%, ∼10%, ∼9%, ∼7% and ∼6% respectively). The other 31 VOCs contributed ∼42% to this factor, but their individual contributions were $\leq$ 5% each (Figure 5.4). It was observed that garbage/trash burning activities were more intense during evening hours of winter in the Kathmandu Valley. Table 5.6 shows a comparison of the aromatics/benzene emission ratios obtained from the PMF, with previously reported aromatics/benzene ratios for waste and trash burning, and with the emission ratios of grab samples that were collected in the Kathmandu Valley near the source (a household waste fire). It can be seen that the aromatics/benzene emission

Table 5.6: Emission ratios of VOCs/benzene for acetonitrile and aromatic hydrocarbons derived from the PMF model for the factor attributed to Residential biofuel use and burning household waste and comparison with previously reported studies and the grab sample collected at the point source

	Kathmandu PMF	Kathmandu grab samples	Household waste burning[1]	Trash burning[2]	Scrap tires burning[1]
Acetonitrile	0.23	0.77	-	0.10	-
Toluene	0.34	0.34	0.45	0.37	0.74
C8-aromatics	0.25	0.25	0.31	0.10	1.06
C9-aromatics	0.12	0.08	-	0.03	0.04
Styrene	0.18	0.16	0.72	0.89	0.40
Naphthalene	0.11	0.09	0.02	0.13	0.49

1. Lemieux et al. (2004); 2. Stockwell et al. (2015)

ratios of the PMF output are in excellent agreement with the values obtained for grab samples collected in the Kathmandu Valley.

The garbage burning grab samples were collected near the measurement site (∼200 m in the northern direction, upwind of Bode; 27.690°N, 85.395°E) on 7 December 2014 between 15:00-15:03 LT. The whole air samples were collected in a 2 litre glass flask that had been validated for the stability of VOCs (Chandra et al., in preparation) and were analyzed within 38 hours of the collection (on 9 December 2014 between 03:42-04:05 LT). The whole air samples were diluted by a factor of 10 using VOC free zero air. The average background instrumental signals while measuring VOC free zero air were subtracted from each m/z channel. At least 10 cycles (∼10 minutes) of data were measured. Figure 5.7 shows pictures of the grab sample collection and the instrumental setup used for the analysis.

There is some agreement with the emission ratios reported in previous studies, though all of these previous studies found higher emission ratios for styrene. This could indicate, that the composition of household waste in the Kathmandu Valley is different (less thermocol, plastic and more biomass) or that the source profile is mixed with that of a second source, with similar spatial and temporal characteristics. Residential biofuel use is expected to have a similar temporal profile and did not appear as a separate factor in the PMF solution. Therefore, Factor 2 was attributed to residential biofuel use and waste disposal sources collectively.

Figure 5.7: Collection of garbage burning grab samples in the Kathmandu Valley (on left) and the instrumental setup for the analysis (on right)

5.4.4 Factor 3 - Mixed industrial emissions

This factor explained 66% of the total ethanol, which is used as an industrial solvent. Moreover, ∼20-25% of the total propyne, propene, acetonitrile, dimethyl sulfide (DMS) and furan were also present in this factor. All these compounds have industrial sources (Karl et al., 2003; Kim et al., 2008) as they are widely used as solvents/reactants in various industrial processes and can be emitted during combustion processes. Therefore, Factor 3 was attributed to mixed industrial emissions. Most of the VOC mass in this factor was contributed by propyne (∼16%), acetaldehyde (∼15%), ethanol (∼10%), propene (∼9%), methanol (∼9%), benzene (∼8%) and acetone+propanal (∼5%). The emissions reflect both release of chemicals used in the industrial units as well as emissions associated with combustion of a variety of fuels including biofuels. The other 30 VOCs jointly contributed only ∼28% of the total VOC mass and their individual contribution were $\leq$ 5% each. The emission strength of industrial sources is typically constant throughout the day and hence the observed mass concentrations are driven by boundary layer dynamics. The diel box and whisker plot (Figure 5.8) shows a gradual increase in the mass concentrations throughout the night. The highest mass concentration are observed just after sunrise, when the inversion in the mountain Valley is most shallow. This shallow early morning boundary layer is caused by the cold pooling of air at night, which results in an accumulation of cold air at the Valley bottom. The rising sun first warms the upper part

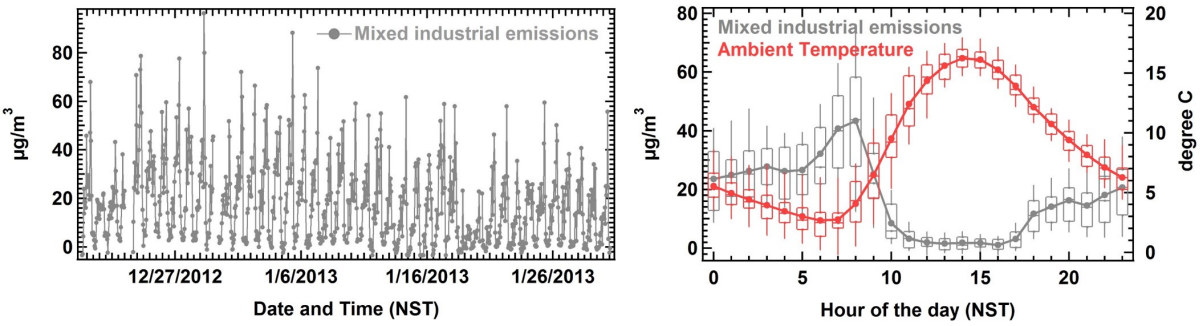

Figure 5.8: Timeseries and diel box and whisker plot for Factor 3 (Mixed industrial emissions)

of the Valley's atmosphere, while the Valley bottom is still in the shade of the surrounding mountains. Once direct sunlight reaches the Valley bottom, warming and thermally driven convection breaks the shallow boundary layer and wind speeds increase, increasing turbulent mixing under a growing boundary layer. The daytime mass concentrations of the mixed industrial emissions are hence an inverse of the temperature and wind speed profile (Figure 5.8).

5.4.5 Factor 4 - Biomass co-fired brick kilns

The diel box and whisker plot of factor 4 (Figure 5.9) shows a profile that is similar to the profile of mixed industrial emissions, indicating that this factor should be attributed to a source that operates 24/7, as its mass loadings, too, represent an inverse of the temperature and wind speed profile. The timeseries of Factor 4 showed sudden increase from 4 January 2013 at exactly the time when brick kilns in the Kathmandu Valley became operational (refer Chapter 4).

Benzene (∼23%) contributed most to the total VOC mass of Factor 4. In addition acetaldehyde (∼10%), propyne (∼8%), toluene (∼8%), acetone (∼7%), acetic acid (∼5%) and xylenes (∼5%) also contributed significantly to the total VOC mass. The other 30 VOCs contributed ∼34% to the total VOC mass of this factor, but their individual contribution were $\leq$ 5% each. Overall, factor 4 explained ∼37% of total benzene and ∼24% of the total acetonitrile mass loading.

It is reported that brick kilns in the Kathmandu Valley burn large quantity of biomass, wood and crop residues along with coal (Stone et al. (2010); Chapter 4) that can lead

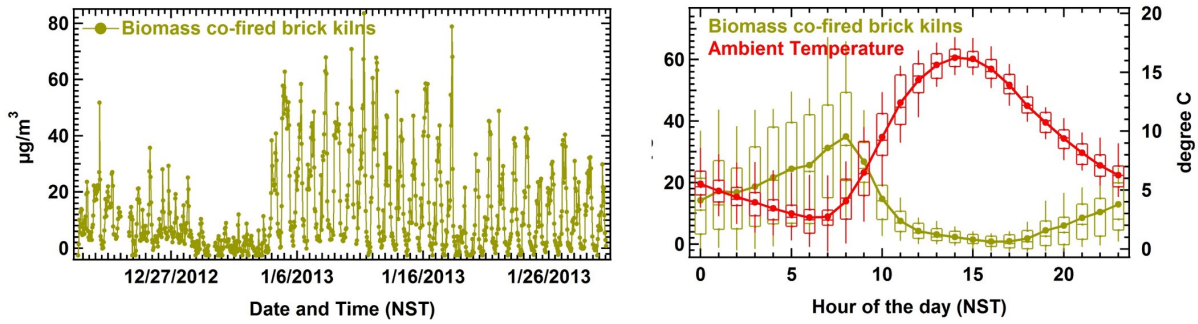

Figure 5.9: Timeseries and diel box and whisker plot for Factor 4 (Biomass co-fired brick kilns)

to significant emission of aromatics and acetonitrile (Akagi et al. (2011); Yokelson et al. (2013); Chapter 3). Therefore Factor 4 was attributed to the biomass co-fired brick kilns and the conditional probability function analysis (Section 5.4.10) is consistent with this assignment.

5.4.6 Factor 5 - Unresolved industrial emissions

Factor 5 explained ∼48% of total 1,3-butadiyne, ∼35% of total methanol , ∼30% of total acetonitrile and ∼27% of the total propanenitrile and ∼24% of the total nitromethane. 1,3-butadiyne is used in the production of several polymers and acetonitrile and propene can be side products in this process. Propanenitrile is used to start acrylic polymerization reactions in industrial processes. The largest use of methanol worldwide is as feedstock for the plastic industry and nitromethane is used in the synthesis of several important pharmaceutical drugs. Nitromethane is also emitted from combustion of diesel fired generators (Inomata et al., 2013; Sekimoto et al., 2013; Inomata et al., 2014) which are used as a back-up power source by both small and large industrial units. It is, therefore, likely that miscellaneous nearby industries contributed significantly to the unresolved factor. The diel profile of Factor 5 (Figure 5.10) showed morning and evening peaks (at 09:00-10:00 LT and 17:00 LT, respectively), which is not typical for industrial emissions, but this factor always had a high background with average mass loadings of ∼20 μg m^{-3} throughout. The timeseries and diel profile (Figure 5.10) of this factor did not reveal characteristics that could be related uniquely to a known emission source.

Factor 5.10 displayed elevated daytime mass concentrations and an evening peak that

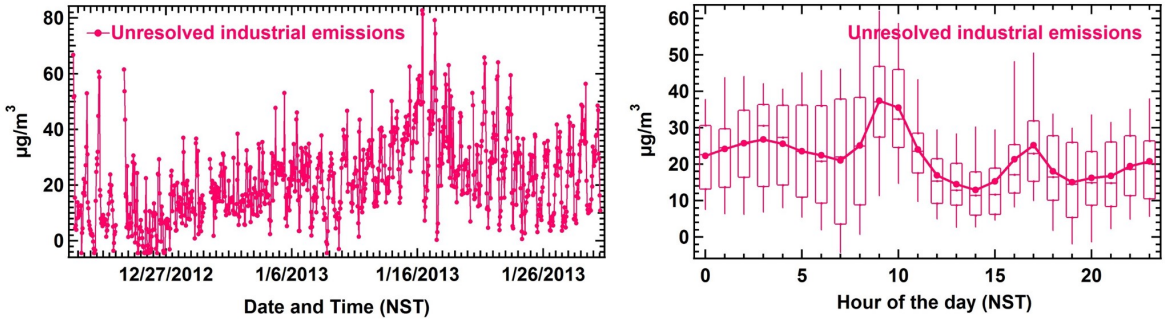

Figure 5.10: Timeseries and diel box and whisker plot for Factor 5 (Unresolved industrial emissions)

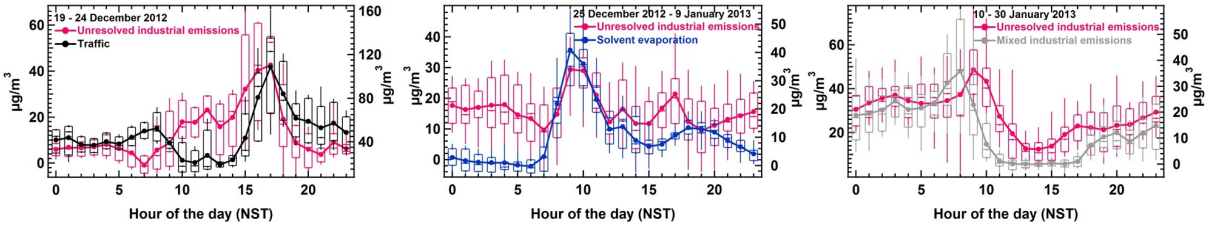

Figure 5.11: Comparison of the diel profile of the unresolved industrial emissions with that of traffic (19-24 December 2012), solvent evaporation (25 December 2012-9 January 2013) and mixed industrial emissions (10-30 January 2013)

occurs slightly before the traffic peak in the early evening during the first part of the SusKat-ABC campaign (till 25 December). Towards the end of the campaign (from 10 January onwards), the same factor had diurnal variations that showed some similarity to profiles of both the solvent evaporation (morning peak) and mixed industrial emissions (slow rise throughout evening and nighttime) factors. Between 25 December 2012 and 10 January 2013, diurnal patterns are weak and peaks in the unresolved factor seem to coincide with peaks in the solvent evaporation factor. This comparison of the diel profiles is shown in Figure 5.11. Since this factor seems to contain contributions of multiple sources and potentially the photooxidation products of their emissions, this factor was termed as the unresolved industrial emissions factor.

Most of the total VOC mass of Factor 5 was due to oxygenated VOCs like methanol (∼14%), acetic acid (∼11%), acetaldehyde (∼9%), acetone (∼9%) and formic acid (∼9%) but benzene, propyne and propene also contributed > 5% (∼9%, ∼6% and ∼6%, respectively) to the total VOC mass of this factor. The other 29 VOCs together contributed only ∼27% to this factor and their individual contributions were less than 5%.

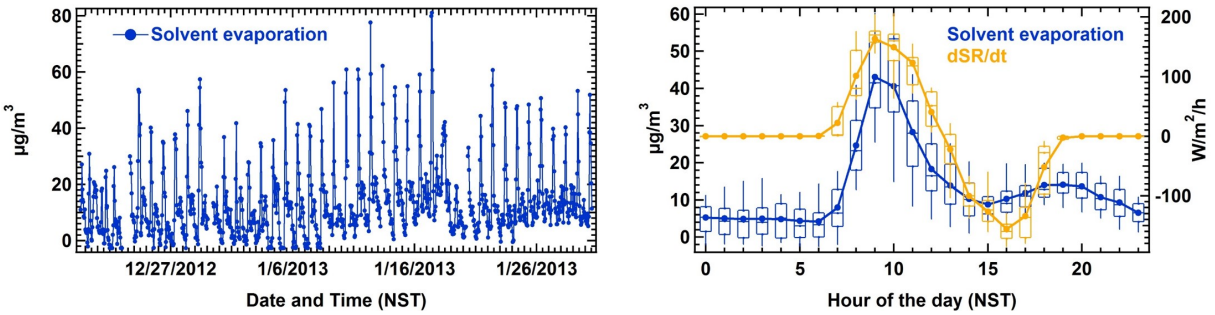

Figure 5.12: Timeseries and diel box and whisker plot for Factor 6 (Solvent evaporation)

5.4.7 Factor 6 - Solvent evaporation

Factor 6 explains approximately 25-40% of the compounds containing the aldehyde functional group. It explained ∼39% of the acetaldehyde, ∼27% of total formaldehyde and ∼23% of 2-furaldehyde. Moreover, ∼28% of the total acetic acid and ∼23% of the total methylglyoxal were explained by this factor. Acetaldehyde and acetic acid contributed ∼40% and ∼27% respectively to the total VOC mass of Factor 6 while formic acid, formaldehyde, acetone and ethanol together contributed ∼15% (∼5%, ∼4% and ∼3%, respectively) to the total VOC mass of this factor. The other 31 species contributed only ∼18%. The diel profile (Figure 5.12) of this factor correlates best with the increase in rates of temperature (dT/dt, $R^2 = 0.41$) and solar radiation (dSR/dt, $R^2 = 0.38$) during the daytime hours (between 06:00-17:00 LT; as can be seen in Table 5.7). Factor 6 showed a sharp peak directly after sunrise between 08:00-10:00 LT. This time coincides with the maximum increase in both temperature and solar radiation. Average mass loadings of ∼45 μg m^{-3} were observed during this period. The sharp peaks observed in this factor during morning hours could be explained by the Kathmandu Valley meteorology. After sunrise when air temperatures start to rise, the boundary layer continues to be shallow till direct sunlight reaches the Valley bottom. The accumulation of compounds in a shallow boundary layer contributes to high ambient concentrations. The dilution due to the rising boundary layer and daytime westerly winds in the Valley reduces the concentrations subsequently.

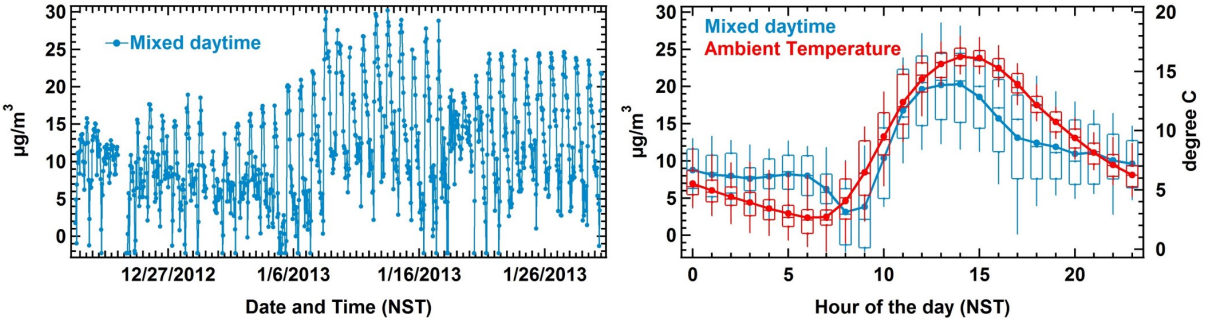

Figure 5.13: Timeseries and diel box and whisker plot for Factor 7 (Mixed daytime)

5.4.8 Factor 7 - Mixed daytime

Formic acid and acetic acid contributed most to the total VOC mass of Factor 7 (∼25% and ∼13%, respectively) while propyne, methanol and acetone together contributed ∼26% (∼10%, ∼8% and ∼8%, respectively). The other 32 species collectively contributed ∼36% to this factor but their individual contributions were ≤ 5%. Like factor 6, this factor, too, has a pre-dominance of oxygenated compounds (that could be due to photooxidation) with a minor contribution from VOCs such as acetonitrile and propyne which can be emitted from primary emission sources (Hao et al., 1996; Andreae and Merlet., 2001; Akagi et al., 2011). The diel profile of this factor (Figure 5.13) is similar to that of the ambient temperature and solar radiation with an average mass concentration of ∼20 μg m^{-3} between 12:00-14:00 LT.

Approximately 41% of the total formamide, ∼37% of total acetamide and ∼40% of total isocyanic acid are explained by this factor. Both formamide and acetamide can be produced by hydroxyl radical initiated photooxidation of primary amines (such as methyl amine) and in turn can photochemically form isocyanic acid upon being oxidized by hydroxyl radicals (Roberts et al. (2014); Ge et al. (2011); Chapter 4). In addition 34% of the formic acid and 23% of the formaldehyde mass was explained by this factor. The timeseries (Figure 5.13) of this factor showed higher baseline concentrations during second part of the measurement period when primary emissions were higher due to both biomass burning and biomass co-fired brick kiln emissions as described in the Chapter 4 of this thesis. During this intense biomass burning period, specific VOCs such as isocyanic acid, formamide and acetamide showed enhancement in their background concentrations. This

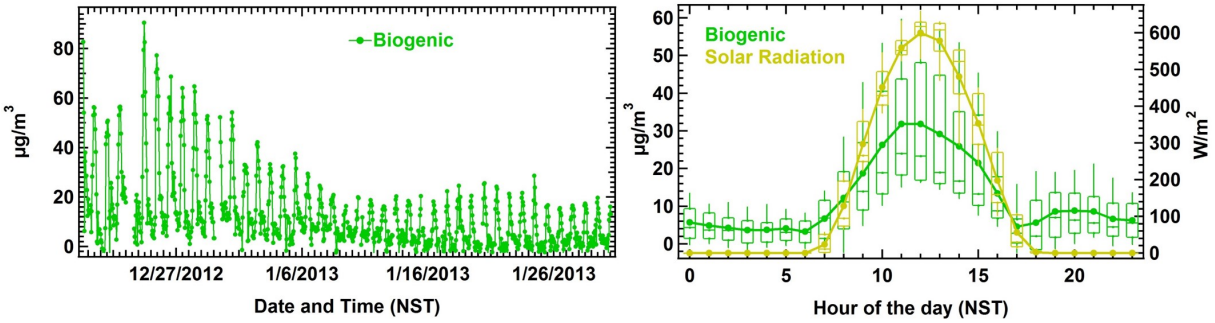

Figure 5.14: Timeseries and diel box and whisker plot for Factor 8 (Biogenic emissions)

is likely due to the higher emissions of precursor alkyl amines and other N-containing compounds from the incomplete combustion of biomass (Stockwell et al., 2015) which can form formamide and acetamide via photooxidation. Photooxidation of these amides lead to the formation of isocyanic acid. Due to the contribution from both photooxidation and primary emissions, this factor was attributed as the mixed daytime factor.

5.4.9 Factor 8 - Biogenic emissions

Factor 8 explains more of the total isoprene mass than any of the other factors (∼33%) and shows a distinct daytime peak with the highest mass loadings of ∼32 μg m^{-3} observed between 11:00-12:00 LT (Figure 5.14). The diel profile (Figure 5.14) of this factor correlates best with solar radiation (R^2 = 0.33; as can be seen in Table 5.7) during the daytime hours (between 06:00-17:00 LT). Nighttime average concentrations of this factor were always less than 10 μg m^{-3}. The timeseries profile showed very high daytime mass loadings up to ∼80 μg m^{-3} for the first part of the campaign (19 December 2012-2 January 2013) and lower mass loadings as the time progresses. This is also consistent with the observation of deciduous trees in the Kathmandu Valley shedding their leaves during peak winter (refer Chapter 4). Therefore, the factor was attributed to biogenic emissions. Most of the total VOC mass in this factor was associated with oxygenated VOCs namely acetaldehyde, acetic acid, acetone and formic acid which contributed ∼21%, ∼15%, ∼11% and ∼10% respectively to Factor 8. Isoprene contributed ∼8% to the total VOC mass. The other 32 VOCs together contributed ∼35%.

To summarize, based on the characteristics observed in the factor profiles, factor timeseries and diel plots, Factor 1 was attributed to traffic (TR), Factor 2 was attributed to

Table 5.7: Correlation coefficient (r) between the PMF resolved factors and other independent meteorological parameters (solar radiation, ambient temperature, change in solar radiation, change in ambient temperature, wind speed, wind direction, relative humidity and absolute humidity) for a) daytime period (06:00-17:00 LT) and b) nighttime period (17:00-06:00 LT)

a)	SE	MD	BG	RB+WD	BK	MI	UI	TR	SR	AT	△SR	△AT	WS	RH	AH
SE	1.00	-													
MD	-0.22	1.00	-												
BG	-0.01	-0.01	1.00	-											
RB+WD	-0.01	-0.35	0.10	1.00	-										
BK	0.23	-0.55	-0.31	0.18	1.00	-									
MI	0.07	-0.68	-0.28	0.51	0.54	1.00	-								
UI	0.55	-0.49	-0.17	-0.24	0.37	0.06	1.00	-							
TR	0.05	-0.33	0.27	0.21	-0.19	0.17	-0.02	1.00	-						
SR	0.23	0.58	0.57	-0.35	-0.51	-0.65	-0.16	-0.10	1.00	-					
AT	-0.11	0.74	0.31	-0.41	-0.74	-0.79	-0.23	-0.07	0.71	1.00	-				
△SR	0.62	-0.47	0.15	0.14	0.38	0.29	0.46	-0.08	0.11	-0.46	1.00	-			
△AT	0.64	-0.06	0.33	-0.06	0.03	-0.07	0.28	-0.04	0.50	0.02	0.67	1.00	-		
WS	-0.35	0.57	-0.05	-0.23	-0.50	-0.48	-0.39	0.00	0.13	0.63	-0.71	-0.45	1.00	-	
RH	0.10	-0.82	-0.31	0.42	0.65	0.74	0.37	0.10	-0.75	-0.91	0.45	-0.05	-0.62	1.00	-
AH	0.21	-0.27	0.08	0.02	-0.17	-0.11	0.49	0.11	-0.02	0.13	0.20	0.16	-0.11	0.25	1.00
b)	SE	MD	BG	RB+WD	BK	MI	UI	TR	SR	AT	△SR	△AT	WS	RH	AH
SE	1.00	-													
MD	0.14	1.00	-												
BG	-0.25	-0.18	1.00	-											
RB+WD	0.34	-0.10	0.58	1.00	-										
BK	-0.20	-0.38	-0.07	-0.33	1.00	-									
MI	-0.25	-0.60	0.08	0.04	0.32	1.00	-								
UI	0.29	-0.29	-0.58	-0.47	0.38	-0.03	1.00	-							
TR	0.17	-0.36	0.36	0.46	-0.24	0.14	-0.24	1.00	-						
SR	0.10	0.11	0.05	-0.04	-0.17	-0.28	-0.01	0.32	1.00	-					
AT	0.47	0.36	0.15	0.48	-0.59	-0.58	-0.18	0.37	0.44	1.00	-				
△SR	-0.17	-0.22	-0.03	-0.02	0.25	0.38	0.04	-0.34	-0.83	-0.59	1.00	-			
△AT	-0.12	0.00	-0.06	-0.21	0.09	0.08	0.08	-0.11	-0.09	-0.14	0.21	1.00	-		
WS	0.30	0.43	-0.02	0.07	-0.35	-0.53	-0.09	0.15	0.55	0.70	-0.78	-0.15	1.00	-	
RH	-0.59	-0.49	-0.07	-0.44	0.40	0.48	0.25	-0.26	-0.44	-0.80	0.59	0.16	-0.66	1.00	-
AH	0.04	-0.06	0.18	0.26	-0.43	-0.33	0.03	0.21	0.05	0.55	-0.08	-0.05	0.21	0.04	1.00

SE = Solvent evaporation; MD = Mixed daytime; BG = Biogenic; RB+WD = Residential biofuel use and waste disposal; BK = Biomass co-fired brick kilns; MI = Mixed industrial emissions; UI = Unresolved industrial emissions; TR = Traffic; SR = Solar radiation; AT = Ambient temperature; △SR = Change in solar radiation (dSR/dt); △AT = Change in ambient temperature (dT/dt); WS = Wind speed; RH = Relative humidity; AH = Absolute humidity

residential biofuel use and waste disposal (RB+WD), Factor 3 was attributed to mixed industrial emissions (MI), Factor 4 was attributed to biomass co-fired brick kilns (BK), Factor 5 to unresolved industrial emissions (UI), Factor 6 was attributed to solvent evaporation (SE), Factor 7 was attributed to mixed daytime source (MD) and Factor 8 was attributed to biogenic VOC emissions (BG). Table 5.7 shows the calculated correlation coefficients between the PMF resolved source factors and the independent meteorological parameters.

It can be seen from Table 5.7 that during daytime, the solvent evaporation (SE) factor correlated best with the rate of change in solar radiation and the rate of change in ambient temperature (r = 0.62 and 0.64, respectively). This supports the assignment to solvent evaporation as the process of evaporation is governed by temperature changes. However, the change of the saturation vapor pressure for a temperature change from 5°C to 20°C for the dominant compounds (acetaldehyde and acetic acid) is small (less than a factor of 1.3; (Betterton and Hoffmann., 1988; Johnson et al., 1996)) and, therefore, does not ac-

count for the observed magnitude of increase (by a factor of ∼5) between 06:00-09:00 LT. Instead, the temperature dependence of the solubility of these compounds in an aqueous solution (factor 5-7) would explain a change of this magnitude. The solvent evaporation factor strongly anti-correlated with RH during the nighttime and correlated well with the unresolved industrial (UI) factor (r = 0.55) during daytime. It is, therefore, possible that the sources of the solvent evaporation and unresolved industrial emission may be identical or at least spatially co-located. We hypothesize, that compounds, that firstly display a significant solubility in aqueous solution and secondly a strong temperature dependence of the solubility are attributed to this separate factor. At night, soluble compounds partition into the aqueous phase of the fog aerosol and hence their mixing ratios will not build up in the nocturnal boundary layer to the same extent as those of less soluble compounds. Those compounds with a high temperature dependence on solubility like acids and aldehydes will rapidly shift to the gas phase from their nocturnal fog water reservoir when temperatures increase in the morning and their solubility decreases, which manifests itself in a disproportionate (considering only evaporation) increase of their mixing ratios at that time.

The mixed daytime factor (MD) correlated with solar radiation, ambient temperature and wind speed (r = 0.58, 0.74 and 0.57, respectively). The biogenic factor (BG) had the best correlation with solar radiation (r = 0.57) during daytime, consistent with its attribution to biogenic emissions. During daytime, the mixed industrial emissions and biomass co-fired brick kiln emissions had very low mass concentration due to the boundary layer dilution and ventilation effect of high westerly winds in the Kathmandu Valley (as discussed in Chapter 4). The ambient RH was also lower during the daytime. Therefore, both the mixed industrial emissions and brick kilns emission showed positive correlations with ambient RH (r = 0.65 and 0.74, respectively). During nighttime, no significant correlation was observed between the PMF resolved factors except the correlation of the biogenic factor with the residential biofuel use and waste disposal (RB+WD) factor (r = 0.58) which indicates that the high emissions of oxygenated VOCs and isoprene from residential biofuel use and waste disposal source could result in a minor misattribution of the combustion derived emissions to the biogenic factor.

5.4.10 Conditional probability functions (CPF) to determine source directionality

Figure 5.15 shows the Conditional Probability Function (CPF) plots that were used to examine the spatial profile of the eight different PMF source factors. For the CPF plots, only data with wind speed > 0.5 m s^{-1} were considered. Six factors namely traffic, residential biofuel use and waste disposal, mixed industrial emissions, unresolved industrial emissions, solvent evaporation and biomass co-fired brick kilns could be associated clearly to the anthropogenic activities and are, therefore, likely to be impacted by spatially fixed sources, while one factor (mixed daytime) was related to photochemistry. One factor, the biogenic emissions, is natural but can also be attributed to spatially fixed sources such as forests.

The CPF plot for the traffic factor showed maximum conditional probability (0.4-0.7) from the W-NW direction where the Kathmandu city center and the busiest traffic intersections were located. The conditional probability for the SW and NE wind direction ranged from 0.2-0.4. Two cities namely Patan and Bhaktapur, respectively, are located upwind of the site in these directions. The lowest conditional probability was observed for the SE wind direction.

The residential biofuel use and waste disposal factor, showed a high conditional probability of emissions exceeding the mean for air masses reaching the site from most wind directions (0.5-0.7 for NW-N, $\sim$0.4 for N-NE and S-SW and 0.2 for E-S), indicating that this source is spatially distributed throughout the Kathmandu Valley. Only for the wind sector from SW-NW the conditional probability of this source is low. The reason for this low conditional probability is, that every day in the afternoon winds from the western mountain passes reach the receptor site. The same wind direction is extremely rare after sunset and during the early morning hours, when residential biofuel use and waste disposal mostly occur. Consequently, the conditional probability plot shows low conditional probabilities for this wind sector.

The mixed industrial emissions factor showed the highest conditional probability of air masses with above average mass loadings reaching the receptor site from the NE to SE wind sector (p = 0.4-0.6), where Bhaktapur industrial area is located within a distance

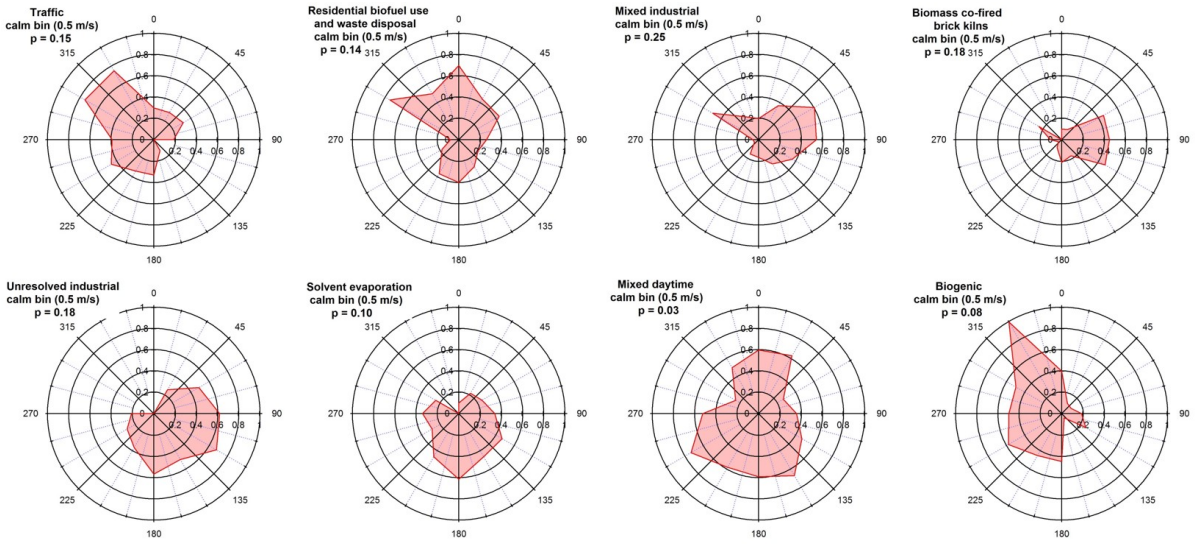

Figure 5.15: CPF plots for all source factors resolved by PMF showing wind directional dependency for different source categories

of 3-4 km upwind of the receptor site. Conditional probabilities of 0.2-0.4 were observed for the NW wind direction where Balaju industrial area is located.

For brick kilns the highest conditional probability was observed for air masses reaching the receptor site from the NE-SE (p ∼0.4), which had several active brick kilns near the Bhaktapur industrial area, which was ∼2 km upwind of the receptor site.

It is interesting to note that the unresolved industrial emissions factor shows a clear directional dependence (p = 0.5-0.7 for the NE-SW wind sector) indicating that this factor, too, can be attributed to spatially fixed sources in Bhaktapur and Patan industrial area. Polymer production, manufacturing industries for adhesives, paints and/or pharmaceuticals upwind of the site likely contributed towards the VOC mass of the unresolved industrial factor.

The solvent evaporation factor, too, shows high conditional probabilities for the SE-SW wind direction (Patan industrial area) and low conditional probabilities for the NW-NE wind direction. The conditional probability function shows significant overlap with that of the unresolved industrial emissions factor. It is therefore highlights the plausibility that solvent/chemical evaporation from industrial units is responsible for this factor.

Within the calm bin of wind speeds < 0.5 m s^{-1} the maximum conditional probabilities were observed for mixed industrial emissions, unresolved industrial emissions and brick

kilns (0.25, 0.18 and 0.18, respectively) which indicates that emissions from these sources were tend to accumulate in a shallow boundary layer during stagnant conditions in the Kathmandu Valley. Therefore, using taller chimney stacks, at least for combustion sources to prevent accumulation of emissions in a shallow boundary layer could potentially improve the air quality of the Valley during foggy nights.

The mixed daytime factor shows no obvious directional dependence for the conditional probability of recording values above the average at the receptor site ($p > 0.3$ for all directions). Slightly higher conditional probabilities ($p \sim 0.6$) are recorded for air masses reaching the receptor site from the N-NE and S-SW wind direction.

The biogenic factor showed high conditional probabilities for air masses reaching the receptor site form the SW to N direction ($p = 0.5$-1) where few forested areas such as Nilbarahi jungle and Gokarna forest were located. Also forested areas in mountain slopes in the SW and NW direction and the midday fetch region being frequently from this sector explains the directional dependency of the biogenic factor.

The CPF analysis of the PMF model output clearly indicates that spatially fixed sources are responsible for a significant fraction of the overall VOC mass loadings and opens up the possibility to identify and mitigate emissions or at least the build-up of pollutants in a shallow inversion.

5.4.11 Source contribution to total VOC mass loading and comparison with emission inventory

Figure 5.16 shows the pie chart summarizing contributions of individual sources to the total VOC mass loading. Total VOC mass loading was calculated by summing up the concentrations of individual VOCs (in μg m^{-3}). The distribution shows that biogenic sources and the mixed daytime factor contributed only 10% and 9.2%, respectively to the total VOC mass loading while all the anthropogenic/anthropogenic influenced sources contributed $\sim$80% to the total.

According to two widely used emission inventories, namely REAS v2.1 (Regional Emission inventory in ASia) and EDGAR v4.2 (Emissions Database for Global Atmospheric Research) (Kurokawa et al., 2013; Olivier et al., 1994) and the existing Nepalese in-

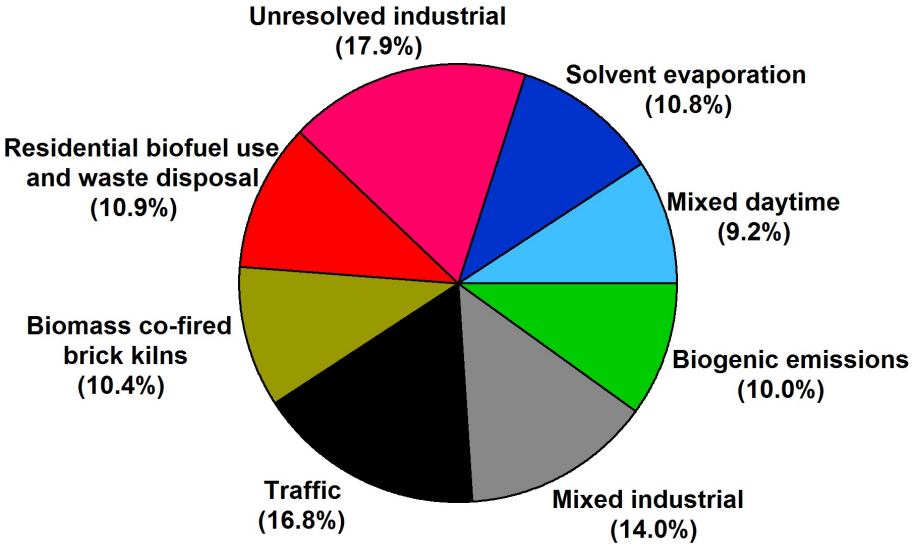

Figure 5.16: Pie chart showing source contribution to total VOC mass loading

ventory obtained from the International Centre for Integrated Mountain Development's (ICIMOD) database, residential biofuel use is considered to be the pre-dominant source of VOC emissions in the Kathmandu Valley (as shown in Figure 5.17). The Nepalese and EDGAR inventory estimate ∼80% of the total VOC emissions in the Valley to be due to residential biofuel use whereas the REAS inventory estimates that ∼51% of the total VOC emissions originate from residential/commercial biofuel use. According to the REAS inventory, agricultural/waste burning is considered to be the second most dominant contributor (∼27%), followed by solvent use and industrial emissions (collective contribution ∼20%). The EDGAR inventory considers solvent use and mixed industrial emissions to represent the second most important source. Collectively they are considered to contribute ∼10% to the total VOC mass followed by waste burning (∼8%). The Nepalese inventory considers solvent and paint use to be the second largest contributor to the VOC emissions. Traffic was considered to contribute only between ∼1.4% (in the Nepalese inventory) to a maximum of ∼2.6% (in EDGAR inventory) of the total VOC emissions. This stands in stark contrast to the results of our PMF run, which indicate traffic contributes ∼20% of the total VOC mass loadings, solvent evaporation and industrial solvent/chemical usage accounts for ∼36% of the total VOC mass loadings (unresolved industrial emissions +

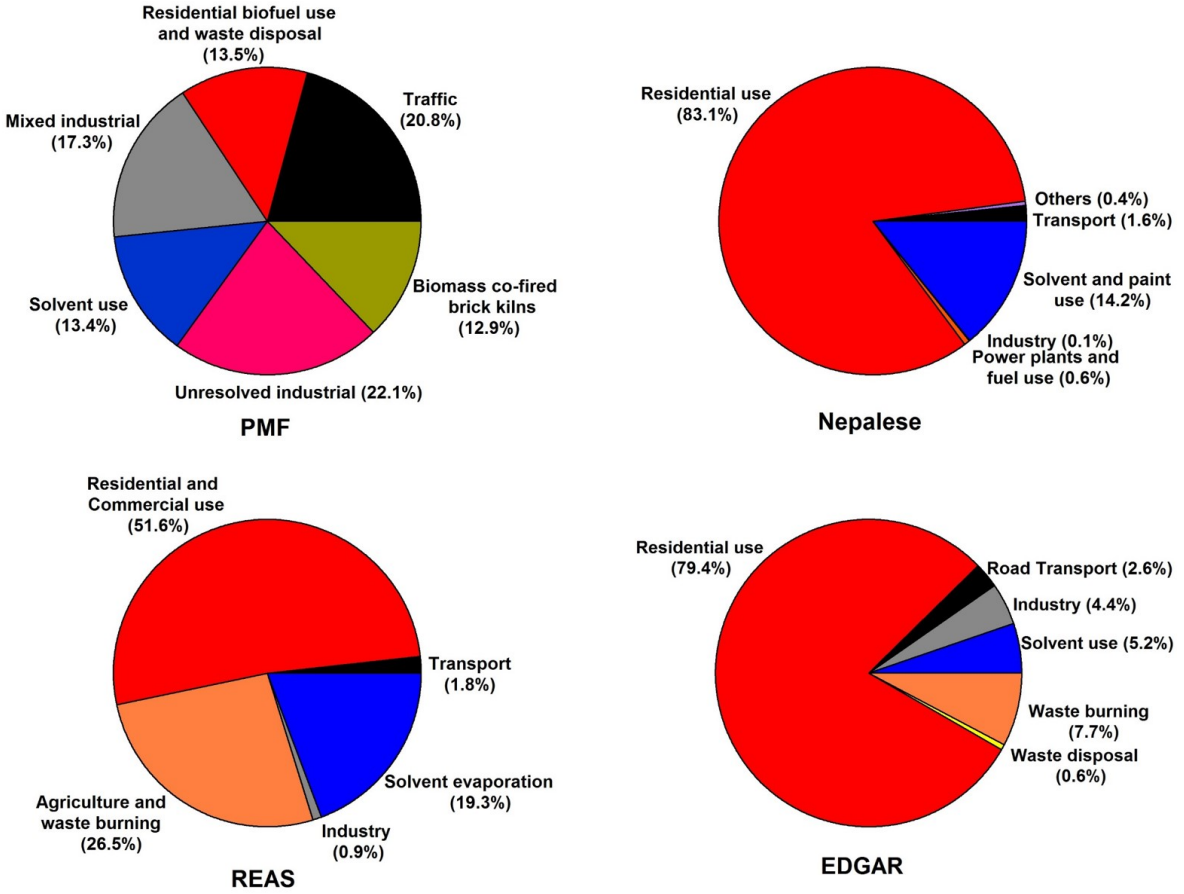

Figure 5.17: Pie charts showing comparison of the PMF derived source contribution with NMVOCs source contribution according to REAS, existing Nepalese and EDGAR emission inventory

solvent evaporation) and other industrial emissions (mixed industrial emissions + brick kilns) account for ∼30% of the total VOC mass. Residential fuel use and waste disposal do not feature prominently in our PMF solution (∼14%). Our ratio of the contribution of industries/traffic-ratio and solvent use/traffic-ratio agrees with that of the EDGAR emission inventory ∼2:1. However, the overall fraction of the total anthropogenic VOC mass contributed by these three sources is only ∼12% in the EDGAR emission inventory, while it amounts ∼86% in our PMF solution. The comparison suggests that the VOC mass contributed by residential solid biofuel use and waste disposal is overestimated by a factor of ∼8 in current emission inventories or the emissions from traffic and industrial sources are underestimated significantly in the current emission inventory.

Biomass co-fired brick kilns are an atypical industrial source in the Kathmandu Valley, and contributed significantly (∼15%) to the total VOC mass loading. The existing Nepalese

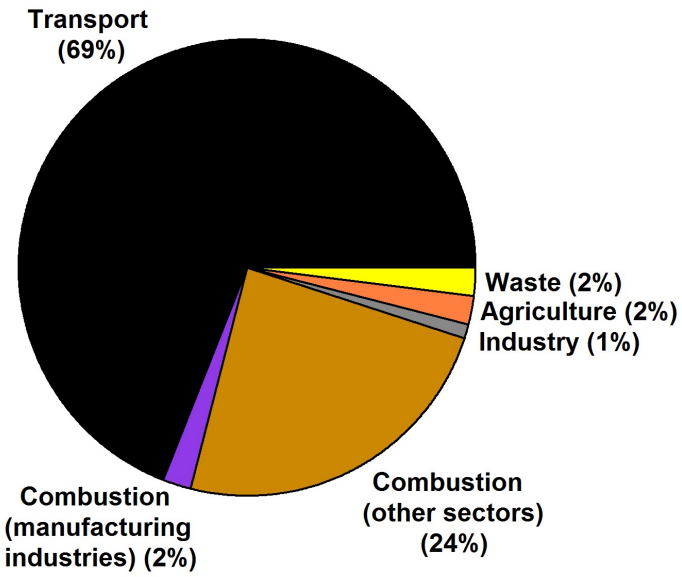

Figure 5.18: Pie chart showing emissions of particulate matter (PM_{10} and $PM_{2.5}$) and CO from different sectors in Kathmandu

inventory considers contributions of brick kilns only to the emission of particulate matter (PM_{10} and $PM_{2.5}$). The emission inventories do not include VOC emissions from brick kilns in the Kathmandu Valley. Therefore, including emissions sources such as brick kilns in the existing emission inventory would certainly improve the representation of VOC emissions in the Kathmandu Valley.

According to the recent air quality assessment report of ICIMOD (Pradhan et al., 2012), total emissions of particulate matter (PM_{10} and $PM_{2.5}$) and carbon monoxide (CO) are estimated to be dominated by road transport (69%) as can be seen in Figure 5.18. Higher PM levels in transport were attributed to the re-suspension of dust by vehicles. Combustion processes in residential, commercial and forestry sectors collectively had the second largest contribution to PM and CO. The contribution from different emission sources to PM and CO in the Kathmandu Valley are similar to that of higher aromatic VOCs (toluene, C8-aromatics and C9-aromatics; refer Figure 5.19) obtained from the PMF solution.

5.4.12 Source contribution to individual VOCs

Figure 5.19 represents the pie charts showing contribution of the eight source factors to individual VOCs such as acetonitrile, benzene, styrene, toluene, sum of C8-aromatics (xylenes and ethylbenzene) and sum of C9-aromatics (trimethylbenzenes and propylbenzene). Maximum contribution to the acetonitrile mass concentration was observed from the unresolved industrial emission sources (∼30%) followed by the biomass co-fired brick kilns emission (∼24%) and mixed industrial emission (∼20%) factors. Residential biofuel use and waste disposal features only fourth (∼18%). The same sources also contribute most to benzene emissions, indicating that fuel usage, rather than its application as solvent/chemical reagents in industrial processes is responsible for most of the industrial acetonitrile emissions. It also indicates that industrial rather than residential biofuel usage contributes more towards outdoor air pollution. Most of the benzene (which is a human carcinogen) can be attributed to biomass co-fired brick kilns (∼37%), mixed industrial (∼17%) and unresolved industrial (∼18%) sources. Residential biofuel use again featured only fourth as far as the contribution towards mixing ratios of this compound in the outdoor environment is concerned. Table 5.8 shows a comparison of VOCs/benzene emission ratios for four PMF derived sources (residential biofuel use and waste disposal, biomass co-fired brick kilns, mixed industrial and unresolved industrial sources) to the emission ratios obtained from the grab samples collected for garbage burning in the Kathmandu Valley and the previously reported emission ratios for waste burning, wood burning and charcoal burning sources.

Residential biofuel use and waste disposal contributed ∼28% of the total styrene which emitted significantly from waste burning. However, traffic was found to be equally important as a styrene source (∼37%) in the Kathmandu Valley. Recently, styrene has been detected from traffic and was found to have high emission ratios with respect to benzene after cold startup of engines and in LPG fuel (Alves et al., 2015). Biomass co-fired brick kilns and mixed industrial emissions also contribute significantly (∼21% and ∼14%, respectively) towards styrene mass loadings. Traffic was found to be the most important source of higher aromatics including toluene, C8-aromatics, and C9-aromatics (> 60%). Biomass co-fired brick kilns were the second largest contributors towards their mass load-

Table 5.8: Emission ratios of VOCs/benzene for acetonitrile and aromatic hydrocarbons derived from the PMF model for different sources and comparison with the ratios for the garbage burning grab samples and different source categories reported in previous studies

	RB+WD	BK	MI	UI	Grab samples	Waste burning[1]	Wood burning[2]	Charcoal burning[2]
Acetonitrile	0.23	0.14	0.25	0.36	0.77	0.10	-	-
Toluene	0.34	0.35	0.18	0.30	0.34	0.37	0.05	0.59
C8-aromatics	0.18	0.06	0.08	0.00	0.25	0.10	-	0.63
C9-aromatics	0.25	0.22	0.06	0.12	0.08	0.03	-	-
Styrene	0.12	0.09	0.09	0.04	0.16	0.89	-	-
Naphthalene	0.11	0.15	0.20	0.05	0.09	0.13	-	-

1. (Stockwell et al., 2015); 2. (Tsai et al., 2003); RB+WD = Residential biofuel use and waste disposal; BK = Biomass co-fired brick kilns; MI = Mixed industrial emissions; UI = Unresolved industrial emissions

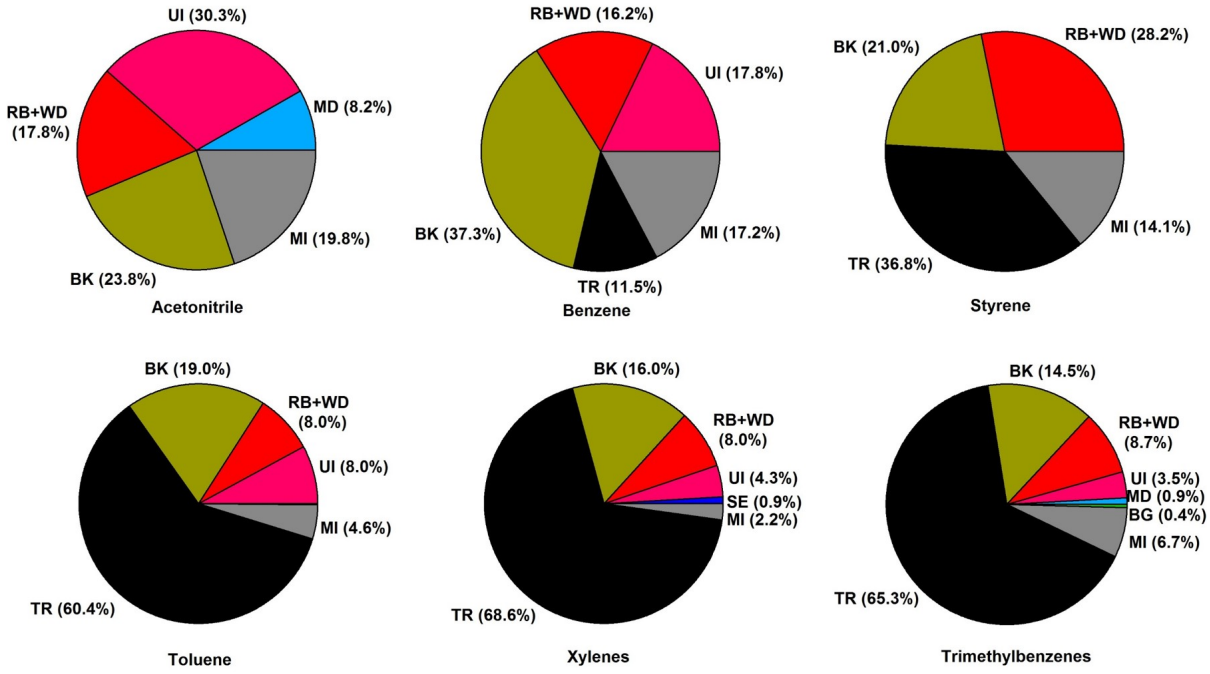

Figure 5.19: Pie charts showing contribution of PMF derived source factors to acetonitrile and aromatic VOCs

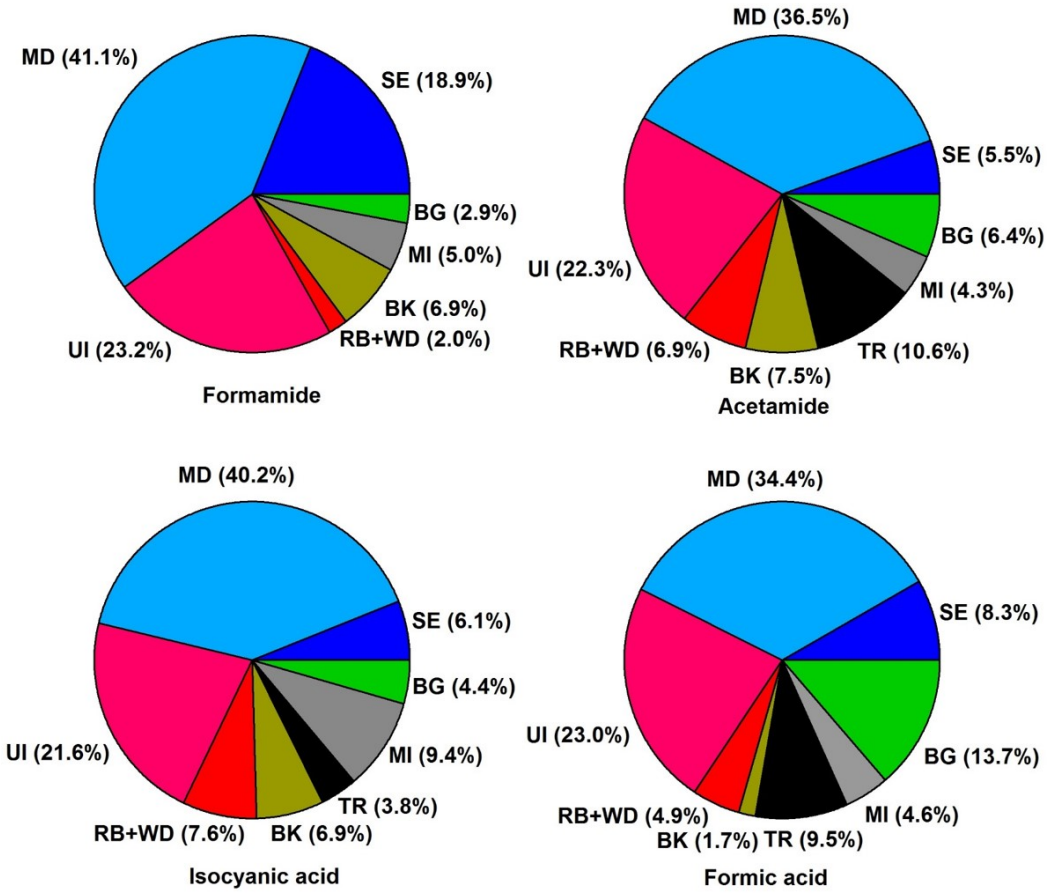

Figure 5.20: Pie charts showing contribution of PMF derived sources to formamide, acetamide, isocyanic acid and formic acid

ings, while residential biofuel usage and waste disposal ranked third.

Figure 5.20 shows the pie charts summarizing contributions of PMF derived sources to two newly quantified compounds in the Kathmandu Valley, namely formamide and acetamide along with isocyanic acid and formic acid. All these compounds showed maximum contribution from the mixed daytime factor (∼34% to ∼41%) due to the photooxidation source. As discussed previously in this thesis (Chapter 4 and Section 5.4.8 of this chapter), both formamide and acetamide are formed primarily as a result of photooxidation of amine compounds and N-containing compounds. These can be emitted from the various inefficient combustion processes in the Kathmandu Valley. Photooxidation of these amides further forms isocyanic acid. Apart from the mixed daytime source, unresolved industrial emissions factor also contributed significantly to all these compounds (∼22% to ∼23%)

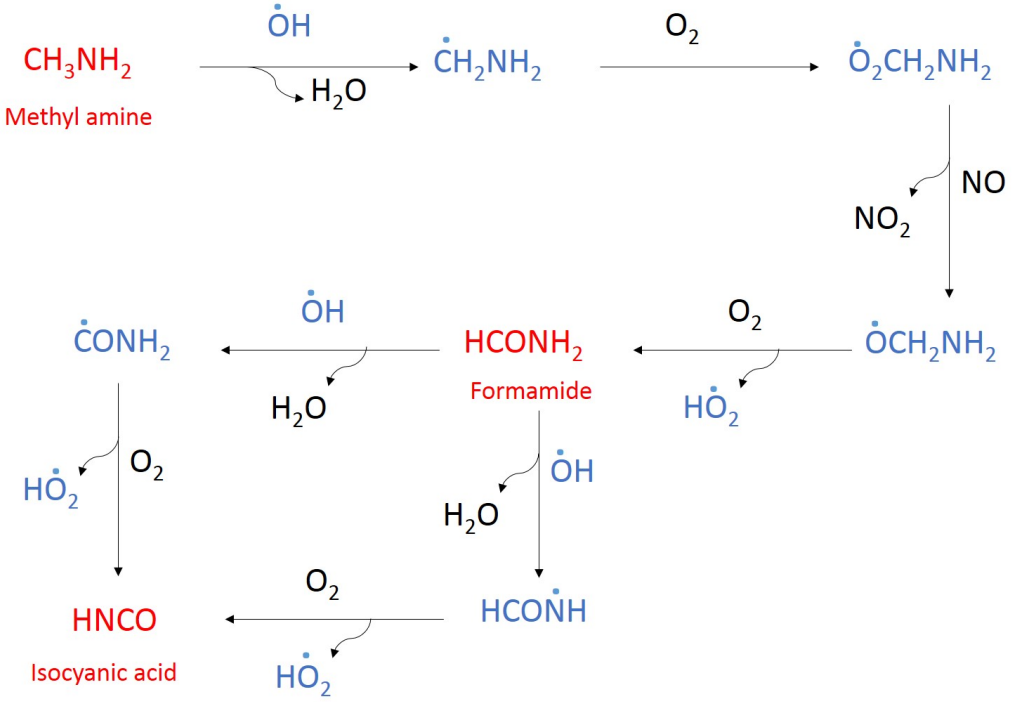

Figure 5.21: Reaction schematic for the formation of formamide and isocyanic acid (blue colored species represents radicals)

as they are used as reactants (e.g., formic acid is used as reactant to produce formamide in industries) or produced during different industrial processes (such as formamide is produced in pharmaceuticals and plastic industries). Solvent evaporation factor contributed ∼19% to formamide while biogenic factor contributed ∼14% to formic acid. Contribution from all the other sources to these VOCs were $< 10\%$.

Figure 5.21 represents the reaction schematic of the proposed mechanism for the formation of formamide, acetamide and isocyanic acid based on the previous laboratory experiments which shows that photooxidation of alkyl amines leads to the formation of formamide and acetamide which undergoes further photooxidation to form isocyanic acid which can have severe health impact at concentration thresholds above 1 ppb (Roberts et al., 2014, 2011). This thesis provides the first ever ambient evidence of the photochemical source of isocyanic acid by quantification of both the amides (the precursor) and isocyanic acid (the product) collectively and the source apportionment of these compounds in the Kathmandu Valley.

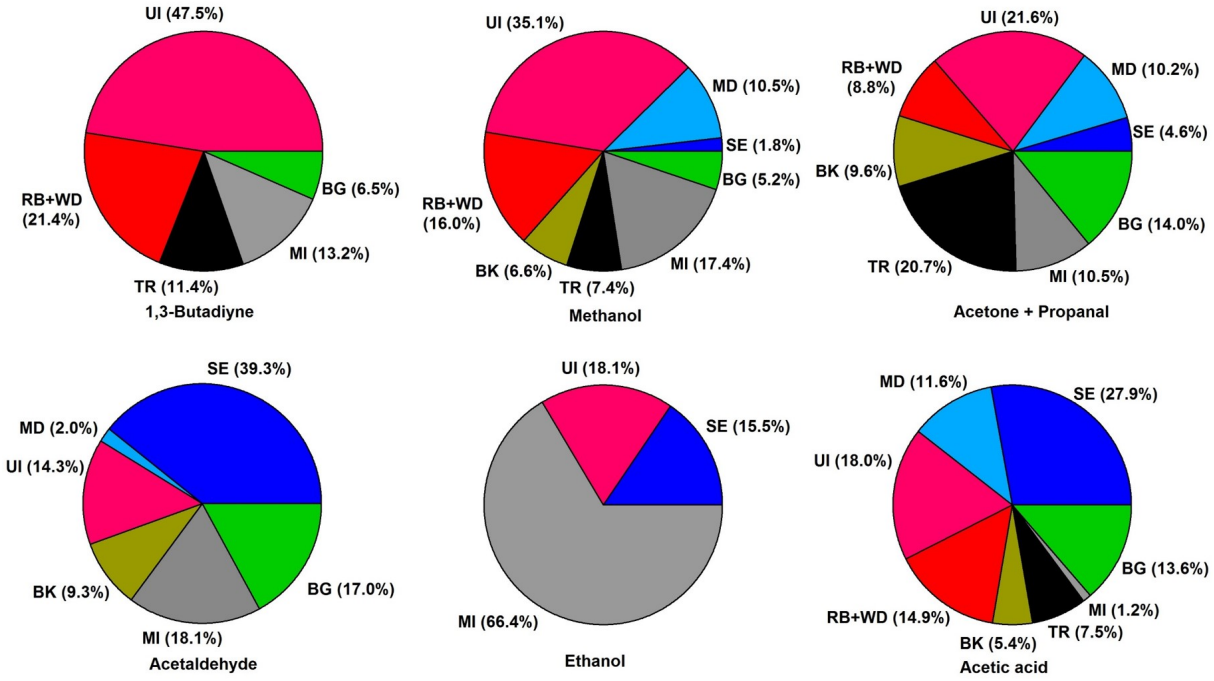

Figure 5.22: Pie charts showing contribution of PMF derived sources to 1,3-butadiyne and oxygenated VOCs such as methanol, acetone, acetaldehyde, ethanol and acetic acid

Figure 5.22 represents the pie charts showing contribution of the eight sources derived from PMF to 1,3-butadiyne and oxygenated compounds namely methanol, acetone, acetaldehyde, ethanol and acetic acid. It can be seen from Figure 5.22 that emissions of all these compounds in the Kathmandu Valley were dominated by different industrial activities. The total unresolved industrial emissions factor dominated the contribution to 1,3-butadiyne (∼48%), methanol (∼35%) and acetone (∼22%). Residential biofuel use and waste disposal also contributed significantly to 1,3-butadiyne (∼21%) and methanol (∼16%). Traffic was found to have significant contribution to acetone (∼21%). It is known that acetaldehyde, ethanol and acetic acid are used as solvents in different industries and it was found that industrial sources obtained from PMF (mixed industrial + unresolved industrial + solvent evaporation) together contributed ∼72% of total acetaldehyde, 100% of total ethanol and ∼47% of total acetic acid. Biogenic sources also had significant contribution to acetaldehyde and acetic acid (∼17% and ∼14%, respectively) whereas residential biofuel use and waste disposal contributed to ∼15% of the total acetic acid.
Figure 5.23 represents a timeseries of daily mean relative contribution of the PMF derived sources during SusKat-ABC campaign. As discussed in chapter 4 of this thesis the

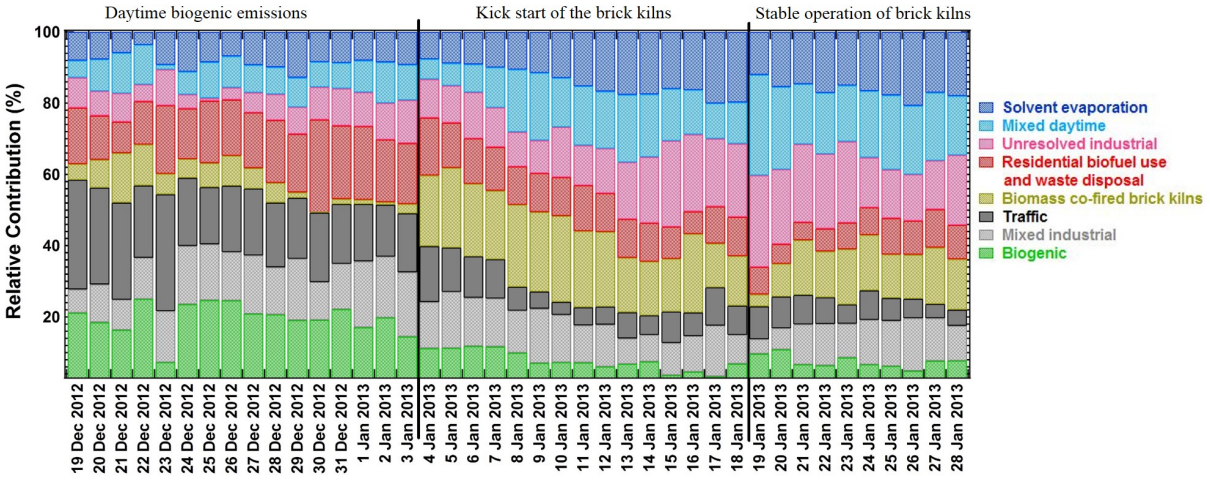

Figure 5.23: Daily mean relative contribution of sources during SusKat-ABC campaign

whole campaign can be divided into three different periods based on the measurements - first period (from the start of the campaign till 3 January 2013) was associated with high daytime isoprene emissions due to strong biogenic emission , the second period (4-18 January 2013) was marked by enhancements in acetonitrile and benzene concentrations due to the kick start of the biomass co-fired brick kilns in the Kathmandu Valley and in the third period (19 January till the end of the campaign), more oxygenated VOCs were observed which was believed to be due to the stable operation of the brick kilns and more contribution from the industrial sources. PMF derived results also supports these observation as can be seen in Figure 5.11. It can be seen that from the start of the campaign till 3 January 2013 contribution of PMF derived biogenic sources were $> 20\%$ for most of the time while contribution from the brick kilns emission factor was negligible ($\leq 5\%$). From 4 January till 18 January 2013, the contribution of brick kilns increased significantly ($\sim$20% to $\sim$40%) as the brick kilns in the Kathmandu Valley became operational. After 18 January till the end of the campaign the contribution of brick kilns become lower due to its stable operation.

During the first period, contribution of traffic was found to be more ($\sim$20% to $\sim$30%) as compared to the rest of the campaign likely because of Kathmandu city being the more frequently sampled fetch region during this period. The higher contribution of the mixed daytime source during the second and third part of the campaign was due to the early morning and daytime photooxidation of the precursor compounds which were emitted as

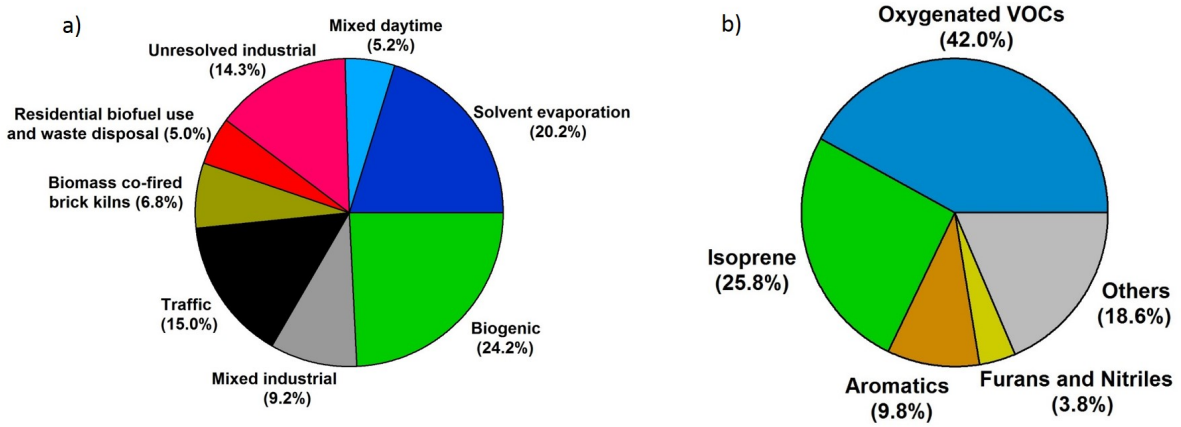

Figure 5.24: Pie charts showing daytime O_3 production potential obtained a) from the source contribution using PMF and b) from the measurements performed in the Kathmandu Valley

a result of biomass co-fired brick kilns and other biomass burning emissions during these periods. The mixed industrial emissions factor contributed almost equally throughout the campaign (contributing ∼10% to ∼15%) but the solvent evaporation and the unresolved industrial emissions factor contributed more during the second and third part of the campaign (increase of ∼10%).

5.4.13 Source contribution to daytime ozone production potential and SOA formation

Figure 5.24a represents the source contribution to daytime O_3 production potential while Figure 5.24b represents the contribution of different classes of compounds measured in the Kathmandu Valley to the daytime O_3 production potential as discussed in Chapter 4 of this thesis. The daytime O_3 production potential for individual sources was calculated by summing up the O_3 production potential for the individual compounds which was calculated according to the method described by Sinha et al. (2012). The distribution of the daytime O_3 production potential obtained from the measurements (Figure 5.24b) shows that ∼78% of total daytime O_3 production potential was due to the contribution from isoprene and oxygenated VOCs which indicated dominance of biogenic emissions and photochemistry in the Kathmandu Valley even in the winter time. But the distribution of different sources obtained from PMF to daytime O_3 production potential shows that

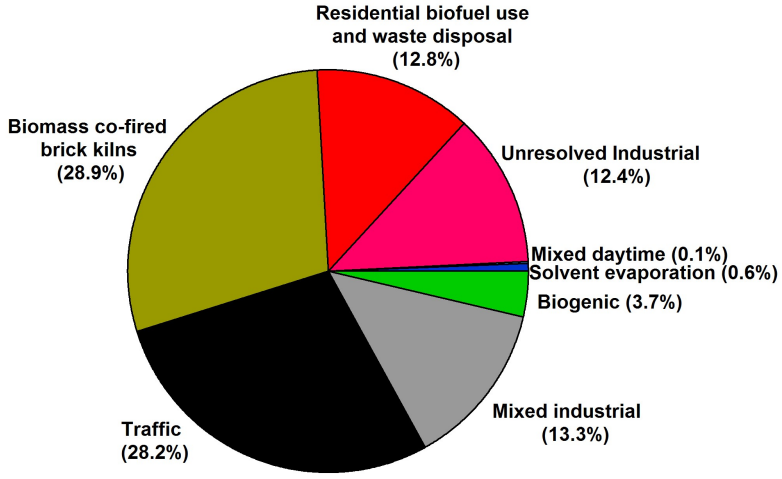

Figure 5.25: Pie chart showing source contribution to SOA formation

the biogenic factor together with the photochemistry factor (mixed daytime) contributed only ∼30% of total O_3 production potential. The remaining ∼70% was contributed by anthropogenic sources. While solvent evaporation contributed most (∼20%) to the total daytime O_3 production potential, traffic and unresolved industrial emission stood second and third in terms of anthropogenic ozone precursor emissions. Residential biofuel use and waste disposal, and biomass co-fired brick kilns while potentially important from a human health perspective, contributed only a minor fraction of the total anthropogenically emitted ozone precursors.

SOA production was calculated using the concentrations and the known SOA yields for benzene, toluene, styrene, xylene, trimethylbenzenes, naphthalene and isoprene (Ng et al., 2007; Chan et al., 2009; Yuan et al., 2013; Kroll et al., 2006). As the biomass co-fired brick kilns and the traffic factor contains most of the reactive aromatic compounds, they appeared to be the dominant contributors to SOA production (as shown in Figure 5.25) in the Kathmandu Valley.

5.5 Conclusions

The PMF model results reveal several new insights regarding the source apportionment of VOCs in the Kathmandu Valley. Speciation of VOCs in the emission inventory for Nepal only includes compound classes (e.g., alkanes, alkenes etc.) and not specific compounds. Also, the existing emission inventories (e.g., REAS v2.1, EDGAR v4.2; Kurokawa et al. (2013); Olivier et al. (1994)) and Nepalese inventory (ICIMOD)) are highly uncertain as there has been no validation using in-situ measurements of these mostly bottom up inventories which rely on fuel and source emission factors measured in other technologically different regions of the world (mostly US and Europe). By using the specific VOC emission tracer data measured in the Kathmandu Valley and constraining the PMF with measured source profiles of complex sources (e.g., biomass co-fired brick kilns, residential solid biofuel use and waste disposal), it is shown that the contribution from sources such as residential solid biofuel use and waste disposal is overestimated in current emission inventories. At the same time, the emissions from traffic and industrial sources are underestimated in the current emission inventory. The presence of elevated concentrations of several health relevant VOCs (e.g., benzene) could be attributed to the biomass co-fired brick kiln sources.

This study has provided quantitative information regarding the contributions of the major VOC sources in the Kathmandu Valley. This will enable focused mitigation efforts by policy makers to improve the air quality of the Kathmandu Valley by reducing emissions of both toxic VOCs and secondary pollutants. The results will also enable significant improvements in existing VOC emission inventories so that chemical-transport models can be parameterized more faithfully over the South Asian region and the air quality - climate predictions by models become more reliable.

Chapter 6

Conclusions: Major findings and outlook

On a regional scale in the agricultural regions and villages of north-western India, paddy residue burning may dominate benzenoid emissions from traffic and industrial sources and the impact of crop residue burning from India on the global budget of benzenoids will require further such studies in different seasons and regions of India.

Every year during Oct-Nov, $\sim 90\%$ of the days are influenced by paddy residue burning in the north-western Indo Gangetic Plain (IGP). These events are similar to the event chosen here for the case study in terms of emissions and spatio-temporal character. Recent works from our group using 3-year and 2-year long measurements (Chandra and Sinha, 2016; Kumar et al., 2016) further demonstrate the representativeness of such events in the north-western IGP. It is disconcerting to note that several paddy growing regions of India are also regions with very high prevalence of cancer (e.g., Malwa belt in Punjab). The exposure of the population to sustained high levels of carcinogenic benzenoids in the air they breathe for several months in a year could certainly be a contributory factor to cancer prevalence and warrants detailed multidisciplinary epidemiological and environmental studies. It is worth mentioning that though the Ministry of Environment and Forests, Government of India stipulated new ambient air quality standards (NAAQS) in 2009 regarding permissible exposure to benzene in air (NAAQS for benzene: annual average < 1.6 ppb), no standards are available for the other benzenoids. Currently, the

national monitoring network for benzenoid VOCs is very sparse and does not even exist for methyl cyanide, for which this thesis reports the first measurements. Future efforts should focus on national monitoring of ambient benzenoids using online analytical techniques to establish their spatial and temporal variability and constrain contribution of its different sources for mitigation.

This thesis has comprehensively characterized the chemical composition of air in the Kathmandu Valley in terms of speciated volatile organic compounds during the SusKat-ABC wintertime campaign. The measurements performed at high time resolution (every minute) and high mass resolution ($m/\Delta m > 4200$) enabled us to identify a multitude of compounds based on their monoisotopic masses and hence exact molecular formula. Novel insights could be acquired regarding chemical processes related to ozone and secondary organic aerosol formation in a complex chemical environment affected by mountain meteorology and both anthropogenic and biogenic sources (even in winter).

A total of 71 ion peaks were observed in the mass spectra of PTR-TOF-MS that were above the detection limit of the instrument. Out of these, 37 species that had average ambient concentrations greater than 200 ppt during the campaign could be identified with reasonable confidence based on (1) spectral characteristics observed at a particular m/z in a 0.005 amu bin relative to the ion peak, (2) ambient diel profiles and (3) correlation with specific emission tracer molecules such as acetonitrile (a biomass burning tracer). 200 ppt cut off was also chosen as an additional quality control measure so as to ensure attribution of ion peaks in the mass spectra only to the compounds present in the ambient air and not due to instrumental reasons. Among these 37 species, 8 contained nitrogen, 15 contained oxygen, 13 were hydrocarbons and one contained sulfur. Based on chemical signatures of tracer compounds such as acetonitrile and isoprene, two periods with contrasting emission influences were identified during the campaign and investigated in detail. period 1 (19 December 2012–2 January 2013) was characterized by high daytime biogenic emissions of isoprene (average isoprene concentrations in period 1 and period 2 were 1.66 and 0.97 ppb, respectively) and the absence of operational brick kilns (and hence their emissions); while period 2 (4 January 2013–18 January 2013) was marked by high acetonitrile (average concentration during this Period was 1.34 ppb), benzene (3.46 ppb) and isocyanic acid (1.03 ppb) due to emissions from the biomass co-fired brick kilns and

other biofuel/biomass burning activities. A clear distinction of isoprene from furan, which had distinct emission profiles, highlighted the importance of deploying a PTR-TOF-MS for VOC measurements in the Kathmandu Valley.

Two "new" compounds which have not been reported in any previous ambient study namely, formamide (CH_3NO); protonated m/z = 46.029; campaign average 0.76 ppb) and acetamide (C_2H_5NO; protonated m/z = 60.051; campaign average 0.39 ppb) and are involved in photochemical formation of isocyanic acid were also detected. The average total reactive carbon (sum of the average mixing ratios of all the 37 species reported in this study) was 175.8 ppbC to which propyne, acetaldehyde, benzene, acetic acid, acetone, propene and toluene collectively contributed more than 60%. Isoprene concentrations as high as 3 ppb were observed frequently during the daytime, in the early part of the campaign (December 2012) and could be traced to biogenic emissions from vegetation in fetch regions upwind of the site.

The concentration ranking in the average VOC mixing ratios during our wintertime deployment was acetaldehyde (8.8 ppb) > methanol (7.4 ppb) > acetone + propanal (4.2 ppb) > benzene (2.7 ppb) > toluene (1.5 ppb) > isoprene (1.1 ppb) > acetonitrile (1.1 ppb) > C8-aromatics ($\sim$ 1 ppb) > furan ($\sim$ 0.5 ppb) > C9-aromatics (0.4 ppb). The results suggest that the emission sources of oxygenated and aromatic VOCs in the Kathmandu Valley are different compared to several cities such as Paris and London, likely due to the emissions from biomass co-fired brick kilns, open burning of biomass (e.g. garden waste, agro-residue burning and garbage burning) and extensive use of diesel generators. In comparison to wintertime mixing ratios reported from several sites elsewhere in the world, the mixing ratios of acetaldehyde ($\sim$ 9 ppb), acetonitrile ($\sim$ 1 ppb) and isoprene ($\sim$ 1 ppb) in the Kathmandu Valley are among the highest measured anywhere in the world. The major sources of propyne, propene, benzene, and propanenitrile in the Valley appeared to be biomass burning as concentrations of all these compounds correlated well with the biomass burning tracer acetonitrile ($r^2 > 0.7$) and had diel emission profiles similar to that of acetonitrile.

The top three contributing compounds to the total calculated VOC OH reactivity due to 33 compounds were: acetaldehyde (24.0%), isoprene (20.2%), and propene (18.7%), which collectively accounted for ca. 63% of the campaign averaged total VOC OH reac-

tivity of 12.3 s^{-1}. Oxygenated VOCs and isoprene collectively accounted for more than 68% (72% for period 1 and 68% for period 2) of the total ozone production potential. Based on known SOA yields of compounds and the ambient concentrations measured in the Kathmandu Valley, it was estimated that the relative SOA production potential of VOCs was in the following order: benzene > naphthalene > toluene > xylenes > monoterpenes > trimethylbenzenes > styrene > isoprene. Several VOCs known to enhance health risks for cancer, cataract and pulmonary diseases were detected in the ambient air. The synergistic effect of these VOCs on air toxicity is difficult to quantify but likely significant. The prominent ones were: isocyanic acid, formamide, acetamide, naphthalene and nitromethane for which this study presents the first measurements in ambient air from South Asia along with benzene, a human carcinogen.

Although like all urban environment, contribution of traffic sources to ambient VOCs is significant in the Kathmandu Valley, another anthropogenic source which occupies central importance in the Kathmandu Valley (due to inefficient combustion) are the biomass co-fired brick kilns. While we did not measure particulate matter emissions from the biomass co-fired brick kilns in the Kathmandu Valley during our deployment, previous studies by Pariyar et al. (2013) and Raut. (2003) have reported and documented massive increases in PM_{10} and TSP for periods marked by the operation of the brick kilns relative to periods when they were not operational . The study conducted by Clean Energy Nepal (Raut., 2003) showed that 8 h averaged concentrations of air pollutants such as Total Suspended Particulate (TSP) , PM_{10}, SO_2 and NO_x were three times higher during the brick kiln operating period relative to the period they were not operational at the same location. The mass concentration of PM_{10} increased from 218μgm^{-3} to 603μgm^{-3} while TSP increased from 265μgm^{-3} to 634μgm^{-3}. Note that these were primarily Fixed Chimney Bull Trench Brick Kilns, similar to the ones that impacted our measurements. The Bull Trench kilns are an old and inefficient technology, which have been banned even in their place of origin, India, but continue to dominate the Kathmandu Valley landscape. Thus a major conclusion of this study is that replacing the existing brick kiln technology with cleaner and more efficient brick kiln technology would aid air pollution mitigation efforts significantly. While much has been learnt about wintertime VOC speciation in Kathmandu from this study, and the first comprehensive dataset has been acquired, long

term measurements and further field intensives are required.

Future studies need to focus on what happens in the Valley on seasonal and inter-annual timescales. Of particular interest would be assessing the concentrations of isoprene and acetaldehyde in summer as their contributions to atmospheric chemical processes due to higher biogenic emissions and photochemistry would be expected to be even greater at that time of the year in the Kathmandu Valley. Assessment of source specific emission ratios (inter VOC) for the major sources (brick kilns, diesel generator exhaust, leaf litter fires etc.) and improvement of existing emission inventories using the in-situ data should be undertaken. The comparison and estimation of the fraction of isoprene from vegetation and combustion will also be presented in Chapter 5 of this thesis in which source apportionment of VOCs will be performed using positive matrix factorization (PMF) model. Comprehensive air quality and policy recommendations based on all the data acquired during the SusKat-ABC study and from other sites in the Kathmandu Valley will be reported soon by Rupakheti et al. (2016) Panday et al. (2016).

The PMF model results reveal several new insights regarding the source apportionment of VOCs in the Kathmandu Valley. Speciation of VOCs in the emission inventory for Nepal only includes compound classes (e.g., alkanes, alkenes etc.) and not specific compounds. Also, the existing emission inventories (e.g., REAS v2.1, EDGAR v4.2; Kurokawa et al. (2013); Olivier et al. (1994)) and Nepalese inventory (ICIMOD)) are highly uncertain as there has been no validation using in-situ measurements of these mostly bottom up inventories which rely on fuel and source emission factors measured in other technologically different regions of the world (mostly US and Europe). By using the specific VOC emission tracer data measured in the Kathmandu Valley and constraining the PMF with measured source profiles of complex sources (e.g., biomass co-fired brick kilns, residential solid biofuel use and waste disposal), it is shown that the contribution from sources such as residential solid biofuel use and waste disposal is overestimated in current emission inventories. At the same time, the emissions from traffic and industrial sources are underestimated in the current emission inventory. The presence of elevated concentrations of several health relevant VOCs (e.g., benzene) could be attributed to the biomass co-fired brick kiln sources.

This study has provided quantitative information regarding the contributions of the ma-

jor VOC sources in the Kathmandu Valley. This will enable focused mitigation efforts by policy makers to improve the air quality of the Kathmandu Valley by reducing emissions of both toxic VOCs and secondary pollutants. The results will also enable significant improvements in existing VOC emission inventories so that chemical-transport models can be parameterized more faithfully over the South Asian region and the air quality - climate predictions by models become more reliable.

List of Figures

1.1 Variation of temperature at different layers of the atmosphere (Source: James E. Girard, Principles of Environmental Chemistry, 2010, 'Reproduced with kind permission from Jones & Bartlett Learning, Burlington, Massachusetts, United States') 3
1.2 Spatial and temporal scales of variability for reactive constituents of the atmosphere (Source: Seinfeld and Pandis, Atmospheric Chemistry and Physics: From Air Pollution to Climate Change, Second Edition, 2006, 'Reproduced with kind permission from John Wiley & Sons Ltd., UK') . . 4
1.3 Ozone isopleth diagram showing dependence of ozone production on emissions of VOCs and NO_x (Source: Daniel J. Jacob, Introduction to Atmospheric Chemistry, 1999, 'Reproduced with kind permission from Princeton University Press, New Jersey, United States') 11
1.4 Schematic of first generation product formation from VOCs (Source: Hallquist et al. (2009)) 12
1.5 World map showing previous VOC speciation studies including PTR-MS technique (Figure adapted from: Guenther et al. (2006)). Red square shows no study performed in South Asia before 2011 15

2.1 Schematic of chromatographic separation (Source: Dwayne E. Heard, Analytical Techniques for Atmospheric Measurement, 2006, 'Reproduced with kind permission from John Wiley & Sons Ltd., UK') 19
2.2 Flow diagram of a generic gas chromatography based system 20
2.3 Schematic of a flame ionization detector (FID) (Source: Agilent Technologies, Santa Clara, California, USA) 23

2.4 Schematic of a) PTR-Q-MS (Figure adapted from M. Schwarzmann, 2001) and b) PTR-TOF-MS (Source: Ionicon analytik GmbH, Innsbruck, Austria) 29
2.5 Schematic of a quadrupole mass analyzer (Source: Ionicon analytik GmbH, Innsbruck, Austria) 30
2.6 Contribution of components of applied potential for different directions (x, y and z- axis) in a quadrupole (Source: Hoffmann and Stroobant, Mass Spectrometry Principles and Applications, 2007, 'Reproduced with kind permission from John Wiley & Sons Ltd., UK') 31
2.7 Schematic of a linear time-of-flight (LTOF) mass analyzer (Source: Hoffmann and Stroobant, Mass Spectrometry Principles and Applications, 2007, 'Reproduced with kind permission from John Wiley & Sons Ltd., UK') . . 34
2.8 Schematic of a reflectron time-of-flight (RTOF) mass analyzer (Source: Hoffmann and Stroobant, Mass Spectrometry Principles and Applications, 2007, 'Reproduced with kind permission from John Wiley & Sons Ltd., UK') 35
2.9 Schematic of continuous dynodes or channeltrons (Source: Hoffmann and Stroobant, Mass Spectrometry Principles and Applications, 2007, 'Reproduced with kind permission from John Wiley & Sons Ltd., UK') 37

3.1 72-hour back trajectories of air masses that arrived at 18:30 IST in Mohali and Delhi on 5 October 2012 and 3 November 2012 (also shown are the 96 hour MODIS fire count data as red markers) 46
3.2 Ambient mixing. ratios (n = 570) in ppb of methyl cyanide, carbon monoxide, nitrogen oxides, toluene and benzene from 18:00-03:30 IST duirng Period 1 (black cross; non-fire influenced) and Period 2 (red triangles) fire influenced 48

4.1 Location of the measurement site (Bode; red circle) along with surrounding cities (Kathmandu, brown circle; Patan, blue circle and Bhaktapur, pink circle), brick kilns (white markers), major industries (yellow triangles), forest areas (green tree symbols), airport (blue marker) and major river path (sky blue path) in the Google Earth image of the Kathmandu Valley (obtained on 22 May 2015 at 14:55 LT) 58

4.2 a) Schematic of wind flow during different times of the day in the Kathmandu Valley. b) Box and whisker plots of the measured meteorological parameters (wind speed, wind direction, solar radiation, relative humidity and ambient temperature) at the Bode site (16-30 January 2013) 60

4.3 Compound specific normalized sensitivities at different relative humidities (RH 60%, 75% and 90%) for acetonitrile, acetaldehyde, isoprene and benzene during the calibration experiment performed on 10 January 2013. Horizontal bars reflect the error due to the MFC flows and the accuracy of the VOC gas standard whereas vertical bars reflect the precision error (2σ) of the measurements 65

4.4 a) Normalized response of calibration factors ("CF", ncps ppb^{-1}) vs mass (calibrated species labeled by name) overlaid with linearly fitted mass-dependent transmission curve (black markers and dotted line). Approximate calibration factors for all observed masses where explicit calibrations were not available were determined using separate linear approximations namely b) oxygenated (blue) and c) hydrocarbon (green) species 66

4.5 Illustrative mass spectra (30 second average) of isocyanic acid obtained at 09:24 LT on 13 January 2013 72

4.6 Time series of one minute time resolution data for the mixing ratios of methanol, acetaldehyde, and the sum of acetone and propanal (top panel); isoprene (second panel from top); acetonitrile and furan (second panel from bottom); benzene, toluene, the sum of C8-aromatics (xylene isomers and ethyl benzene) and the sum of C9-aromatics (isomers of trimethylbenzenes and propylbenzenes) (bottom panel) during SusKat-ABC campaign 74

4.7 Comparison of wintertime VOC mixing ratios measured in the Kathmandu Valley with wintertime VOC mixing ratios at selected urban sites elsewhere in the world 78

4.8 Box and whisker plots showing average, median and variability (10^{th}, 25^{th}, 75^{th} and 90^{th} percentile) for some major VOCs in the Kathmandu Valley during Period 1 and Period 2 80

4.9 Comparison of diel box and whisker profiles of several rarely measured or previously unreported ambient VOCs with more frequently measured VOCs/emission tracers 86

4.10 **(a)** Polar annulus plot of isoprene for the period 16–30 January 2013 highlighting the spatio-temporal variation of isoprene and its biogenic sources; **(b)** co-variation of daytime isoprene concentrations with solar radiation on 18 January, 2013. 90

4.11 Diel profiles of the calculated total VOC OH reactivity (with 10^{th} and 90^{th} percentile contributions represented by the grey shaded region) and the major VOC contributors 92

4.12 Pie charts showing contribution of different class of compounds to total ozone formation potential **(a)** for Period 1 (19 December 2012-2 January 2013) and **(b)** for Period 2 (4 January 2013-18 January 2013) 94

5.1 Correlation between estimated and observed VOC concentrations 110

5.2 Comparison of the diel profiles of biogenic emissions, mixed daytime and solvent evaporation factors before and after nudging 112

5.3 Comparison of the G-space plots between a) biomass co-fired brick kilns and mixed industrial emissions and b) residential biofuel use and waste disposal and traffic before and after nudging 114

5.4 Factor profiles of the eight sources obtained by PMF analysis 117

5.5 Timeseries and diel box and whisker plot for Factor 1 (Traffic) 118

5.6 Timeseries and diel box and whisker plot for Factor 2 (Residential biofuel use and waste disposal) 119

5.7 Collection of garbage burning grab samples in the Kathmandu Valley (on left) and the instrumental setup for the analysis (on right) 121

5.8 Timeseries and diel box and whisker plot for Factor 3 (Mixed industrial emissions) 122

5.9 Timeseries and diel box and whisker plot for Factor 4 (Biomass co-fired brick kilns) 123

5.10 Timeseries and diel box and whisker plot for Factor 5 (Unresolved industrial emissions) . . . 124
5.11 Comparison of the diel profile of the unresolved industrial emissions with that of traffic (19-24 December 2012), solvent evaporation (25 December 2012-9 January 2013) and mixed industrial emissions (10-30 January 2013) 124
5.12 Timeseries and diel box and whisker plot for Factor 6 (Solvent evaporation) 125
5.13 Timeseries and diel box and whisker plot for Factor 7 (Mixed daytime) . . 126
5.14 Timeseries and diel box and whisker plot for Factor 8 (Biogenic emissions) 127
5.15 CPF plots for all source factors resolved by PMF showing wind directional dependency for different source categories . . . 131
5.16 Pie chart showing source contribution to total VOC mass loading . . . 133
5.17 Pie charts showing comparison of the PMF derived source contribution with NMVOCs source contribution according to REAS, existing Nepalese and EDGAR emission inventory . . . 134
5.18 Pie chart showing emissions of particulate matter (PM_{10} and $PM_{2.5}$) and CO from different sectors in Kathmandu . . . 135
5.19 Pie charts showing contribution of PMF derived source factors to acetonitrile and aromatic VOCs . . . 137
5.20 Pie charts showing contribution of PMF derived sources to formamide, acetamide, isocyanic acid and formic acid . . . 138
5.21 Reaction schematic for the formation of formamide and isocyanic acid (blue colored species represents radicals) . . . 139
5.22 Pie charts showing contribution of PMF derived sources to 1,3-butadiyne and oxygenated VOCs such as methanol, acetone, acetaldehyde, ethanol and acetic acid . . . 140
5.23 Daily mean relative contribution of sources during SusKat-ABC campaign 141
5.24 Pie charts showing daytime O_3 production potential obtained a) from the source contribution using PMF and b) from the measurements performed in the Kathmandu Valley . . . 142
5.25 Pie chart showing source contribution to SOA formation . . . 143

List of Tables

1.1 Overview of some important VOCs in the troposphere: approximate atmospheric lifetimes, major sources, sinks and global budgets 8

2.1 Common adsorbents used in GC and their respective volatility range . . . 22

2.2 Proton affinities of different species present in the atmosphere (from proton affinity list provided by Ionicon Analytik GmbH, Innsbruck, Austria) . . . 25

3.1 Enhancement ratios during the period not influenced by crop residue burning (clean period; 18:00-03:30) and period influenced by crop residue burning (18:00-03:30), typical chemical lifetimes, ozone and secondary organic aerosol formation potentials of the measured species 49

4.1 Principal operational settings for PTR-TOF-MS parameters 64

4.2 Most likely identity of VOCs (having average mixing ratios > 0.2 ppb) detected at specific protonated m/z ratios, molecular formula, likely mass assignment, reference of previous mass assignment, sensitivity, limit of detection (LOD), average ambient mixing ratios ($\pm$ 1σ) 69

4.3 Top fifteen contributing VOCs to the total reactive carbon during SusKat-ABC campaign 73

4.4 Top ten contributing VOCs to the total OH reactivity during SusKat-ABC campaign 93

5.1 Statistical parameters for the measured species used as PMF input 109

5.2 Diagnostic for the results of the positive matrix factorization (PMF) model run 110

5.3 Inter VOC emission ratios used for biogenic, solvent evaporation and mixed daytime factors to nudge the PMF model and the corresponding emission ratios before and after nudging 113
5.4 Comparison of aromatics/benzene ERs (emission ratios) obtained from PMF (before and after nudging), respective grab samples and the 3 stone firewood source reported in Stockwell et al. (2015) 115
5.5 Emission ratios of VOCs/benzene for aromatic hydrocarbons derived from the PMF model for factor attributed to traffic and comparison of ERs with previous studies for traffic source profiles 119
5.6 Emission ratios of VOCs/benzene for acetonitrile and aromatic hydrocarbons derived from the PMF model for the factor attributed to Residential biofuel use and burning household waste and comparison with previously reported studies and the grab sample collected at the point source 120
5.7 Correlation coefficient (r) between the PMF resolved factors and other independent meteorological parameters (solar radiation, ambient temperature, change in solar radiation, change in ambient temperature, wind speed, wind direction, relative humidity and absolute humidity) for a) daytime period (06:00-17:00 LT) and b) nighttime period (17:00-06:00 LT) 128
5.8 Emission ratios of VOCs/benzene for acetonitrile and aromatic hydrocarbons derived from the PMF model for different sources and comparison with the ratios for the garbage burning grab samples and different source categories reported in previous studies 137

Bibliography

Ahammed, Y. N., Reddy, R. R., Gopal, K. R., Narasimhulu, K., Basha, D. B., Reddy, L. S. S., and Rao, T. V. R.: Seasonal variation of the surface ozone and its precursor gases during 20012003, measured at Anantapur (14.62N), a semi-arid site in India, Atmospheric Research, 80, 151-164, doi:10.1016/j.atmosres.2005.07.002, 2006.

Akagi, S. K., Yokelson, R. J., Wiedinmyer, C., Alvarado, M. J., Reid, J. S., Karl, T., Crounse, J. D., and Wennberg, P. O.: Emission factors for open and domestic biomass burning for use in atmospheric models, Atmos. Chem. Phys., 11, 4039-4072, doi:10.5194/acp-11-4039-2011, 2011.

Akagi, S. K., Yokelson, R. J., Burling, I. R., Meinardi, S., Simpson, I., Blake, D. R., McMeeking, G. R., Sullivan, A., Lee, T., Kreidenweis, S., Urbanski, S., Reardon, J., Griffith, D. W. T., Johnson, T. J., and Weise, D. R.: Measurements of reactive trace gases and variable O3 formation rates in some South Carolina biomass burning plumes, Atmos. Chem. Phys., 13, 1141-1165, doi:10.5194/acp-13-1141-2013, 2013.

Al-Naiema, I., Estillore, A. D., Mudunkotuwa, I. A., Grassian, V. H., and Stone, E. A.: Impacts of co-firing biomass on emissions of particulate matter to the atmosphere, Fuel, 162, 111-120, doi:10.1016/j.fuel.2015.08.054, 2015.

Alves, C. A., Lopes, D. J., Calvo, A. I., Evtyugina, M., Rocha, S., and Nunes, T.: Emissions from Light-Duty Diesel and Gasoline in-use Vehicles Measured on Chassis Dynamometer Test Cycles, Aerosol and Air Quality Research, doi:10.4209/aaqr.2014.01.0006, 2015.

Anderson, M. J., Daly, E. P., Miller, S. L., and Milford, J. B.: Source apportionment of exposures to volatile organic compounds: II. Application of receptor models

to TEAM study data, Atmospheric Environment, 36, 3643-3658, doi:10.1016/S1352-2310(02)00280-7, 2002.

Andreae, M. O., and Merlet, P.: Emission of trace gases and aerosols from biomass burning, Global Biogeochemical Cycles, 15, 955-966, doi:10.1029/2000gb001382, 2001.

Andreae, M. O., and Raemdonck, H.: Dimethyl Sulfide in the Surface Ocean and the Marine Atmosphere - a Global View, Science, 221, 744-747, 1983.

Aoki, N., Inomata, S., and Tanimoto, H.: Detection of C1C5 alkyl nitrates by proton transfer reaction time-of-flight mass spectrometry, International Journal of Mass Spectrometry, 263, 12-21, doi:10.1016/j.ijms.2006.11.018, 2007.

Ashworth, K., Wild, O., Eller, A. S. D., and Hewitt, C. N.: Impact of Biofuel Poplar Cultivation on Ground-Level Ozone and Premature Human Mortality Depends on Cultivar Selection and Planting Location, Environmental Science & Technology, 49, 8566-8575, doi:10.1021/acs.est.5b00266, 2015.

Atkinson, R.: Atmospheric chemistry of VOCs and NO_x, Atmospheric Environment, 34, 2063-2101, doi:10.1016/S1352-2310(99)00460-4, 2000

Atkinson, R., and Arey, J.: Atmospheric Degradation of Volatile Organic Compounds, Chemical Reviews, 103, 4605-4638, doi:10.1021/cr0206420, 2003.

Atkinson, R., Baulch, D. L., Cox, R. A., Crowley, J. N., Hampson, R. F., Hynes, R. G., Jenkin, M. E., Rossi, M. J., and Troe, J.: Evaluated kinetic and photochemical data for atmospheric chemistry: Volume I - gas phase reactions of O_x, HO_x, NO_x and SO_x species, Atmos. Chem. Phys., 4, 1461-1738, doi:10.5194/acp-4-1461-2004, 2004.

Atkinson, R., Baulch, D. L., Cox, R. A., Crowley, J. N., Hampson, R. F., Hynes, R. G., Jenkin, M. E., Rossi, M. J., Troe, J., and Subcommittee, I.: Evaluated kinetic and photochemical data for atmospheric chemistry: Volume II - gas phase reactions of organic species, Atmos. Chem. Phys., 6, 3625-4055, doi:10.5194/acp-6-3625-2006, 2006.

Badarinath, K. V. S., Chand, T. R. K., and Prasad, V. K.: Agriculture crop residue

burning in the Indo-Gangetic Plains - A study using IRS-P6 AWiFS satellite data, Current Science, 91(8), 1085-1089, 2006.

Barletta, B., Meinardi, S., Simpson, I. J., Khwaja, H. A., Blake, D. R., and Rowland, F. S.: Mixing ratios of volatile organic compounds (VOCs) in the atmosphere of Karachi, Pakistan, Atmospheric Environment, 36, 3429-3443, doi:10.1016/S1352-2310(02)00302-3, 2002.

Barletta, B., Meinardi, S., Sherwood Rowland, F., Chan, C. Y., Wang, X., Zou, S., Yin Chan, L., and Blake, D. R.: Volatile organic compounds in 43 Chinese cities, Atmospheric Environment, 39, 5979-5990, doi:10.1016/j.atmosenv.2005.06.029, 2005.

Barnes, I., Solignac, G., Mellouki, A., and Becker, K. H.: Aspects of the Atmospheric Chemistry of Amides, Chem. Phys. Chem., 11, 3844-3857, doi:10.1002/cphc.201000374, 2010.

Betterton, E. A., and Hoffmann, M. R.: Henry's law constants of some environmentally important aldehydes, Environmental Science & Technology, 22, 1415-1418, doi:10.1021/es00177a004, 1988.

Blake, R. S., Monks, P. S., and Ellis, A. M.: Proton-Transfer Reaction Mass Spectrometry, Chemical Reviews, 109(3), 861-896, doi:10.1021/cr800364q, 2009.

Bon, D. M., Ulbrich, I. M., de Gouw, J. A., Warneke, C., Kuster, W. C., Alexander, M. L., Baker, A., Beyersdorf, A. J., Blake, D., Fall, R., Jimenez, J. L., Herndon, S. C., Huey, L. G., Knighton, W. B., Ortega, J., Springston, S., and Vargas, O.: Measurements of volatile organic compounds at a suburban ground site (T1) in Mexico City during the MILAGRO 2006 campaign: measurement comparison, emission ratios, and source attribution, Atmos. Chem. Phys., 11, 2399-2421, doi:10.5194/acp-11-2399-2011, 2011.

Borbon, A., Fontaine, H., Veillerot, M., Locoge, N., Galloo, J. C., and Guillermo, R.: An investigation into the traffic-related fraction of isoprene at an urban location, Atmospheric Environment, 35, 3749-3760, doi:10.1016/S1352-2310(01)00170-4, 2001.

Borbon, A., Gilman, J. B., Kuster, W. C., Grand, N., Chevaillier, S., Colomb, A., Dolgorouky, C., Gros, V., Lopez, M., Sarda-Esteve, R., Holloway, J., Stutz, J., Petetin, H., McKeen, S., Beekmann, M., Warneke, C., Parrish, D. D., and de Gouw, J. A.: Emission ratios of anthropogenic volatile organic compounds in northern mid-latitude megacities: Observations versus emission inventories in Los Angeles and Paris, Journal of Geophysical Research: Atmospheres, 118, 2041-2057, doi:10.1002/jgrd.50059, 2013.

Borduas, N., da Silva, G., Murphy, J. G., and Abbatt, J. P. D.: Experimental and Theoretical Understanding of the Gas Phase Oxidation of Atmospheric Amides with OH Radicals: Kinetics, Products, and Mechanisms, The Journal of Physical Chemistry A, 119 (19), 42984308, doi:10.1021/jp503759f, 2014.

Brown, S. G., Frankel, A., and Hafner, H. R.: Source apportionment of VOCs in the Los Angeles area using positive matrix factorization, Atmospheric Environment, 41, 227-237, doi:10.1016/j.atmosenv.2006.08.021, 2007.

Brown, S. G., Eberly, S., Paatero, P., and Norris, G. A.: Methods for estimating uncertainty in PMF solutions: Examples with ambient air and water quality data and guidance on reporting PMF results, Science of The Total Environment, 518519, 626-635, doi:10.1016/j.scitotenv.2015.01.022, 2015.

Bryan, A. M., Bertman, S. B., Carroll, M. A., Dusanter, S., Edwards, G. D., Forkel, R., Griffith, S., Guenther, A. B., Hansen, R. F., Helmig, D., Jobson, B. T., Keutsch, F. N., Lefer, B. L., Pressley, S. N., Shepson, P. B., Stevens, P. S., and Steiner, A. L.: In-canopy gas-phase chemistry during CABINEX 2009: sensitivity of a 1-D canopy model to vertical mixing and isoprene chemistry, Atmos. Chem. Phys., 12, 8829-8849, doi:10.5194/acp-12-8829-2012, 2012.

Buzcu, B., and Fraser, M. P.: Source identification and apportionment of volatile organic compounds in Houston, TX, Atmospheric Environment, 40, 2385-2400, doi:10.1016/j.atmosenv.2005.12.020, 2006.

Carlton, A. G., Wiedinmyer, C., and Kroll, J. H.: A review of Secondary Organic Aerosol (SOA) formation from isoprene, Atmos. Chem. Phys., 9, 4987-5005, doi:10.5194/acp-9-4987-2009, 2009.

Central Bureau of Statistics: Nepal Population and Housing Census Report 2011, 1, 2011.

Chan, A. W. H., Kautzman, K. E., Chhabra, P. S., Surratt, J. D., Chan, M. N., Crounse, J. D., Krten, A., Wennberg, P. O., Flagan, R. C., and Seinfeld, J. H.: Secondary organic aerosol formation from photooxidation of naphthalene and alkylnaphthalenes: implications for oxidation of intermediate volatility organic compounds (IVOCs), Atmos. Chem. Phys., 9, 3049-3060, doi:10.5194/acp-9-3049-2009, 2009.

Chandra, B. P., and Sinha, V.: Contribution of post-harvest agricultural paddy residue fires in the N.W. Indo–Gangetic Plain to ambient carcinogenic benzenoids, toxic isocyanic acid and carbon monoxide, Environment International, 88, 187-197, doi:10.1016/j.envint.2015.12.025, 2016.

Chen, W. T., Shao, M., Lu, S. H., Wang, M., Zeng, L. M., Yuan, B., and Liu, Y.: Understanding primary and secondary sources of ambient carbonyl compounds in Beijing using the PMF model, Atmos. Chem. Phys., 14, 3047-3062, 10.5194/acp-14-3047-2014, 2014.

Christian, T. J., Kleiss, B., Yokelson, R. J., Holzinger, R., Crutzen, P. J., Hao, W. M., Saharjo, B. H., and Ward, D. E.: Comprehensive laboratory measurements of biomass-burning emissions: 1. Emissions from Indonesian, African, and other fuels, Journal of Geophysical Research: Atmospheres, 108, 4719, doi:10.1029/2003jd003704, 2003.

Christian, T. J., Kleiss, B., Yokelson, R. J., Holzinger, R., Crutzen, P. J., Hao, W. M., Shirai, T., and Blake, D. R.: Comprehensive laboratory measurements of biomass-burning emissions: 2. First intercomparison of open-path FTIR, PTR-MS, and GC-MS/FID/ECD, J. Geophys. Res., 109, D02311, doi:10.1029/2003jd003874, 2004.

Crutzen, P. J., and Andreae, M. O.: Biomass Burning in the Tropics: Impact on Atmospheric Chemistry and Biogeochemical Cycles, Science, 250, 1669-1678, doi:10.1126/science.250.4988.1669, 1990.

Davidson, C. I., Lin, S. F., Osborn, J. F., Pandey, M. R., Rasmussen, R. A., and Khalil, M. A. K.: Indoor and outdoor air pollution in the Himalayas, Environmental Science & Technology, 20, 561-567, doi:10.1021/es00148a003, 1986.

de Foy, B., Varela, J. R., Molina, L. T., and Molina, M. J.: Rapid ventilation of the Mexico City basin and regional fate of the urban plume, Atmos. Chem. Phys., 6, 2321-2335, doi:10.5194/acp-6-2321-2006, 2006.

de Gouw, J. A., Goldan, P. D., Warneke, C., Kuster, W. C., Roberts, J. M., Marchewka, M., Bertman, S. B., Pszenny, A. A. P., and Keene, W. C.: Validation of proton transfer reaction-mass spectrometry (PTR-MS) measurements of gas-phase organic compounds in the atmosphere during the New England Air Quality Study (NEAQS) in 2002, Journal of Geophysical Research: Atmospheres, 108, doi:10.1029/2003jd003863, 2003.

de Gouw, J. A.: Validation of proton transfer reaction-mass spectrometry (PTR-MS) measurements of gas-phase organic compounds in the atmosphere during the New England Air Quality Study (NEAQS) in 2002, Journal of Geophysical Research: Atmospheres, 108, doi:10.1029/2003jd003863, 2003.

de Gouw, J., and Warneke, C.: Measurements of volatile organic compounds in the Earth's atmosphere using proton-transfer-reaction mass spectrometry, Mass Spectrometry Reviews, 26, 223-257, doi:10.1002/mas.20119, 2007.

de Gouw, J. A., Welsh-Bon, D., Warneke, C., Kuster, W. C., Alexander, L., Baker, A. K., Beyersdorf, A. J., Blake, D. R., Canagaratna, M., Celada, A. T., Huey, L. G., Junkermann, W., Onasch, T. B., Salcido, A., Sjostedt, S. J., Sullivan, A. P., Tanner, D. J., Vargas, O., Weber, R. J., Worsnop, D. R., Yu, X. Y., and Zaveri, R.: Emission and chemistry of organic carbon in the gas and aerosol phase at a sub-urban site near Mexico City in March 2006 during the MILAGRO study, Atmos. Chem. Phys., 9, 3425-3442, doi:10.5194/acp-9-3425-2009, 2009.

Department of Plant Resources, Nepal :Bulletin of Department of Plant Resources,Nepal 37, 2015.

Dolgorouky, C., Gros, V., Sarda-Esteve, R., Sinha, V., Williams, J., Marchand, N., Sauvage, S., Poulain, L., Sciare, J., and Bonsang, B.: Total OH reactivity measurements in Paris during the 2010 MEGAPOLI winter campaign, Atmos. Chem. Phys., 12, 9593-9612, doi:10.5194/acp-12-9593-2012, 2012.

Draxler, R. R., and Rolph, G. D.: HYSPLIT - Hybrid Single Particle Lagrangian Integrated Trajectory Model, Model access via NOAA ARL READY Website http://ready.arl.noaa.gov/HYSPLIT.php, NOAA Air Resources Laboratory, College Park, MD.

Dutta, C., Som, D., Chatterjee, A., Mukherjee, A. K., Jana, T. K., and Sen, S.: Mixing ratios of carbonyls and BTEX in ambient air of Kolkata, India and their associated health risk, Environ. Monit. Assess., 148, 97-107, doi:10.1007/s10661-007-0142-0, 2009.

Filella, I., and Peȟuelas, J.: Daily, weekly, and seasonal time courses of VOC concentrations in a semi-urban area near Barcelona, Atmospheric Environment, 40, 7752-7769, doi:10.1016/j.atmosenv.2006.08.002, 2006.

Finlayson-Pitts, B. J., and Pitts, Jr. J. N.: Chemistry of the Upper and Lower Atmosphere, Academic Press, ISBN: 978-0-12-257060-5, 2000.

Fleming, Z. L., Monks, P. S., and Manning, A. J.: Review: Untangling the influence of airmass history in interpreting observed atmospheric composition, Atmospheric Research, 104105, 1-39, doi:10.1016/j.atmosres.2011.09.009, 2012.

Gadi, R., Kulshrestha, U. C., Sarkar, A. K., Garg, S. C., and Parashar, D. C.: Emissions of SO_2 and NO_x from biofuels in India, Tellus B, 55, 787-795, doi:10.1034/j.1600-0889.2003.00065.x, 2003.

Gaimoz, C., Sauvage, S., Gros, V., Herrmann, F., Williams, J., Locoge, N., Perrussel, O., Bonsang, B., dÁrgouges, O., Sarda-Estéve, R., and Sciare, J.: Volatile organic compounds sources in Paris in spring 2007. Part II: source apportionment using positive matrix factorisation, Environmental Chemistry, 8, 91-103, doi:dx.doi.org/10.1071/EN10067, 2011.

Gaur, A., Tripathi, S. N., Kanawade, V. P., Tare, V., and Shukla, S. P.: Four-year measurements of trace gases (SO_2, NO_x, CO, and O_3) at an urban location, Kanpur, in Northern India, Journal of Atmospheric Chemistry, 71, 283-301, doi:10.1007/s10874-014-9295-8, 2014.

Ge, X., Wexler, A. S., and Clegg, S. L.: Atmospheric amines - Part I. A review, Atmospheric Environment, 45, 524-546, doi:10.1016/j.atmosenv.2010.10.012, 2011.

Geron, C., Harley, P., and Guenther, A.: Isoprene emission capacity for US tree species, Atmos. Environ., 35, 3341–3352, doi:10.1016/S1352-2310(00)00407-6, 2001.

Ghude, S., Jain, S. L., Arya, B. C., Beig, G., Ahammed, Y. N., Kumar, A., and Tyagi, B.: Ozone in ambient air at a tropical megacity, Delhi: characteristics, trends and cumulative ozone exposure indices, Journal of Atmospheric Chemistry, 60, 237-252, doi:10.1007/s10874-009-9119-4, 2008.

Giles, J.: Hikes in surface ozone could suffocate crops, Nature, 435, 7-7, doi:10.1038/435007a, 2005.

Gilman, J. B., Lerner, B. M., Kuster, W. C., Goldan, P. D., Warneke, C., Veres, P. R., Roberts, J. M., de Gouw, J. A., Burling, I. R., and Yokelson, R. J.: Biomass burning emissions and potential air quality impacts of volatile organic compounds and other trace gases from fuels common in the US, Atmos. Chem. Phys., 15, 13915–13938, doi:10.5194/acp-15-13915-2015, 2015.

Girard J. E.: Principles of Environmental Chemistry, Third Edition, ISBN-13: 9781449693527, Jones & Bartlett Publishers, 2014.

Grosjean, D., Grosjean, E., and Williams, E. L.: Atmospheric chemistry of olefins: a product study of the ozone-alkene reaction with cyclohexane added to scavenge hydroxyl radical, Environmental Science & Technology, 28, 186-196, doi:10.1021/es00050a026, 1994.

Grosjean, E., Rasmussen, R. A., and Grosjean, D.: Ambient levels of gas phase pollutants in Porto Alegre, Brazil, Atmospheric Environment, 32, 3371-3379, doi:10.1016/S1352-2310(98)00007-7, 1998.

Guenther, A., Hewitt, C. N., Erickson, D., Fall, R., Geron, C., Graedel, T., Harley, P., Klinger, L., Lerdau, M., McKay, W. A., Pierce, T., Scholes, B., Steinbrecher, R., Tallamraju, R., Taylor, J., and Zimmerman, P.: A global model of natural volatile organic

compound emissions, Journal of Geophysical Research: Atmospheres, 100, 8873-8892, doi:10.1029/94jd02950, 1995.

Guenther, A., Karl, T., Harley, P., Wiedinmyer, C., Palmer, P. I., and Geron, C.: Estimates of global terrestrial isoprene emissions using MEGAN (Model of Emissions of Gases and Aerosols from Nature), Atmos. Chem. Phys., 6, 3181-3210, doi:10.5194/acp-6-3181-2006, 2006.

Guo, H., Wang, T., and Louie, P. K. K.: Source apportionment of ambient non-methane hydrocarbons in Hong Kong: Application of a principal component analysis/absolute principal component scores (PCA/APCS) receptor model, Environmental Pollution, 129, 489-498, doi:10.1016/j.envpol.2003.11.006, 2004.

Guo, H., Wang, T., Blake, D. R., Simpson, I. J., Kwok, Y. H., and Li, Y. S.: Regional and local contributions to ambient non-methane volatile organic compounds at a polluted rural/coastal site in Pearl River Delta, China, Atmospheric Environment, 40, 2345-2359, doi:10.1016/j.atmosenv.2005.12.011, 2006.

Guo, H., So, K. L., Simpson, I. J., Barletta, B., Meinardi, S., and Blake, D. R.: C1-C8 volatile organic compounds in the atmosphere of Hong Kong: Overview of atmospheric processing and source apportionment, Atmospheric Environment, 41, 1456-1472, doi:10.1016/j.atmosenv.2006.10.011, 2007.

Gupta, P. K.; Sahai, A.; Singh, N.; Dixit, C. K.; Singh, D. P.; Sharma, C.; Tiwari, M. K.; Gupta, R. K.; and Garg, S. C.: Residue burning in rice-wheat cropping system: causes and implications, Current Science, 87(12), 1713-1717, 2004.

Gurung, A., and Bell, M. L.: Exposure to airborne particulate matter in Kathmandu Valley, Nepal, J. Expos. Sci. Environ. Epidemiol., 22, 235-242, http://www.nature.com/jes/journal/v22/n3/suppinfo/jes201214s1.html, 2012.

Haggen-Smit, A. J.: Chemistry and Physiology of Los Angeles Smog, Air Pollution, 44, 1342-1346, doi:10.1021/ie50510a045, 1952.

Hallquist, M., Wenger, J. C., Baltensperger, U., Rudich, Y., Simpson, D., Claeys, M., Dommen, J., Donahue, N. M., George, C., Goldstein, A. H., Hamilton, J. F., Her-

rmann, H., Hoffmann, T., Iinuma, Y., Jang, M., Jenkin, M. E., Jimenez, J. L., Kiendler-Scharr, A., Maenhaut, W., McFiggans, G., Mentel, T. F., Monod, A., Prvt, A. S. H., Seinfeld, J. H., Surratt, J. D., Szmigielski, R., and Wildt, J.: The formation, properties and impact of secondary organic aerosol: current and emerging issues, Atmos. Chem. Phys., 9, 5155-5236, doi:10.5194/acp-9-5155-2009, 2009.

Hansel, A., Jordan, A., Holzinger, R., Prazeller, P., Vogel, W., and Lindinger, W.: Proton transfer reaction mass spectrometry: on-line trace gas analysis at the ppb level, International Journal of Mass Spectrometry and Ion Processes, 149150, 609-619, doi:10.1016/0168-1176(95)04294-U, 1995.

Hao, W. M., Ward, D. E., Olbu, G., and Baker, S. P.: Emissions of CO_2, CO, and hydrocarbons from fires in diverse African savanna ecosystems, Journal of Geophysical Research: Atmospheres, 101, 23577-23584, doi:10.1029/95JD02198, 1996.

Heard, D. E.: Analytical Techniques for Atmospheric Measurement, Blackwell Publishing Ltd, ISBN: 978-1-4051-2357-0, 2006.

Hellèn, H., Tykkä, T., and Hakola, H.: Importance of monoterpenes and isoprene in urban air in northern Europe, Atmospheric Environment, 59, 59-66, doi:10.1016/j.atmosenv.2012.04.049, 2012.

Henze, D. K., Seinfeld, J. H., Ng, N. L., Kroll, J. H., Fu, T. M., Jacob, D. J., and Heald, C. L.: Global modeling of secondary organic aerosol formation from aromatic hydrocarbons: high- vs. low-yield pathways, Atmos. Chem. Phys., 8, 2405-2420, doi:10.5194/acp-8-2405-2008, 2008.

Heigenmoser, A., Liebner, F., Windeisen, E., and Richter, K.: Investigation of thermally treated beech (Fagus sylvatica) and spruce (Picea abies) by means of multifunctional analytical pyrolysis-GC/MS, Journal of Analytical and Applied Pyrolysis, 100, 117-126, doi:10.1016/j.jaap.2012.12.005, 2013.

Hewitt, C. N.: Reactive Hydrocarbons in the Atmosphere, Academic Press, ISBN: 978-0-12-346240-4, San Diego, 1999

Ho, K. F., Lee, S. C., Ho, W. K., Blake, D. R., Cheng, Y., Li, Y. S., Ho, S. S. H., Fung, K., Louie, P. K. K., and Park, D.: Vehicular emission of volatile organic compounds (VOCs) from a tunnel study in Hong Kong, Atmos. Chem. Phys., 9, 7491-7504, doi:10.5194/acp-9-7491-2009, 2009.

Hoffmann, E. D., and Stroobant, V.: Mass Spectrometry Principles and Applications: Third Edition, John Wiley & Sons Ltd, ISBN: 978-0-470-03310-4, 2007.

Holzinger, R., Warneke, C., Hansel, A., Jordan, A., Lindinger, W., Scharffe, D. H., Schade, G., and Crutzen, P. J.: Biomass burning as a source of formaldehyde, acetaldehyde, methanol, acetone, acetonitrile, and hydrogen cyanide, Geophysical Research Letters, 26, 1161-1164, doi:10.1029/1999gl900156, 1999.

Hoque, R. R., Khillare, P. S., Agarwal, T., Shridhar,V., Balachandran, S.: Spatial and temporal variation of BTEX in the urban atmosphere of Delhi, India, Science of The Total Environment, 392(1), 30-40, doi:10.1016/j.scitotenv.2007.08.036, 2008.

Hwa, M. Y., Hsieh, C. C., Wu, T. C., and Chang, L. F. W.: Real-world vehicle emissions and VOCs profile in the Taipei tunnel located at Taiwan Taipei area, Atmospheric Environment, 36, 1993-2002, doi:10.1016/S1352-2310(02)00148-6, 2002.

Iinuma, Y., Kahnt, A., Mutzel, A., Böge, O., and Herrmann, H.: Ozone-Driven Secondary Organic Aerosol Production Chain, Environmental Science & Technology, 47, 3639-3647, doi:10.1021/es305156z, 2013.

Inomata, S., Tanimoto, H., Kato, S., Suthawaree, J., Kanaya, Y., Pochanart, P., Liu, Y., and Wang, Z.: PTR-MS measurements of non-methane volatile organic compounds during an intensive field campaign at the summit of Mount Tai, China, in June 2006, Atmos. Chem. Phys., 10, 7085-7099, doi:10.5194/acp-10-7085-2010, 2010.

Inomata, S., Tanimoto, H., Fujitani, Y., Sekimoto, K., Sato, K., Fushimi, A., Yamada, H., Hori, S., Kumazawa, Y., Shimono, A., and Hikida, T.: On-line measurements of gaseous nitro-organic compounds in diesel vehicle exhaust by proton-transfer-reaction mass spectrometry, Atmospheric Environment, 73, 195-203, doi:10.1016/j.atmosenv.2013.03.035, 2013.

Inomata, S., Fujitani, Y., Fushimi, A., Tanimoto, H., Sekimoto, K., and Yamada, H.: Field measurement of nitromethane from automotive emissions at a busy intersection using proton-transfer-reaction mass spectrometry, Atmospheric Environment, 96, 301-309, doi:10.1016/j.atmosenv.2014.07.058, 2014.

IPCC: Impacts, Adaptation and Vulnerability : Working Group II Contribution to the Intergovernmental Panel on Climate Change : Fifth Assessment Report (AR5): Summary for Policymakers. , Intergovernmental Panel on Climate Change. Working Group Impacts, 2013.

Jacob, D.: Introduction to Atmospheric Chemistry, ISBN: 9781400841547, Princeton University Press, 1999.

Jardine, K., Yañez-Serrano, A. M., Williams, J., Kunert, N., Jardine, A., Taylor, T., Abrell, L., Artaxo, P., Guenther, A., Hewitt, C. N., House, E., Florentino, A. P., Manzi, A., Higuchi, N., Kesselmeier, J., Behrendt, T., Veres, P. R., Derstroff, B., Fuentes, J. D., Martin, S. T., and Andreae, M. O.: Dimethyl sulfide in the Amazon rain forest, Global Biogeochemical Cycles, 29, 2014GB004969, doi:10.1002/2014gb004969, 2015.

Jerrett, M., Burnett, R. T., Pope, C. A., Ito, K., Thurston, G., Krewski, D., Shi, Y., Calle, E., and Thun, M.: Long-Term Ozone Exposure and Mortality, New England Journal of Medicine, 360, 1085-1095, doi:10.1056/NEJMoa0803894, 2009.

Johnson, B., Betterton, E., and Craig, D.: Henry's law coefficients of formic and acetic acids, Journal of Atmospheric Chemistry, 24, 113-119, doi:10.1007/bf00162406, 1996.

Jones, C. E., Hopkins, J. R., and Lewis, A. C.: In situ measurements of isoprene and monoterpenes within a south-east Asian tropical rainforest, Atmos. Chem. Phys., 11, 6971-6984, doi:10.5194/acp-11-6971-2011, 2011.

Jones, C. E., Kato, S., Nakashima, Y., and Kajii, Y.: A novel fast gas chromatography method for higher time resolution measurements of speciated monoterpenes in air, Atmos. Meas. Tech., 7, 1259-1275, doi:10.5194/amt-7-1259-2014, 2014.

Jordan, A., Haidacher, S., Hanel, G., Hartungen, E., Märk, L., Seehauser, H., Schottkowsky, R., Sulzer, P., and Märk, T. D.: A high resolution and high sensitivity proton-transfer-reaction time-of-flight mass spectrometer (PTR-TOF-MS), International Journal of Mass Spectrometry, 286, 122-128, doi:10.1016/j.ijms.2009.07.005, 2009.

Jorquera, H., and Rappenglück, B.: Receptor modeling of ambient VOC at Santiago, Chile, Atmospheric Environment, 38, 4243-4263, doi:10.1016/j.atmosenv.2004.04.030, 2004.

Karl, T., Jobson, T., Kuster, W. C., Williams, E., Stutz, J., Shetter, R., Hall, S. R., Goldan, P., Fehsenfeld, F., and Lindinger, W.: Use of proton-transfer-reaction mass spectrometry to characterize volatile organic compound sources at the La Porte super site during the Texas Air Quality Study 2000, Journal of Geophysical Research: Atmospheres, 108, 4508, doi:10.1029/2002jd003333, 2003.

Karl, T. G., Christian, T. J., Yokelson, R. J., Artaxo, P., Hao, W. M., and Guenther, A.: The Tropical Forest and Fire Emissions Experiment: method evaluation of volatile organic compound emissions measured by PTR-MS, FTIR, and GC from tropical biomass burning, Atmos. Chem. Phys., 7, 5883-5897, doi:10.5194/acp-7-5883-2007, 2007.

Karl, T., Harley, P., Emmons, L., Thornton, B., Guenther, A., Basu, C., Turnipseed, A., and Jardine, K.: Efficient Atmospheric Cleansing of Oxidized Organic Trace Gases by Vegetation, Science, 330, 816-819, doi:10.1126/science.1192534, 2010.

Kesselmeier, J., Bode, K., Hofmann, U., Müller, H., Schäfer, L., Wolf, A., Ciccioli, P., Brancaleoni, E., Cecinato, A., Frattoni, M., Foster, P., Ferrari, C., Jacob, V., Fugit, J. L., Dutaur, L., Simon, V., and Torres, L.: Emission of short chained organic acids, aldehydes and monoterpenes from Quercus ilex L. and Pinus pinea L. in relation to physiological activities, carbon budget and emission algorithms, Atmospheric Environment, 31, Supplement 1, 119-133, doi:10.1016/S1352-2310(97)00079-4, 1997.

Kesselmeier, J., and Staudt, M.: Biogenic Volatile Organic Compounds (VOC): An Overview on Emission, Physiology and Ecology, Journal of Atmospheric Chemistry, 33, 23-88, doi:10.1023/a:1006127516791, 1999.

Kim, E., Brown, S. G., Hafner, H. R., and Hopke, P. K.: Characterization of non-methane volatile organic compounds sources in Houston during 2001 using positive matrix factorization, Atmospheric Environment, 39, 5934-5946, doi:10.1016/j.atmosenv.2005.06.045, 2005.

Kim, K. H., Hong, Y. J., Pal, R., Jeon, E. C., Koo, Y. S., and Sunwoo, Y.: Investigation of carbonyl compounds in air from various industrial emission sources, Chemosphere, 70, 807-820, doi:10.1016/j.chemosphere.2007.07.025, 2008.

Kitada, T., and Regmi, R. P.: Dynamics of Air Pollution Transport in Late Wintertime over Kathmandu Valley, Nepal: As Revealed with Numerical Simulation, Journal of Applied Meteorology, 42, 1770-1798, doi:10.1175/1520-0450(2003)042<1770:doapti>2.0.co;2, 2003.

Koppmann, R., von Czapiewski, K., and Reid, J. S.: A review of biomass burning emissions, part I: gaseous emissions of carbon monoxide, methane, volatile organic compounds, and nitrogen containing compounds, Atmos. Chem. Phys. Discuss., 5, 10455-10516, doi:10.5194/acpd-5-10455-2005, 2005.

Kristensson, A., Johansson, C., Westerholm, R., Swietlicki, E., Gidhagen, L., Wideqvist, U., and Vesely, V.: Real-world traffic emission factors of gases and particles measured in a road tunnel in Stockholm, Sweden, Atmospheric Environment, 38, 657-673, doi:10.1016/j.atmosenv.2003.10.030, 2004.

Kroll, J. H., Ng, N. L., Murphy, S. M., Flagan, R. C., and Seinfeld, J. H.: Secondary Organic Aerosol Formation from Isoprene Photooxidation, Environmental Science & Technology, 40, 1869-1877, doi:10.1021/es0524301, 2006.

Kulshrestha, U. C., Jain, M., and Parashar, D. C.: Concentrations and behaviour of surface O_3, NO and NO_2, Indian J Radio & Space Physics, 26, 82-84, 1997.

Kumar, V., and Sinha, V.: VOC–OHM: A new technique for rapid measurements of ambient total OH reactivity and volatile organic compounds using a single proton transfer reaction mass spectrometer, International Journal of Mass Spectrometry, 374, 55-63, doi:10.1016/j.ijms.2014.10.012, 2014.

Kumar, V., Sarkar, C. and Sinha, V.: Influence of post harvest crop residue fires on surface ozone mixing ratios in the N.W. IGP analyzed using two years of continuous in-situ trace gas measurements. J. Geophys. Res. Atmos., 120, 10.1002/2015JD024308, 2016.

Kumar, A., and Tyagi, S. K.: Benzene and toluene profiles in ambient air of Delhi as determined by active sampling and GC analysis, Journal of Scientific and Industrial Research, 65, 252-257, 2006.

Kurokawa, J., Ohara, T., Morikawa, T., Hanayama, S., Janssens-Maenhout, G., Fukui, T., Kawashima, K., and Akimoto, H.: Emissions of air pollutants and greenhouse gases over Asian regions during 20002008: Regional Emission inventory in ASia (REAS) version 2, Atmos. Chem. Phys., 13, 11019-11058, doi:10.5194/acp-13-11019-2013, 2013.

Lal, S., Naja, M., and Subbaraya, B. H.: Seasonal variations in surface ozone and its precursors over an urban site in India, Atmospheric Environment, 34, 2713-2724, doi:10.1016/S1352-2310(99)00510-5, 2000.

Lal, S., Sahu, L. K., Venkataramani, S., Rajesh, T. A., and Modh, K. S.: Distributions of O_3, CO and NMHCs over the rural sites in central India, Journal of Atmospheric Chemistry, 61, 73-84, doi:10.1007/s10874-009-9126-5, 2008.

Lal, S., Sahu, L. K., Venkataramani, S., and Mallik, C.: Light non-methane hydrocarbons at two sites in the Indo-Gangetic Plain, Journal of Environmental Monitoring : JEM, 14, 1159-1166, doi:10.1039/c2em10682e, 2012.

Langford, B., Davison, B., Nemitz, E., and Hewitt, C. N.: Mixing ratios and eddy covariance flux measurements of volatile organic compounds from an urban canopy (Manchester, UK), Atmos. Chem. Phys., 9, 1971-1987, doi:10.5194/acp-9-1971-2009, 2009.

Langford, B., Nemitz, E., House, E., Phillips, G. J., Famulari, D., Davison, B., Hopkins, J. R., Lewis, A. C., and Hewitt, C. N.: Fluxes and concentrations of volatile organic compounds above central London, UK, Atmos. Chem. Phys., 10, 627-645, doi:10.5194/acp-10-627-2010, 2010.

Larssen, S., F. Gram, I. Haugsbakk, J. Huib, X. Olsthoorn, A. S. Giri, R. Shah, M. L. Shrestha, A. and Shrestha, B.: Urban Air Quality Management Strategy in Asia: Kathmandu Valley Report, World Bank, Washington, D. C., 1997.

Lee, A., Goldstein, A. H., Kroll, J. H., Ng, N. L., Varutbangkul, V., Flagan, R. C., and Seinfeld, J. H.: Gas-phase products and secondary aerosol yields from the photooxidation of 16 different terpenes, Journal of Geophysical Research: Atmospheres, 111, D17305, doi:10.1029/2006jd007050, 2006.

Leighton, P. A.: Photochemistry of Air Pollution, Academic Press, New York, p. 59, 1961.

Lelieveld, J., Crutzen, P. J., Ramanathan, V., Andreae, M. O., Brenninkmeijer, C. A. M., Campos, T., Cass, G. R., Dickerson, R. R., Fischer, H., de Gouw, J. A., Hansel, A., Jefferson, A., Kley, D., de Laat, A. T. J., Lal, S., Lawrence, M. G., Lobert, J. M., Mayol-Bracero, O. L., Mitra, A. P., Novakov, T., Oltmans, S. J., Prather, K. A., Reiner, T., Rodhe, H., Scheeren, H. A., Sikka, D., and Williams, J.: The Indian Ocean Experiment: Widespread Air Pollution from South and Southeast Asia, Science, 291, 1031-1036, 10.1126/science.1057103, 2001.

Lelieveld, J., Dentener, F. J., Peters, W., and Krol, M. C.: On the role of hydroxyl radicals in the self-cleansing capacity of the troposphere, Atmos. Chem. Phys., 4, 2337-2344, doi:10.5194/acp-4-2337-2004, 2004.

Lemieux, P. M., Lutes, C. C., and Santoianni, D. A.: Emissions of organic air toxics from open burning: a comprehensive review, Progress in Energy and Combustion Science, 30, 1-32, doi:10.1016/j.pecs.2003.08.001, 2004.

Leuchner, M., and Rappenglück, B.: VOC source-receptor relationships in Houston during TexAQS-II, Atmospheric Environment, 44, 4056-4067, doi:10.1016/j.atmosenv.2009.02.029, 2010.

Levy, H.: Normal Atmosphere: Large Radical and Formaldehyde Concentrations Predicted, Science, 173, 141-143, doi:10.1126/science.173.3992.141, 1971

Li, Q., Steele, P. H., Yu, F., Mitchell, B., and Hassan, E. B. M.: Pyrolytic spray increases levoglucosan production during fast pyrolysis, Journal of Analytical and Applied Pyrolysis, 100, 33-40, doi:10.1016/j.jaap.2012.11.013, 2013.

Lindinger, W., Hansel, A., and Jordan, A.: On-line monitoring of volatile organic compounds at pptv levels by means of proton-transfer-reaction mass spectrometry (PTR-MS) medical applications, food control and environmental research, International Journal of Mass Spectrometry and Ion Processes, 173, 191-241, doi:10.1016/s0168-1176(97)00281-4, 1998.

Liu, Y., Shao, M., Lu, S., Chang, C. C., Wang, J. L., and Chen, G.: Volatile Organic Compound (VOC) measurements in the Pearl River Delta (PRD) region, China, Atmos. Chem. Phys., 8, 1531-1545, doi:10.5194/acp-8-1531-200, 2008.

Liu, Y., Shi, Q., Zhang, Y., He, Y., Chung, K. H., Zhao, S., and Xu, C.: Characterization of Red Pine Pyrolysis Bio-oil by Gas ChromatographyMass Spectrometry and Negative-Ion Electrospray Ionization Fourier Transform Ion Cyclotron Resonance Mass Spectrometry, Energy and Fuels, 26, 4532-4539, doi:10.1021/ef300501t, 2012.

Lockhart, J., Blitz, M. A., Heard, D. E., Seakins, P. W., and Shannon, R. J.: The Mechanism of the Reaction of OH with Alkynes in the Presence of Oxygen, J Phys Chem A, doi:10.1021/jp404233b, 2013.

Majumdar, D., Mukherjeea, A. K., and Sen, S.: BTEX in Ambient Air of a Metropolitan City, Journal of Environmental Protection, 02, 11-20, doi:10.4236/jep.2011.21002, 2011.

Mannschreck, K., Gilge, S., Plass-Duelmer, C., Fricke, W., and Berresheim, H.: Assessment of the applicability of NO-NO_2-O_3 photostationary state to long-term measurements at the Hohenpeissenberg GAW Station, Germany, Atmos. Chem. Phys., 4, 1265-1277, doi:10.5194/acp-4-1265-2004, 2004.

Marandino, C. A., de Bruyn, W. J., Miller, S. D., Prather, M. J., and Saltzman, E. S.: Oceanic uptake and the global atmospheric acetone budget, Geophysical Research Letters, 32, L15806 1-4, doi:10.1029/2005gl023285, 2005.

Martinez, M., Harder, H., Ren, X., Lesher, R. L., and Brune, W. H.: Measuring atmospheric naphthalene with laser-induced fluorescence, Atmos. Chem. Phys., 4, 563-569, doi:10.5194/acp-4-563-2004, 2004.

Miller, S. L., Anderson, M. J., Daly, E. P., and Milford, J. B.: Source apportionment of exposures to volatile organic compounds. I. Evaluation of receptor models using simulated exposure data, Atmospheric Environment, 36, 3629-3641, doi:10.1016/S1352-2310(02)00279-0, 2002.

Millet, D. B., Jacob, D. J., Custer, T. G., de Gouw, J. A., Goldstein, A. H., Karl, T., Singh, H. B., Sive, B. C., Talbot, R. W., Warneke, C., and Williams, J.: New constraints on terrestrial and oceanic sources of atmospheric methanol, Atmos. Chem. Phys., 8, 6887-6905, doi:10.5194/acp-8-6887-2008, 2008.

Millet, D. B., Guenther, A., Siegel, D. A., Nelson, N. B., Singh, H. B., de Gouw, J. A., Warneke, C., Williams, J., Eerdekens, G., Sinha, V., Karl, T., Flocke, F., Apel, E., Riemer, D. D., Palmer, P. I., and Barkley, M.: Global atmospheric budget of acetaldehyde: 3-D model analysis and constraints from in-situ and satellite observations, Atmos. Chem. Phys., 10, 3405-3425, doi:10.5194/acp-10-3405-2010, 2010.

Misztal, P. K., Hewitt, C. N., Wildt, J., Blande, J. D., Eller, A. S. D., Fares, S., Gentner, D. R., Gilman, J. B., Graus, M., Greenberg, J., Guenther, A. B., Hansel, A., Harley, P., Huang, M., Jardine, K., Karl, T., Kaser, L., Keutsch, F. N., Kiendler-Scharr, A., Kleist, E., Lerner, B. M., Li, T., Mak, J., Nlscher, A. C., Schnitzhofer, R., Sinha, V., Thornton, B., Warneke, C., Wegener, F., Werner, C., Williams, J., Worton, D. R., Yassaa, N., and Goldstein, A. H.: Atmospheric benzenoid emissions from plants rival those from fossil fuels, Scientific Reports, 5, 12064, doi:10.1038/srep12064, 2015.

Mohan Rao, A. M., Pandit, G. G., Sain, P., Sharma, S., Krishnamoorthy, T. M., and Nambi, K. S. V.: Non-methane hydrocarbons in industrial locations of Bombay, Atmospheric Environment, 31, 1077-1085, doi:10.1016/S1352-2310(96)00266-X, 1997.

Molina, L. T., Kolb, C. E., de Foy, B., Lamb, B. K., Brune, W. H., Jimenez, J. L.,

Ramos-Villegas, R., Sarmiento, J., Paramo-Figueroa, V. H., Cardenas, B., Gutierrez-Avedoy, V., and Molina, M. J.: Air quality in North America's most populous city – overview of the MCMA-2003 campaign, Atmos. Chem. Phys., 7, 2447-2473, doi:10.5194/acp-7-2447-2007, 2007.

Monks, P. S.: Gas-phase radical chemistry in the troposphere, Chemical Society Reviews, 34, 376-395, doi:10.1039/b307982c, 2005.

Morino, Y., Ohara, T., Yokouchi, Y., and Ooki, A.: Comprehensive source apportionment of volatile organic compounds using observational data, two receptor models, and an emission inventory in Tokyo metropolitan area, Journal of Geophysical Research: Atmospheres, 116, doi:10.1029/2010jd014762, 2011.

Müller, M., Graus, M., Ruuskanen, T. M., Schnitzhofer, R., Bamberger, I., Kaser, L., Titzmann, T., Hörtnagl, L., Wohlfahrt, G., Karl, T., and Hansel, A.: First eddy covariance flux measurements by PTR-TOF, Atmos. Meas. Tech., 3, 387-395, doi:10.5194/amt-3-387-2010, 2010.

Müller, M., Graus, M., Wisthaler, A., Hansel, A., Metzger, A., Dommen, J., and Baltensperger, U.: Analysis of high mass resolution PTR-TOF mass spectra from 1,3,5-trimethylbenzene (TMB) environmental chamber experiments, Atmos. Chem. Phys., 12, 829-843, doi:10.5194/acp-12-829-2012, 2012.

Na, K., and Pyo Kim, Y.: Chemical mass balance receptor model applied to ambient C2-C9 VOC concentration in Seoul, Korea: Effect of chemical reaction losses, Atmospheric Environment, 41, 6715-6728, doi:10.1016/j.atmosenv.2007.04.054, 2007.

Nakashima, Y., Kamei, N., Kobayashi, S., and Kajii, Y.: Total OH reactivity and VOC analyses for gasoline vehicular exhaust with a chassis dynamometer, Atmospheric Environment, 44, 468-475, doi:10.1016/j.atmosenv.2009.11.006, 2010.

Nelson, P. F., Li, C. Z., and Ledesma, E.: Formation of HNCO from the Rapid Pyrolysis of Coals, Energy & Fuels, 10, 264-265, doi:10.1021/ef950183o, 1996.

Ng, N. L., Kroll, J. H., Chan, A. W. H., Chhabra, P. S., Flagan, R. C., and Seinfeld, J. H.: Secondary organic aerosol formation from m-xylene, toluene, and benzene, Atmos. Chem. Phys., 7, 3909-3922, doi:10.5194/acp-7-3909-2007, 2007.

Ng, N. L., Chhabra, P. S., Chan, A. W. H., Surratt, J. D., Kroll, J. H., Kwan, A. J., McCabe, D. C., Wennberg, P. O., Sorooshian, A., Murphy, S. M., Dalleska, N. F., Flagan, R. C., and Seinfeld, J. H.: Effect of NO_x level on secondary organic aerosol (SOA) formation from the photooxidation of terpenes, Atmos. Chem. Phys., 7, 5159-5174, doi:10.5194/acp-7-5159-2007, 2007.

Norris, G., Vedantham, R., Wade, K., Zahn, P., Brown, S., Paatero, P., Eberly, S., and Foley, C.: Guidance Document for PMF Applications with the Multilinear Engine, EPA 600/R-09/032, 2009.

Olivier, J. G. J., Bouwman, A. F., van der Maas, C. W. M., and Berdowski, J. J. M.: Emission Database for Global Atmospheric Research (EDGAR), in: Non-CO_2 Greenhouse Gases: Why and How to Control?, edited by: van Ham, J., Janssen, L. J. H. M., and Swart, R. J., Springer Netherlands, 93-106, 1994.

Olivier, J. G. J., Bouwman, A. F., van der Maas, C. W. M., Berdowski, J. J. M., Veldt, C., Bloos, J. P. J., Visschedijk, A. J. H., Zandveld, P. Y. J., and Haverlag, J. L.: A set of global emission inventories of green house gases and ozone depleting substances for all anthropogenic and natural sources on a per country basis and on 10 by 10 grid, in Description of EDGAR version 2.0, National Institute of public health and environment: Bilthoven, The Neatherlands., 66-71., 1996.

Olson, D. A., Norris, G. A., Seila, R. L., Landis, M. S., and Vette, A. F.: Chemical characterization of volatile organic compounds near the World Trade Center: Ambient concentrations and source apportionment, Atmospheric Environment, 41, 5673-5683, doi:10.1016/j.atmosenv.2007.02.047, 2007.

Paatero, P., and Tapper, U.: Positive matrix factorization: A non-negative factor model with optimal utilization of error estimates of data values, Environmetrics, 5, 111-126, doi:10.1002/env.3170050203, 1994.

Paatero, P.: Least squares formulation of robust non-negative factor analysis, Chemometrics and Intelligent Laboratory Systems, 37, 23-35, doi:10.1016/S0169-7439(96)00044-5, 1997.

Paatero, P.: The Multilinear Engine-A Table-Driven, Least Squares Program for Solving Multilinear Problems, Including the n-Way Parallel Factor Analysis Model, Journal of Computational and Graphical Statistics, 8, 854-888, doi:10.1080/10618600.1999.10474853, 1999.

Paatero, P., Hopke, P. K., Song, X. H., and Ramadan, Z.: Understanding and controlling rotations in factor analytic models, Chemometrics and Intelligent Laboratory Systems, 60, 253-264, doi:10.1016/S0169-7439(01)00200-3, 2002.

Paatero, P., and Hopke, P. K.: Rotational tools for factor analytic models, Journal of Chemometrics, 23, 91-100, doi:10.1002/cem.1197, 2009.

Padhy, P. K., and Varshney, C. K.: Emission of volatile organic compounds (VOC) from tropical plant species in India, Chemosphere, 59, 1643-1653, doi:10.1016/j.chemosphere.2005.01.046, 2005.

Panday, A. K., and Prinn, R. G.: Diurnal cycle of air pollution in the Kathmandu Valley, Nepal: Observations, Journal of Geophysical Research: Atmospheres, 114, D09305, doi:10.1029/2008jd009777, 2009.

Panday, A. K., Prinn, R. G., and Schär, C.: Diurnal cycle of air pollution in the Kathmandu Valley, Nepal: 2. Modeling results, Journal of Geophysical Research: Atmospheres, 114, D21308, doi:10.1029/2008jd009808, 2009.

Panday, A. K., Adhikary, B., Praveen, P. S., Mahata, K. S., and Rupakheti, M.: Meteorology and air pollution transport in the Kathmandu Valley, Nepal, in preparation, 2016.

Pariyar, S. K., Das, T., and Ferdous, T.: Environment and Health Impact for Brick Kilns in Kathmandu Valley, International Journal of Scientific & Technology Research, 2, 2013.

Park, J. H., Goldstein, A. H., Timkovsky, J., Fares, S., Weber, R., Karlik, J., and Holzinger, R.: Eddy covariance emission and deposition flux measurements using proton transfer reaction – time of flight-mass spectrometry (PTR-TOF-MS): comparison with PTR-MS measured vertical gradients and fluxes, Atmos. Chem. Phys., 13, 1439-1456, doi:10.5194/acp-13-1439-2013, 2013.

Paton-Walsh, C., Smith, T. E. L., Young, E. L., Griffith, D. W. T., and Guérette, É. A.: New emission factors for Australian vegetation fires measured using open-path Fourier transform infrared spectroscopy Part 1: Methods and Australian temperate forest fires, Atmos. Chem. Phys., 14, 11313-11333, doi:10.5194/acp-14-11313-2014, 2014.

Patton, R. L., and Garraway, M. O.: Ozone-induced necrosis and increased peroxidase activity in hybrid poplar (Populus sp.) leaves, Environmental and Experimental Botany, 26, 137-141, doi:10.1016/0098-8472(86)90006-7, 1986.

Platt, U. A., and Stutz, J.: Differential Optical Absorption Spectroscopy: Physics of Earth and Space Environments, pp. 575, doi:10.1007/978-3-540-75776-4 2, 2008.

Pollmann, J., Helmig, D., Hueber, J., Plass-Dülmer, C., and Tans, P.: Sampling, storage, and analysis of C2-C7 non-methane hydrocarbons from the US National Oceanic and Atmospheric Administration Cooperative Air Sampling Network glass flasks, Journal of Chromatography A, 1188, 75-87, doi:10.1016/j.chroma.2008.02.059, 2008.

Pradhan, B. B., Dangol, P. M., Bhaunju, P. M., and Pradhan, S.: Rapid Urban Assessment of Air Quality for Kathmandu, Nepal: Summary, ICIMOD, 2012.

Presto, A. A., Huff Hartz, K. E., and Donahue, N. M.: Secondary Organic Aerosol Production from Terpene Ozonolysis. 2. Effect of NO_x Concentration, Environmental Science & Technology, 39, 7046-7054, doi:10.1021/es050400s, 2005.

Pudasainee, D., Sapkota, B., Shrestha, M. L., Kaga, A., Kondo, A., and Inoue, Y.: Ground level ozone concentrations and its association with NO_x and meteorological parameters in Kathmandu Valley, Nepal, Atmospheric Environment, 40, 8081-8087, doi:10.1016/j.atmosenv.2006.07.011, 2006.

Putero, D., Cristofanelli, P., Marinoni, A., Adhikary, B., Duchi, R., Shrestha, S. D., Verza, G. P., Landi, T. C., Calzolari, F., Busetto, M., Agrillo, G., Biancofiore, F., Di Carlo, P., Panday, A. K., Rupakheti, M., and Bonasoni, P.: Seasonal variation of ozone and black carbon observed at Paknajol, an urban site in the Kathmandu Valley, Nepal, Atmos. Chem. Phys., 15, 13957-13971, doi:10.5194/acp-15-13957-2015, 2015.

Ramana, M. V., Ramanathan, V., Podgorny, I. A., Pradhan, B. B., and Shrestha, B.: The direct observations of large aerosol radiative forcing in the Himalayan region, Geophysical Research Letters, 31, L05111, doi:10.1029/2003gl018824, 2004.

Rappenglück, B., Schmitz, R., Bauerfeind, M., Cereceda-Balic, F., von Baer, D., Jorquera, H., Silva, Y., and Oyola, P.: An urban photochemistry study in Santiago de Chile, Atmospheric Environment, 39, 2913-2931, doi:10.1016/j.atmosenv.2004.12.049, 2005.

Rasmussen, R. A., and Khalil, M. A. K.,: Atmospheric benzene and toluene, Geophysical Research Letters, 10(11), 1096-1099, doi:10.1029/GL010i011p01096, 1983.

Raut, A. K.: Brick Kilns in Kathmandu Valley: Current status, environmental impacts and future options, Himalayan Journal of Sciences, 1, doi:10.3126/hjs.v1i1.189, 2003.

Regmi, R. P., Kitada, T., and Kurata, G.: Numerical Simulation of Late Wintertime Local Flows in Kathmandu Valley, Nepal: Implication for Air Pollution Transport, Journal of Applied Meteorology, 42, 389-403, doi:10.1175/1520-0450(2003)042<0389:nsolwl>2.0.co;2, 2003.

Rizzo, M. J., and Scheff, P. A.: Utilizing the Chemical Mass Balance and Positive Matrix Factorization models to determine influential species and examine possible rotations in receptor modeling results, Atmospheric Environment, 41, 6986-6998, doi:10.1016/j.atmosenv.2007.05.008, 2007.

Roberts, J. M., Veres, P. R., Cochran, A. K., Warneke, C., Burling, I. R., Yokelson, R. J., Lerner, B., Gilman, J. B., Kuster, W. C., Fall, R., and de Gouw, J.: Isocyanic acid in the atmosphere and its possible link to smoke-related health effects, Proceedings of the National Academy of Sciences, doi:10.1073/pnas.1103352108, 2011.

Roberts, J. M., Veres, P., VandenBoer, T. C., Warneke, C., Graus, M., Williams, E. J., Lefer, B. L., Brock, C. A., Bahreini, R., Öztürk, F., Middlebrook, A. M., Wagner, N. L., Dubè, W. P. A., and de Gouw, J. A.: New insights into atmospheric sources and sinks of isocyanic acid, HNCO, from recent urban and regional observations, Journal of Geophysical Research: Atmospheres, 119, 1060-1072, doi:10.1002/2013JD019931, 2014.

Rolph, G. D.: Real-time Environmental Applications and Display sYstem (READY) Website (http://www.ready.noaa.gov). NOAA Air Resources Laboratory, College Park, MD.

Ropkins, K., and Carslaw, D. C.: openair - Data Analysis Tools for the Air Quality Community, The R Journal 4, 20-29, 2012.

Rosenfeld, D., Lohmann, U., Raga, G. B., O'Dowd, C. D., Kulmala, M., Fuzzi, S., Reissell, A., and Andreae, M. O.: Flood or Drought: How Do Aerosols Affect Precipitation?, Science, 321, 1309-1313, doi:10.1126/science.1160606, 2008.

Rupakheti, M., Panday, A. K., Lawrence, M. G., Kim, S. W., Sinha, V., Kang, S. C., Naja, M., Park, J. S., Hoor, P., Holben, B., Sharma, R. K., Mues, A., Mahata, K. S., Bhardwaj, P., Sarkar, C., Rupakheti, D., Regmi, R. P., and Gustafsson, Ö.: Air pollution in the Himalayan foothills: Overview of the SusKat-ABC international air pollution measurement campaign in Nepal, in preparation, 2016.

Ruuskanen, T. M., Müller, M., Schnitzhofer, R., Karl, T., Graus, M., Bamberger, I., Hörtnagl, L., Brilli, F., Wohlfahrt, G., and Hansel, A.: Eddy covariance VOC emission and deposition fluxes above grassland using PTR-TOF, Atmos. Chem. Phys., 11, 611-625, doi:10.5194/acp-11-611-2011, 2011.

Sahai, S., Sharma, C., Singh, D. P., Dixit, C. K., Singh, N., Sharma, P., Singh, K., Bhatt, S., Ghude, S., Gupta, V., Gupta, R. K., Tiwari, M. K., Garg, S. C., Mitra, A. P., and Gupta, P. K.: A study for development of emission factors for trace gases and carbonaceous particulate species from in situ burning of wheat straw in agricultural fields in india, Atmospheric Environment, 41(39), 9173-9186, doi:10.1016/j.atmosenv.2007.07.054, 2007.

Sahu, L. K., and Lal, S.: Distributions of C2-C5 NMHCs and related trace gases at a tropical urban site in India, Atmospheric Environment, 40, 880-891, doi:10.1016/j.atmosenv.2005.10.021, 2006.

Sanhueza, E., Holzinger, R., Kleiss, B., Donoso, L., and Crutzen, P. J.: New insights in the global cycle of acetonitrile: release from theocean and dry deposition in the tropical savanna of Venezuela, Atmos. Chem. Phys., 4, 275-280, doi:10.5194/acp-4-275-2004, 2004.

Sarkar, C., Kumar, V. and Sinha, V.: Massive emissions of carcinogenic benzenoids from paddy residue burning in North India, Curr. Sci., 104, 1703-1706, 2013.

Sarkar, C., Sinha, V., Kumar, V., Rupakheti, M., Panday, A., Mahata, K. S., Rupakheti, D., Kathayat, B., and Lawrence, M. G.: Overview of VOC emissions and chemistry from PTR-TOF-MS measurements during the SusKat-ABC campaign: high acetaldehyde, isoprene and isocyanic acid in wintertime air of the Kathmandu Valley, Atmos. Chem. Phys., 16, 3979-4003, doi:10.5194/acp-16-3979-2016, 2016.

Sasaki, J., Aschmann, S. M., Kwok, E. S. C., Atkinson, R., and Arey, J.: Products of the Gas-Phase OH and NO_3 Radical-Initiated Reactions of Naphthalene, Environmental Science & Technology, 31, 3173-3179, doi:10.1021/es9701523, 1997.

Schmitz, R.: Modelling of air pollution dispersion in Santiago de Chile, Atmospheric Environment, 39, 2035-2047, doi:10.1016/j.atmosenv.2004.12.033, 2005.

Seco, R., Peñuelas, J., Filella, I., Llusià, J., Molowny-Horas, R., Schallhart, S., Metzger, A., Müller, M., and Hansel, A.: Contrasting winter and summer VOC mixing ratios at a forest site in the Western Mediterranean Basin: the effect of local biogenic emissions, Atmos. Chem. Phys., 11, 13161-13179, doi:10.5194/acp-11-13161-2011, 2011.

Seinfeld, J. H., and Pandis, S. N.: Atmospheric Chemistry and Physics: From Air Pollution to Climate Change, Second Edition, ISBN: 978-0-471-72018-8, 2006.

Sekimoto, K., Inomata, S., Tanimoto, H., Fushimi, A., Fujitani, Y., Sato, K., and Yamada, H.: Characterization of nitromethane emission from automotive exhaust, Atmospheric Environment, 81, 523-531, doi:10.1016/j.atmosenv.2013.09.031, 2013.

Shao, M., Lu, S., Liu, Y., Xie, X., Chang, C., Huang, S., and Chen, Z.: Volatile organic compounds measured in summer in Beijing and their role in ground-level ozone formation, Journal of Geophysical Research: Atmospheres, 114, D00G06, doi:10.1029/2008jd010863, 2009.

Sharma, R. K., Bhattarai, B. K., Sapkota, B. K., Gewali, M. B., and Kjeldstad, B.: Black carbon aerosols variation in Kathmandu Valley, Nepal, Atmospheric Environment, 63, 282-288, doi:10.1016/j.atmosenv.2012.09.023, 2012.

Sharma, U. K., Kajii, Y., and Akimoto, H.: Characterization of NMHCs in downtown urban center Kathmandu and rural site Nagarkot in Nepal, Atmospheric Environment, 34, 3297-3307, doi:10.1016/S1352-2310(99)00485-9, 2000.

Shim, C., Wang, Y., Singh, H. B., Blake, D. R., and Guenther, A. B.: Source characteristics of oxygenated volatile organic compounds and hydrogen cyanide, Journal of Geophysical Research: Atmospheres, 112, doi:10.1029/2006jd007543, 2007.

Simon, V., Dumergues, L., Bouchou, P., Torres, L., and Lopez, A.: Isoprene emission rates and fluxes measured above a Mediterranean oak (Quercus pubescens) forest, Atmospheric Research, 74, 49-63, doi:10.1016/j.atmosres.2004.04.005, 2005.

Singh, H. B., Kanakidou, M., Crutzen, P. J., and Jacob, D. J.: High concentrations and photochemical fate of oxygenated hydrocarbons in the global troposphere, Nature, 378, 50-54, 1995.

Singh, H. B., Salas, L. J., Chatfield, R. B., Czech, E., Fried, A., Walega, J., Evans, M. J., Field, B. D., Jacob, D. J., Blake, D., Heikes, B., Talbot, R., Sachse, G., Crawford, J. H., Avery, M. A., Sandholm, S., and Fuelberg, H.: Analysis of the atmospheric distribution, sources, and sinks of oxygenated volatile organic chemicals based on measurements over the Pacific during TRACE-P, Journal of Geophysical Research: Atmospheres, 109, D15S07 1-20, doi:10.1029/2003jd003883, 2004.

Singh, D.: Centre terms smog as extreme pollution, in Hindustan Times, December 1, 2012: New Delhi., Front Page., 2012

Sinha, V., Williams, J., Meyerhöfer, M., Riebesell, U., Paulino, A. I., and Larsen, A.: Air-sea fluxes of methanol, acetone, acetaldehyde, isoprene and DMS from a Norwegian fjord following a phytoplankton bloom in a mesocosm experiment, Atmos. Chem. Phys., 7, 739-755, doi:10.5194/acp-7-739-2007, 2007.

Sinha, V., Custer, T. G., Kluepfel, T., and Williams, J.: The effect of relative humidity on the detection of pyrrole by PTR-MS for OH reactivity measurements, International Journal of Mass Spectrometry, 282, 108-111, doi:10.1016/j.ijms.2009.02.019, 2009.

Sinha, V., Williams, J., Lelieveld, J., Ruuskanen, T. M., Kajos, M. K., Patokoski, J., Hellen, H., Hakola, H., Mogensen, D., Boy, M., Rinne, J., and Kulmala, M.: OH Reactivity Measurements within a Boreal Forest: Evidence for Unknown Reactive Emissions, Environmental Science & Technology, 44, 6614-6620, doi:10.1021/es101780b, 2010.

Sinha, V., Williams, J., Diesch, J. M., Drewnick, F., Martinez, M., Harder, H., Regelin, E., Kubistin, D., Bozem, H., Hosaynali-Beygi, Z., Fischer, H., Andrès-Hernàndez, M. D., Kartal, D., Adame, J. A., and Lelieveld, J.: Constraints on instantaneous ozone production rates and regimes during DOMINO derived using in-situ OH reactivity measurements, Atmos. Chem. Phys., 12, 7269-7283, doi:10.5194/acp-12-7269-2012, 2012.

Sinha, V., Kumar, V., and Sarkar, C.: Chemical composition of pre-monsoon air in the Indo-Gangetic Plain measured using a new air quality facility and PTR-MS: high surface ozone and strong influence of biomass burning, Atmos. Chem. Phys., 14, 5921-5941, doi:10.5194/acp-14-5921-2014, 2014.

Sinha, B., Singh Sangwan, K., Maurya, Y., Kumar, V., Sarkar, C., Chandra, B. P., and Sinha, V.: Assessment of crop yield losses in Punjab and Haryana using two years of continuous in-situ ozone measurements, Atmos. Chem. Phys., 15, 9555-9576, doi:10.5194/acp-15-9555-2015, 2015.

Sommariva, R., de Gouw, J. A., Trainer, M., Atlas, E., Goldan, P. D., Kuster, W. C., Warneke, C., and Fehsenfeld, F. C.: Emissions and photochemistry of oxygenated VOCs in urban plumes in the Northeastern United States, Atmos. Chem. Phys., 11, 7081-7096, doi:10.5194/acp-11-7081-2011, 2011.

Španél, P., and Smith, D.: Selected ion flow tube studies of the reactions of H_3O^+, NO^+, and O_2^+ with some chloroalkanes and chloroalkenes, International Journal of Mass Spectrometry, 184, 175-181, doi:10.1016/S1387-3806(98)14296-3, 1999.

Sprung, D., Jost, C., Reiner, T., Hansel, A., and Wisthaler, A.: Acetone and acetonitrile in the tropical Indian Ocean boundary layer and free troposphere: Aircraft-based intercomparison of AP-CIMS and PTR-MS measurements, Journal of Geophysical Research: Atmospheres, 106, 28511-28527, doi:10.1029/2000jd900599, 2001.

Srivastava, A.: Source apportionment of ambient VOCS in Mumbai city, Atmospheric Environment, 38, 6829-6843, doi:10.1016/j.atmosenv.2004.09.009, 2004.

Srivastava, A.: Variability in VOC concentrations in an Urban Area of Delhi, Environ. Monit. Assess., 107, 363-373, doi:10.1007/s10661-005-3546-8, 2005.

Srivastava, A., Joseph, A. E., Patil, S., More, A., Dixit, R. C., and Prakash, M.: Air toxics in ambient air of Delhi, Atmospheric Environment, 39, 59-71, doi:10.1016/j.atmosenv.2004.09.053, 2005.

Srivastava, A., Joseph, A. E., More, A., and Patil, S.: Emissions of VOCs at Urban Petrol Retail Distribution Centres in India (Delhi and Mumbai), Environ Monit Assess, 109, 227-242, doi:10.1007/s10661-005-6292-z, 2005.

Srivastava, A., Sengupta, B., and Dutta, S. A.: Source apportionment of ambient VOCs in Delhi City, Science of The Total Environment, 343, 207-220, doi:10.1016/j.scitotenv.2004.10.008, 2005c.

Srivastava, A., Joseph, A. E., and Devotta, S.: Volatile organic compounds in ambient air of Mumbai-India, Atmospheric Environment, 40, 892-903, doi:10.1016/j.atmosenv.2005.10.045, 2006.

Srivastava, A., and Devotta, S.: Indoor Air Quality of Public Places in Mumbai, India in Terms of Volatile Organic Compounds, Environ. Monit. Assess., 133, 127-138, doi:10.1007/s10661-006-9566-1, 2007.

Staehelin, J., Keller, C., Stahel, W., Schläpfer, K., and Wunderli, S.: Emission factors from road traffic from a tunnel study (Gubrist tunnel, Switzerland). Part III: Results of organic compounds, SO_2 and speciation of organic exhaust emission, Atmospheric Environment, 32, 999-1009, doi:10.1016/S1352-2310(97)00339-7, 1998.

Stemmler, K., Bugmann, S., Buchmann, B., Reimann, S., and Staehelin, J.: Large decrease of VOC emissions of Switzerland's car fleet during the past decade: results from a highway tunnel study, Atmospheric Environment, 39, 1009-1018, doi:10.1016/j.atmosenv.2004.10.010, 2005.

Stockwell, C. E., Veres, P. R., Williams, J., and Yokelson, R. J.: Characterization of biomass burning emissions from cooking fires, peat, crop residue, and other fuels with high-resolution proton-transfer-reaction time-of-flight mass spectrometry, Atmos. Chem. Phys., 15, 845-865, doi:10.5194/acp-15-845-2015, 2015.

Stone, E. A., Schauer, J. J., Pradhan, B. B., Dangol, P. M., Habib, G., Venkataraman, C., and Ramanathan, V.: Characterization of emissions from South Asian biofuels and application to source apportionment of carbonaceous aerosol in the Himalayas, Journal of Geophysical Research: Atmospheres, 115, D06301, doi:10.1029/2009jd011881, 2010.

Streets, D. G., Yarber, K. F., Woo, J. H., and Carmichael, G. R.: Biomass burning in Asia: Annual and seasonal estimates and atmospheric emissions, Global Biogeochem. Cycles, 2003. 17(4), doi:10.1029/2003GB002040, 2003.

Tani, A., Hayward, S., Hansel, A., and Hewitt, C. N.: Effect of water vapour pressure on monoterpene measurements using proton transfer reaction-mass spectrometry (PTR-MS), International Journal of Mass Spectrometry, 239, 161-169, doi:10.1016/j.ijms.2004.07.020, 2004.

Taylor, W. D., Allston, T. D., Moscato, M. J., Fazekas, G. B., Kozlowski, R., and Takacs, G. A.: Atmospheric photodissociation lifetimes for nitromethane, methyl nitrite, and methyl nitrate, International Journal of Chemical Kinetics, 12, 231-240, doi:10.1002/kin.550120404, 1980.

Tsai, S. M., Zhang, J., Smith, K. R., Ma, Y., Rasmussen, R. A., and Khalil, M. A. K.: Characterization of Non-Methane Hydrocarbons emitted from various Cookstoves used in China, Environmental Science & Technology, 37, 2869-2877, doi:10.1021/es026232a, 2003.

Venkataraman, C., Habib, G., Kadamba, D., Shrivastava, M., Leon, J. F., Boucher, O., and Streets, D. G.: Emissions from open biomass burning in India: Integrating the inventory approach with high-resolution Moderate Resolution Imaging Spectroradiometer (MODIS) active-fire and land cover data, Global Biogeochem. Cycles, 20(2): p. GB2013, doi:10.1029/2005GB002547, 2006.

Wang, Z., S. J. Nicholls, E. R. Rodriguez, O. Kummu, S. Hörkko, J. Barnard, W. F. Reynolds, E. J. Topol, J. A. DiDonato, and S. L. Hazen, Protein carbamylation links infammation,smoking, uremia, and atherogenesis, Nature Medicine, 13, 1176-1184, 2007

Warneck, P., and Williams, J.: The Atmospheric Chemist's Companion: Numerical Data for use in the Atmospheric Sciences, Springer Dordrecht Heidelberg London New York, doi:10.1007/978-94-007-2275-0, 2012.

Warneke, C., van der Veen, C., Luxembourg, S., de Gouw, J. A., and Kok, A.: Measurements of benzene and toluene in ambient air using proton-transfer-reaction mass spectrometry: calibration, humidity dependence, and field intercomparison, International Journal of Mass Spectrometry, 207, 167-182, doi:10.1016/S1387-3806(01)00366-9, 2001.

Warneke, C., de Gouw, J. A., Kuster, W. C., Goldan, P. D., and Fall, R.: Validation of Atmospheric VOC Measurements by Proton-Transfer- Reaction Mass Spectrometry Using a Gas-Chromatographic Preseparation Method, Environmental Science & Technology, 37, 2494-2501, doi:10.1021/es026266i, 2003.

Warneke, C., de Gouw, J. A., Goldan, P. D., Kuster, W. C., Williams, E. J., Lerner, B. M., Jakoubek, R., Brown, S. S., Stark, H., Aldener, M., Ravishankara, A. R., Roberts, J. M., Marchewka, M., Bertman, S., Sueper, D. T., McKeen, S. A., Meagher, J. F., and Fehsenfeld, F. C.: Comparison of daytime and nighttime oxidation of biogenic and anthropogenic VOCs along the New England coast in summer during New England

Air Quality Study 2002, Journal of Geophysical Research: Atmospheres, 109, D10309, doi:10.1029/2003jd004424, 2004.

Warneke, C., McKeen, S. A., de Gouw, J. A., Goldan, P. D., Kuster, W. C., Holloway, J. S., Williams, E. J., Lerner, B. M., Parrish, D. D., Trainer, M., Fehsenfeld, F. C., Kato, S., Atlas, E. L., Baker, A., and Blake, D. R.: Determination of urban volatile organic compound emission ratios and comparison with an emissions database, Journal of Geophysical Research: Atmospheres, 112, D10S47, doi:10.1029/2006jd007930, 2007.

Warneke, C., Roberts, J. M., Veres, P., Gilman, J., Kuster, W. C., Burling, I., Yokelson, R., and de Gouw, J. A.: VOC identification and inter-comparison from laboratory biomass burning using PTR-MS and PIT-MS, International Journal of Mass Spectrometry, 303, 6-14, doi:10.1016/j.ijms.2010.12.002, 2011.

Watson, J. G., Chow, J. C., and Fujita, E. M.: Review of volatile organic compound source apportionment by chemical mass balance, Atmospheric Environment, 35, 1567-1584, doi:10.1016/S1352-2310(00)00461-1, 2001.

Wentzell, J. J. B., Liggio, J., Li, S. M., Vlasenko, A., Staebler, R., Lu, G., Poitras, M. J., Chan, T., and Brook, J. R.: Measurements of Gas phase Acids in Diesel Exhaust: A Relevant Source of HNCO?, Environmental Science & Technology, 47, 7663-7671, doi:10.1021/es401127j, 2013.

Williams, J., Pöschl, U., Crutzen, P. J., Hansel, A., Holzinger, R., Warneke, C., Lindinger, W., and Lelieveld, J.: An Atmospheric Chemistry Interpretation of Mass Scans Obtained from a Proton Transfer Mass Spectrometer Flown over the Tropical Rainforest of Surinam, Journal of Atmospheric Chemistry, 38, 133-166, doi:10.1023/a:1006322701523, 2001.

WHO Guidelines for Indoor Air Quality: Selected Pollutants (ed. Theakston, F.), World Health Organization: WHO Regional Office for Europe, Copenhagen, Denmark, 2010, pp. 1-454

Xu, X., Stee, L. L. P., Williams, J., Beens, J., Adahchour, M., Vreuls, R. J. J., Brinkman, U. A., and Lelieveld, J.: Comprehensive two-dimensional gas chromatog-

raphy (GC × GC) measurements of volatile organic compounds in the atmosphere, Atmos. Chem. Phys., 3, 665-682, doi:10.5194/acp-3-665-2003, 2003.

Yassaa, N., Meklati, B. Y., Brancaleoni, E., Frattoni, M., and Ciccioli, P.: Polar and non-polar volatile organic compounds (VOCs) in urban Algiers and saharian sites of Algeria, Atmospheric Environment, 35, 787-801, doi:10.1016/S1352-2310(00)00238-7, 2001.

Yokelson, R. J., Burling, I. R., Gilman, J. B., Warneke, C., Stockwell, C. E., de Gouw, J., Akagi, S. K., Urbanski, S. P., Veres, P., Roberts, J. M., Kuster, W. C., Reardon, J., Griffith, D. W. T., Johnson, T. J., Hosseini, S., Miller, J. W., Cocker Iii, D. R., Jung, H., and Weise, D. R.: Coupling field and laboratory measurements to estimate the emission factors of identified and unidentified trace gases for prescribed fires, Atmos. Chem. Phys., 13, 89-116, doi:10.5194/acp-13-89-2013, 2013.

Yoshino, A., Nakashima, Y., Miyazaki, K., Kato, S., Suthawaree, J., Shimo, N., Matsunaga, S., Chatani, S., Apel, E., Greenberg, J., Guenther, A., Ueno, H., Sasaki, H., Hoshi, J. y., Yokota, H., Ishii, K., and Kajii, Y.: Air quality diagnosis from comprehensive observations of total OH reactivity and reactive trace species in urban central Tokyo, Atmospheric Environment, 49, 51-59, doi:10.1016/j.atmosenv.2011.12.029, 2012.

Young, P. J., Emmons, L. K., Roberts, J. M., Lamarque, J. F., Wiedinmyer, C., Veres, P., and VandenBoer, T. C.: Isocyanic acid in a global chemistry transport model: Tropospheric distribution, budget, and identification of regions with potential health impacts, Journal of Geophysical Research: Atmospheres, 117, doi:10.1029/2011jd017393, 2012.

Yu, Y., Panday, A., Hodson, E., Galle, B., and Prinn, R.: Monocyclic Aromatic Hydrocarbons in Kathmandu During the Winter Season, Water, Air, and Soil Pollution, 191, 71-81, doi:10.1007/s11270-007-9607-6, 2008.

Yu, Y., Galle, B., Panday, A., Hodson, E., Prinn, R., and Wang, S.: Observations of high rates of NO_2-HONO conversion in the nocturnal atmospheric boundary layer in Kathmandu, Nepal, Atmos. Chem. Phys., 9, 6401-6415, doi:10.5194/acp-9-6401-2009, 2009.

Yuan, B., Shao, M., de Gouw, J., Parrish, D. D., Lu, S., Wang, M., Zeng, L., Zhang, Q., Song, Y., Zhang, J., and Hu, M.: Volatile organic compounds (VOCs) in urban air: How chemistry affects the interpretation of positive matrix factorization (PMF) analysis, Journal of Geophysical Research: Atmospheres, 117, D24302, doi:10.1029/2012jd018236, 2012.

Yuan, B., Hu, W. W., Shao, M., Wang, M., Chen, W. T., Lu, S. H., Zeng, L. M., and Hu, M.: VOC emissions, evolutions and contributions to SOA formation at a receptor site in Eastern China, Atmos. Chem. Phys., 13, 8815-8832, doi:10.5194/acp-13-8815-2013, 2013.

Zhang, Q., Streets, D. G., Carmichael, G. R., He, K. B., Huo, H., Kannari, A., Klimont, Z., Park, I. S., Reddy, S., Fu, J. S., Chen, D., Duan, L., Lei, Y., Wang, L. T., and Yao, Z. L.: Asian emissions in 2006 for the NASA INTEX-B mission, Atmos. Chem. Phys., 9, 5131-5153, doi:10.5194/acp-9-5131-2009, 2009.

Zhang, Z., Lin, L., and Wang, L.: Atmospheric oxidation mechanism of naphthalene initiated by OH radical. A theoretical study, Physical Chemistry Chemical Physics, 14, 2645-2650, doi:10.1039/c2cp23271e, 2012.

Zhao, R., Lee, A. K. Y., Wentzell, J. J. B., McDonald, A. M., Toom-Sauntry, D., Leaitch, W. R., Modini, R. L., Corrigan, A. L., Russell, L. M., Noone, K. J., Schroder, J. C., Bertram, A. K., Hawkins, L. N., Abbatt, J. P. D., and Liggio, J.: Cloud partitioning of isocyanic acid (HNCO) and evidence of secondary source of HNCO in ambient air, Geophysical Research Letters, 41, 6962-6969, doi:10.1002/2014gl061112, 2014.